

University of Nottingham
UK | CHINA | MALAYSIA



OPTICS & PHOTONICS
UNIVERSITY OF NOTTINGHAM

Development and characterisation of optogenetic tools for non-invasive control of cellular functions in epithelia

Victoria Ciampani

A thesis presented for the degree of

Doctor of Philosophy

Electrical and Electronic Engineering

University of Nottingham

United Kingdom

01.03.19

Abstract

Living organisms are constantly working to maintain homeostasis, a status of physiological balance, which is required for stable cellular functionalities. Internal and external factors act to disrupt homeostatic conditions, against which the organisms have to counteract in a continuous dynamic equilibrium. Epithelial cells, which demarcate the interface of the inside and the outside world and discriminate different compartments in animal organisms, are responsible for maintaining compartmental and bodily homeostasis. Epithelia constitute a diverse and heterogeneous tissue in the human body: their physiological functions are based on simple processes, such as the transport of ions and water through the layer to regulate fluid composition and preserve homeostasis. Impairments in such processes are often rooted in dysfunctions of the molecular structures behind these mechanisms, namely ion channels, transporters and pumps, and result in a variety of pathological conditions. Consequently, epithelia are rich targets for the development of drugs and therapies and there is growing interest in their study. The study of epithelial volume regulation and fluid transport has classically been invasive, drawing on electrophysiology and pharmacology to dissect and control ion transport for detailed characterisation of their physiology.

The subject of this thesis is to create and optimise optogenetic tools to control and study vital properties of epithelial cells in future, such as their regulation of ion fluxes and volume flow. Optogenetics, a recently-born field of biotechnologies, mainly explored in neurophysiology to achieve precisely-timed generation of action potentials of selected populations of neurons, employs photon-gated channels and pumps to achieve control of ion flows across the membrane of genetically modified cells using light. The underlying thesis explored in this study is that the introduction and activation of these structures in epithelia, if sustained, could be capable of providing non-invasive control of epithelial membrane ion fluxes, homeostasis and cell volume, thus contributing to a complete vision of both pathophysiology and normophysiology of the tissue. In particular, the light-gated non selective cation channel Channelrhodopsin-2 from the green algae *Chlamydomonas reinhardtii* and the electrogenic chloride pump Halorhodopsin from the halophilic bacterium *Natronomonas pharaonis* will be harnessed in this thesis

to create a novel toolkit for the manipulation of epithelial membrane fluxes relevant to the control of cell volume and fluid handling in a model for the human retinal pigment epithelium (RPE), whose dysfunctions have been associated to a variety of pathological conditions, eventually leading to blindness.

The first half of this study focused on investigating the feasibility of introducing the optogenetic constructs Channelrhodopsin-2 (ChR2) and Halorhodopsin (eNpHR) into ARPE-19, an epithelial cell line derived from the human eye and routinely employed as an *in vitro* model of the RPE. Different approaches for the delivery of these opsin genes to the cells were evaluated and transfection was optimised both for ChR2 and eNpHR, following which the functionality of the channels, i.e. their ability to respond to light stimuli and drive the permeable ions through the membrane of the epithelial cells, was assessed. Activity of the optogenetic proteins was confirmed by the use of ion-sensitive fluorophores, in the case of ChR2 the calcium-sensitive Fura-2. Preliminary experiments performed using wild-type ChR2 (wtChR2), did not evidence major membrane ion permeability changes upon light exposure, as evaluated by calcium imaging.

To overcome limitations of wtChR2, which is characterised by low channel conductance and rapid, slowly-reversible gating, my work moved to the selection and generation of point mutants of ChR2, designed to both modify overall membrane flux and longevity of the conducting state. Four single amino acid mutations were designed, generated and optimised in epithelially-targeted plasmids and promoters via site-directed mutagenesis, in order to screen for the most suitable mutants for controlling membrane ion dynamics in epithelial cells. Among the tested mutants, ChR2 variants L132C, H134R and T159C showed, through functional experiments, to be capable of providing optical control of the ARPE-19 cells, to the extent of controlling calcium dynamics. Moreover, implementation of a conventional microscope with specific optical filters and components resulted in the development of an integrated tool for the simultaneous photostimulation of the light-gated proteins and the recording of ion dynamics through the monitoring of ion-sensitive fluorescent indicators. Changes in ion permeabilities across the epithelial cell membrane and readout of cell output following light stimuli were achieved optically, removing the need for pharmacological agents or invasive mi-

croelectrodes.

In conclusion, this work presents the design, creation and characterisation of a set of tools for a previously unreported application of light-gated optogenetic channels for the study of epithelial physiological processes, with the final goal of achieving non-invasive control of epithelial membrane ion fluxes and dynamics.

Contents

1 Background and literature review **15**

1.1 Epithelia 18

1.1.1 Structure and function 18

1.1.2 Epithelial transport 20

1.1.3 Conventional methodologies to study epithelial transport 25

1.1.4 The retinal pigment epithelium (RPE) 28

1.2 Rhodopsins 35

1.2.1 Channelrhodopsin 39

1.2.2 Halorhodopsin 54

1.3 Genetic engineering 59

1.4 Optical engineering 68

1.5 From microbial rhodopsins to optogenetics 71

2 Materials and Methods **81**

2.1 Molecular biology 81

2.1.1 Plasmid design and description 81

2.1.2 Plasmid sequence validation 83

2.1.3 Site-directed mutagenesis 86

2.1.4 Plasmid amplification and purification 89

2.2 Cell culture 91

2.2.1 General cell culture procedures 91

2.3 Cytotoxicity assessments 92

2.3.1 MTS assay: opsin cytotoxicity 92

2.3.2 Live/dead assay: all-trans retinal (ATR) cytotoxicity 94
2.4 Transfection 95
2.4.1 Transfection optimisation 95
2.4.2 Evaluation of transfection efficiency 97
2.5 Localisation study 99
2.6 Optogenetic stimulation: calcium imaging 99
2.7 Microscopy 101
2.7.1 Development of the imaging system 101
2.7.2 Power measurements 103
2.8 Statistical analysis 105

3 Optimising the expression of optogenetic actuators in ARPE-19 cells 107
3.1 Optimisation of delivery of wtChR2 and eNpHR genes to the retinal pigment epithelial cell line ARPE-19 108
3.1.1 Flow cytometric evaluation of transfection efficiency 108
3.1.2 Evaluation of cytotoxicity of optogenetic actuators in epithelia . 113
3.1.3 Expression study of optogenetic actuators by fluorescence imaging 114
3.1.4 Membrane localisation study 116
3.2 Functionality of wtChR2 in ARPE-19 cells assessed with calcium imaging 122

4 Creation and characterisation of ChR2 mutants in the ARPE-19 cell line 127
4.1 Genetic engineering of ChR2 mutants for applications in epithelial physiology 128
4.1.1 Screening of ChR2 mutants 128
4.1.2 Generation of ChR2 variants with modified channel properties for applications in epithelial physiology 129
4.1.3 Cytotoxicity study of *all-trans* retinal 131
4.2 Expression of ChR2 mutants in the ARPE-19 cell line 134
4.2.1 Flow cytometric evaluation of mutant ChRs expression in ARPE-19 cells 134

4.2.2 Study of expression levels of ChR2 mutants by fluorescence imaging 135
4.2.3 Membrane localisation study of the expression of ChR2 mutants in the ARPE-19 cell line 140
4.3 Functionality of ChR2 mutants in retinal epithelial cells 143
4.3.1 Fura-2 ratiometric calcium imaging of ChR2 mutants 143
4.3.2 Characterisation of ChR2 mutants L132C, T159C and H134R properties in the ARPE-19 cell line 151

5 Conclusions and Future Work **161**

List of Figures

1.1 General schematics of ion channels, transporters and pumps, responsible for the mainteinance of homeostasis in living organisms. 16

1.2 Epithelia schematic, focusing on the main transport paths across the epithelial layer. 21

1.3 Regulatory volume decrease and increase processes. 23

1.4 Fluorescence spectra of the calcium-sensitive dye Fura-2. 28

1.5 General anatomy of the human eye and location of the retinal pigment epithelium (RPE) 30

1.6 Retinal pigment epithelium schematics 31

1.7 Transepithelial transport across the RPE 34

1.8 Retinal *cis-trans* photoisomerisation in animal and microbial rhodopsins 37

1.9 Channelrhodopsin-2 from *Chlamydomonas reinhardtii* and Halorhodopsin from *Natronomonas pharaonis* in their natural environment. 38

1.10 The crystal structure of the C1C2 chimera, showing the main architectural features of channelrhodopsins, including the retinal binding pocket. 41

1.11 The crystal structure of ChR2 is shown as a 3UG9-derived pore. 42

1.12 Mechanism of action of the light-gated cation channel Channelrhodopsin-2. 44

1.13 Channelrhodopsin-2 photocycle. 45

1.14 Channelrhodopsin-2 most relevant amino acids involved in kinetics and channel properties are highlighted in the 3D protein structure. 48

1.15 ChR2 mutant H134R compared to wild-type ChR2 49

1.16 Substitution of amino acid C128 in ChR2 structure results in slower off-kinetics of the optogenetic channel. 50

1.17 ChR2 mutant E123T (ChETA) compared to wild-type ChR2 50

1.18 Mutation of the leucine 132 with a cysteine results in six-fold calcium permeability increase in ChR2. 51
1.19 ChR2 T159C mutant compared to wild-type ChR2 and other engineered ChR2 . . . 52
1.20 The crystal structure of halorhodopsin from *Natronomonas pharaonis*. 55
1.21 Mechanism of action of the light-driven chloride pump Halorhodopsin from *Natronomonas pharaonis* 56
1.22 Photocycle reactions of the electrogenic chloride pump Halorhodopsin from *Natronomonas pharaonis* (NpHR) 57
1.23 Mechanism of chloride uptake from the extracellular space and release into the cytoplasm of the electrogenic chloride pump Halorhodopsin from *Natronomonas pharaonis* 58
1.24 Comparison of expression patterns of *Natronomonas pharaonis* halorhodopsin (NpHR) and its enhanced version (eNpHR) for reduced endoplasmic reticulum accumulation in cultured hippocampal neurons. 59
1.25 Genetic engineering schematics 61
1.26 Lipofection schematic mechanism. 64
1.27 Magnetic-nanoparticle-based transfection schematics. 65
1.28 pcDNA3.1 plasmid vector map 66
1.29 Post-translational protein trafficking schematics. 67
1.30 Multitude of optogenetic constructs grouped based on their kinetic properties, activation wavelengths and activity type when introduced in mammalian cells 72
1.31 Activation spectra of Channelrhodopsin-2 and Halorhodopsin. 74
1.32 Optogenetics conceptual schematics. 75

2.1 Simplified schematics of main components of pcDNA3.1 plasmids for ChR2 and eNpHR 2.0. 81
2.2 pcDNA3.1 ChR2-hChR2(H134R)-mCherry plasmid vector map 82
2.3 Sequence alignment of wtChR2 showing integrity of sequence after subcloning. . . . 84
2.4 Sequence alignment of eNpHR showing integrity of sequence after subcloning. 85
2.5 Site-directed mutagenesis schematics. 86
2.6 Site-directed mutagenesis schematics. 87
2.7 Blue-white screening for the evaluation of mutagenesis efficiency. 89

2.8 Cells transfected with magnetofection reagents shown on the magnetic plate used to induce the process. 97
2.9 Schematics of the imaging setup used for photostimulation experiments. 101
2.10 Fluorescence spectra of molecules used in photostimulation experiments. 102

3.1 Transfection optimisation: comparison of different transfection reagents tested for the delivery of the optogenetic constructs to retinal pigment epithelial cells. 110
3.2 Flow cytometry data for evaluation of transfection efficiency of wild type Channelrhodopsin-2 and *Natronomonas pharaonis* Halorhodopsin. 112
3.3 Histograms showing efficiency of Lipofectamine-mediated transfection of wtChR2 and eNpHR. 112
3.4 Cytotoxicity assessment of optogenetic constructs. 113
3.5 Fluorescent images of ARPE-19 cells expressing the optogenetic construct wild-type ChR2. 114
3.6 Fluorescent images of ARPE-19 cells expressing the optogenetic construct eNpHR. . 115
3.7 Fluorescent images of ARPE-19 cells co-expressing ChR2 and eNpHR. 116
3.8 Membrane localisation study of wtChR2 in ARPE-19 cells. 118
3.9 Membrane localisation study of eNpHR in ARPE-19 cells. 119
3.10 Confocal images showing membrane localisation study of wtChR2 and eNpHR co-transfected in ARPE-19 cells. 120
3.11 Localisation study of wtChR2 and eNpHR in ARPE-19 cells. 121
3.12 Fura-2 ratiometric measurements of Ca^{2+} dynamics in ARPE-19 cells expressing wtChR2. 123

4.1 DNA and protein sequences validation of ChR2 mutants created by site-directed mutagenesis. 130
4.2 Chromatograms confirming the introduction of point mutations in wt-ChR2 sequence following site-directed mutagenesis. 130
4.3 Protein sequence validation of ChR2 mutants created by site-directed mutagenesis. . 131
4.4 Fluorescence images reporting cytotoxicity of *all-trans* retinal in the ARPE-19 cell line. 133
4.5 Study of cytotoxicity of *all-trans* retinal in the ARPE-19 cell line. 134

4.6 Flow cytometry data showing transfection efficiency of ChR2 mutants in the ARPE-19 cell line with or without supplementation of 1μM *all-trans* retinal. 135
4.7 Study of the expression patterns of mutants generated by site-directed mutagenesis. . 137
4.8 20X confocal images reporting study of expression levels of ChR2(H134R) mutant at different time points post-transfection. 138
4.9 63X confocal images reporting study of expression levels of ChR2(H134R) mutant at different time points post-transfection. 139
4.10 Confocal images showing sub-cellular localisation of ChR2 mutants in ARPE-19 cells. 141
4.11 Membrane localisation study of ChR2 mutants. 142
4.12 Calcium transients in ARPE-19 cells generated by the photoactivation of ChR2-L132C mutant. 145
4.13 Effects of *all-trans* retinal supplementation on the activity of ChR2 mutant L132C. . 146
4.14 L132C causes calcium transients in ARPE-19 cells in 2 mM Ca^{2+} solution. 147
4.15 Calcium transients in ARPE-19 cells generated with the photoactivation of ChR2-T159C mutant. 148
4.16 Effects of *all-trans* retinal supplementation on the activity of ChR2 mutant T159C. . 148
4.17 Calcium transients in ARPE-19 cells generated with the photoactivation of ChR2-H134R mutant. 149
4.18 Calcium transients in ARPE-19 cells generated with the photoactivation of ChR2-C128A mutant. 150
4.19 Fura-2 ratiometric measurements of ARPE-19 cells expressing the ChR2 mutant E123T. 151
4.20 Calcium influx in ARPE-19 cells mediated by mutants H134R, L132C and T159C. . 152
4.21 Comparison of ChR2 mutant H134R, L132C, T159C responses versus increasing lenght of blue light stimulus. 153
4.22 Comparison of ChR2 mutant H134R, L132C, T159C responses versus increasing light intensities. 154
4.23 Comparison of the recovery kinetics of ChR2 mutants H134R, L132C, T159C. . . . 155
4.24 Effects of *all-trans* retinal supplementation on ARPE-19 autofluorescence. 157
4.25 Retinal cycle and by-production of the fluorophore A2E 158

4.26 Fluorescence spectra of lipofuscin and A2E fluorophores, by-products of the retinoid metabolism in the Retinal Pigment Epithelium (RPE) 159

5.1 Fluorescence emission spectra of chloride-sensitive indicator MQAE at different chloride concentrations. 163

List of Tables

1.1 ChR variants designed to overcome heterologous expression of the light-gated channel in mammalian systems. 53

2.1 Table of PCR primers used for site-directed mutagenesis. 88

2.2 Table of optical filters used in the present study for optogenetic phosostimulation experiments 103

2.3 Table of power measurements of the blue light used for photostimulation of ChR2 . . 104

2.4 Table of power measurements of the blue light used for photostimulation of ChR2 in the FuraLED/TwinLED unit (CairnResearch) 105

Abbreviations

A2E : N-retinyledin-N-retinylethanolamin

AMD : Age-related Macular Degeneration

ARPE-19 : human-derived retinal pigment epithelium cell line

ATR : *all-trans* retinal

BR : Bacteriorhodopsin

BRB : Blood-Retina Barrier

C128A : Channelrhodopsin-2 C128A mutant

CatCh : Calcium-Translocating Channelrhodopsin 2

CF : Cystic Fibrosis

CFTR : Cystic Fibrosis Transmembrane Regulator

ChETA : Channelrhodopsin-2 mutant E123T with accelerated kinetics

ChR2 : Channelrhodopsin-2

CNV : choroidal neo-vascularisation

DMEM : Dulbecco-Modified Minimal Essential Medium

DNA : deoxyribonucleic acid

DPBS : Dulbecco's phosphate buffer saline

E123T : Channelrhodopsin-2 E123T mutant

eNpHR : enhanced *Natronomonas pharaonis* Halorhodopsin

ER : endoplasmic reticulum

EYFP : Enhanced Yellow Fluorescent Protein

FBS : Fetal Bovine Serum

GPCR = G-protein coupled receptor

H134R : Channelrhodopsin-2 H134R mutation HBSS = Hank's Balanced Salt Solution

HR : Halorhodopsin

L132C : Channelrhodopsin-2 L132C mutant

LED : light-emitting diode

MTS : 3-(4,5-dimethylthiazol-2-yl)-5-(3-carboxymethoxyphenyl)-2-(4-sulfophenyl)-2H-tetrazolium

Na^+/K^+-ATPase : sodium-potassium ATPase

ND : neutral density

NKCC : sodium potassium chloride co-transporter

pcDNA3.1 : circular plasmid for constitutive expression

PCR : polymerase chain reaction

PDB : Protein Data Bank

PE : phosphatidylethanolamine

PEDF : Pigment Epithelium Derived Factor

PFA : Paraformaldehyde

POS : photoreceptor outer segments

RNA : ribonucleic acid

RP : Retinitis Pigmentosa

RPE : Retinal Pigment Epithelium

$RSBH^+$: protonated retinal Schiff base

SEM : standard error of the mean

SLM : Spatial Light Modulator

T159C : Channelrhodopsin-2 T159C mutant

TEER : Trans-Epithelial Electrical Resistance

VEGF : Vascular Endothelial Growth Factor

WGA : Wheat Germ Agglutinin

WGA-CF405 : CF405-conjugated WGA

wtChR2 : wild-type Channelrhodopsin-2

Chapter 1

Background and literature review

Living organisms are defined and maintained by membranes, boundaries which determine what is part of the organism, i.e. inside such boundary, and what is outside and therefore extraneous to the form of life under examination. But life is also grounded in the exchange of resources between the outside and the inside, a continuous balancing process which is vital for all organisms.

The fine control of the transport of useful molecules towards the inside and the ability to keep harmful compounds or other potentially dangerous beings on the outside is critical for survival. Evolution has developed many different mechanisms to tune such selective transport but the basic principles are shared across all domains of life. Fundamentally, the generation of an action potential in a human neuron and the movement of unicellular photosynthetic green algae towards light to maximise energy production are both based on similar simple processes, i.e. movements of ions across the membranes. From this perspective, when primordial single cells have evolved into more complex organisms, the 'in' and 'out' discrimination has been passed on from the phospsholipid bilayer of a single cell to contiguous layers of cells that can act as a selective barrier around tissues and compartments, which allow for regulated gas and metabolite exchange whilst protecting from pathogen invasion.

Biological membranes are composed of a phospholipid bilayer, which restricts uncontrolled movement of molecules from the intracellular to the extracellular compartment and viceversa [Ikonen, 2001]. Small hydrophobic molecules, gas and small uncharged polar molecules can diffuse freely across the membrane but the flow of ionic species and

charged or big molecules is restricted and finely controlled. Membrane transport of solutes is made possible by specialised protein structures, such as ion channels, transporters and pumps, proteins embedded in the phospholipid bilayer, which control the distribution of ions and molecules across the membrane and, therefore, are responsible for cellular homeostasis [Dubyak, 2004]. These transport proteins contribute to the generation of a concentration gradient across cellular membranes, i.e. they maintain unequal intracellular and extracellular ion compositions. The electrochemical ion gradient is the foundation of numerous cellular vital functions, from the conduction of neuronal signal, to muscle contraction and sensory processes [Koch and Barish, 1994; Nielsen and Overgaard, 1996]. Transport proteins in the cell membrane can be categorised in different groups, responsible for active and passive transport, based on their transport characteristics, schematically represented in Figure 1.1.

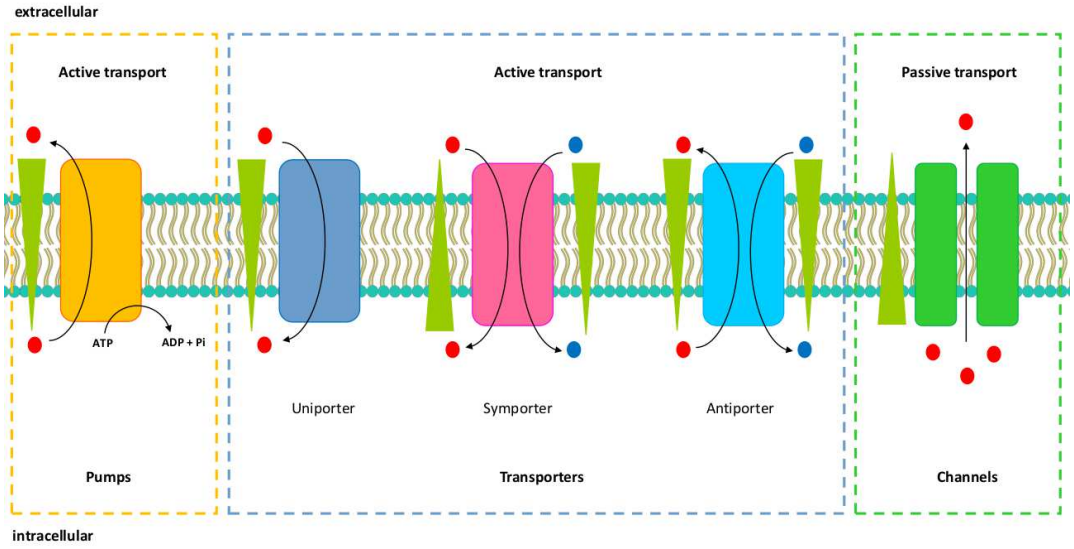


Figure 1.1: **General schematics of ion channels, transporters and pumps, responsible for the mainteinance of homeostasis in living organisms.** They can be categorised in two groups, responsible for active and passive transport, based on their transport characteristics. Pumps transport ions against their concentration gradients (represented by a triangle pointing to the compartment with the lower concentration) by exploiting, for instance, ATP hydrolysis as a source of energy. Uniporters carry one ion species or molecule at a time by binding it and assisting it across the membrane. Symporters are co-transporters which transport two or more ions in the same direction. They allow the movement of one ionic species against its concentration gradient by coupling it to the flow of another ionic species down its gradient. Antiporters have a similar activity to symporter but, instead of driving ions in the same direction, they transport two ionic species in opposite directions. Channels conduct a specific ion or molecule down their concentration gradient and they are responsible for passive transport. Channels can be gated by voltage, ligands or light and once opened they allow for the passive flow of permeable ions or molecules through the pore. *Original drawing.*

A variety of pathologies arises from failure or flaws in membrane transport mechanisms [Ashcroft, 1999], and there is growing interest in studying the molecular bases of

these processes. Ion channels and transporters are in fact among the main targets for the pharmacology of a variety of pathological conditions [Bagal et al., 2012; Clare et al., 2000; Triggle, 2007], from cardiac pathologies [Viola et al., 2009] to neurological disorders [Yogeeswari et al., 2004]. Our knowledge on ion transporters, channels and pumps derives from observations acquired with a variety of methodologies. Crystallography analysis of the 3D structure of the proteins provided information on the spatial organisation of these macromolecules [Rees et al., 2000]. Electrical investigation of cellular properties by means of electrophysiology approaches enlightened details of the electrical activities of channels and pumps in terms of their kinetics and stoichiometry, in combination with pharmacological agents as tools to modulate protein activities [Soria and Ceña, 1998]. Ion-sensitive indicators have been employed to study ion dynamics, again combined with pharmacological tools to tune membrane transport protein functionality [Tsien, 1989]. The use of chemical compounds to activate (agonists) or inhibit (antagonists) the activity of a specific transporter and study the consequent effects on the cells or tissues represent an invaluable tool to modulate membrane transport [Jones, 1993; White and Cohen, 1992]. Pharmacological agents, however, possess considerable limitations, e.g. they can lack specificity and reversibility [Neyton and Paoletti, 2006]. A new technique in the field of biotechnology, optogenetics, shows promising features to become very useful in the study of membrane transport by manipulating it non-invasively in response to light [Deisseroth, 2011]. So far, optogenetic techniques have been mainly used to study the function of excitable cells such as neurons [Boyden et al., 2005] and therefore their role in the behaviour of organ systems and animal models [Nagel et al., 2005a; Zhao et al., 2011]. Expanding the remit of optogenetic interventions in ion transport processes into other cell types has the potential to aid researchers understanding the molecular basis of ion transport and homeostasis across biological membranes in health and disease.

1.1 Epithelia

1.1.1 Structure and function

Epithelia represent the boundary between the body and its surroundings and between fluid compartments within organisms. They are constituted of sheets of cells coating the external surface (skin) and the internal cavities of the body and organs (kidney, stomach, intestine, lung, bladder, reproductive organs, etc) and specialisation of epithelia constitute exocrine and endocrine glands. Epithelia are classified in different groups based on their morphology (squamous, cuboidal, columnar) and organisation (simple, stratified, pseudostratified) of the cells constituting them. Functions of epithelia include:

- **protection**: epithelia protect the body or the organs from infections and exogenous harmful or toxic molecules; these cells allow for gas and metabolite exchange (lungs, digestive tract) whilst preventing pathogen invasion [Peterson and Artis, 2014].

- **secretion**: epithelial tissue secrete a variety of molecules depending on the organ they are found in. Glands are composed of epithelial tissue; endocrine glands secrete hormones; exocrine glands secrete mucus, sweat, saliva. Epithelia in the gastrointestinal tract produce digestive enzymes and secrete them in the lumen of the digestive organs [Barrett and Keely, 2000; Nathanson and Boyer, 1991; Rogers, 2007].

- **absorption**: epithelial cells lining the intestine absorb nutrients, which are then delivered to the blood stream for nutrition of the organism [Kiela and Ghishan, 2016]; epithelia of the kidney and the eye reabsorb fluid to excrete it as waste and preserve ion and fluid balance [Burg and Orloff, 1968; Marmor, 2000].

- **transport**: epithelial cells, like the retinal epithelium in the eye, are able to perform vectorial transport of nutrients in one direction and metabolites in the opposite direction [Quinn and Miller, 1992].

- **regulation**: numerous epithelia produce growth factors for the mainteinance of organ homeostasis [Adamis et al., 1993].

The distinguishing parts of epithelia are: epithelial cells, tight junctions and the basement membrane where the cells are anchored [Lewis, 1996]. Epithelial cells are differentiated, polarised cells which are arranged in contiguous sheets. Tight junctions (TJs) are multi-component structures constituted by proteins embedded within and protruding from the cell membranes of adjacent cells [Niessen, 2007]; numerous proteins contribute to the formation of TJs [Mitic and Anderson, 1998], among which occludins, claudins and junction adhesion molecules (JAMs) play a major role [Steed et al., 2010]. TJs bind the cells to one another (adhesion) and restrict movement of substances between them (segregation), blocking the paracellular diffusion path [Anderson and Van Itallie, 1995]. They are also responsible for the barrier function of numerous epithelia [Förster, 2008], protecting the tissue and the organisms from pathogen invasion. By interacting with similar structures on neighbour cells, TJs separate an apical from a basolateral domain in the membrane of epithelial cells. TJs therefore dictate epithelial polarity by segregating distinct populations of membrane transport proteins to one of the two membrane compartments [Cereijido et al., 1998]. Based on the resistive properties of the tight junctions, epithelia can be categorised as leaky, if resistance through the paracellular pathway is low (R_j<100 Ωcm^2), or tight, where intercellular resistance is high (R_j>500 Ωcm^2).

The basement membrane is a layer of extracellular matrix (ECM) which acts as a scaffolding element, upon which epithelial cells can grow, a driver for polarised differentiation and as a selective mechanical barrier discriminating which substances can enter the epithelial layer [Hay, 1993; Manninen, 2015]. Different macromolecules, such as collagen, glycoproteins and enzymes, mainly proteases, can be found in the ECM. Anchoring of the epithelial cells to the basement membrane is achieved by interactions of protein structures on the cells surface, such as integrins, with other proteins protruding from the ECM, such as laminins and collagen [Theocharis et al., 2016].

The chief and defining characteristic of epithelial cells is their ability to segregate an apical and a basolateral compartment of the plasma membrane and target comple-

mentary protein structures involved in the regulation of solute concentrations to either domain of the cell membrane in a highly controlled way [Cereijido et al., 1996; Ortega and Welling, 2018]. Asymmetric distribution of lipids and proteins in biological cells can be either a transient characteristic, for instance during cell division, or is a permanent trait of cellular organisation, as it happens in neurons, spermatozoa and epithelial cells [Bradke and Dotti, 1998; Ladha, 1998; Simons and Wandinger-Ness, 1990]. Polarisation of epithelia is a complex, multi-factorial process, which is not yet fully understood, but is driven by receptor-mediated interactions with both the basement membrane [Manninen, 2015] and adjacent cells through tight junction complexes [Cereijido et al., 1998]. Segregation of ion transporters, channels and other regulative proteins specifically to one domain of the epithelial cell membrane appears to be influenced by post-translational modifications and targeting sequences in expressed proteins, which are transported and directed to defined membrane compartments by a variety of interactions with subcellular organelles and the cytoskeleton [Legouis et al., 2003; Li and Gundersen, 2008; Mostov et al., 2003; Simons and Wandinger-Ness, 1990; Weisz and Rodriguez-Boulan, 2009].

1.1.2 Epithelial transport

Epithelial transport is one of the main tasks of epithelia and it depends on the asymmetric structural organisation of epithelial cells. Epithelial trasport is rooted in the polarisation of the epithelial cell layer and the segregation of specific membrane transporters, pumps and channels to the apical or the basolateral membrane compartments of the cells [Matter and Mellman, 1994]. Transport of molecules through the epithelial layer can follow two main paths: the paracellular or the transcellular path. Transcellular transport describes transport through the layer of cells (i.e. intracellular); it is vectorial, requires energy and relies on the distribution of cell-type-specific transport proteins targeted to one of the two domains of the plasma membrane. Paracellular transport happens between the cells (i.e. intercellular); it is passive, energy-independent and is the result of the gradients generated by the transcellular transport, as modulated by the properties of the tight junctions [Anderson, 2001]. A schematic representation of

epithelia and the key transport paths across the layer are shown in Figure 1.2.

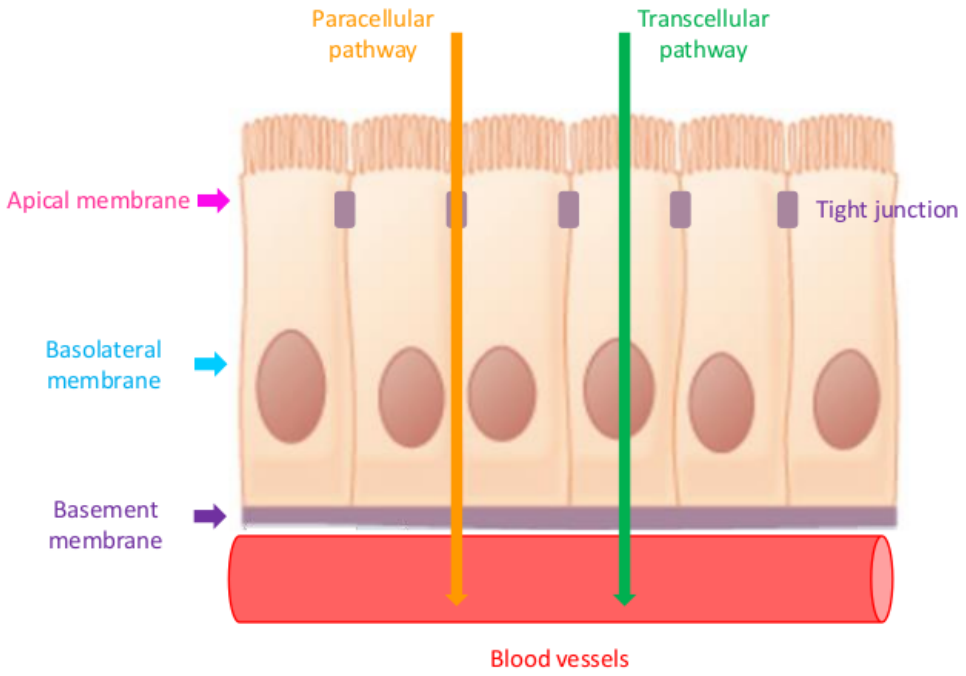


Figure 1.2: **Epithelia schematic, focusing on the main transport paths across the epithelial layer.** Schematic representation of a layer of epithelial cells showing the distinguishing features of the tissue responsible for its function. Epithelia are constituted by a packed layer of cells, solidly held together by tight junctions, adhesive protein structures that prevent uncontrolled transport via the paracellular pathway. Tight junctions divide the epithelial cell membrane into two compartments, an apical domain, facing the lumen of the organ, and a basolateral domain, anchored to the basement membrane and facing the blood stream underneath. Epithelial functionality depends on the ability to target specific transport proteins to one of the two membrane domains, thereby allowing vectorial transcellular transport. Transepithelial transport is responsible for uptake of nutrients from the blood vessels and secretion of growth factors or excretion of metabolites into the circulation stream. Transport across epithelia is fundamental for the mainteinance of ion and fluid balance in the organ where the epithelium is located. *Original drawing.*

The ionic gradient in most epithelial cells is generated by the sodium-potassium ATPase (Na^+/K^+ ATPase), which transports three sodium ions outside the cells and two potassium ions inside the cells, against their concentration gradients using ATP hydrolysis as driving force for its operation [Clausen et al., 2017]. The Na^+/K^+ ATPase is localised at the basolateral membrane in all epithelia, with the exception of the retinal pigment epithelium (RPE) and the choroid plexus, which express the pump in the brushed border of their apical membrane [Gundersen et al., 1991; Masuzawa et al., 1984]. The unilateral expression of the Na^+/K^+ ATPase in epithelial cells is the result of the complex processes defining epithelial polarity. Understanding epithelial functions depend strongly on the study of localisation of membrane transport structures to the apical or basolateral compartments and on the synergistic activity with other

proteins in order to achieve the directional movement of substances across the epithelial layer [Cereijido et al., 2008; Hamann, 2002; Miller and Steinberg, 1977]. Ion and fluid transport are finely intertwined in epithelia [Fischbarg, 2010; Lang et al., 1998; Larsen and Hoffmann, 2016; Larson and Spring, 1987; Spring, 1998]. By controlling the dynamic equilibrium of ions across epithelial cells, one controls also, to a certain extent, water transport. Water transport across epithelia is still a controversial topic. There are evidences supporting water movement based on solute gradient either through specialised pores in the membrane, aquaporins [Stamer et al., 2003], or other still debated routes [Fischbarg, 2010, 2018]. Fluid transport between isotonic solutions has also been theorised [Mathias, 1985]. Moreover, depending on the type of epithelium under examination, tight or leaky, water can follow different paths across the layer of cells, either through the paracellular or transcellular routes [Kawedia et al., 2007; Reuss, 2001]. The correct movement of fluid in a tissue is connected to the conservation of homeostasis, therefore it is a finely-regulated process. When water equilibrium at the interface of a biological membrane is perturbed, the cells conteract it by two mechanisms: RVD (Regulatory Volume Decrease) or RVI (Regulatory Volume Increase), schematically represented in Figure 1.3. During RVD, osmotically swollen cells release K^+, Cl^-, organic osmolytes, and water. A variety of cell membrane transport mechanisms are involved in RVD such as swelling-activated Cl^- channels and swelling-activated K^+ channels [Kubo and Okada, 1992; Stutzin and Hoffmann, 2006]. On the other hand, the RVI response occurs by gain of water, Na^+ and Cl^-. In the majority of cells, RVI is mediated by the $Na^+/K^+/2Cl^-$ cotransporter (NKCC), and the Na^+/Cl^- symporter. In other cases, an important role is played by the parallel activation of the Na^+/H^+ exchanger (NHE) and $Cl^-/HCO3^-$ anion exchanger [Eveloff and Warnock, 1987].

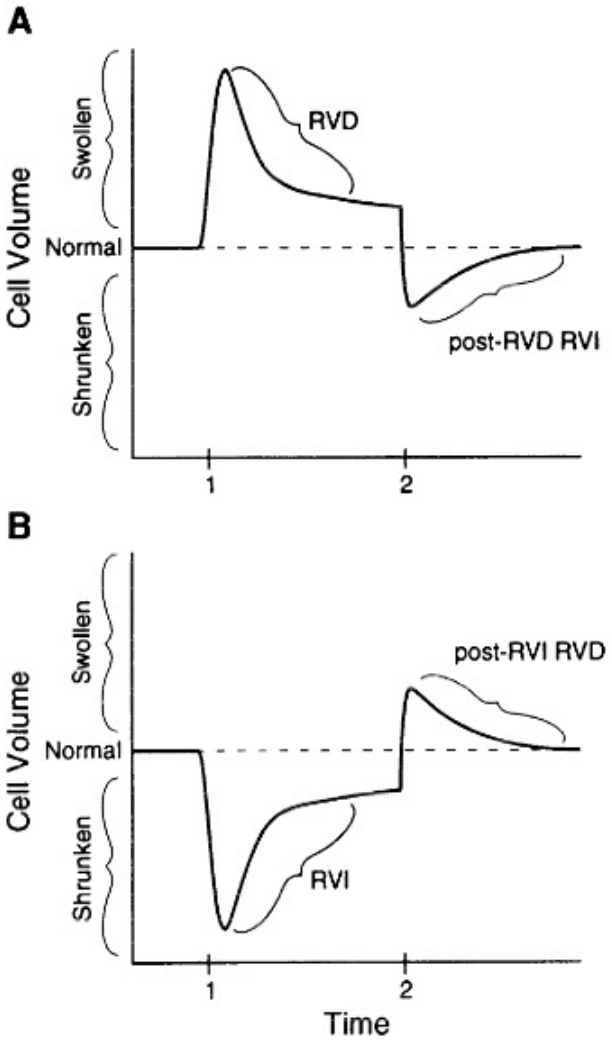


Figure 1.3: **Regulatory volume decrease and increase processes. A** Cell swelling in epithelial cells following alterations in equilibrium conditions, either by changes in ionic gradients in response to hyposmotic solution or addition of pharmacological agents to the cultured cells. Cells counteract such perturbation by opening specific channels in order to restore physiological fluid balance, a process called RVD (Regulatory Volume Decrease). **B** Cell shrinking caused by bathing in hyperosmotic solution initiates the opposite regulatory process, RVI (Regulatory Volume Increase), activating transport dynamics to ensure system equilibrium. Adapted from [Srinivas et al., 2003].

An involvement of Ca^{2+} in the signaling cascade leading to RVD has previously been demonstrated, where increasing intracellular calcium levels were reflected in signaling pathways activating K^+ and Cl^- outward fluxes resulting in a loss of ions, water, and recovery of initial cell volume [McCarty and O'Neil, 1992]. Entering the cells, calcium can perform a variety of functions, among which opening Ca^{2+}-activated K^+ channels to help bringing membrane potential and volume to homeostasis. Fluid transport across epithelia, depending on their configuration as tight or leaky, remains one of the most debated topics in physiology and, according to Hans Ussing, might represent the last unanswered question in the field of epithelial physiology [Fischbarg, 2010]. Alterations in epithelial functionality, especially regarding their ion and volume transport activities, are often the cause of diseases or conditions in the body. Cystic fibrosis (CF) [Cutting, 2015], autosomal polycystic kidney disease (APKD) [González-Perrett et al., 2001], retinitis pigmentosa (RP) [Davidson et al., 2009; Jones et al., 2016], age-related macular degeneration (AMD) [Nowak, 2006] and hypertension [Hummler, 2003] are all examples of conditions where epithelial transport is altered. Impairments in epithelial transport can either be caused by genetic mutations (so-called "channelopathies", where aberrant transport is the primary cause of the disease) [Kim, 2014; Planells-Cases and Jentsch, 2009] or by incorrect localisation of the transporters in the membrane domain where they normally provide for homeostasis [Wilson et al., 1991]. For instance, cystic fibrosis is the result of mutations in the gene for the chloride channel CFTR (Cystic Fibrosis Transmembrane Regulator), involved in a variety of processes like mucus production and fluid secretion which, when impaired, cause chronic pulmonary and pancreatic failures, often exacerbated by chronic bacterial infections in the compromised tissues [Cutting, 2015]. Channelopathies can affect all organs in the human body and the number of known diseases is increasing, mainly due to a deepening knowledge of the role of ion channels in pathophysiology [Hübner and Jentsch, 2008]. In the gastrointestinal tract, deregulated epithelial barrier function has been reported in conditions such as Chrohn's disease [Zeissig et al., 2007] and the irritable bowel syndrome (IBS) [Beyder and Farrugia, 2016]. In the eye, changes in the functionality of the retinal pigment epithelium (RPE) have been linked to the pathophysiology of a variety of retinal

pathologies and degenerations, eventually leading to blindness [R Sparrrow et al., 2010]. The RPE are involved in the etiology of such conditions [Kent et al., 2000], often due to impairments in their tasks and contribution to the formation of ocular edema [Marmor, 2000]. In numerous ophtalmic diseases, in fact, disruption of the blood-retina barrier (BRB) caused by defects in RPE functionality or structure is reflected in water accumulation and failures of tissue homeostasis [Marmor, 2000; R Sparrrow et al., 2010]. A deeper understanding of epithelial functions, especially regarding trans-layer transport processes, is therefore needed for the progression of intervention and treatment of several pathologies.

1.1.3 Conventional methodologies to study epithelial transport

Epithelial physiology can be studied with a variety of methodologies, some of which have been in use for decades. Understanding ion, solute and solvent transport across epithelia involves investigating the activity of carriers, channels or pumps responsible for the translocation of ionic species or molecules.

Pharmacological approaches have been employed to clarify the involvement of a specific transport protein in complex processes by blocking or enhancing its activity and analysing the resulting response of the system [Haas and McManus, 1983; Liu et al., 2000]. In addition to their use as research tools, channel blockers are also routinely employed in the treatment of many diseases, where the role of the transport processes are understood in sufficient detail to become targets for graded modulation by clinicians. Some conditions possess pathophysiology which is tractable through changes in the activity of membrane channels, such as calcium-channel blockers for the treatment of hypertension [Triggle, 2007]. Bridging the gap between research tool and therapy requires detailed understanding of both the physiology and pharmacology if potential undesired side effects of the compounds used are to be minimised.

The primary approach to study epithelial functions and characterise their electrical properties, is via electrophysiology techniques [Santacroce et al., 2018]. Many epithelia produce, in fact, a spontaneous transcellular potential, even when bathed in identical extracellular solutions on both sides of the layer, while the ability to restrict ion move-

ments across the layer can be seen as a resistive property. Therefore, epithelia can be studied electrically using Ohm's law to describe the flow of ions through the cell layer, while exploiting pharmacology and/or the selective disruption of either apical or basolateral membranes with detergents or chemicals [Lewis and Wills, 1982; Wills, 1981]. Native tissue explants, such as the gut epithelium, can be inserted into bicameral Ussing chambers for such work, while *in vitro* studies can exploit simple trans-epithelial electrical resistance (TEER) and voltage measurements using cultures of epithelial cells on porous substrates designed to simulate the epithelial environment *in vivo*, which allows the exchange of ions and water through the polarised layer of cells [Cereijido et al., 1978; Li et al., 2004; Srinivasan et al., 2015; Yeste et al., 2018]. At a single-cell level, electrophysiology techniques allow for the study of current or voltage changes by keeping one of the two variables constant (*clamping*) and measuring the other (voltage or current clamp, respectively). The technique involves the use of glass microelectrodes that, impaled into or in contact with the cells, enable measurements of their electrical behaviour across the entire cell membrane (sharp microelectrodes/whole-cell patch clamp) or in patches of membrane demarcated by the electrode orifice (patch clamp) [Dunlop et al., 2008]. Fluctuations in ion dynamics are recorded as changes in the electrical currents measured in either the current- or voltage-clamp regimes; more sensitive and selective information can be obtained by means of ion-sensitive electrodes [Voipio et al., 1998]. The main limitation of electrophysiological methodologies is represented by the complexity of the experimental procedures and equipment, which is poorly scalable or requires highly-trained personnel or expensive high-throughput instruments capable of performing such measurements via microfluidic chips.

Sharing the advantages of specificity and sensitivity, while additionally being relatively simple and highly scalable, ion-sensitive fluorophores have also become commonly-used tools to monitor the concentration dynamics accompanying epithelial ion transport. Fluorescent indicators of ion activities, such as Indo-1, Fluo-4, Fura-2 (for Ca^{2+}) and SPQ, MQAE (for Cl^-), represent a variety of chemicals whose optical properties are modulated by local free ion concentrations [Minta et al., 1989; Roe et al., 1990; Verkman, 1990]. Activity of ion-sensitive indicators is based on different mechanisms, from

collisional quenching to spectral shift of the dyes due to conformation or electrical changes when bound to the ion of interest. Loading cultured epithelial cells with such molecules by direct injection, electroporation or enzymatic cleavage, enables monitoring of ion fluctuations over time, in response to perturbation of ion equilibrium by means of drugs or alterations of ion composition of the extracellular solution [Tsien, 1989].

Calcium imaging, for instance, is a well-established technique to study calcium signals in a wide variety of contexts [Grynkiewicz et al., 1985; Regehr et al., 1989]. Free intracellular calcium is extremely low at resting conditions for most cell types, therefore even a slight increase can be appreciated with the right indicators. Fura-2 AM, the acetoxymethylester form of the calcium-sensitive dye Fura-2, can permeate the cell membrane and once internalised its AM group is cleaved by intracellular esterases; the dye becomes impermeable and is therefore trapped inside the cells. Its fluorescence emission at 510 nm varies when in its calcium-free and calcium-bound forms, when excited at 340 nm and 380 nm (Figure 1.4), thus allowing for ratiometric evaluation of intracellular calcium concentration changes [Roe et al., 1990]. The ratiometric approach ensures quantitative data, since it takes into account differences in morphology within different parts of single cells or between cell types, which might affect signal variations. Also, it evens out volume changes resulting from ion movements that would dilute or concentrate the dye, thus resulting in false changes in intensity [Dustin, 2000].

Genetically-encoded fluorophores for specific ions and signalling cascades have also been developed for the spontaneous or directed expression within particular cell types and cellular compartments [McCombs and Palmer, 2008].

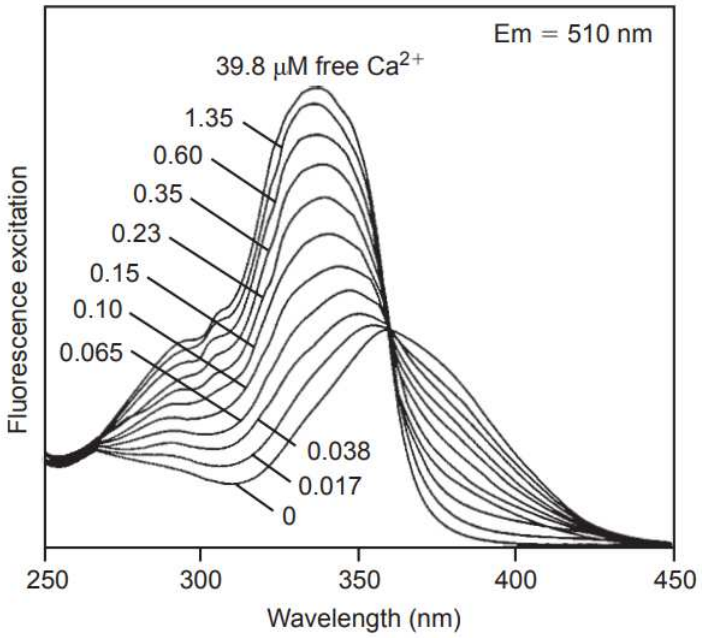


Figure 1.4: **Fluorescence spectra of the calcium-sensitive dye Fura-2.** Fura-2 is a ratiometric UV-excitable calcium indicator that allows for the precise evaluation of changes in intracellular calcium concentration after perturbation of equilibrium. Fura-2 is excited at 340 nm and 380 nm and the ratio of the fluorescence recorded at 510 nm when excited at such wavelengths is directly related to the intracellular free calcium. The calcium-bound 340 nm signal increases upon calcium concentration rises in the cells, while the 380 nm unbound signal decreases following calcium influx in the cells. Once internalised, Fura-2 dye is trapped inside the cells. Therefore, by calculating the ratio of fluorescence emission when the dye is excited at 340 nm and 380 nm, calcium dynamics are calculated. Adapted from [Johnson, 1998].

1.1.4 The retinal pigment epithelium (RPE)

The retinal pigment epithelium (RPE) is a monolayer of pigmented epithelial cells involved in the formation of the blood-retina barrier at the interface of the subretinal space and the choroidal blood stream at the back of the eye [Strauss, 2011], as represented in Figure 1.5. The RPE is composed of cuboidal epithelial cells, joined together by tight junctions, which contribute to the formation of the blood-retina barrier (BRB), a physiological barrier that controls ion and water flux into and out of the retina [Rizzolo, 2007]. Alterations to the integrity of the BRB are involved in the onset of pathologies such as diabetic retinopathy and age-related macular degeneration (AMD) [Feher et al., 2006; Imamura et al., 2006; Liang and Godley, 2003a]. Depending on the severity of the BRB compromise, diseases caused by alterations of transport across the barrier can result in different degrees of vision loss.

In the human eye, the RPE performs a variety of tasks (summarised in Figure 1.6) to maintain homeostasis of the eye during the visual process [Strauss, 2005]. Being a

layer of pigmented cells, it absorbs light focused onto the retina by the lens, reducing photodamage and production of reactive oxygen species (ROS) following light exposure [Bok, 1993]. An increase in photo-oxidative stress is considered as the main cause for age-related macular degeneration (AMD) [Beatty et al., 2000; Liang and Godley, 2003b], so the RPE plays a protective role in this context. The RPE is also involved in phagocyotosis and renewal of the photoreceptor outer segments (POS). Upon light absorption and degradation, damaged POS are uptaken by the RPE, where they are processed and renewed [Kevany and Palczewski, 2010]. Failure of the phagocytosis process leads to the accumulation of photo-damaged molecules in the sub-retinal space, often resulting in degenerative conditions of the eye [Finnemann et al., 2002].

Furthermore, photoreceptors are unable to regenerate *all-trans* retinal into *11-cis* retinal after conversion of light energy into electrical signals; the RPE is responsible for the reisomerisation of retinal to its functional form for the progression of the visual cycle [Gollapalli et al., 2003; Redmond et al., 1998].

Finally, the RPE secretes a variety of growth factors, including the vascular endothelial growth factor (VEGF) [Adamis et al., 1993] and the pigment epithelium-derived factor (PEDF) [Bouck, 2002], which are trophic for both the epithelial layer and the choriocapillaries underneath [Saint-Geniez et al., 2009]. Changes in growth factor secretion result in proliferative diseases in the retina [Frank, 1997], mostly due to choroidal neovascularisation (CNV) [Tong and Yao, 2006], subsequent to or in parallel with inflammation [Bhutto et al., 2006; Ohno-Matsui et al., 2001]. Furthermore, growth-factor secretion is strongly connected to calcium dynamics [Ikeda et al., 2006; Strauss, 2005]. Secretion of growth factors has been associated to triggering an increase in intracellular calcium, which, in return, activates phosphorylation of more growth factors in the RPE. Calcium acts as a regulator of RPE cellular functions [Wimmers et al., 2007], therefore its transport within the cells is finely regulated by expression of Ca^{2+}-transporting and Ca^{2+}-binding proteins and their localisation in specific compartments of the cell membrane.

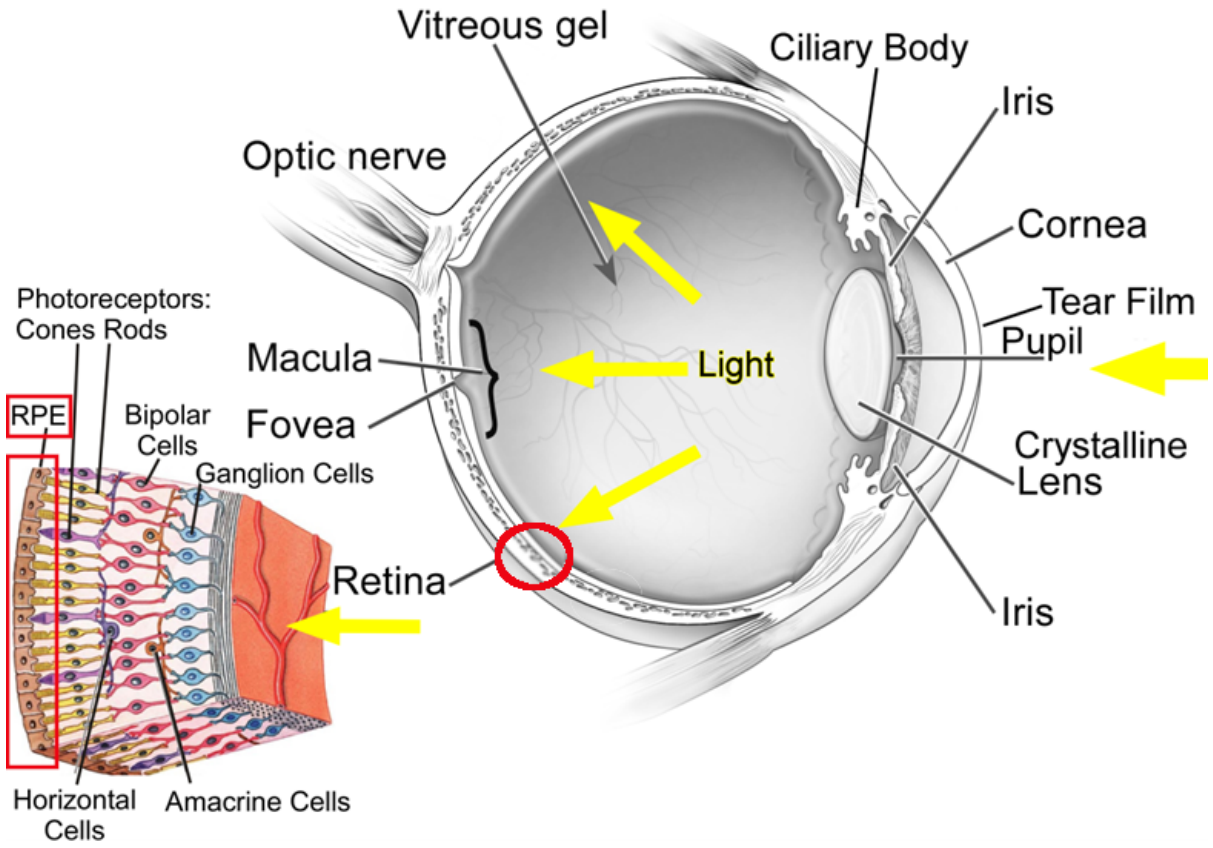


Figure 1.5: **General anatomy of the human eye and location of the retinal pigment epithelium (RPE).** A portion of the retina is circled in red and details are shown in the inset. The RPE is highlighted in red to show its location at the back of the eye beneath the photo-sensitive elements of the retina, crucial for its functionality. Yellow arrows represent direction of incident light on the eye. Adapted from [Vera-Díaz and Doble, 2012].

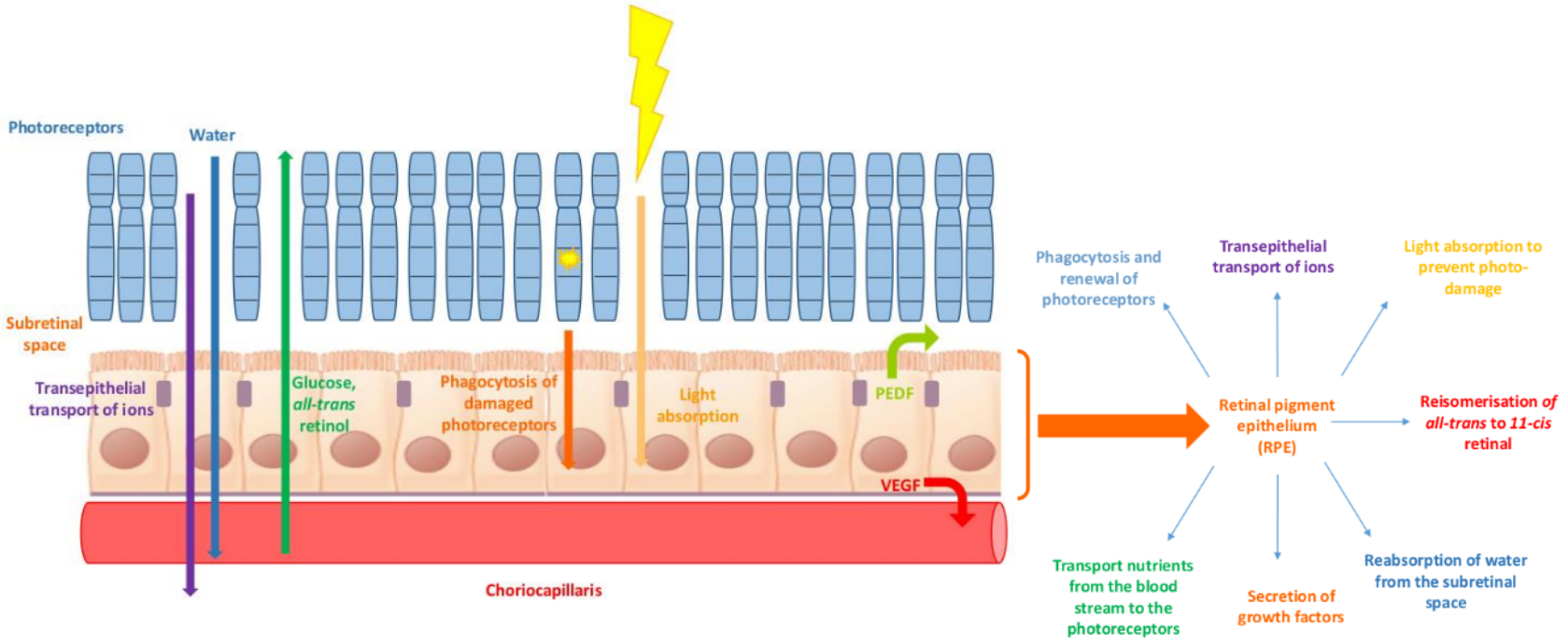


Figure 1.6: **Retinal pigment epithelium (RPE) schematics** The diagram is showing a schematic representation of the retinal pigment epithelium (RPE) *in vivo* and summarises its core functions in the retinal environment. The RPE is located at the back of the eye, where it performs a variety of tasks to support vision. During the visual cycle, the photoreceptors are unable to reisomerise *all-trans* retinal to *11-cis* retinal. This task is also performed by the RPE, which then exports *11-cis* retinal to the photoreceptors for the beginning of a new visual cycle. Following light exposure, lipids and proteins in the outer segments of photoreceptors are damaged; the RPE is responsible for phagocytosis and renewal of damged photoreceptor outer segments. Moreover, with its pigmentation the RPE absorbs photons from the retina, reducing oxidative photodamage of the tissue. As part of the blood-retina barrier (BRB), the RPE transports nutrients, ions and water between the photoreceptors in the subretinal space and the choriocapillaris. Transport of water is vital for mainteinance of intraocular pressure and is mainly achieved as an osmotic consequence of directional ion transport through the RPE layer. Furthermore, the RPE secretes a variety of growth factors into the blood stream, including the vascular endothelial growth factor (VEGF) and the pigment epithelium-derived growth factor (PEDF). *Original drawing.*

Moreover, the RPE is responsible for the mainteinance of the immune privilege of the eye, which ensures preservation of the health of the organ and protects it from inflammatory responses [Forrester and Xu, 2012; Niederkorn and Kaplan, 2007]. Secretion of immunosuppressive factors by the RPE contributes to block the activation of $CD8^+$ and $CD4^+$ cells [Farrokh-Siar et al., 1999], in order to reduce post-inflammatory edema in the ocular region.

Crucially, the RPE is responsible for transepithelial transport of ions, nutrients and water between the photoreceptors and the choriocapillaris layer [Wimmers et al., 2007]. From the blood vessels, the RPE takes glucose, *all-trans* retinol and other nutrients and delivers them to the photoreceptors. In the opposite direction, the RPE exploits the electrochemical gradient generated by the Na^+/K^+ ATPase, located in the apical membrane, to vectorially transport ions [de la Cour Dornonville, 1993] and therefore reabsorb water from the subretinal space to the blood stream [Chihara and Nao-i, 1985; Tsuboi, 1987]. Control of intraocular pressure is paramount and failure of the RPE reabsorption of fluid can lead to edema, i.e. pathological swelling of the tissue [Marmor, 2000]. Because the RPE is a tight epithelium, in fact, water cannot diffuse freely through the paracellular route [Stamer et al., 2003]. Transport of water across the epithelial layer mainly follows K^+ and Cl^- gradients [Kennedy, 1994; Marmor, 1990], as schematically represented in Figure 1.7 and it is thought to be mostly transcellular. Alterations of epithelial transport processes are reflected in dysfunctions of the eye, where decrease of the transport activity causes retinal degeneration [Feher et al., 2006; Imamura et al., 2006; Marmor, 2000; R Sparrrow et al., 2010].

The correct functionality of ion transport pathways is crucial to the variety of tasks performed by the RPE to preserve homeostasis, dysregulation of which is either altered by mutations in the genes for transport proteins or arises from dysfunction or misregulation of the transporters, themselves. Reduced RPE chloride transport also plays an important role in the etiology of macular edema, a complication of most ophtalmic pathological conditions. Vectorial transport of chloride from the subretinal space to the choriocapillaris layer beneath the RPE is in fact the driving force for the reabsorption of excess water from the retina [Wimmers et al., 2007]. Therefore, study of ion channels

in the RPE is extremely relevant to understand involvement of different transport proteins in the pathophysiology of the eye. A variety of pathological conditions in the eye has been associated to impairments in RPE functionality. AMD, for instance, is a degenerative disorder caused by damage of the photoreceptor cells in the retina; its initial pathogenesis was found linked to failures in the RPE layer [Green et al., 1985; McLeod et al., 2009], mostly of oxidative nature [Liang and Godley, 2003a]. AMD is a complex disease, whose onset is determined by numerous factors, among which lipofuscin, drusen [Crabb et al., 2002], inflammation [Anderson et al., 2002] and vascularisation, in the case of the wet form of AMD [Nowak, 2006]. Choroidal neovascularisation (CNV) [Grossniklaus and Green, 2004] originates from the overproduction of growth factors, such as VEGF, or the decreased secretion of anti-angiogenic factors, such as PEDF [Spilsbury et al., 2000; Tong and Yao, 2006]. Both factors are produced and secreted by the RPE, as described above. Therefore, multiple roles for the RPE in the development of retinal degeneration have been reported [Bhutto et al., 2006; Imamura et al., 2006] and there is growing interest in understanding these processes, in order to cure them.

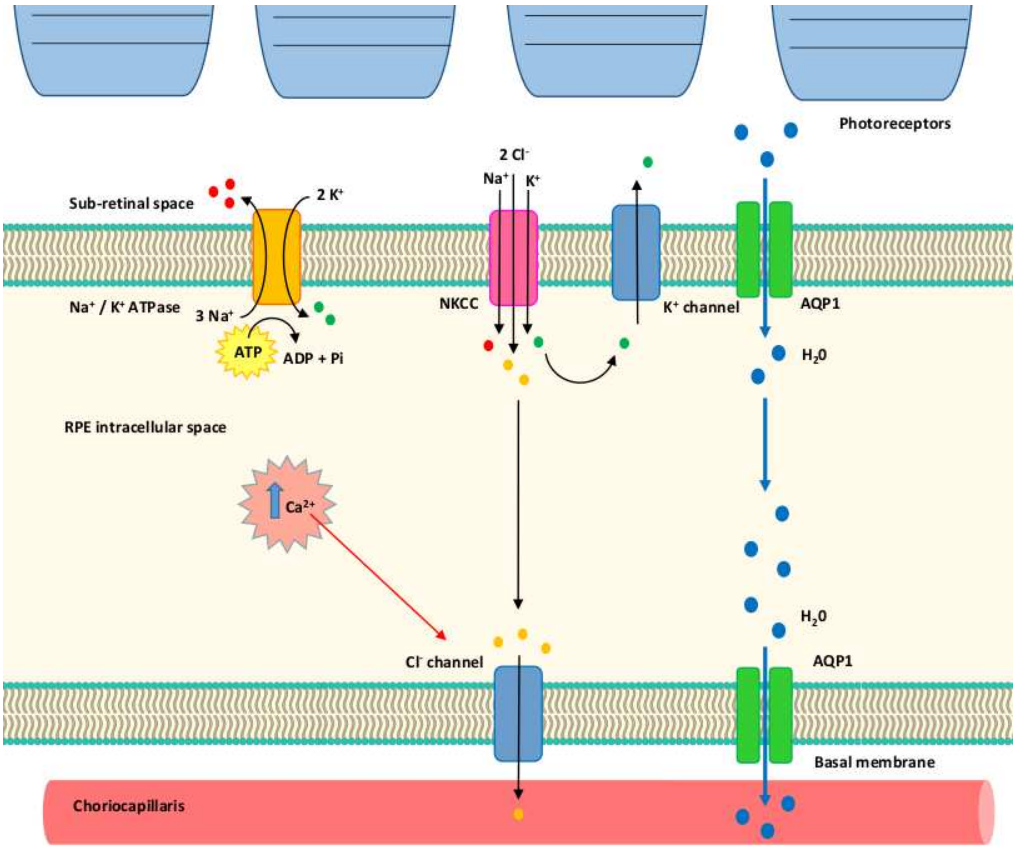


Figure 1.7: **Transepithelial transport across the RPE.** Main transporters of the RPE are schematically shown, to outline the core steps of ion and vectorial water transport across the epithelial layer. The driving force for transepithelial transport is provided by the sodium-potassium ATPase (Na^+/K^+ ATPase), located in the apical membrane of the RPE. K^+ is recycled back to the sub-retinal space by K^+ channels ($Kir_{7.1}$), resulting in the establishment of a gradient for Na^+ in the intracellular environment. Such gradient results in the internalisation of K^+ and Cl^- by means of the sodium-potassium-chloride co-transporter (NKCC) on the apical side. At this stage, a Cl^- gradient is generated and Cl^- channels, such as Best1, CFTR and ClC-2) extrude excess Cl^- from the basal domain of the RPE. The flow of Cl^- across the retinal epithelial layer represents the main driving force for water reabsorption from the sub-retinal space by the activity of aquaporin channels (AQP1), according to osmosis, while Na^+ flux to satisfy electroneutrality occurs via the cation-selective tight junctions. *Original drawing.*

Due to the RPE location at the back of the retina, *in vivo* studies are very challenging, therefore *in vitro* models have been established and routinely exploited for experimental procedures. One of the best characterised models for the RPE is the ARPE-19 cell line[Dunn et al., 1996], first developed in the 1980s, which is used in the present work as an epithelial cell model. The ARPE-19 cells have been obtained from selective trypsinisation of a primary culture of epithelial cells from the eye of a human donor. Cultures of ARPE-19 cells retain many features of the RPE [Mannermaa et al., 2010; Philp et al., 2003] although there are evidences of differences in the behaviour when cultured for the development of models for transepithelial transport [Ablonczy

et al., 2011]. Ablonczy and colleagues reported that, despite the ability of ARPE-19 cells to form a monolayer of cells when grown on porous filters, such a monolayer was not tight but rather leaky and $< 50\ \Omega cm^2$. They also noted a reduction in the production of growth factors, such as VEGF and PEDF, of the ARPE-19 cells compared to fetal human RPE (fhRPE). Nevertheless, Ablonczy and colleagues remark that these conclusions are quantitative, more than qualitative, therefore they do not mine the valuable contribution of studies performed on the ARPE-19 cell line to disclose functional characteristics of the RPE. Besides these observations, the ARPE-19 cell line represents an accessible and less ethically-concerning alternative to primary cultures of epithelial cells from the human eye, such as the fhRPE.

Insights in the processes described above will prove useful for a better understanding of basic processes in epithelia and in the RPE, in particular. The following section describes the molecular tools harnessed in the present work to control ion dynamics in epithelial cells using photonics, i.e. light-gated channels and pumps from the microbial world.

1.2 Rhodopsins

The main molecular tools of optogenetic research are rhodopsins, naturally-occurring light sensors which are expressed by a variety of organisms, ranging from prokaryotes to eukaryotes. The word rhodopsin comes from the Greek *rhodon* meaning rose and *opsis* meaning sight, and together they refer to the red-coloured pigment in the eyes. The colour red originates from retinal, a vitamin A-derivative pigment bound to the protein structure and responsible for the light-sensing activity of these proteins [Ernst et al., 2013]. Rhodopsins are a big family of proteins involved in diverse mechanisms from vision to adaptation to the environment [Ernst et al., 2013]. Structurally, they are retinylidene proteins, composed of a protein moiety, the opsin, bound to a chromophore, retinal, to form a composite structure referred to as rhodopsin . The amino acid sequence of rhodopsins alternates lipophilic and lipophobic regions which organise in seven transmembrane helices. The chromophore retinal exists in different conformation [Rowan III et al., 1974], *cis* or *trans*, depending on the class of rhodopsins it

interacts with and its isomerisation state, as summarised in Figure 1.8.

Opsins have been categorised in two classes: type I or microbial and type II or vertebrate rhodopsins [Ernst et al., 2013]. Type I rhodopsins are found in microorganisms from bacteria to algae and are mainly involved in metabolic processes, such as phototaxis (i.e. movement towards light) [Sineshchekov et al., 2002a] or adaptation to extreme environmental conditions [Fendrihan et al., 2006; Lanyi, 1985] and, therefore, survival. This family includes proton pumps, like Bacteriorhodopsin [Lanyi, 2004] from *Halobacterium salinarum* or Archaerhodopsin from Halobacteria [Sugiyama et al., 1989], cation channels, such as Channelrhodopsins from unicellular algae and anion pumps, like Halorhodopsins from Halobacteriacea [Lanyi, 1985]. A small sub-group in this family is also involved in sensory processes [Spudich, 2006], such as sensory rhodopsin II found in Archaea, which transduces photon signals into protein phosphorylation and bacterial movement. Bacteriorhodopsin was the first membrane protein whose crystallographic structure was obtained in the 1970s [Oesterhelt and Stoeckenius, 1971]; from the 3D structure of this protein and phylogenetic and bioinformatic studies, more and more procaryotic rhodopsins were identified [Brown and Jung, 2006].

Upon light absorption, the *all-trans* retinal molecule covalently bound to type I opsins isomerises to *13-cis* retinal (see Figure 1.8), inducing a conformational change in the trans-membrane helices [Ernst et al., 2013]. Reorganisation of the opsin structure widens the channel pore, thus allowing permeable ions to cross the plasma membrane. For the most part, type I opsins form themselves the light-gated channels [Nagel et al., 2003] or pumps [Schobert and Lanyi, 1982] and modification of the retinal conformations is responsible for ion channel gating and activity.

On the other hand, in type II rhodopsins sensing activity and phototransduction are performed by distinct portions of the protein. Type II opsins are in fact a specialised group of G-protein coupled receptors (GPCR) [Palczewski, 2006], mainly involved in photosensory processes, such as vision, in vertebrate organisms. Isomerisation of *11-cis* to *all-trans* retinal (see Figure 1.8) bound to the opsin moiety changes its structure [Patel et al., 2004] and, subsequently, such modification activates a heterotrimeric G protein which will then initiate a cascade of reactions and transduce the signal intra-

cellularly [Filipek et al., 2003; Schoenlein et al., 1991].

To avoid confusion in the present work, it is important to highlight, that microbial (type I) rhodopsins are here heterologously expressed in human cells for optogenetic purposes. The reason behind this crossover is mainly residing in the photocycle of mammalian rhodopsins that convert retinal back into its *all-trans* form at the end of the photo-reactions of the visual cycle, therefore accumulating the chromophore in its *all-trans* configuration [Ernst et al., 2013]. Enzymatic regeneration of *11-cis* retinal is performed in vision organs by the activity of specialised cells, for instance the RPE in the human eye.

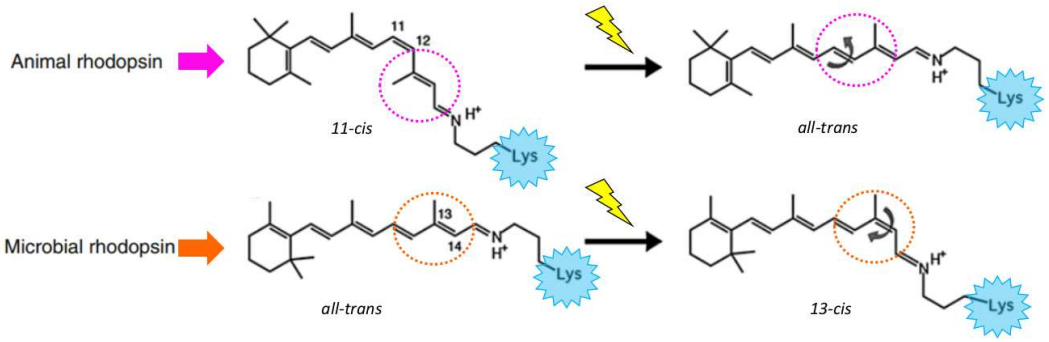


Figure 1.8: **Retinal *cis-trans* photoisomerisation in animal and microbial rhodopsins.** In animal, type II, rhodopsins *11-cis* retinal is bound to the opsin moiety via a protonated Schiff base, usually a Lysine on one of the seven transmembrane alpha helices. During the visual cycle in vertebrate, upon light absorption, *11-cis* retinal isomerises to *all-trans* retinal and it is then reisomerised to the functional *11-cis* form. In microorganisms, on the other hand, *all-trans* retinal is converted to *13-cis* retinal upon photon absorption and induces a conformational change in the protein structure by interacting with a charged amino acid in the binding pocket. Structural reorganisation of the transmembrane helices results in the opening of the light-gated channel and subsequent flow of permeable ions. Adapted from [Yawo et al., 2015].

In the interest of the present work, two type I rhodopsins will be described in more details, Channelrhodopsin from the unicellular green algae *Chlamydomonas reinhardtii* and Halorhodopsin from the halophilic bacterium *Natronomonas pharaonis*, schematically represented in Figure 1.9.

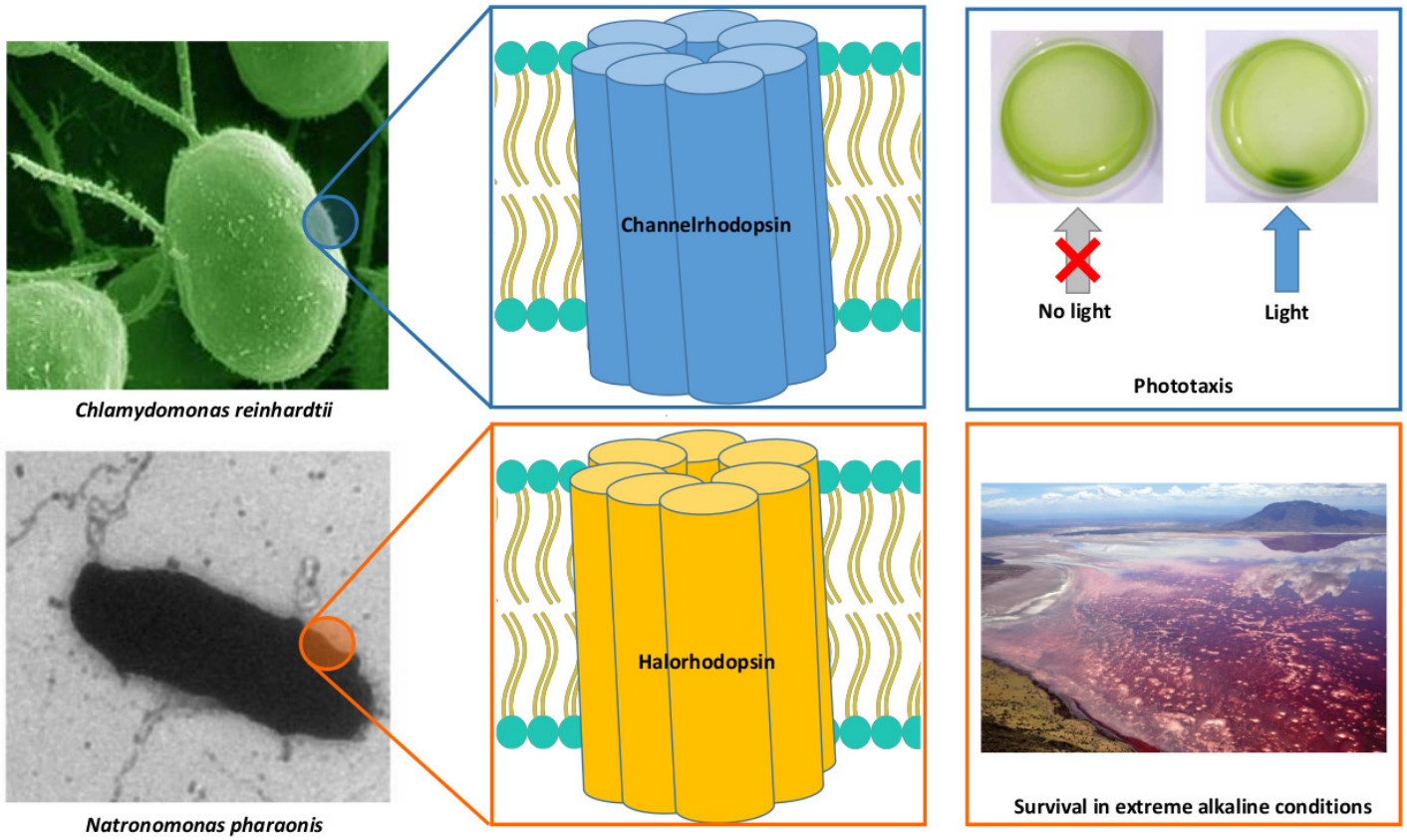


Figure 1.9: **Channelrhodopsin-2 (ChR2) from *Chlamydomonas reinhardtii* and Halorhodopsin (eNpHR) from *Natronomonas pharaonis* in their natural environment.** The figure outlines ChR2 and eNpHR functions in their natural hosts. ChR2 is a naturally-occurring non-selective cation channel found in the membrane of the green algae *C. reinhardtii*. In the algae, ChR2 mediates phototaxis, the process of moving towards light to maximise photosynthetic activity of the organisms. On the other hand, eNpHR is an electrogenic chloride pump found in the membrane of halophilic bacteria *N. pharaonis*, populating alkali lakes. eNpHR allows bacteria to survive in extreme alkaline conditions with its chloride pumping activity.

1.2.1 Channelrhodopsin

Channelrhodopsin refers to a broad subset of rhodopsins mainly found in photomotile green algae [Nagel et al., 2005b]. Channelrhodopsin-1 (ChR1) and Channelrhodopsin-2 (ChR2), both from the green algae *Chlamydomonas reinhardtii*, were the first two proteins of this group to be discovered and, later on, introduced into mammalian cells, where their light-gated activity was exploited for optogenetic purposes [Nagel et al., 2003]. ChR-1 mainly shows permeability to H^+ [Nagel et al., 2002] and was therefore less intriguing for optogenetic applications, while ChR2 is a non-selective cation channel, permeable to Na^+, K^+, H^+ and Ca^{2+}, depending on their gradient across the membrane. In *C. reinhardtii* ChRs allow unicellular algae to couple the signal from sunlight into flagellar movement to swim towards light (phototaxis) [Sineshchekov et al., 2002b; Witman, 1993] and maximise photosynthetic activity.

Studies on *C. reinhardtii* behaviour were pioneered by Andrei Faminzin 150 years ago: these single-cell algae were first found in the river Neva in Russia and Faminzin was the first one to notice their peculiar motility in response to blue light, as shown in Figure 1.9. However, it was not until the 1970s that such behaviour was explained with the discovery and the isolation of prokaryotic rhodopsins and the determination of Bacteriorhodopsin crystal structure, considered for decades a model for all microbial rhodopsin 3D-conformation [Oesterhelt and Stoeckenius, 1971].

1.2.1.1 Channelrhodopsin structure

Channelrhodopsin 1 and 2 (ChR1 and ChR2) are microbial rhodopsins weighing 76 kDa; they are composed of 712 and 737 amino acids, respectively. The protein moieties of channelopsin 1 and 2 were identified as the two cDNA sequences encoding for ChR1 and 2, thought to be involved in sensory processes of the green algae [Nagel et al., 2005b]. Half the protein sequence is responsible for the organisation in a seven-transmembrane helix configuration (7-TM) and therefore embedding of the protein into the plasma membrane, while the rest encodes for a long hydrophilic C-terminal portion protruding in the cytoplasm (Figure 1.10), that is generally omitted and replaced by fluorescent protein tags for optogenetic applications (Section 1.5). The function of the C-terminal

sequence is still debated, but it is thought to be involved in ChR localisation to the eyespot region of *C. reinhardtii*, the light-sensing organelle in the algae [Mittelmeier et al., 2011]. On the other hand, the N-terminal region is considered to be responsible for dimer formation [Kato et al., 2012]. The truncated version of ChR2, including amino acids 1 to 315 only, that is the sequence forming the 7-TM domain, is the most commonly used ChR for heterologous expression and optical manipulation. The core of the channel pore, shown in Figure 1.10 C and D and in Figure 1.11 accommodates the retinal-binding pocket, where *all-trans* retinal is covalently bound to the protein domain through a protonated Schiff base, generally a lysine on one of the TM helices [Kato et al., 2012].

The retinal chromophore is responsible for ChRs photoreactivity and its interactions with the protein moiety are the foundations of ChRs photocycle and, consequently, their ion channel activity [Ernst et al., 2013; Patel et al., 2004]. Preliminary structural data on ChRs were first obtained in 2011 by cryo-electron microscopy from Müller and colleagues [Müller et al., 2011], who solved ChR2 structure (1-315 aa) to 6 Å, revealing a predominantly dimeric conformation of the protein at the membrane level, formed at the interface of TM3 and TM4. Later in 2012, the crystal structure of a chimaeric protein derived from the fusion of TM1 to TM5 from ChR1 and TM6 and TM7 from ChR2, named C1C2 (3UG9 on the Protein Data Bank), was determined by Kato and colleagues [Kato et al., 2012] and is generally considered a good 3D-model for ChR2 for mutagenesis modifications of the active site of the protein. The retinal-binding pocket is in fact one of the most highly-conserved features across microbial rhodopsins and amino acid modifications have widened the pool of available proteins for heterologous expression in mammals. It is formed at the interface of the TMs, where amino acids protruding in the active site of the protein create a hydrophobic environment, where the chromophore *all-trans* retinal is covalently bound [Okada et al., 2004].

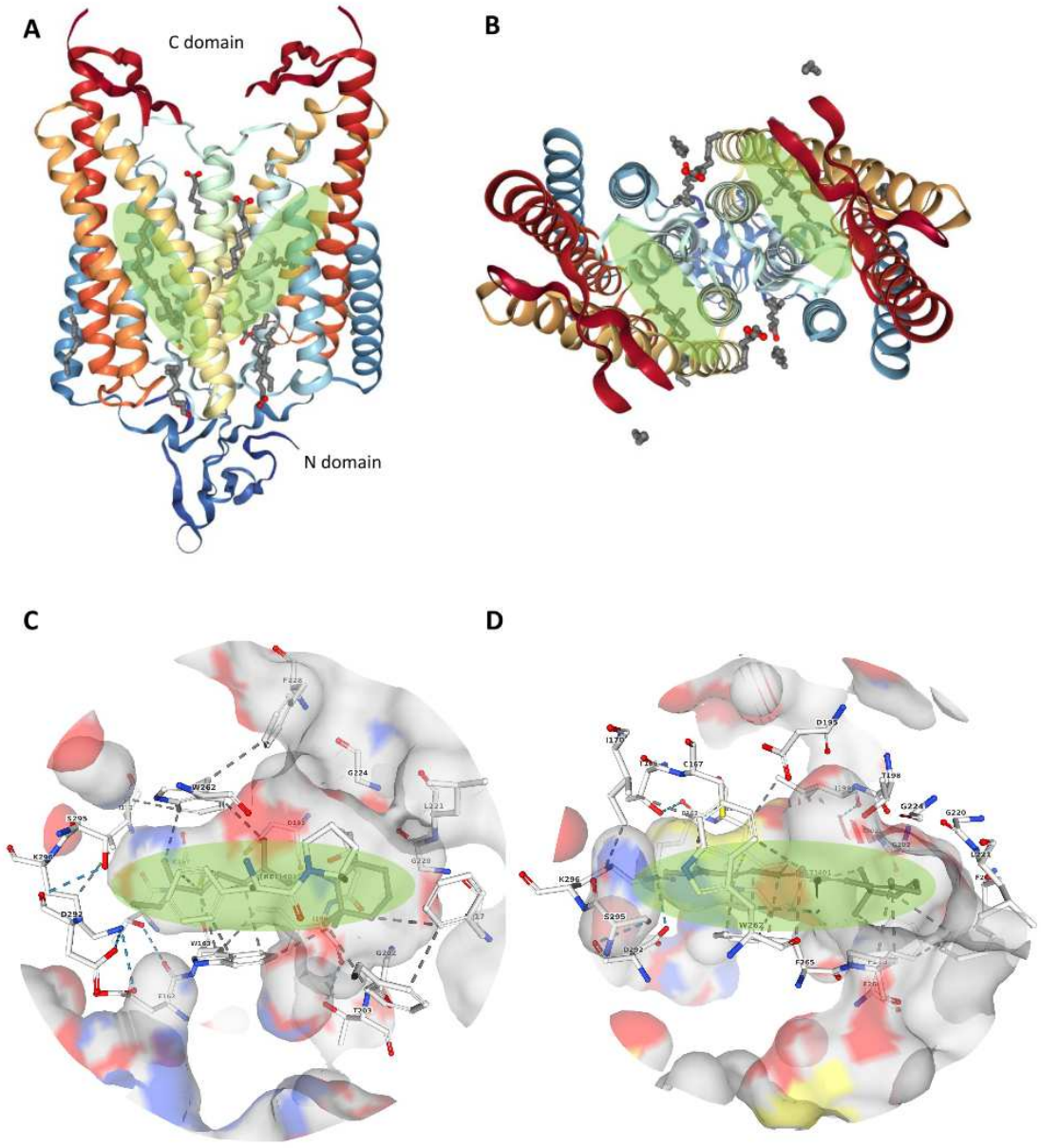


Figure 1.10: **Crystal structure of C1C2 dimer and its core features in the retinal binding pocket.** The crystal structure of the C1C2 dimer in its closed state, viewed parallel to the membrane (**A**) and from the top (**B**). C1C2 consists of the extracellular N domain, seven transmembrane helixes and the intracellular C domain. C1C2 is a chimera of ChR1 and ChR2 from *Chlamydomonas reinhardtii* which reveals the main architectural characteristics of channelrhodopsins, including their interactions with the retinal chromophore in its binding pocket (close-up: **C**, side-view and **D**, top-view). The *all-trans* retinal is coloured in gray and highlighted in green; the main interactions with the side chains of the amino acids protruding in the active site are also shown. (Adapted from 3UG9 deposited structure from the Protein Data Bank (PDB)).

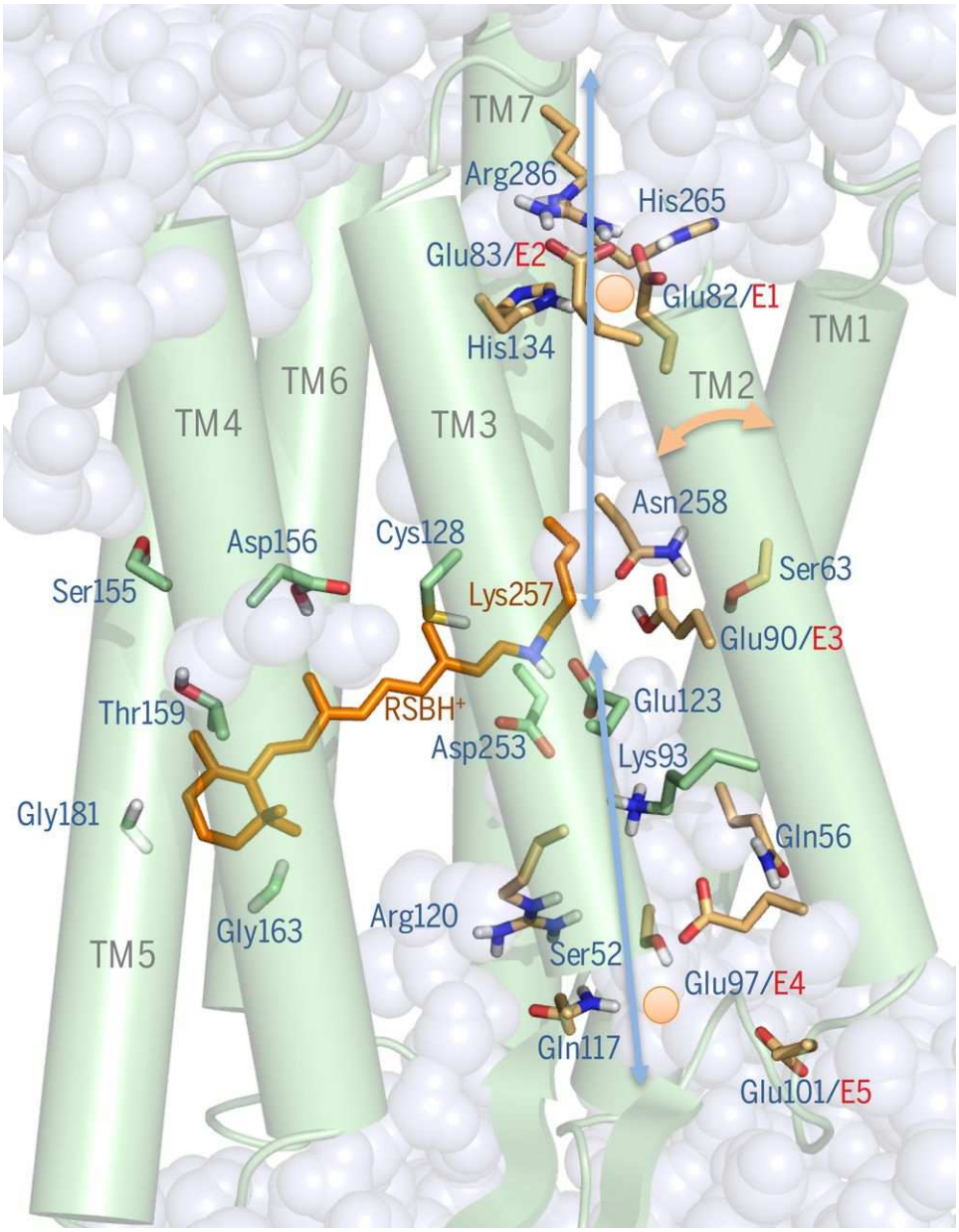


Figure 1.11: **Crystal structure of C1C2 dimer embedded in the phpsholipid bilayer.** The crystal structure of the seven-transmembrane channelrhdopsin truncated chimera C1C2 adapted from 3UG9 structure from the Protein Data Bank (PDB). The protein is shown in the phospholipidic bilayer of the cell membrane as a 7-transmembrane-helix (TM1-TM7) pore with the side chains of the amino acid residues involved in the kinetics of the channel protruding towards the middle of the channel. The chromophore *all-trans* retinal, shown in its protonated Schiff base form (orange), is embedded in the protein core and interacts in its binding pocket with the surrounding lateral chains of the protruding amino acids, shown in their stick form (red, oxygen; blue, nitrogen and white, polar protons). Blue arrows denote the hypothetical permeation pathway throuch the pore. (Adapted from [Deisseroth and Hegemann, 2017])

Before 2011, information regarding ChR structure were derived from sequence homology and bioinformatic comparisons with another microbial rhodopsin, Bacteriorhodopsin, a proton pump found in *Halobacterium salinarum*, whose structure had been determined in the 1970s [Oesterhelt and Stoeckenius, 1971]. Despite primary sequence homology, ChRs show considerable differences when compared to other type I rhodopsins, mainly due to a large number of charged residues in the channel pore [Kato et al., 2012]. Such peculiarity is reflected in the protein functionality, i.e. a non-selective cation channel. The cavity formed by the transmembrane helixes is in fact an electronegative pore rich in protruding aspartates, glutamates and polar residues, permeable to positively charged ions. This cation-conducting pathway is open towards the extracellular side but is occluded on the cytoplasmic side when ChR is in its closed dark state (D470, see Section 1.2.1.2). Upon light absorption and *all-trans* retinal isomerisation to *13-cis* retinal, the protonated Schiff base induces a conformational change in the 7-TM organisation, opening the gate and exposing the pore to surrounding cations and protons, that can flow across the membrane until the channel completes its photocycle again and returns to its closed conformation [Bamann et al., 2008]. During the channel photocycle there is therefore a conversion of retinal isomerisation into channelopsin conformational changes, characterised by the enlargement of the water-filled pore to form a transient cation path. This mechanism is schematically represented in Figure 1.12.

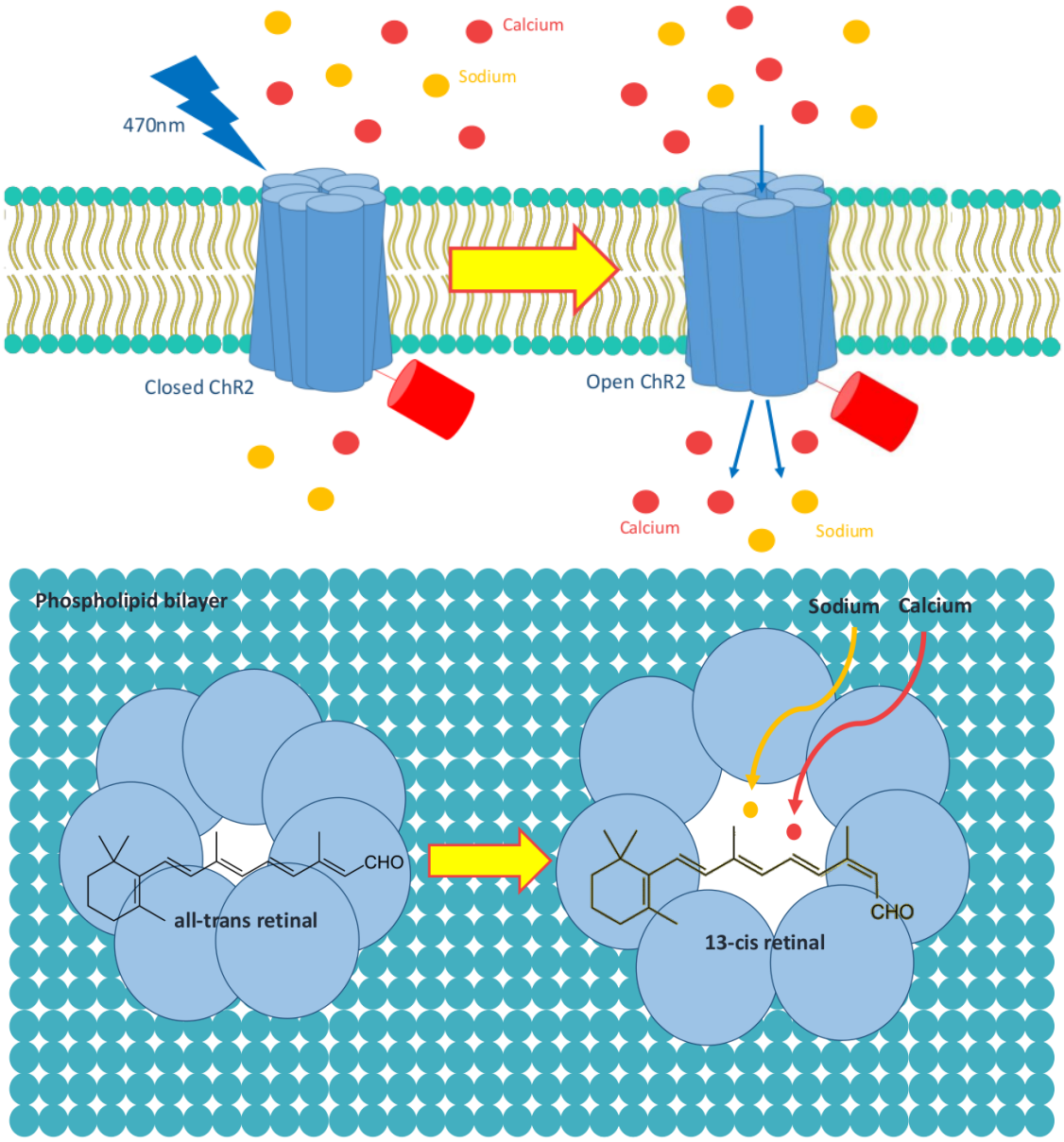


Figure 1.12: **Mechanism of action of the light-gated non selective cation channel Channelrhodopsin-2 (ChR2).** Cartoon showing the mechanism of action of Channelrhodopsin-2 (ChR2). Lateral view of the plasma membrane of a cell expressing ChR2; on the left, the light-switchable, non-selective cation channel (ChR2) is shown in its closed (i.e. non-conducting) state, with its seven transmembrane helixes schematically represented as blue cylinders. mCherry fluorescent tag, that can be used to identify those cells expressing the light-gated channels, is also simplified as a red cylinder connected to one of the helixes. Upon delivery of blue (470 nm) light, represented by the lightning bolt on the top left corner, the protein undergoes a conformational change resulting in the widening of the pore and the flow of permeable ions, mainly sodium and calcium, through the channel. The rise of intracellular cations causes a depolarisation of the cell membrane, feature that has been exploited to trigger action potentials in neurons and study neuronal functions using photonics. Bottom: top view of the plasma membrane of the same cell showing the pore from the extracellular side with a schematic view of the retinal chromophore enclosed in the protein structure; on the left, *all-trans* retinal keeps the channel shut by interacting with amino acid residues in the active site of ChR2. Upon light absorption, *all-trans* retinal photoisomerises to 13-cis retinal, thus modifying its interactions in the binding pocket and generating a cation-conducting pathway for sodium and calcium ions as shown on the right of the top view. *Original drawing.*

1.2.1.2 Channelrhodopsin photocycle

The function of Channelrhodopsin, similarly to that of other microbial opsins, is regulated by a cycle of protein conformational changes that is initiated by light absorption, the so-called photocycle (outlined in Fig.1.13). The different intermediates of the cycle are characterised by spectral changes in the retinal chromophore, which, because intertwined with the protein α-helices, are reflected in the plasticity of the channel and transition from an open state to a closed state [Nikolic et al., 2009].

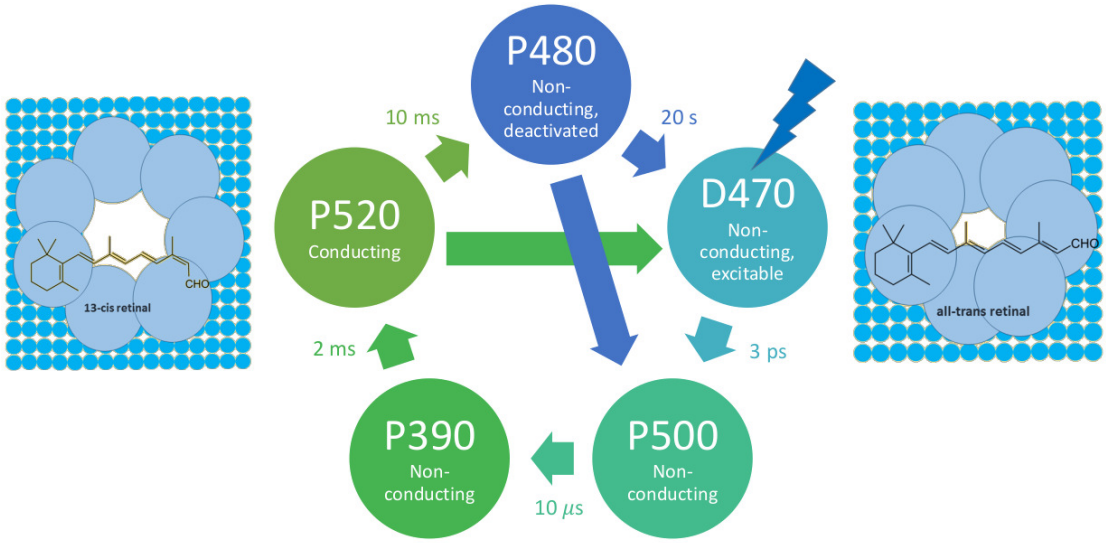


Figure 1.13: **Channelrhodopsin 2 (ChR2) photocycle:** scheme showing the photocycle of Channelrhodopsin-2; numbers indicate the maximum absorption wavelength for each of the intermediate states of the channel. The photocycle is initiated by blue light stimulation and absorption (indicated by the lightning bolt on the D470 configuration). Following photoisomerisation of *all-trans* retinal to 13-*cis* retinal and deprotonation of the retinal Schiff base, ChR2 transitions to two non-conducting states, namely P500 and P390 in few milliseconds, and eventually turns into the channel open state, P520. The photocycle is then completed when the final intermediate, P480, where the protein is deactivated and in a non-conducting state, reverts back to the dark state D470 that will again be responsive to 470 nm blue light, after reprotonation of the Schiff base. The photocycle can also be short-circuited by acting on the photoreactive intermediates: P520 can be converted into D470 by green light while P480 can be converted by blue light into the early P500 intermediate. *Original drawing.*

The photocycle starts with the dark-adapted ground state D470 where *all-trans* retinal is bound to a positively-charged amino acid in its binding pocket to form the protonated retinal Schiff base ($RSBH^+$). Upon absorption of a photon, *all-trans* retinal photoisomerises to *13-cis* retinal on carbon 13, resulting in a twist of the protein backbone [Radu et al., 2009; Ritter et al., 2008] and transition to the P500 intermediate in 3 ps [Ernst et al., 2008]. The photocycle then proceeds to P390, the blue-shifted intermediate that indicates the deprotonation of the Schiff base (t=10 μs). The P520

conducting state of ChR2 is then formed in a lifetime of 2 ms, where *13-cis* retinal is inducing the channel to open exposing the negatively charges of the inner pore and allowing cations to flow towards the intracellular space. The decay rate from P520 to P480 determines the closing kinetics of the channel and is in the range of 10 ms for wild type ChR2, but can be as long as 52 seconds for some of the step-function channelrhodopsin mutants. Recovery to the ground state is then characterised by the isomerisation of *13-cis* retinal and the reprotonation of the Schiff base to the initial light-responsive intermediate [Stehfest and Hegemann, 2010; Verhoefen et al., 2010].

1.2.1.3 Channelrhodopsin mutants

Heterologous expression of ChR2 in mammalian cells, dictating the birth of optogenetics, initially presented considerable drawbacks, slowing down the potential breakthrough of the technique. Among these, considerable differences between the expression pathway and membrane delivery of the rhodopsin channels from lower organisms were addressed by removing the C-terminal of the protein and using the truncated version as the wild-type for preliminary heterologous expressions [Nagel et al., 2003]. The need to overcome wild-type ChR2 limitations was further achieved by genetic engineering of the channel structure, to generate a pool of ChR2 variants with improved channel properties for optogenetic applications and expression in animal systems [Lin, 2011]. Most reported variants of ChR2 present single or multiple amino acid changes in the retinal-binding pocket, since by modifying the interaction of the opsin with the light-sensitive chromophore it is possible to modify ChR2 progression through the photocycle (described in 1.2.1.2), therefore channel properties.

Genetic modification of ChR2 structure focused on these main characteristics:

- **channel conductance:** wtChR2 conductance has been estimated to be below 1 pS, therefore less than the average conductance of common ion channels in the membrane [Bamann et al., 2008];
- **kinetics of the channel:** the opening and closing rates of channelrhodopsin are influenced by the channel photocycle (Section 1.2.1.2) and the spectral changes of the retinal chromophore [Lin et al., 2009b];

- **ion selectivity:** ChR2 is a non-selective cation channel, permeable to H^+, Na^+, K^+ and Ca^{2+}. Permeability can therefore be influenced by extracellular solution composition, pH and transmembrane potential [Nagel et al., 2005b];

- **desensitisation:** excessive light stimulation can desensitise the channel and recovery from such desensitisation can only be achieved after long permanence in the dark [Nagel et al., 2003];

- **light sensitivity:** the range of light intensity required to open ChR2, without desensitising it, is very narrow and it can represent an obstacle when trying to reach threshold for activation, without actually inhibiting the channel [Ishizuka et al., 2006];

- **successful delivery to the plasma membrane and expression level:** initial studies reported ChR2 aggregates when the protein was heterologously expressed in neurons, thus reducing the number of light-responsive channels [Lin et al., 2009a].

When it became clear that the above-mentioned issues were slowing down the potential breakthrough of exploiting microbial opsins in neuroscience, researchers started working on problematic features of ChR2 in order to improve its function.
In the next section some of the most commonly used ChR2 mutants will be described, with particular attention to the ones used in this thesis (H134R, C128A, E123T, T159C and L132C), which are highlighted in Figure 1.14. Broader excellent reviews on the topic can be found in [Knöpfel et al., 2010; Lin, 2011; McIsaac et al., 2015; Wietek and Prigge, 2016].

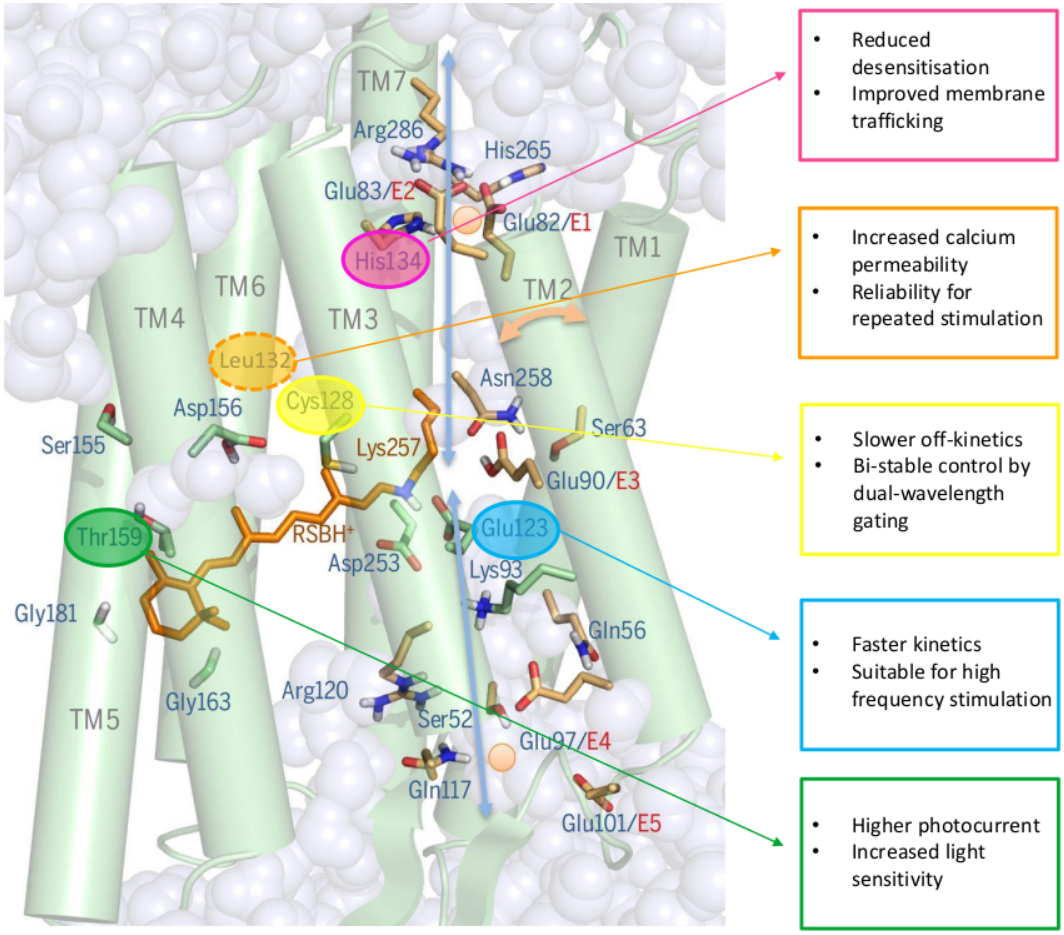


Figure 1.14: **Amino acids involved in the interactions with the retinal chromophore, therefore main targets of site-directed mutagenesis to generate ChR2 variants.** ChR2 is shown as the 3UG9 pore embedded in the plasma membrane with the *all-trans* retinal chromophore as the protonated retinal Schiff base ($RSBH^+$) in orange in the active site of the protein. Amino acids involved in the main interactions in the retinal binding pocket are highlighted with different colours. Adapted from [Deisseroth and Hegemann, 2017].

ChR2 H134R was one of the first mutants designed to overcome ChR2 limitations [Lin et al., 2009b; Nagel et al., 2005a]. Its main features involve a modest reduction in desensitisation combined with a higher plasma membrane delivery rate. On the other hand, ChR2 H134R is characterised by a slight decrease in light sensitivity and slower channel closing kinetics when compared to wt-ChR2 (Figure 1.15). ChR2 H134R has been used to successfully depolarise neurons both *in vitro* and in the living animal.

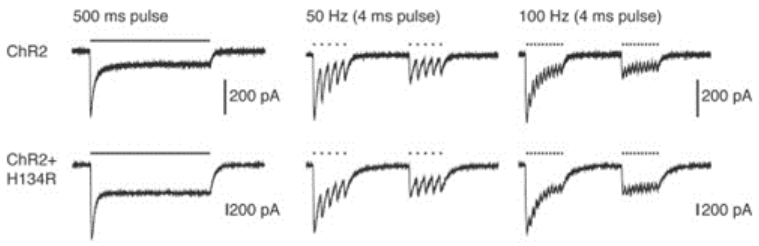


Figure 1.15: **ChR2 mutant H134R compared to wild-type ChR2.** H134R mutant is compared to wtChR2 for its ability to reliably generate photocurrents when heterologously expressed in animal cells. Note comparative scale of current yielded. Adapted from [Lin, 2012].

ChR2 C128A belongs to the group of Step Function Opsins (SFO) or bi-stable opsins, characterised by slower channel closing kinetics (Figure 1.16) due to prolonged lifetime of the P520 intermediate in the photocycle. Closing kinetics can be reduced by exposure to longer wavelength of light (530 nm) after the one used for activation (470 nm). SFO variants, including also D156A, C128S, C128T and the combination of some of these single point mutants, enable ON/OFF control of membrane depolarisation by modification of the conducting state lifetime. Cys128 is a very relevant residue in the structure of ChR2, forming the DC gate together with Asp156 (D156) [Nack et al., 2010]. Mutations in both residues (C128A/D156A) freeze the photocycle in the conducting state P520 (see Figure 1.13). The DC gate in ChR2 corresponds to the DT (D115 and T90) gate in Bacteriorhodopsin, which is in close proximity to the C11/C12 carbons of the protonated retinal Schiff base ($RSBH^+$). Mutation of Thr90 to alanine or valine in Bacteriorhodopsin resulted in slowing the channel closing kinetics, due to an accumulation of intermediate non-conducting states in the photocycle. In 2009 Berndt and colleagues reasoned that a similar approach could have been used to create a ChR2 variant with longer closing rate (τ_{off}) by mutating the cysteine analogue of Thr90 for a threonine (C128T), alanine (C128A) or serine (C128S); these three mutants are characterised by closing constants of 2 ms, 52 s and 106 s, respectively. The dual wavelength control of SFO mutants is caused by the longer lifetime of the P520 intermediate in these mutants. When exposed to short pulses of green light (520 nm) P520 can revert to the ground dark state D470, which can be opened again by a blue light pulse, enabling short-circuiting of the photocycle [Berndt et al., 2008].

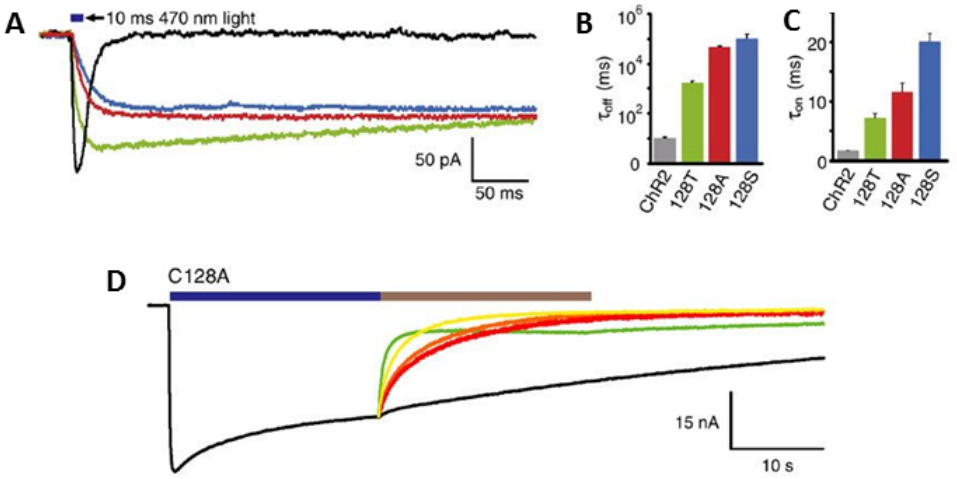


Figure 1.16: **Substitution of amino acid C128 in ChR2 structure results in slower off-kinetics of the optogenetic channel.** Photocurrents recorded in hippocampal neurons (**A**) show slower channel closing kinetics of the C128 mutants, namely C128A (red), C128S (blue) and C128T (green), compared to wild-type ChR2 (black). **B** and **C** report closing and opening kinetics of these mutants, respectively. **D** shows photocurrents generated by the C128A mutant expressed in *Xenopus laevis* oocyes (black trace). Coloured traces report reduction of channel closing timescale by exposing ChR2-C128A to longer wavelength light stimuli (green=530 nm; yellow=546 nm; orange=570 nm; red= 600 nm). Image modified from [Berndt et al., 2008].

ChR2 E123T, also known as ChETA (**Ch**annelrhodopsin **ET** **A**ccelerated), was also one of the first ChR2 mutants to be developed with a slight increase in kinetics but reduced photcurrent; the reduced photocurrent can be advantageous to compensate for desensitisation in the case of overexpression of the channel. The negatively charged glutamate in position 123 was substituted with a polar non-charged threonine, resulting in a destabilised active conformation of retinal, allowing for faster reisomerisation kinetics (Figure 1.17) [Gunaydin et al., 2010]. The relatively small red-shifted activation peak (495 nm) of ChETA may be beneficial in combination with Fura-2 for calcium imaging experiments [Lin, 2011], reducing the undesired activaton of ChR2 by means of the UV wavelength used for excitation of the calcium-sensitive dye (340 nm and 380 nm).

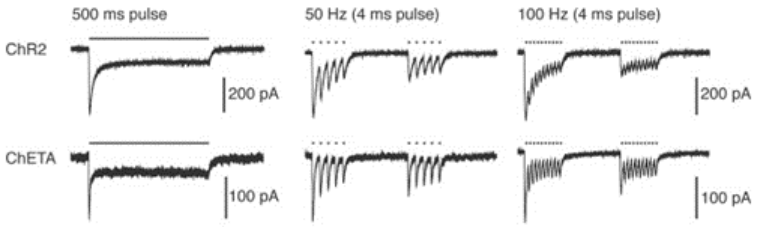


Figure 1.17: **ChR2 mutant E123T (ChETA) compared to wild-type ChR2.** ChETA mutant is compared to wtChR2 for its ability to reliably generate photocurrents when heterologously expressed in animal cells. Note relative size of current bars. Adapted from [Lin, 2012].

ChR2 L132C is a ChR2 mutant with a six-fold increased calcium permeability compared to wt-ChR2, therefore named CatCh (**Ca**lcium **t**ranslocating **Ch**R2). It was first developed by Kleinlogel and colleagues in 2011 and it is able to generate higher photocurrents when expressed in hippocampal neurons. The ability of CatCh to mainly drive calcium through the membrane also makes it a good candidate for calcium imaging experiments, amplifying the signal resulting from primary calcium flow, although it has been reported that secondary calcium fluxes might actually be responsible for the rise in fluorescence when performing calcium imaging, possibly due to voltage-gated calcium channels opening in response to membrane depolarisation. CatCh was obtained by genetically engineering a lysine in position 132 into a cysteine (L132C), as shown in Figure 1.18; selection of the mutagenic site was based on the homology model with the Sensory Rhodopsin 2 structure (PDB 1H2S). After removal of the leucine's methyl group, a cavity is formed in the retinal binding pocket, resulting in an increased permeability for ions such as calcium, characterised by higher steric hindrance [Kleinlogel et al., 2011a].

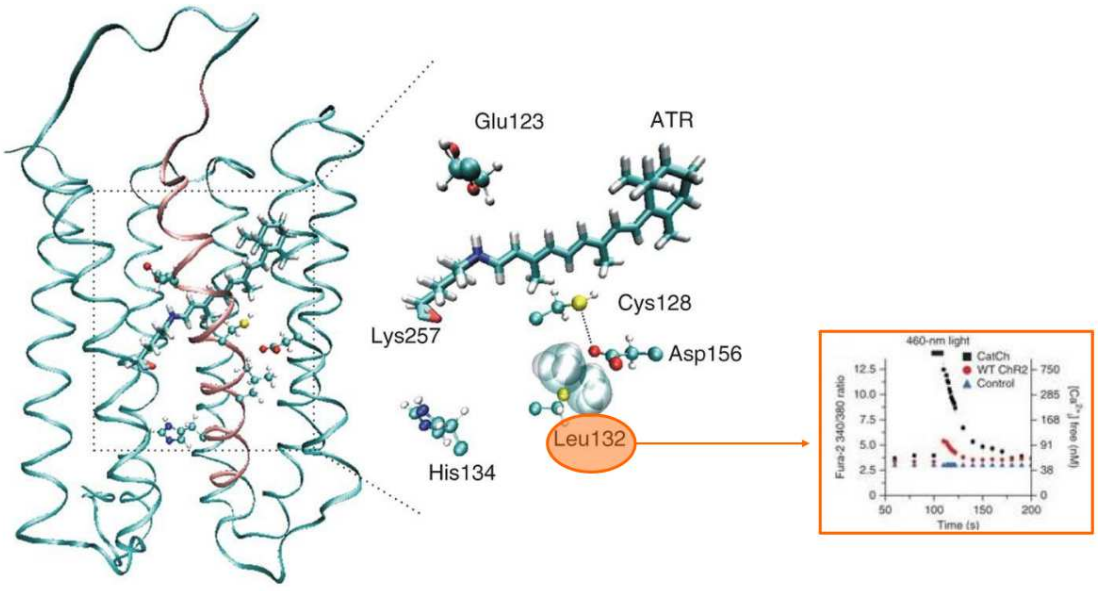


Figure 1.18: **Mutation of the leucine 132 with a cysteine results in six-fold calcium permeability increase in ChR2.** ChR2 homology model based on sensory rhodopsin 2 (1H2S on the PDB) shows Leu132 interacting with the Asp156/Cys128 gate in the active site of the pore. Mutation of Leu132 to a Cys results in an increase in the permeability of ChR2 to calcium ions, due to the formation of a more flexible pore in the mutant. Inset: Fura-2 measurements of calcium dynamics show a six-fold increase in calcium influx for L132C (or CatCh-Calcium Translocating Channelrhodopsin-2) compared to the wild-type ChR2. Adapted from [Kleinlogel et al., 2011a].

ChR2 T159 is another amino acid involved in the retinal binding process; it is in

direct contact with D156 and mutation of the threonine to a cysteine dramatically increased photocurrent amplitudes (Figure 1.19), depending on the expression system (oocytes, neurons), while at the same time improved light sensitivity of the channel [Berndt et al., 2011]. **T159C** has been combined with other point mutations, such as H134R or E123T to compensate for channel opening delay after photostimulation [Berndt et al., 2011].

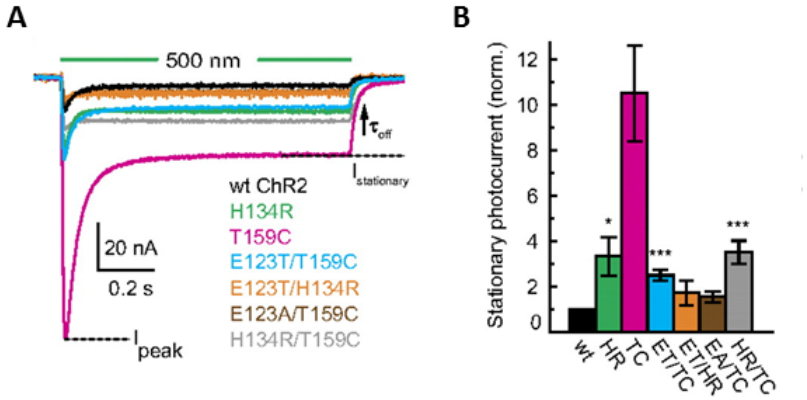


Figure 1.19: **ChR2 T159C mutant compared to wild-type ChR2 and other engineered ChR2.** Mutation of Thr159 in the retinal binding pocket changes amplitudes of photocurrents generated by ChR2. **A** Photocurrents in *X. laevis* oocytes are higher in T159C compared to other engineered ChR2. **B** Combination of T159C mutation with other reported amino acid substitution in the active site of ChR2 do not enhance its activity. Adapted from [Berndt et al., 2011].

From this brief overview of ChR2 variants, whose properties are summarised in Table 1.1 it should be clear how the serendipity of introducing an algal ion channel in mammalian neurons was only the first step of the dawn of optogenetics and how only through the synergism of meticulous research in structural chemistry, biochemistry and genetic engineering ChR2 could become a very useful tool in the hands of (but not only) neurobiologists.

ChR variant (Mutation)	**Main features**	**Activation wavelength** (nm)	**Opening rate τ_{on}** (ms)	**Closing rate τ_{off}** (ms)	**Reference**
wtChR2 (Naturally-occurring ChR2 1-315 aa)	Small channel conductance Strong desensitisation Poor heterologous expression	470	1.21	13.5	[Nagel et al., 2003]
H134R	Reduced desensitisation Slower kinetics	460	1.92	17.9	[Lin et al., 2009b]
ChETA (E123T)	Fast kinetics Red-shifted activation	495	0.8	8	[Gunaydin et al., 2010]
CatCh (L132C)	Increased calcium permeability Minimal desensitisation to long stimulation	470	0.5	10	[Kleinlogel et al., 2011a]
Step-Function Opsins (C128X, D156A)	Slow off kinetics Dual wavelength ON/OFF control	470	8-20	50000-100000	[Berndt et al., 2008]
ChEF/ChIEF (ChR1-ChR2 chimaera)	Increased membrane trafficking Minimal desensitisation	450-490	1.56	12-24	[Lin et al., 2009b]
ChD (ChR1-ChR2 chimaera)	Reduced desensitisation	450	1.5	8	[Lin et al., 2009b]

Table 1.1: **ChR variants designed to overcome heterologous expression of the light-gated channel in mammalian systems.** The table summarises the main features of the ChR mutants genetically engineered from the naturally-occurring ChR to achieve highly precise spatio-temporal control of mammalian cell functions. *Original table.*

1.2.2 Halorhodopsin

Halorhodopsin is a light-activated electrogenic chloride pump found in the membrane of halophilic (from Greek 'salt lovers') bacteria, which prosper in extremely saline environments [Schobert and Lanyi, 1982]. One of the most commonly used halorhodopsins for optogenetic purposes is NpHR (*Natronomonas pharaonis* halorhodopsin), which will be described in more details in this section. It is a naturally-occurring halorhodopsin found in the membrane of bacteria populating the alkaline lake Natron in Tanzania, characterised by a pH of about 11. Such extreme alkaline conditions cause low extracellular proton concentrations, that affect membrane-linked bioenergetics [Ihara et al., 2008]. *Natronomonas* is in fact an aerobic organism and it gains energy mainly through cellular respiration; difficulties in generating a proton gradient through the cell membrane would be reflected in lower ATP synthesis and therefore reduced survival rates [Falb et al., 2005]. To compensate for the lack of protons in the highly alkaline surroundings, *N. pharaonis* exploits the photon-dependent inward chloride current to generate an intracellular negative environment and maximise proton flow and therefore ATP synthesis.

The inwardly directed chloride pump activity of halorhodopsin, discovered about 10 years after bacteriorhodopsin, came from an observation of Schobert and Lanyi in the early 1980s [Schobert and Lanyi, 1982]; they noticed that when growing in the absence of extracellular chloride, the bacteria were not able to hyperpolarise their membrane, thus the conclusion that chloride, and not protons like in bacteriorhodopsin, were transported through this protein. The detailed mechanism of chloride transport through *N. pharaonis* halorhodopsin is still debated and modifications to its photocycle and the interchange of structure intermediates are often revised [Sato et al., 2005].

Halorhodopsin presents high sequence similarities with other microbial opsins: its structure is in fact that of a seven-transmembrane-helix protein, with the chromophore *all-trans* retinal (ATR) enclosed in the structure, as reported in Figure 1.20.

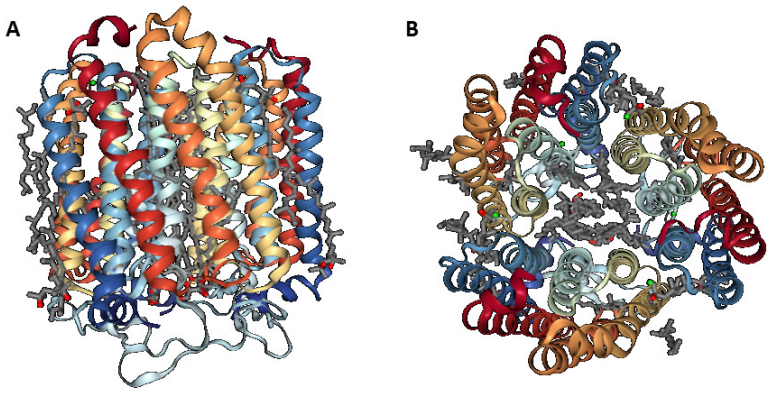


Figure 1.20: **The crystal structure of halorhodopsinfrom Halorodopsin from *Natronomonas pharaonis***. The ground state of the chloride pump halorhodopsin is shown in its crystal structure obtained by Kouyama and colleagues as deposited on the Protein Data Bank (PDB identification number 3A7K). (Adapted from the PDB, Protein Data Bank)

Preliminary structural information about halorhodopsin was obtained by cryo-electron microscopy and later on its crystallographic structure was determined, being one of the first membrane protein structures to be unravelled by X-ray crystallography [Guijarro et al., 2006; Kolbe et al., 2000; Kouyama et al., 2010]. The ionic environment surrounding the retinal cofactor strongly influences Halorhodopsin spectral characteristics. In ChR2, ATR photoisomerises at 470 nm, whilst in Halorhodopsin the pump activity is triggered by light at 580 nm, due to interactions of the amino acids in the active site with the protonated retinal Schiff base ($RSBH^+$) formed by retinal and a lysine [Jardón-Valadez et al., 2014]. Figure 1.21 represents Halorhodopsin mechanism of action in a schematic diagram.

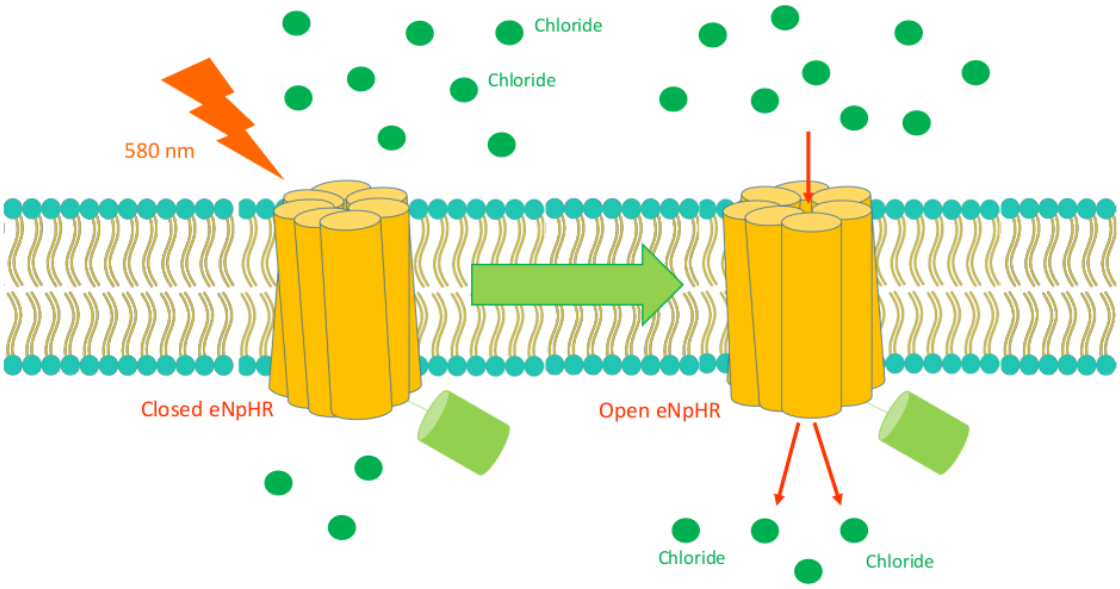


Figure 1.21: **Mechanism of action of the light-gated electrogenic chloride pump Halorhodopsin from *Natronomonas pharaonis* (eNpHR).** Cartoon showing the mechanism of action of eNpHR. Lateral view of the plasma membrane of a cell expressing eNpHR; on the left, the light-gated eNpHR is shown in its closed (i.e. non-conducting) state, with its seven transmembrane helixes schematically represented as yellow cylinders. An EYFP fluorescent tag, that can be used to identify the cells expressing the light-gated pumps, is also simplified as a green cylinder connected to one of the helices. Upon delivery of amber (580 nm) light, represented by the lightning bolt on the top left corner, the protein undergoes a conformational change resulting in the widening of the pore on the extracellular side first, and the following pumping of chloride through the channel inside the cell. The rise of intracellular chloride causes hyperpolarisation of the cell membrane, feature that has been exploited to silence action potentials in neurons and study neuronal functions using photonics. *Original drawing.*

Isomerisation of *all-trans* retinal to the *13-cis* isoform initiates halorhodopsin photocycle which, similarly to other type I rhodopsins, is characterised by the succession of protein intermediate states following retinal spectral changes until reisomerisation to the *all-trans* form (simplified in Figure 1.22) [Fastermann et al., 2000; Mizuno et al., 2018]. Halorhodopsin photocycle intermediates are indicated as $NpHR_{575}$, K, $L1_{520}$, $L2_{520}$, N_{510}, O_{605} and NpHR', where the numbers represent the absorption maximum (λ_{max}) of the respective isoform. The photocycle is unidirectional, as for Channelrhodopsin, but the reverse reaction from O_{605} to N_{510} has been reported [Kouyama et al., 2018].

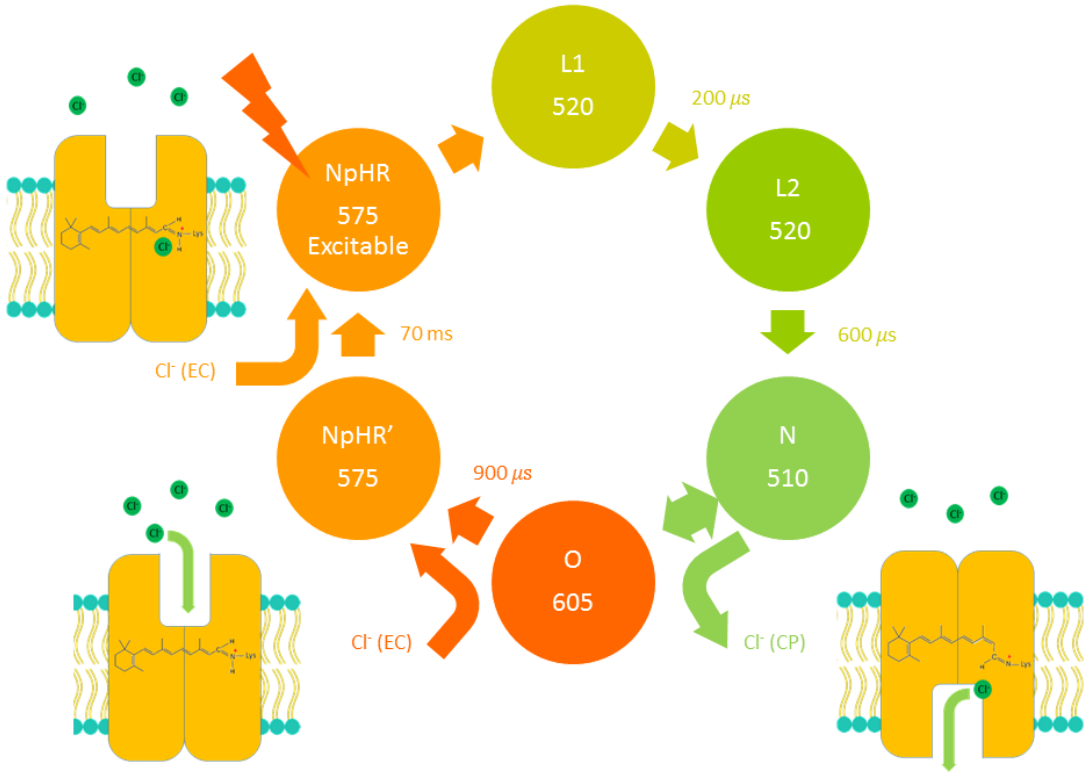


Figure 1.22: **Photocycle reactions of the electrogenic chloride pump Halorhodopsin from *Natronomonas pharaonis* (NpHR). The schematic represents the photocycle of NpHR and drawings report circulation of Cl^- ions through the pump.** The numbers indicate the maximum absorption wavelength for each of the intermediate states of the pump. Chloride is uptaken from the extracellular environment by the O intermediate and is stored in the active site of the protein, due to interactions with the positively-charged retinal Schiff base ($RSBH^+$) formed by the retinal chromophore and the lysine. The photocycle is initiated by amber light exposure (575 nm) and absorption (indicated by the lightning bolt on the 575 configuration). Following photoisomerisation of *all-trans* retinal to 13-*cis* retinal, the polar environment in the Cl^--binding site is altered and the structure of NpHR modified, to facilitate release of the Cl^- ion on the intracellular side (Cl^- CP, cytoplasmic). *Original drawing.*

Conversely from ChR2, halorhodopsin is a pump, not a channel, therefore the photocycle incorporates the movement of chloride through the protein in two steps: first, chloride is captured from the extracellular solution and binds the active site near the $RSBH^+$ when the protein is in its dark state and the pore is wider towards the outside of the membrane. Subsequently, the chloride ion gets released from the core of the protein to the cytoplasmic side after conformational changes of the helices arrangement and widening of the pore on the intracellular side (Figure 1.23) [Guijarro et al., 2006].

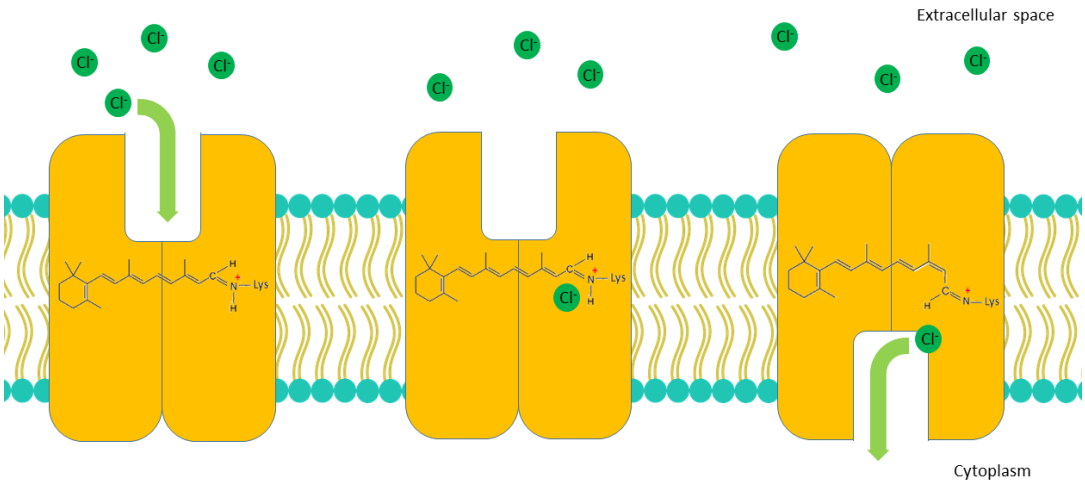


Figure 1.23: **Mechanism of action of the light-driven chloride pump Halorhodopsin from *Natronomonas pharaonis*.** Cartoon showing the mechanism of action of eNpHR, focusing on uptake and release of chloride ions and their flow through the cell membrane, schematically showing chloride interactions with the protonated retinal schiff base in its *all-trans* retinal and *13-cis* retinal forms. First, chloride ions are captured from the extracellular environment and bind to the active site of the protein by electrostatic interactions. Upon light stimulation and conformational changes of the retinal chromophore and the protein structure, chloride ions are driven to the cytoplasmic side of the membrane and released in the intracellular environment. *Original drawing.*

When Channelrhodopsin became an optogenetic tool used to depolarise the membrane of specific subsets of neurons, growing interest in the world of microbial rhodopsins was rediscovered, in the hope to find a suitable candidate to couple ChR2 activity with. Halorhodopsin soon became an ideal candidate, because of its inwardly-directed chloride current and potential to hyperpolarise neurons, thus inhibiting action potential generation [Zhang et al., 2007]. Halorhodopsin is one of the most used silencing opsins, enabling non-invasive inhibition of genetically engineered neurons [Han and Boyden, 2007]. Furthermore, the distinction of ChR2 and HR activation spectra allows for combination of the two proteins in the same population of cells, providing ON/OFF control of cellular functions with light of different wavelengths.

Preliminary attempts at expressing NpHR in neurons were, however, disappointing, mainly because of accumulation of the protein in the endoplasmic reticulum (ER) and unsuccessful delivery to the plasma membrane [Zhao et al., 2008]. Genetic insertion of two peptides in the protein sequence, for membrane delivery and ER escape, enhanced plasma membrane translocation (Figure 1.24) and, subsequently, functionality of the construct, named eNpHR2.0 or simply eNpHR (second generation enhanced halorhodopsin from *N. pharaonis*) [Gradinaru et al., 2008].

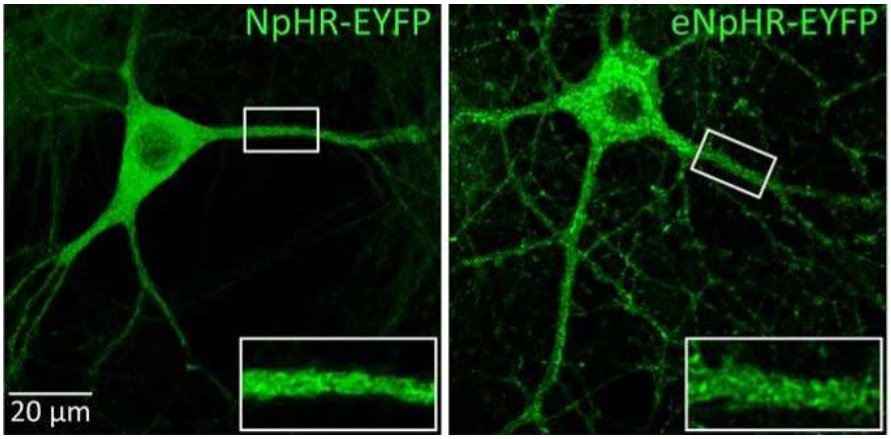


Figure 1.24: **Comparison of expression patterns of *Natronomonas pharaonis* halorhodopsin (NpHR) and its enhanced version (eNpHR) for reduced endoplasmic reticulum accumulation in cultured hippocampal neurons.** Confocal images showing expression patterns of NpHR and eNpHR 2.0 in hippocampal neurons. eNpHR, engineered with the peptide FCYENEV for endoplasmic reticulum escape, does not accumulate in the cytosol like its naturally-occuring variant NpHR. Insets show magnified views of selected regions. Adapted from [Gradinaru et al., 2008].

Optogenetics enables control of genetically-modified cells or tissues exploiting light as a tool to achieve spatiotemporally precise switch of cellular functions. The *optogenetic revolution*, as it has been referred to, was made possible by the simultaneous development of very diverse fields of science, namely genetic engineering, described in Section 1.3, and optical engineering, in Section 1.4, and their union to achieve precise control of cellular processes with photonics.

On one hand, the fine development of recombinant-DNA techniques allowed for the selective creation of light-responsive cells by the expression of optogenetic actuator genes. Furthermore, the modification of microbial rhodopsin structures via genetic engineering propelled the field forward by the creation of molecular probes to suit experimental needs and overcome limitations of the naturally-occurring microbial rhodopsins. On the other hand, progress of optical techniques and devices, such as high-power LEDs (Light Emitting Diodes) and fibre-optic coupled illumination, contributed to increasing spatial and temporal resolution, especially when operating on living animals.

1.3 Genetic engineering

Genetic engineering enables rearranging and hijacking of gene structures and functions *in vitro*. Since its birth in the 1980s, it has revolutionalised the world of biology and

genetics.

Genetics, the study of genes and information they carry, is based on observation of patterns of heredity and how they propagate from one generation to the next. Conversely, genetic engineering is an active branch of molecular biology that allows scientists to alter the genetic components of an organism in order to harness them for a variety of purposes, from research to therapeutics and diagnostics. A schematic diagram of the core procedures in genetic engineering, molecular cloning, is shown in Figure 1.25. The basic principle of genetic engineering is the isolation of single genes from longer sequences of DNA by the use of the "cut and paste" ability provided by restriction enzymes. Restriction enzymes, discovered by Arber, Smith and Nathans in the 1960s, are proteins originally used by bacteria as a defensive mechanism to protect the cells against external sources of genetic material, such as viruses [Arber and Linn, 1969; Nathans and Smith, 1975]. They recognise highly conserved and specific short palindromic sequences of DNA and cleave the strand, fragmenting the exogenous genetic material and preventing its integration in the genome. This feature has been exploited in molecular biology to isolate single genes from longer sequences of DNA or even from genomes [Roberts, 2005]. The isolated gene is introduced in a carrier vector, often a plasmid or inactivated viral particle, and then internalised by a foreign organism. Molecular cloning, the amplification of recombinant genetic material exploiting the replication machinery of host cells, is exploited in genetic engineering to obtain multiple copies of the gene of interest. Following amplification, hybrid genetic material can be used for a variety of applications. For instance, by introducing the amplified DNA in host cells and by exploiting them as productive factories, large quantities of recombinant proteins can be obtained. The production of insulin [Johnson, 1983] or clotting factors [Pipe, 2008] for the treatment of diabetes and haemophilia, respectively, are only two examples of the many biosynthetic drugs produced as recombinant proteins and routinely used in the clinic [Dingermann, 2008].

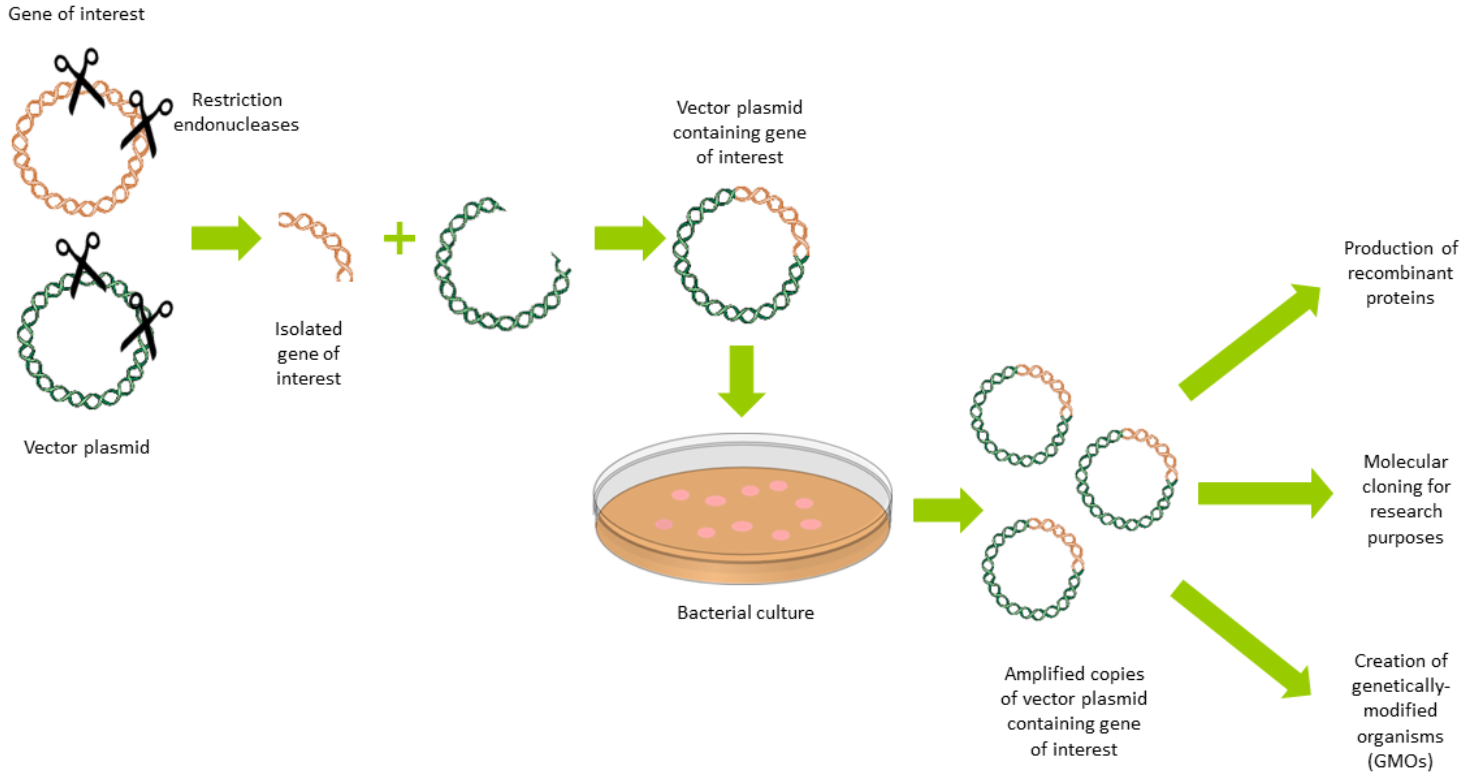


Figure 1.25: **Genetic engineering schematics.** Simplified diagram summarising core steps of the genetic engineering procedure. The gene of interest is removed from its original source by the activity of restriction enzymes (represented as molecular scissors). A molecule of DNA that will work as a carrier vector undergoes the same procedure. When combined, either *in vitro* or *in vivo*, the two fragments will merge in a hybrid DNA molecule containing the gene of interest and other components for amplification or expression in other organisms. Once introduced into host cells, e.g. bacteria, the recombinant DNA can be isolated and used for a variety of applications, from production of bio-synthetic drugs or creation of genetically modified organisms or further research on the gene of interest. *Original drawing.*

Genetically engineered cells have been key players in the last decades of biology, from GMOs (genetically modified organisms) of cereal crop plants in agriculture [Chaudhary and Singh, 2019; Potrykus, 2001] to animal genetic models of pathologies [Ruggeri et al., 2014]. Recombinant DNA techniques allowed for analysis of single gene sequences and functions and the birth of the genomic era, where genes are studied and modified in the light of the whole genetic material defining an organism in a species. At the beginning of this millennium, entire genomes of several species were decoded, by combining molecular cloning and DNA sequencing. DNA sequencing, that is the process of determining the order of nucleotides in a fragment of DNA, was discovered in the 1970s by separate groups of scientists [Maxam and Gilbert, 1977; Sanger et al., 1977]. The "chain termination method", developed by Frederick Sanger, is based on the polymerisation of a strand of DNA template providing the polymerase with both dNTPS and ddNTPS (deoxy and dideoxy-nucleotides). Incorporation of the latter results in termination of the elongation chain, lacking the $3^{'}$ –OH group needed for the bond with the following base in the chain. The ddNTPS are either radioactively or fluorescently labelled for visualisation and reconstruction of the sequence based on the increasingly long fragment on an electrophoresis gel. Sanger methods have been surpassed by Next-Generation (or next-gen or high throughput) sequencing techniques [Metzker, 2010; Shendure and Ji, 2008] for genomics applications, but are still extremely reliable and valuable for validation of sequences in molecular biology. For instance, capillary sequencing, used in the present work for sequence validation (Section 2.1.2), analyses DNA fragments by separating them by size through a long, thin, acrylic-fibre capillary, instead of an electrophoresis gel. The configuration of the capillary allows for the use of extremely high electric fields and, consequently, very rapid separation of DNA fragments is achieved. Automation of these processes resulted in rapid access to huge quantities of genetic data and really allowed the genomic era to thrive [Mullis et al., 1986].

The discovery of the Polymerase Chain Reaction (PCR) by Kary Mullis in the 1980s represents another milestone in the field. The PCR provides an alternative method for the generation of high copy numbers of the same gene, without the use of host cells. By knowing part of the sequence of the gene or DNA portion of interest, short

matching sequences are designed in order to amplify that fragment and introduce desired mutations. Site-directed mutagenesis is a molecular biology technique routinely used to introduce point mutations in the amino acidic sequence of proteins by altering the series of nucleotides in their encoding genes. Mutagenesis of single nucleotides at specific sites highlighted roles of point mutations in the onset of pathologies [Horton, 1997]. An example is the point mutation in the sequence of the haemoglobin gene, resulting in sickle cell anemia. Bioinformatics and site-directed mutagenesis identified and modified amino acids in protein sequences to generate an expanded pool of proteins for the most diverse applications [Rehm, 2001].

Once extracted, modified and analysed with the techniques described above, genetic material can be introduced into host cells via different methods. Genetic material needs in fact to be driven across the membrane of host cells by phyisical or chemical factors, ranging from electroporation to gene gun to the use of specific vectors, all designed to aid internalisation. Such vectors can be cationic molecules, lipid nanoparticles or even viral structures for high delivery efficiencies [Nayerossadat et al., 2012]. Transfection refers to non-viral methods in eukaryotic cell lines, preferred to the terms transformation, more often used to describe non-viral DNA transfer in bacteria, and transduction, used to describe virus-mediated DNA transfer. Transfection methods are generally less toxic to the cells receiving the exogenous DNA [Yin et al., 2017] and are preferred in this work to viral-based ones. Inactivated, i.e. deprived of their virulence factors, viral particles from lentiviruses or adeno-associated viruses, for instance, have been exploited for the introduction of genetic material into host cells and for therapeutic purposes in gene therapy [Kotterman et al., 2015]. Despite their high-efficiency rates, viral vectors present considerable limitations, such as toxicity and risk of uncontrolled mutagenesis [Thomas et al., 2003]. Viral methods have been, however, the gene delivery vectors of choice due to their ability to overcome delivery obstacles in the host cells, especially when studying non-dividing cells [Wagstaff and Jans, 2007]. More recently, non-viral vectors have been developed and optimised for reduced cytotoxicity and increased biocompatibility [Balazs and Godbey, 2011; de Ilarduya et al., 2010; Zhang et al., 2004]. A transfection technique, lipofection is a lipid nanoparticle-based transfection technique,

designed to efficiently deliver genetic material into the cells, schematically represented in Figure 1.26. The liposomes show an overall positive charge at physiological pH and are able to form complexes (lipoplexes) with negatively charged nucleic acids through electrostatic interactions. The association of the lipid-based transfection reagent with nucleic acids results in a tight coating and these cationic complexes are easily internalized by endocytosis.

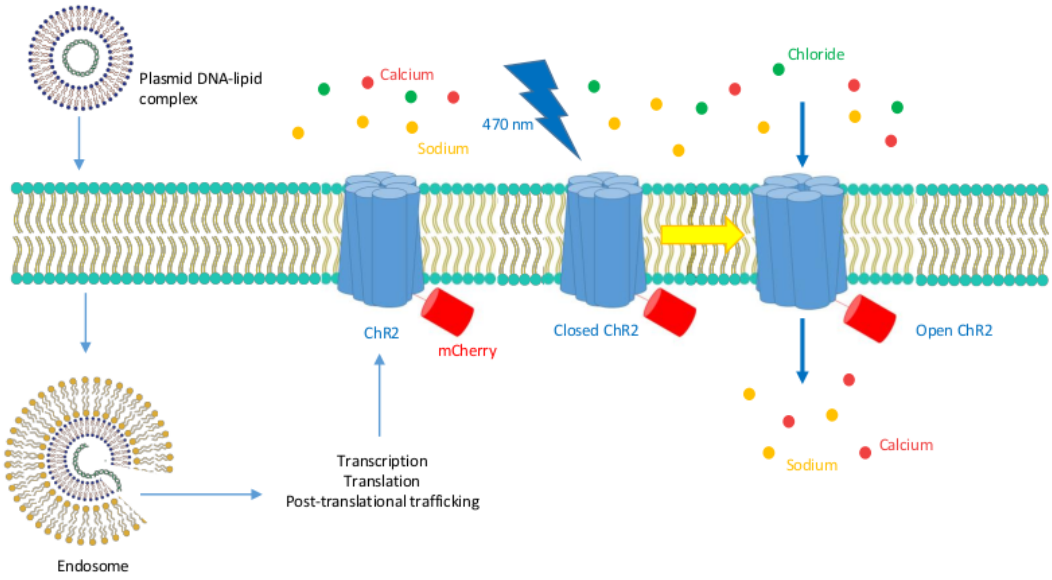


Figure 1.26: **Lipofection schematic mechanism.** DNA molecule are complexed with the lipid nanoparticles, to create a lipoplex, in order to facilitate internalisation through the plasma membrane. Once inside the cells, the endosome is disrupted and the DNA is first transcribed and then translated into protein. The process is based on the packaging of negatively-charged DNA molecules into positively-charged liposomes that can cross the membrane barrier. *Original drawing.*

Magnetofection is an emerging alternative tool to lipofection and can be employed to optimize transfection efficiency *in vitro* (Figure 1.27). It combines the advantages of biochemical (cationic lipids or polymers) and physical (electroporation, gene gun) transfection methods in one system while excluding their inconveniences, such as vector accumulation and toxicity. It can be employed to maximize both viral and non-viral techniques. The basic principle of this methodology is to associate transfection reagents with magnetic nanoparticles. The iron-oxide magnetic nanoparticles are coated with specific cationic molecules that can vary upon applications. The resulting complexes are then transported into the cells by an appropriate magnetic field, which is applied by a specifically designed magnetic plate, placed underneath the culture dish [Plank et al., 2003].

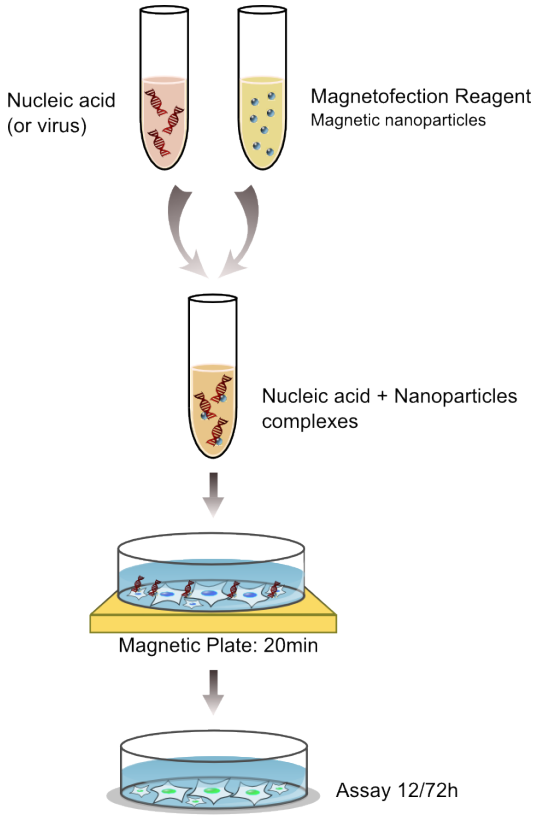


Figure 1.27: **Mechanism of action of magnetofection process.** Magnetofection is a transfection method based on magnetic nanoparticles funcionalised with cationic molecules: the positive charge on the surface of the coated iron oxide nanoparticles attracts and binds DNA that can be then driven inside the cells by the application of a magnetic field. Image courtesy of *OZBiosciences*.

Optimisation of vectors and their components is crucial for the expression of heterologous proteins in host systems. The vector for the delivery of optogenetic constructs in the present work is a pcDNA3.1, a versatile 5.4 kilobase (kb) plasmid designed for high level expression of heterologous proteins in mammalian cells and its main features are summarised in Figure 1.28. pcDNA3.1 contains both a strong promoter for mammalian expression, the cytomegalovirus (CMV) promoter and an origin of replication for cloning in *E.coli* bacterial colonies. Selection of recombinant cells is based on selectable markers, namely the ampicillin(AmpR) and neomycin/kanamycin resistance genes (NeoR/KanR) for bacteria and mammalian cells, respectively. Internalisation of the plasmid confers resistance to specific antibiotics, whose metabolic enzymes are encoded by the same plasmid. Growth in selective media containing the specific antibiotic, selects only cells, which have uptaken the exogenous element of genetic material. The multi-cloning site (MCS) presents restriction sites for a broad variety of endonucleases, in order to facilitate cloning.

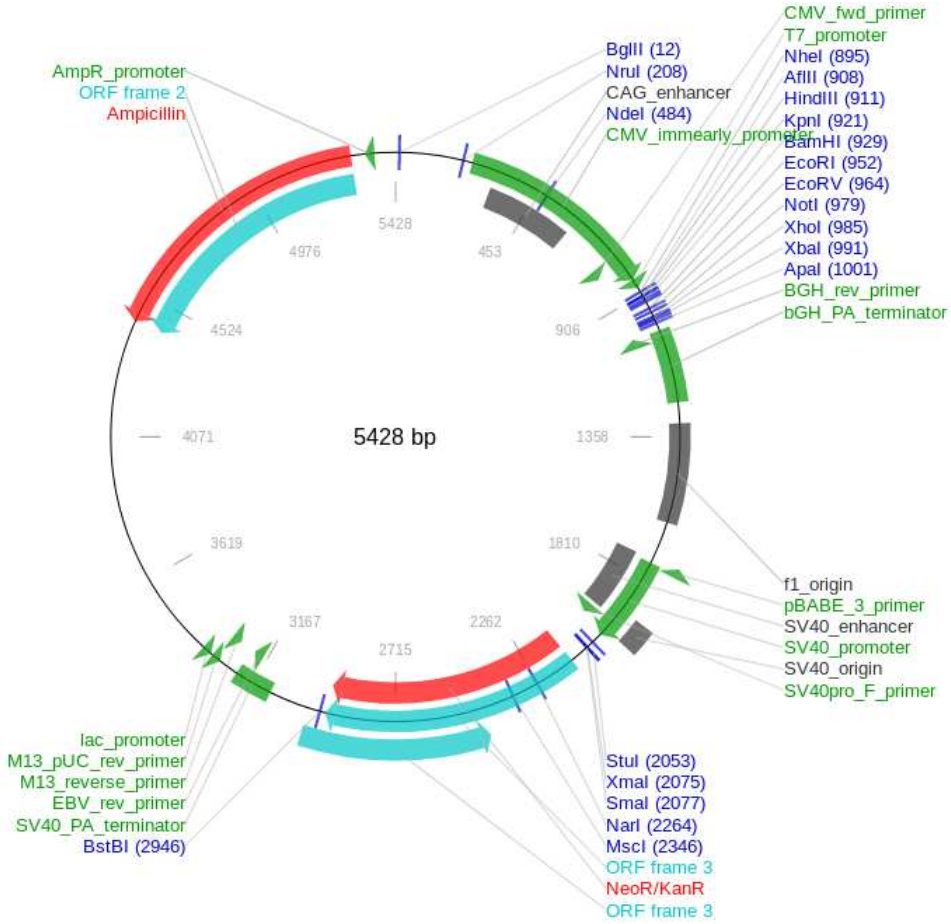


Figure 1.28: **pcDNA3.1(+) blank vector map.** (**A**) where the sequences for hChR2 and eNpHR3.0 were subcloned into from the lentiviral vectors to obtain less neuronally-specific optogenetic constructs for applications in human epithelial physiology. Image from Thermo Fisher Scientific.

Endogenous or exogenous DNA (e.g. deriving from plasmids after transfection) is transcribed into messenger RNA (mRNA) and translated into proteins by ribosomes in the rough endoplasmic reticulum (ER); following synthesis in the ER, proteins are folded and assembled to be packaged into ER-derived vesicles and transported through the trans-Golgi network, where they undergo other functionalisation processes. From the Golgi apparatus, proteins, in this case opsins, travel in transport vesicles towards the membrane, where they are finally embedded and functional (see Figure 1.29). This process is crucial for the correct functionality of the proteins and it is strongly dependent on a wide variety of factors, from the cell line, to the specific protein which is desired to be expressed and the mode of delivery chosen for the application, in the case of exogenous DNA [Grisshammer, 2006].

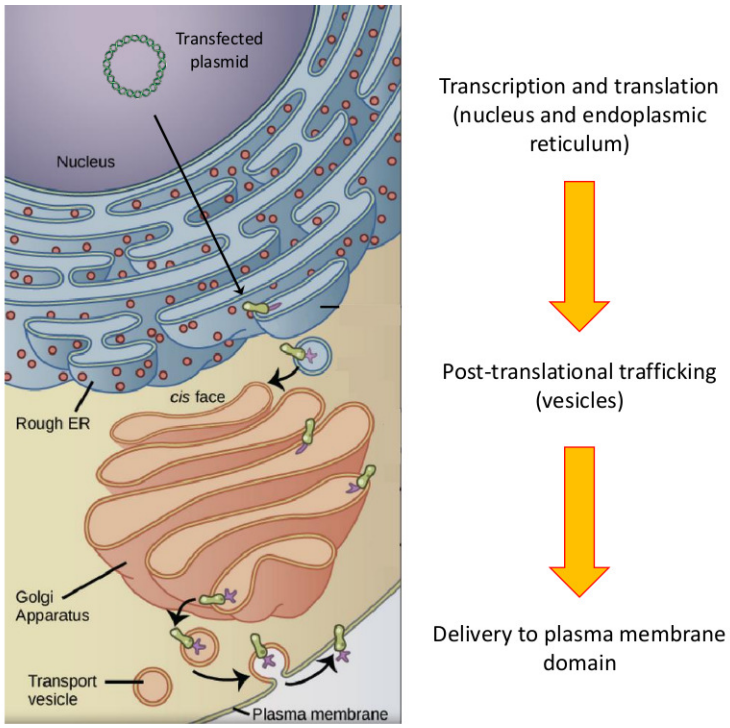


Figure 1.29: **Post-translational protein trafficking schematics.** Schematics summarising post-translational trafficking of membrane-targeted proteins. Following internalisation of transfected plasmid, DNA is transcribed into mRNA in the nucleus and then transcribed into protein in the endoplasmic reticulum (ER). Following translation, the protein is packaged into vesicles and targeted to the plasma membrane. Adapted from *Anatomy and Physiology*.

Therefore, the time that exogenous proteins take to express, can vary and it needs to be assessed for every new set of conditions. Recently, researchers have developed mutants which are more easily delivered to the cell membrane; an example is eNpHR 2.0, engineered with a signal peptide for membrane insertion and an endoplasmic reticulum escaping sequence, to prevent aggregation in the endoplasmic stuctures. Another factor of variability is given by the fluorophore chosen to tag the optogenetic tools; for example, it was observed in zebrafish that *N. pharaonis* halorhodopsin appeared to clump more when expressed fused with the fluorophore mCherry, than to the yellow fluorescent protein YFP [Arrenberg et al., 2009].

Genetic engineering refers to the numerous techniques mentioned above and it enables modification of the genetic material of organisms in order to hijack their molecular processes and either study them or harness their product for further research.

1.4 Optical engineering

Light and biology have been intertwined since the 17^{th} century, when Antonie van Leeuwenhoek was the first man to see microbes by harnessing light with a single-lensed microscope he had built. The primary application of light in cellular biology was therefore visualisation of structures otherwise invisible to the human eye. The discovery and purification of fluorescent proteins in the 1960s represented a huge turning point for microscopy, with the advent of fluorescent imaging techniques both in widefield and confocal configurations [Shimomura, 2009; Tsien, 1998]. Fluorescence proteins could be linked to antibodies for specific structures of the cells, thus allowing for their visualisation. Developments of optical techniques pushed the boundaries of cell imaging constantly further, even beyond the resolution limit dictated by the diffraction of light, with super-resolution microscopy [Huang et al., 2009].

In the late 1980s, scientists realised that light could be used not only as a passive tool to study cellular features but also as an active mean to interact with cellular functions. Techniques like optical trapping and CALI (Chromophore Assisted Laser Inactivation) emerged then, exploiting light as a tool for interfering with cellular processes [Jay and Sakurai, 1999; Liao et al., 1994]. By destroying mutated proteins with high specificity using light as the trigger of the process, CALI raised hope for treatment of degenerative diseases and cancer. Light became a tool to reorganise nature, besides observing it and understanding its processes.

Similar approaches were used to induce tumour cell death by heating gold nanoparticles (hyperthemia) or to activate chemical compounds targeted to the cancerous cells only [Hauck et al., 2008; Huang et al., 2008; Terentyuk et al., 2009].

A very intriguing feature of light for these manipulating applications is its tunability, in terms of spatial and temporal resolutions, and ease of delivery through simple lenses in conventional light microscopes. Conversely, most techniques available to biologists to control cell functions are either quite invasive or present low specificity for the subset of cells under analysis. The use of electrodes or drugs to activate or inhibit certain neurons in the brain of animals and record their outcome in terms of behavioural response are two examples of the limitations of conventional methods to manipulate cell

activities [Mandonnet et al., 2010]. When using electrodes, in fact, it is impossible to select only a specific type of neurons while leaving the surrounding ones unaffected.
By using light as a tool to direct cellular activities, together with molecules that would make only certain cells respond to impulses, cellular events could be controlled in a time- and space-resolved manner with physiological significance.
The first optogenetic control of mammalian cell functions was achieved by widefield illumination, due to its simplicity and tunability. Epi-fluorescent blue (470nm) light was used for the first optogenetic experiments to control the light-gated channel ChR2 both in mammalian cells (HEK293, BHK) and *Xenopus laevis* frog oocytes [Nagel et al., 2003].
In vivo applications, requiring deeper light penetration, benefited from fibre-optic technology that could be inserted directly into the brain of freely-moving animals. Laser or LED-coupled optical fibres of different core diameters were used based on the animal species and light-delivery depth requirements [Aravanis et al., 2007; Kim et al., 2013]. Furthermore, optical fibres and recording electrodes embedded in the same device have been used for stimulation of neurons and simultaneous electrophysiological recording of their response [Katz et al., 2013].
The thriving of semiconductor light sources constituted another advantage for illuminating techniques in optogenetics [Iwai et al., 2011]. Due to their reduced sizes and high power abilities, LEDs were extremely useful in the delivery of light into portable devices that could be implanted in the skull of rats and mice. Development of higher power red LEDs, combined with thin optical fibres and red-shifted variants of Channelrhodopsin, are proving useful for deeper brain stimulations.
Spatial light modulators (SLMs) and other light-patterning devices, like DMD (Dichroic Mirror Devices) were also exploited to change the light intensity over selected regions and to generate illumination patterns based on cellular morphology [Favre-Bulle et al., 2015; Packer et al., 2013]. Digital holography (DH) approaches have been used in a similar fashion to control optogenetic tools with spatial resolution below the optical spot of the illumination device employed to deliver the light stimulus [Reutsky-Gefen et al., 2013].

Scanning wide-field methods are an alternative to light-patterning devices, where the focused laser beam is scanned over the sample. Investigations of synapse connectivity have been taken out with this approach, where single cells are illuminated sequentially by the same source of light and propagation of the action potential is observed in the circuit.

Light has been adopted not only to deliver the channel gating input, but also as a mean to record responses from the cells. An example is the use of fluorescent indicators to monitor the flow of ions moving through the optogenetic channels, such as calcium-sensitive or voltage-sensitive dyes. There are evidences of an all-optogenetic approach, where response of the activation of optogenetic actuators (e.g. ChR2) was recorded by optogenetic sensors (e.g. GECI-Genetically Encoded Calcium Indicators) [Hires et al., 2008].

The rise of optogenetics saw the exponential succession of experiments testing different illumination devices and approaches; most scientists used off-the-shelf components to customise and upgrade the pre-existent microscopy rig to suit light delivery or patterning needs [Chagas et al., 2017]. Conventional microscopes are often not optimised for optogenetic experimental procedures and light delivery is often a limiting factor in optogenetic applications, where activation of light-gated proteins demand specific light intensities, normally in the range of 0.1-10 mW/mm^2. Precise regulation of the light stimuli is required to avoid closure of the channels due to excessive illumination intensity, referred to as desensitisation [Murawski et al., 2016].

Recently, two-photon excitation (2PE) methods have been investigated as an enhancement of optogenetic illuminating techniques [Oron et al., 2012; Prakash et al., 2012]. Scattering and axial incoherence prevent the use of 1PE for sectioning and deeper brain applications. The specificity of photon absorption and the longer wavelengths used in 2PE, make this approach more suitable for optogenetic interrogations in tissues and the living animal in neuroscience, due to the reduced photodamage and increased depth penetration in combination with red-shifted rhodopsin mutants [Lin et al., 2013].

1.5 From microbial rhodopsins to optogenetics

The possibility of selectively targeting and interrogating specific cells in a wider population had long been the dream of biologists, who constantly have to compromise with nature and devise new techniques to study processes that would otherwise be inaccessible in their original niche. *In vitro* studies have been tremendously helpful in understanding complex physiological processes, but the final goal of biology is to study cellular events in the context of other occurencies taking place at the same time in the rest of the tissue, organism and environment as a whole to consider all relevant variables simultaneously. In his 1979 paper "Thinking about the brain" and his 1999 paper "The impact of molecular biology on neuroscience" Francis Crick, father of molecular biology and Nobel Prize for the discovery of the double-helix structure of DNA, hypothesised that the future of neuroscience laid in the fusion of molecular biology and the ability to address only specific populations of neurons, underlying the need for *a method by which all neurons of just one type could be inactivated, leaving the others more or less unaltered.* Later on, he explicitly suggested light as the most intriguing tool to assess highly specific targeting of cellular sub-sets.

Crick's vision was put into life when microbial rhodopsins from algae and bacteria were introduced into mammalian neurons by Deisseroth and colleagues, obtaining control of neuronal function by light with millisecond time-scale resolution [Boyden et al., 2005]. Stimulation of selected neurons was performed by targeting heterologous genes for microbial rhodopsins, later addressed as optogenetic actuators, to specific sets of neurons only, by cell-type specific promoters that would induce expression of ChR2, for instance, in excitatory neurons but not in GABAergic neurons [Nathanson et al., 2009]. Optogenetics tools, both from single-cell organisms and modified with molecular biology techniques, rapidly grew in numbers and applications, as shown in Figure 1.30.

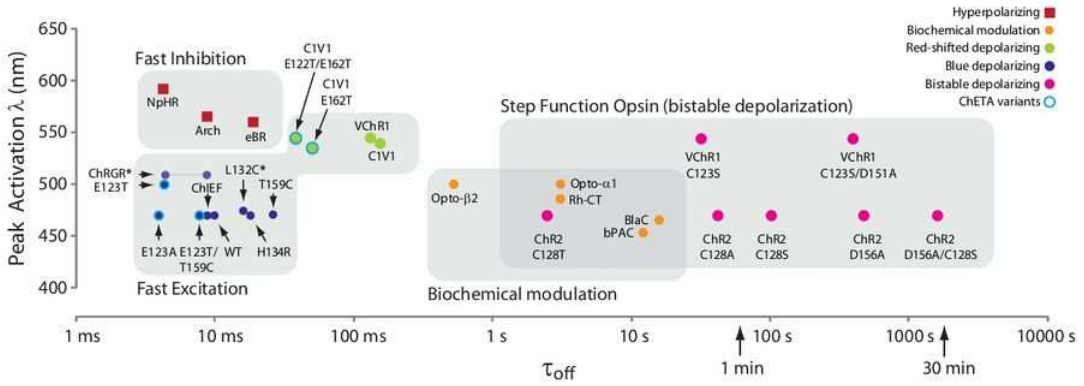


Figure 1.30: **The variety of optogenetic constructs and their diverse features.** Graph showing the still-growing family of optogenetic actuators available up to 2015, grouped based on their kinetic properties (τ_{off}), peak activation wavelengths and type of activity when introduced in other organisms (activation, inhibition, biochemical modulation). On the top left of the graph, inhibitory typeI opsins, the chloride pump halorhodopsin from *Natronomonas pharaonis* (NpHR) and the proton pumps archaerhodopsin and bacteriorhodopsin from the family of Halobacteriaceae. Opto-XRs (Opto-β2, Opto-α1, bPAC), or optogenetic receptors, are grouped in the centre of the graph; these chimeric proteins incorporating a rhodopsin domain and a GPCR domain, can alter intracellular signalling and gene regulation and have been used as biochemical modulators of cell activity. The remaining constructs on the graph represent the main optogenetic exciters that have been used extensively as triggers for the action potential in neurons. Mainly shown here are point mutants of the *Chlamydomonas reinhardtii* Channelrhodopsin-2 (ChR2) such as H134R, C1128A, D156A, E123T, T159C and variants of *Volvox carterii* Channelrhodopsin (VChR1). (Image from openoptogenetics.org.)

The first reported example of optogenetic control of cellular functions dates back to 2002, when Miesenbock and colleagues introduced the so-called ChARGE construct (fusion of the *Drosophila* α subunit of the heterotrimeric G-protein and the photoreceptor genes encoding for arrestin-2 rhodopsin) into vertebrate neurons, making them sensitive to light and localising the response to the cells expressing the construct only [Zemelman et al., 2002]. Although using an animal type II opsin for their experiments, whereas most applications later on employed microbial type I rhodopsins, Miesenbock and colleagues are generally considered among the pioneers of the field of optogenetics. Also pioneering was the work performed by Nagel and colleagues in 2003: ChR1 and ChR2 were introduced in HEK (Human Embryonic Kidney) and BHK (Baby Hamster Kidney) cells, besides *X. laevis* oocytes [Nagel et al., 2003]. Expression of microbial rhodopsins in mammalian cells resulted in the generation of photocurrents, mostly due to ChR2, within the millisecond time scale, recorded by electrophysiology techniques. The first studies on the heterologous expression of channelrhodopsin in different organisms or cells *in vitro* were performed after supplementing the diet or the medium with ATR [Grimm et al., 2017a; Kralj et al., 2012; Nagel et al., 2003]. When optogenetics moved into neuroscience, neurons expressed functional ChR2 also without direct ATR

supplementation, therefore ATR was not considered as a limiting factor for mammalian cells anymore. Mammals store, in fact, a basal level of ATR in their tissue whilst 11-cis retinal, the chromophore that is bound to animal rhodopsins, is not generally abundant in animal cells. This observation was inferred from the first optogenetic studies in neurons, where no ATR was supplemented to the cells in culture. However, neural growth media contain an unspecified amount of retinyl acetate, or other vitamin A derivative, which could indirectly contribute to the availability of ATR in neural cells. In other cell types, in fact, ATR has been proved to contribute to better expression and increased functionality of microbial rhodopsins for optogenetic applications [Yu et al., 2015]. In 2005, Boyden and Deisseroth at Stanford University with the collaboration of Nagel and Hegemann providing the ChR2 construct, managed to depolarise hippocampal neurons expressing ChR2-EYFP without the addition of supplements such as *all-trans* retinal in a single molecule approach [Boyden et al., 2005].

In parallel, first reports of *in vivo* optical manipulation of neuronal function were published by Nagel and Li, who achieved control of cholinergic motorneurons and muscular contractions in the worm *Caenorhabditis elegans* [Nagel et al., 2005a] and control of chick spinal chord activity in chicken embryos by targeted expression of ChR2 in activatory or inhibitory neurons [Li et al., 2005]. Later on, ON/OFF control of neuron activity was achieved by simultaneously expressing ChR2 and hyperpolarising rhodopsins, such as Halorhodopsin, in the same set of neurons. Such intriguing combination was made possible by ChR2 and Halorhodopsin spectral distinction, as shown in Figure 1.31, allowing for mutually exclusive dual control of cellular functions with the two opsins.

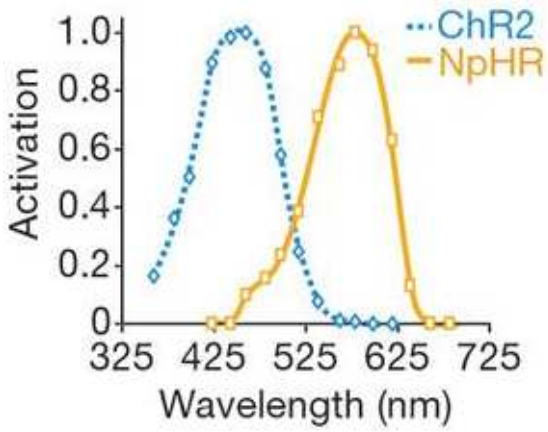


Figure 1.31: **Activation spectra of the optogenetic actuators Channelrhodopsin-2 (ChR2) from *Chlamydomonas reinhardtii* and Halorhodopsin from *Natronomonas pharaonis* (NpHR).** The wavelength distinction between the two peaks allowed for the succesful combination of these two light-gated proteins in neuroscience to achieve ON/OFF control of neuronal functions *in vitro* and *in vivo*. Adapted from [Zhang et al., 2007].

Following these studies, *in vivo* applications of optogenetics became more and more popular and the animal behaviour was widely investigated with these technologies. Transgenic mice expressing ChR2 or HR or both actuators in specific populations of neurons are now commercialised, to provide researchers with a ready-made tool for their behavioural studies [Madisen et al., 2012]. Investigations of functionality of the learning and memory, of rage and addiction and many more neural systems have been made possible by optogenetics and the practicability of interrogating only certain cells at a given time and assessing their effects on the animal behaviour [Adamantidis et al., 2007; Tye and Deisseroth, 2012a; Zhao et al., 2011]. Applications in the freely-moving animal were made possible by the progress of fiber-based technologies, allowing neurobiologists to implant an optical device directly in the brain of mice without restraining animal movement, in most cases core to understanding behavioural response.

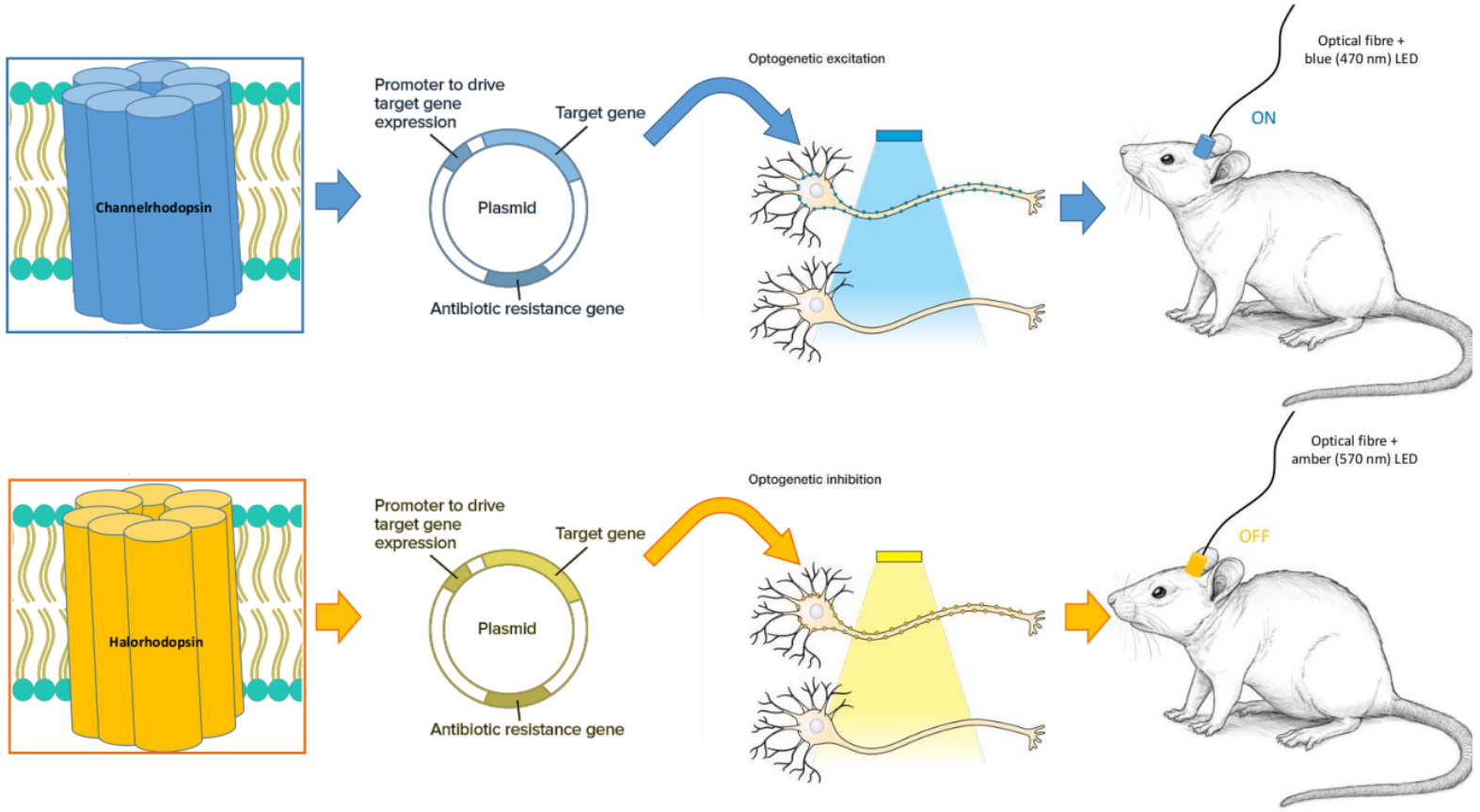


Figure 1.32: **Optogenetics conceptual schematics** The principal of optogenetic techniques to hijack cellular functions lies in the fusion of genetic engineering, microbial light-sensitive proteins and optical engineering. The diagram summarises the basic steps to achieve control of animal behaviour non-invasively using photonics, one of the main breakthrough of optogenetics. Briefly, the genes for light-gated channels, such as Channelrhodopsin-2 (ChR2) and Halorhodopsin (HR), are cloned into DNA carrier vectors. Recombinant DNA molecules are delivered to a specific subset of neurons in the brain of the animals. Expression of the photo-responsive channels allows for modulation of action potentials in genetically-engineered cells only, leaving surrounding neurons unaltered. Simultaneous expression of the two channels enables ON/OFF switch of optogenetic cells, due to depolarisation and hyperpolarisation by means of ChR2 and HR, respectively. Activation or silencing of the modified neurons is reflected in changes in the animal behaviour, which can be studied *in vivo*.

One of the major drawbacks of preliminary optogenetic studies was represented by poor expression or toxicity of the hexogenous microbial rhodopsins in mammalian systems. Expressing an exogenous protein in a cell can in fact result in potential side effects in that specific system [Allen et al., 2015]; therefore, toxicity assessment is always recommended, especially when a specific construct is inserted for the first time in a cell line. Cytotoxicity assessment should ensure that hexogenous proteins, in this case ChR2 and eNpHR, or any structure related to their expression (lipid particles, plasmids, etc.) are not adversely altering cellular well-being or functions. A variety of methodologies can be considered for the task, from histological evaluation of cell's integrity, to assays evaluating cellular metabolic activity, to electrical recordings.
Attempts at optogenetic control of neuronal function in more complex organisms, such as primates, have been performed but only recently they have produced consistent results, due to the fact that expression and functionality of optogenetic tools is highly dependent on the system chosen and requires a certain degree of optimisation. Optical control of heart and skeletal muscle *in vitro* and *in vivo* has also been achieved by different groups in parallel. Other interesting applications of the optogenetic technique include studies on retinal ganglion cells to restore vision in *Retinitis pigmentosa* or blindness and therapy for Parkinson's disease, by genetically-engineered light-responsive dopaminergic neurons [Busskamp et al., 2012; Kravitz et al., 2010]. Optogenetic control of the heart and skeletal muscle has also been reported, where the activity of contractile or pace-maker cells has been hijacked using photostimulation of light-gated ion channels [Arrenberg et al., 2010; Bruegmann et al., 2015].

Widely used in neuroscience to trigger deterministic activity in excitable cells and only recently in non-neuronal cell lines [Arrenberg et al., 2010; Bruegmann et al., 2015; Deneke et al., 2019; Efetova et al., 2013; Krueger et al., 2018; Makadia et al., 2018; Sato et al., 2017], ChR2 and HR both induce ionic fluxes across the cell membrane that would be expected to cause cell swelling and/or an increase in fluid ransport. The speculation behind the present work is that optogenetics may have an unexplored potential application towards clarifying the molecular basis of ubiquitous cellular pro-

cesses such as membrane transport of solutes and fluids, whose impairments are often the causes for a variety of diseases. Complementary with other established techniques, such as Ussing chamber electrophysiology and functional imaging, optogenetics could help unravel grey areas in our knowledge of the health and disease of tissues by imposing non-invasive, reversible and graded precise stimuli to populations or subsets of cells in vitro, in order to unpick the fundamental biophysics associated with homeostasis, volume regulation and fluid transport. While much is known about the ion transport complement in individual epithelia, there remains debate regarding the fundamental mechanisms underlying isotonic fluid transport and volume homeostatis in single cells [Fischbarg, 2010; Mathias, 1985], therefore there is growing interest in studying these phaenomena as a route to unmasking therapeutic strategies and mitigating against their dysregulation. In the present thesis, the applicability of the optogenetic rationale to epithelial cells will be explored, starting from an epithelial cell line derived from the human retina, to validate applicability of the optogenetic toolkit to areas outside neurobiology and widen the interest beyond excitable cells. I will report the construction, optimisation and characterisation of optogenetic tools that can be exploited to study and control cellular functions of epithelia. The tools described in the present work have the potential to be used to obtain a better understanding of the molecular bases of both the physiology of the epithelial tissue and the factors behind its dysfunctions, resulting in the onset of pathologies, such as AMD.

It was my motivation through this work to demonstrate that optogenetics has the potential to become an indispensable aid to biologists in all fields, including epithelial physiology, by providing access to the fundamental ion transport processes at the heart of homeostasis and fluid regulation. Ion transport processes are the foundation of biological life itself, therefore a non-invasive way to control and study such phenomena would prove invaluable to life sciences research.

Epithelial main functions are based on fine tuning of fluid and solutes transport across the cell membrane and across epithelial layers [Lewis, 1996]. Modulating such function with light will allow us to understand further how specific systems and ion transport processes contribute to pathophysiology. In this work, a set of optogenetic tools was

created and employed to achieve precise time- and space-resolved control of epithelial transport.

Chapter 2 contains a delineation of the methodologies used and optimised in the present work. In order to develop an imaging system capable of the different tasks required for the optogenetic control of mammalian cells *in vitro*, considerable effort was devoted, throughout the present study, to the construction of an integrated optical instrument around a conventional inverted light microscope. Implementation of the microscope with specific optical filters and components resulted in the development of a tool for the simultaneous photostimulation of the light-gated proteins and the recording of ion dynamics through the monitoring of ion-sensitive fluorescent indicators. Changes in ion permeabilities across the epithelial cell membrane and readout of cell output following light stimuli were achieved optically, removing the need for pharmacological agents or invasive microelectrodes.

Chapter 3, focused on optimising the expression of the heterologous optogenetic proteins in the epithelial cell line of choice, due to the unreported nature of such expression in the ARPE-19 cells. Screening of diverse approaches to deliver the exogenous genetic material to the ARPE-19 cells was performed in order to optimise the transfection procedure and maximise efficiency of the optogenetic-transformed cells (Section 3.1). Once the most suitable method was identified, tuning of the protocol was performed to maximise delivery efficiency and, therefore, expression. Expression levels of wtChR2 and eNpHR were studied quantitatively, by flow cytometry (Section 3.1.1), to have an index of the optogenetic-modified cells and qualitatively, by confocal fluorescence microscopy, to highlight sub-cellular localisation of the transport proteins (Section 3.1.4). Considering the novel nature of the study, cytotoxicity of microbial rhodopsins in the retinal epithelial cell line was investigated (Section 3.1.2), as recommended by Allen and colleagues in [Allen et al., 2015].

The following step involved assessing the functionality of the channels, i.e. their ability to respond to light stimuli and modify ion permeability across the membrane of the ARPE-19 epithelial cells. Activity of the optogenetic proteins was confirmed by the use of ion-sensitive fluorophores, which allow monitoring of intracellular ion dynamics.

The light-triggered opening of ChR2 and eNpHR should in fact result in a change in ion permeabilities for calcium and chloride, respectively. ChR2 activity was confirmed by studying intracellular calcium concentration changes following activation of the light-responsive optogenetic channel. Calcium was chosen because, besides its permeability through ChR2, it plays an important role in several regulation mechanisms in the RPE, among which volume homeostasis [Wimmers et al., 2007; Wimmers and Strauss, 2007]. Initial research focused on wtChR2 but preliminary experiments demonstrated that the wild-type channel failed to appreciably change calcium dynamics within the ARPE-19 cells (Section 3.2).

To overcome limitations of wtChR2, which is characterised by low channel conductance and rapid, slowly-reversible gating, my work moved to the selection and generation of point mutants of ChR2, designed to both modify overall membrane flux and longevity. Chapter 4 addresses the limitations of the wild type and expands the pool of candidate optogenetic tools to test for epithelial physiology by describing different single amino acid mutants of ChR2 with modified channel properties, generated via site-directed mutagenesis. Four point mutations, namely E123T, C128A, L132C and T159C were introduced into the sequence of ChR2 and characterised for their behaviour in the ARPE-19 cell line. An additional construct, the variant H134R, was purchased from an optogenetic repository and tested alongside the other mutants. These ChR2 variants have been reported in the literature within neuronally-targeted vectors [Lin, 2011]. The present study describes the recreation of defined ChR2 mutants within a more versatile vector (pcDNA3.1) that will be of use to other researchers willing to bring optogenetics outside applications in electrically active tissues into the field of epithelial transport.

Analysis of intracellular calcium dynamics by calcium imaging confirmed functionality of three ChR2 mutants, namely L132C, H134R and T159C in the ARPE-19 cells, with the L132C mutant appearing as the most suitable for combination with calcium imaging experiments (Section 4.3). Mutagenesis-generated variants and the construct H134R from Addgene were characterised in terms of their responsiveness to light irradiance (mW/mm^2), recovery of their response and behaviour in reaction to increasing length of stimuli. These data, reported in Section 4.3.2, are useful for the selection of

the most suitable variant for further investigation of epithelial ion and fluid transport, based on the different properties reported for these ChR2 mutants.

The results reported in this study demonstrate that optogenetic tools like ChR2 can be adapted to control and study the activity of specific ions, such as calcium, on physiological processes in epithelial cell models.

Translating these methods towards the optimised expression of eNpHR in combination with these ChR2 mutants is encouraging for further investigation of epithelial ion and water transport non-invasively using light-sensitive proteins and photonics, in order to provide further insights into these vital processes of epithelial tissues.

Chapter 2

Materials and Methods

2.1 Molecular biology

2.1.1 Plasmid design and description

The plasmids pcDNA3.1 eNpHR-EYFP and pcDNA3.1 wtChR2-mCherry used in the present study were generated by subcloning and kindly provided by collaborators in the group and are schematically represented in Figure 2.1.

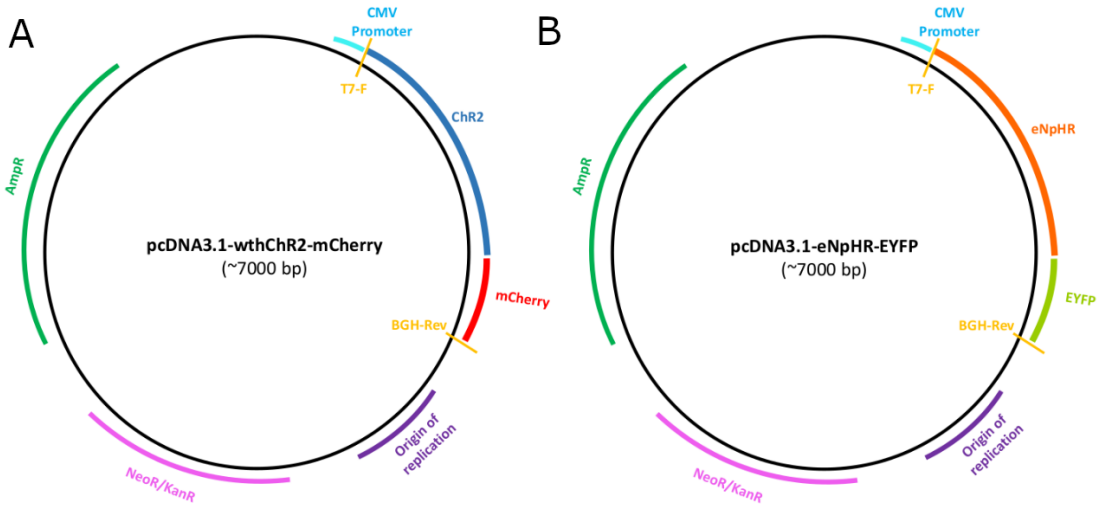


Figure 2.1: **Schematic representation of the high expression level plasmids encoding for the optogenetic tools used in the present thesis.** pcDNA3.1 is a versatile expression vector for most mammalian cell lines. Its main features are summarised in the figure and include: cytomegalovirus (CMV) enhancer-promoter for maximisation of expression in eukaryotic cells; ampicillin resistance gene (AmpR) and an origin of replication for amplification and selection in *E. coli*; neomycin/kanamycin resistance gene (NeoR/KanR) for selection of stable transfectants in mammalian colonies. **A** Plasmid vector for the fusion protein wtChR2-mCherry and **B** eNpHR-EYFP. *Original drawing.*

The enhanced Halorhodopsin gene from *Natronomonas pharaonis* (eNpHR) was

subcloned from pLenti-CaMKIIa-eNpHR-EYFP-WPRE (Addgene 20946) into pcDNA3.1 plasmid. The Channelrhodopsin-2 (ChR2) gene was subcloned from pLenti-CaMKIIa-hChR2(C128A)-EYFP-WPRE (Addgene 20293) into pcDNA3.1 plasmid and the mutation C128A was reverted to the wild type (A128C). pcDNA3.1-hChR2-H134R-mCherry was purchased from Addgene (Addgene, Teddington, UK) (Figure 2.2). All the above plasmids were deposited by Karl Deisseroth laboratory from Stanford University.

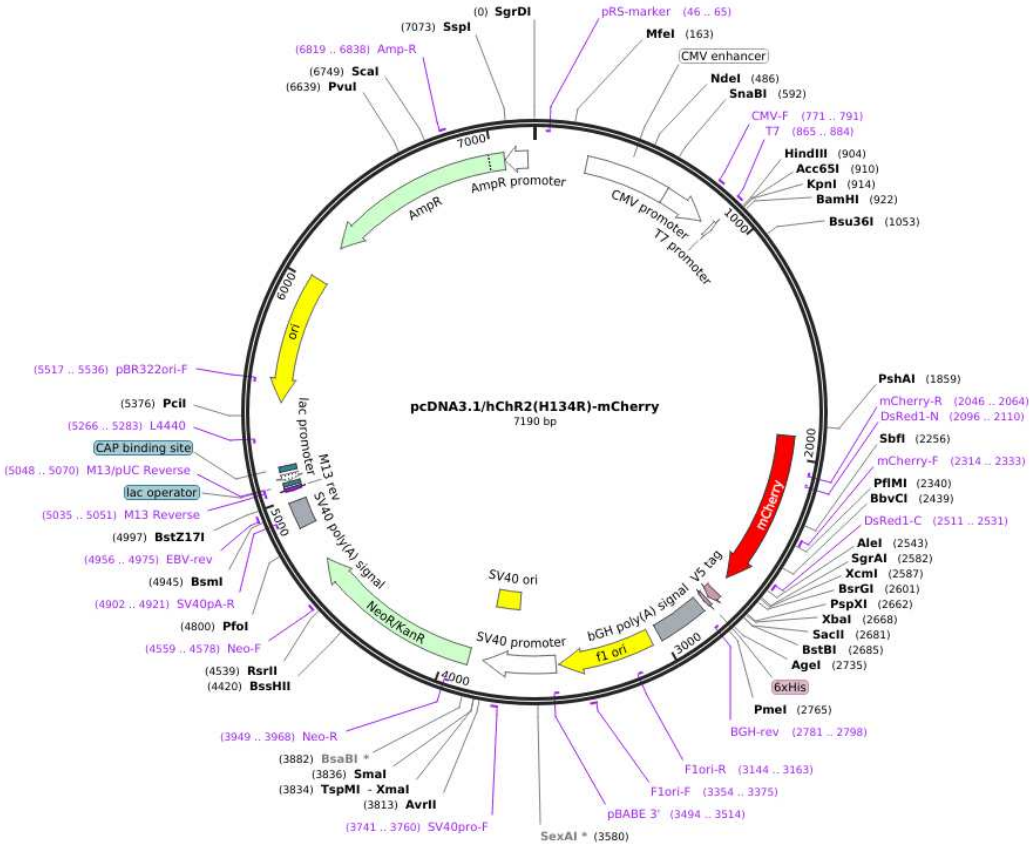


Figure 2.2: **Maps of the plasmid pcDNA3.1-hChR2(H134R)-mCherry**, purchased from Addgene repository to be tested in epithelial cells, alongside ChR2 mutants. Image from Addgene.

For the present study, the ChR2 variant optimised for the *Homo sapiens* codon usage, hChR2, was chosen for better expression in human systems. The enhanced halorhodopsin eNpHR is engineered with an endoplasmic reticulum escaping sequence [Gradinaru et al., 2008], in order to facilitate delivery to the plasma membrane of transfected or transduced cells and avoid accumulation in the endomembranes.

During the subcloning procedure, ChR2 gene was fused in frame with the sequence for mCherry fluorophore, whilst eNpHR fusion to the enhanced yellow fluorescent protein (EYFP) was not modified. The resulting fusion proteins are opsins tagged with two

different fluorophores, whose excitation and emission spectra do not overlap. Moreover, fluorescent tags present no crosstalk with the activation wavelength for either of the two opsins.

2.1.2 Plasmid sequence validation

All plasmids used in the present work were sequenced using Sanger DNA sequencing [Sanger et al., 1977] in the form of capillary sequencing, performed by SourceBioscience (Nottingham, UK). Received plasmids were sequenced to confirm correct insertion of the genes in the multi-cloning site (MCS) of pcDNA3.1 and integrity of the genetic sequence for ChR2 and eNpHR and their fusion to the fluorescent reporters. Results obtained from the forward and reverse primer for each sequence were merged with EMBOSS (European Molecular Biology Open Software Suite) Merger tool [Rice et al., 2000] using the default parameters to obtain the complete sequences and analysed using FinchTV software (Geospiza) for the generation of chromatograms, i.e. the visual representation of the order of nucleotides in a nucleic acid sequence obtained by sequencing methodologies. DNA sequence obtained from Sanger sequencing was translated using Expasy Translate Tool and protein sequences were aligned with Clustal Omega (EMBL-EBI) with the sequences from the lentiviral vectors originally obtained from Addgene. Figures 2.3 and 2.4 show alignment of the open reading frames (ORFs) of wtChR2-mCherry and eNpHR-EYFP with their original viral-encoded sequences. The sub-cloning procedure, performed by our collaborators before this PhD, was successful and did not affect the integrity of the sequences and fusion with the fluorescent tags was confirmed.

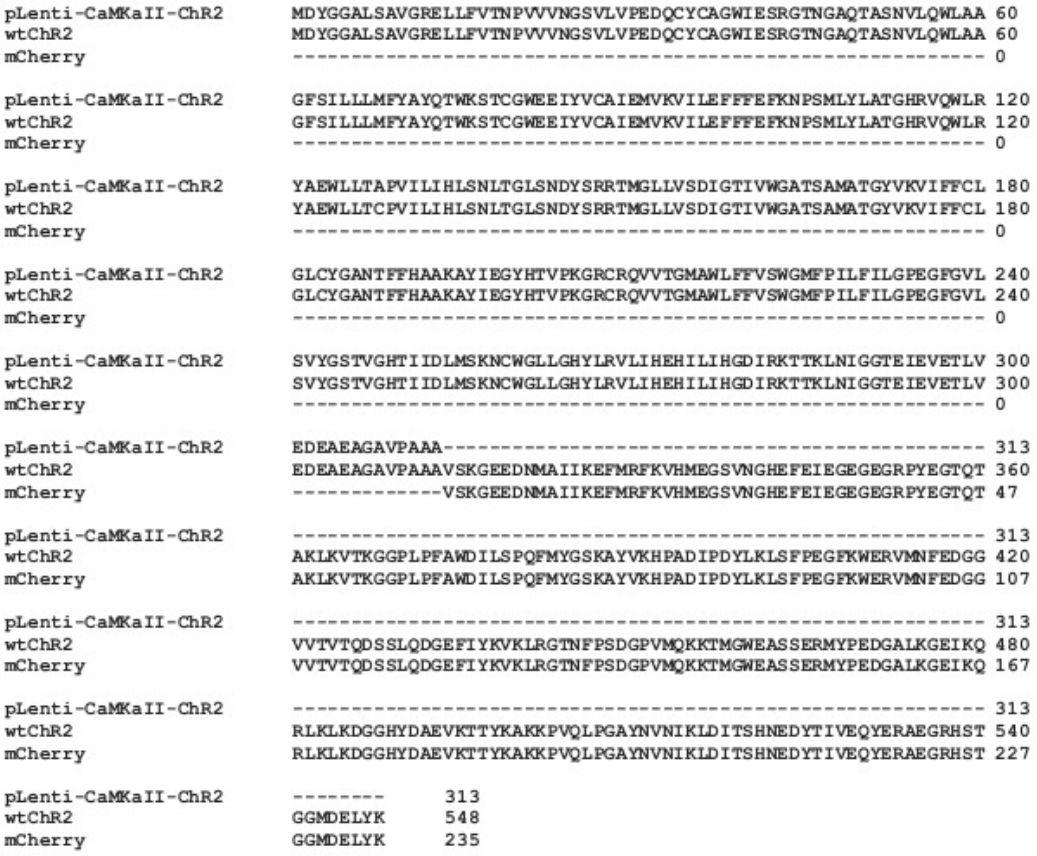


Figure 2.3: **Sequence alignment of wtChR2 showing integrity of sequence after subcloning.** Comparison reveals integrity of the ChR2 sequence and successful fusion with mCherry tag sequence, confirmed by the identity of each amino acid in the alignment. DNA sequence obtained from Sanger sequencing was translated using Expasy Translate Tool and protein sequence was aligned with the ChR2 sequence from pLenti-CaMKIIa-ChR2-EYFP-WPRE vector, from which the protein was originally subcloned from, and mCherry sequence, to which ChR2 was fused to.



Figure 2.4: **Sequence alignment of eNpHR showing integrity of sequence after subcloning.** Comparison reveals integrity of the eNpHR-EYFP fusion protein sequence, confirmed by the identity of each amino acid in the alignment. DNA sequence obtained from Sanger sequencing was translated using Expasy Translate Tool and protein sequence was compared with the eNpHR sequence from pLenti-CaMKIIa-eNpHR-EYFP-WPRE vector, from which the protein was originally subcloned from. Alignment was performed using Clustal Omega (EMBL-EBI) multiple sequence alignment tool.

2.1.3 Site-directed mutagenesis

Site-directed mutagenesis (SDM) 1.3 was performed to create four different point mutants of the protein ChR2 and to compare their properties in epithelial cells in order to overcome limitations of the wild type ChR2. There are several ways of performing SDM: in this case, a Site-directed Mutagenesis Kit (QuikChange II XL, Agilent Technologies, Stockport, UK), schematised in Figure 2.5, was used to create four point mutants of ChR2, namely E123T, C128A, L132C and T159C (for description of mutants in detail see Section 1.2.1.3), according to the schematic SDM workflow shown in Figure 2.6.

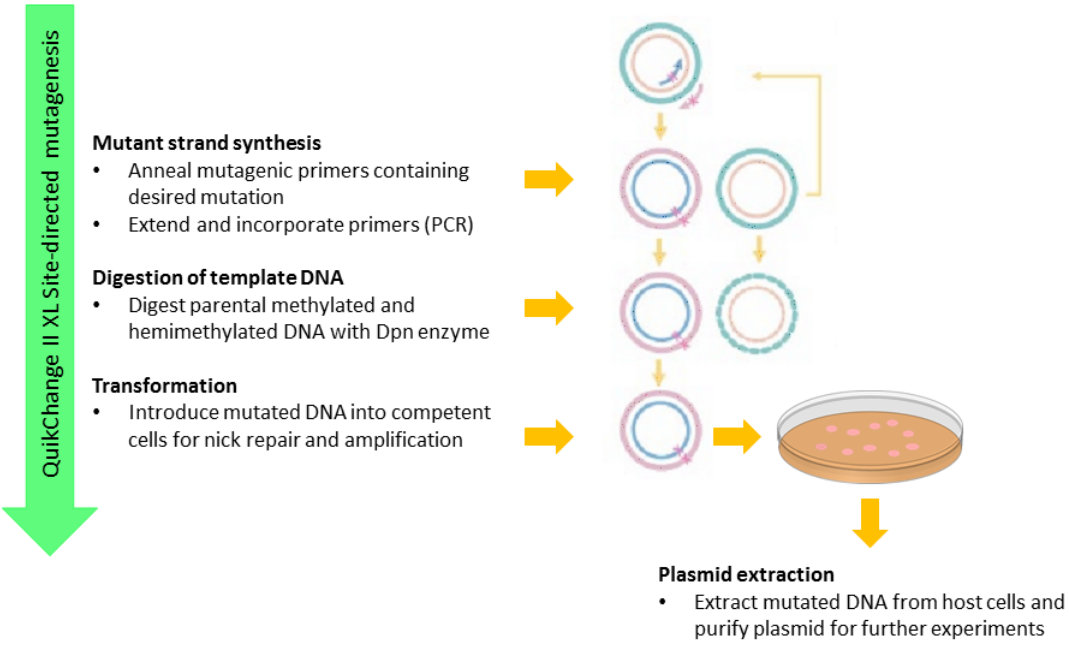


Figure 2.5: **Overview of the core steps of the QuickChange II XL Site-directed Mutagenesis procedure (Agilent Technologies).** The flow chart shows the main steps in the SDM procedure used to create ChR2 point mutants in the present work. Following the mutagenesis procedure, DNA with the desired mutations can be extracted, purified and used for further experiments, such as transfection of mammalian cells. Adapted from Agilent.

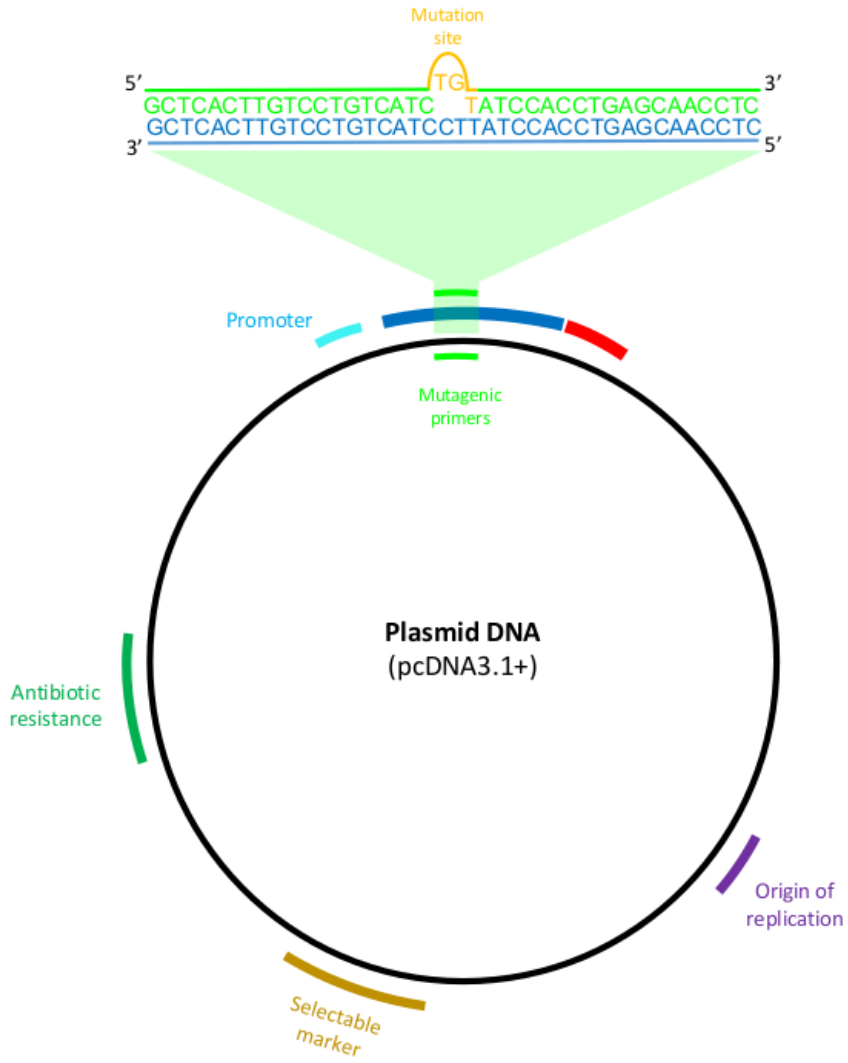


Figure 2.6: **Schematics describing the site-directed mutagenesis process performed to introduce point mutations in the structure of wt ChR2 to generate the mutants E123T, C128A, L132C and T159C.** In the figure, a schematic view of pcDNA3.1 plasmid is shown with the sequences for the wtChR2 and its fluorescent tag mCherry are highlighted in blue and red, respectively. Mutagenic primers are overlayed to the insert sequence in green and the top shows how the mutagenic primer introduces the point mutation, in this case L132C, when annealing with the gene in the plasmid during a polymerase chain reaction (PCR). *Original drawing.*

SDM was carried out following the manufacturer's instructions. Briefly, wtChR2-mCherry in pcDNA3.1 was used as a double-stranded DNA (dsDNA) template for a polymerase chain reaction (PCR). High-performance liquid cromatography-purified (HPLC) primers (Eurofins Genomics) were designed to introduce mutations in the sequence and result in the desired mutant fused to mCherry as a fluorescent tag. The primers' sequences are showed in Table 2.1.

PRIMER	PRIMER SEQUENCE (5'-3')
E123T (f)	CAGTGGCTGCGCTATGCA ACC TGGCTGCTCACTTGTCC
E123T (r)	GGACAAGTGAGCAGCCA GGT TGCATAGCGCAGCCACTG
C128A (f)	CTATGCAGAGTGGCTGCTCACT GCC CCTGTCATCCTTATC
C128A (r)	GATAAGGATGACAGG GGC AGTGAGCAGCCACTCTGCATAG
L123C (f)	GCTCACTTGTCCTGTCATC TGT ATCCACCTGAGCAACCTC
L123C (r)	GAGGTTGCTCAGGTGGAT ACA GATGACAGGACAAGTGAGC
T159C (f)	GTCTCAGACATCGGG TGT ATCGTGTGGGGGGC
T159C (r)	GCCCCCCACACGAT ACA CCCGATGTCTGAGAC

Table 2.1: **List of mutagenic primers, forward (f) and reverse (r) designed and used for the generation of ChR2 variants via site-directed mutagenesis.** Mutated codons are are highlighted and colour-coded for ease of reference throughout this thesis. Length of primers varies between 32 and 40 base pairs (bp), in order to reach a desirable T_m (melting temperature) that would favour annealing with the template strand and therefore maximise the mutagenesis efficiency during the polymerase chain reaction (PCR).

Control and sample PCR reactions were set up using 10 ng dsDNA template, diluted in the recommended reaction buffer, provided with the kit. To demonstrate the efficiency of the QuikChange method, the pWhitescript 4.5-kb control plasmid was used as a mutagenesis control. The control plasmid contains a stop codon (TAA) at the position where a glutamine codon (CAA) would normally appear in the β-galactosidase gene of the pBluescript II SK(-) phagemid, resulting in a truncated, therefore non-functional, enzyme. The oligonucleotide control primers provided with the kit create a point mutation that reverts the truncated protein to the wild type. For screening the colonies that have undergone mutagenesis, a chromogenic substrate known as X-gal is added to the LB agar plate. If functional β -galactosidase is produced, X-gal is hydrolyzed to form 5-bromo-4-chloro-indoxyl, which spontaneously dimerises to produce an insoluble blue pigment called 5,5'-dibromo-4,4'-dichloro-indigo. Isopropyl β-D-1-thiogalactopyranoside (IPTG) is used along with X-gal for blue-white screening. IPTG is a non-metabolizable analog of galactose that induces the expression of lacZ gene. Therefore, following transformation, the blue-phenotype colonies resulting from X-gal metabolism will give an index of the mutagenesis efficiency, as shown in Figure 2.7.

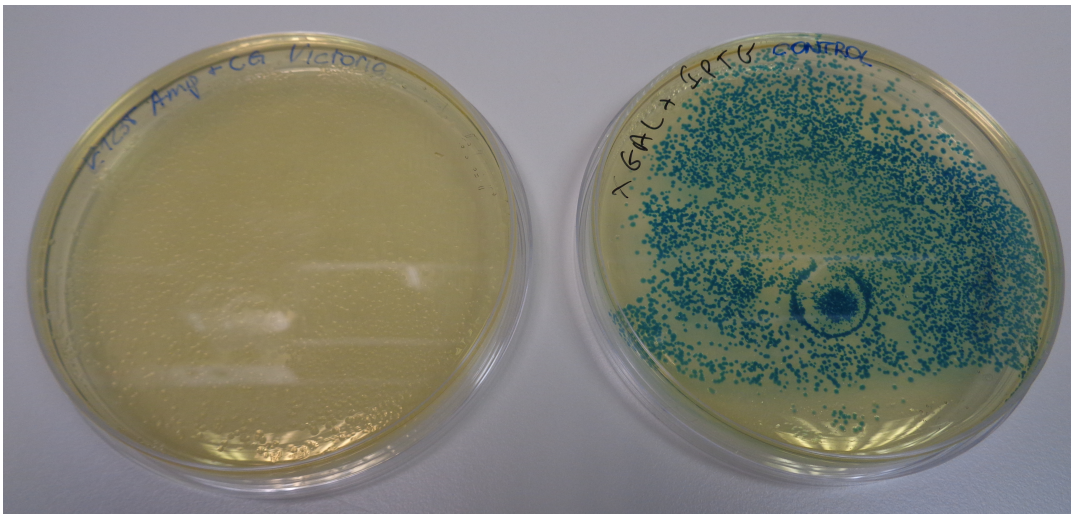


Figure 2.7: **Blue-white screening for the evaluation of mutagenesis efficiency.** Agar plates plated after transformation of bacteria with the mutated sequences of ChR2 (E123T, C128A, L132C, T159C). Mutagenesis control with pBluescript II SK(-) phagemid, right, and representative sample colonies for E123T, left (representative image; data for other mutants not shown). The blue phenotype in the mutagenesis control gives an index of mutagenesis efficiency, in this case the success rate of the introduction of the desired single amino acid mutations in the sequence of wtChR2.

Following mutant strand synthesis, 1 μl DpnI restriction enzyme was added to each amplification reaction and the mixture was incubated at 37°C for an hour. DpnI endonuclease activity is specific for methylated and hemimethylated DNA and was used to digest parental DNA template and to select for mutation-containing newly synthesised DNA. The vector DNA incorporating the desired mutation was then transformed into *Escherichia coli* XL-10 Gold ultracompetent cells and internalisation of the plasmid was induced with thermal shock at 42°C in a water bath for 30 seconds. The transformed cells were then grown for 1 h at 37°C before plating the appropriate volume on agar plates containing ampicillin as the selective antibiotic for pcDNA3.1. Plates were incubated overnight at 37°C: single colonies were then resuspended in liquid culture and grown overnight in a shaking incubator, before proceeding with plasmid extraction (see Section 2.1.4). All plasmids were then sequenced using Sanger capillary sequencing (SourceBioscience, Nottingham, UK) to check for presence of the correct point mutation and integrity of the fusion protein (see Section 2.1.2).

2.1.4 Plasmid amplification and purification

The gene for the H134R mutant of ChR2 was purchased from Addgene (catalogue number: 20938) in a pcDNA3.1(+) vector, fused with the sequence for mCherry fluorescent

protein, provided as bacterial stab in agar. Upon arrival, the plasmid was recovered through the process recommended by the manufacturer.

Briefly, plasmid-containing bacteria were streaked for single colonies onto agar plates (1.5% Select Agar + Circlegrow) in ampicillin selective medium (100 μg/mL). Colonies were left to grow overnight (16-18 h) in a static incubator at 37°C. Following incubation time, single colonies were resuspended in vials containing 5 mL growth medium, supplemented with ampicillin, that is the selective antibiotic for the pcDNA3.1 vector. The vials were incubated again overnight on a shaking incubator at 37°C. On the following day, colonies were amplified in 25 mL growth medium and left growing overnight on the shaking incubator. After incubation, plasmid extraction was performed following the instructions of the QIAGEN MidiPrep Kit (QIAGEN, Manchester, UK). Briefly, the cell suspension was centrifuged for 15 min at 4°C at 5000 rpm (revolutions per minute) to harvest the bacterial cells.

After centrifugation, the supernatant was decanted and the pellets were resuspended in 4 mL of the resuspension buffer P1. 4 mL of the lysis buffer P2 (200 mM NaOH, 1% SDS) were added to the cells and the vial was vigorously inverted to ensure proper mixing and the mixture was incubated for 5 min at room temperature. Four mL of chilled neutralisation buffer P3 (3.0 M potassium acetate, pH 5.5) were added to the tubes and the lysate was poured into the barrel of the QIAfilter cartridge and incubated for 10 min at room temperature.

After incubation, the plunger was gently inserted and the lysate was pressed into new tubes. 1 mL of endotoxin removal buffer (ER) was added to the lysate and the tubes were incubated on ice for 30 min. The endotoxin removal buffer prevents endotoxin molecules from binding to the resin in the QIAGEN-tips allowing purification of DNA containing less than 0.1 endotoxin units per μg plasmid DNA. In the meantime, QIAGEN tips were equilibrated by applying 4 mL of endotoxin-free equilibration buffer QBT (750mM NaCl, 50 mM MOPS, pH 7.0, 15% isopropanol, 0.15% Triton® X-100) and the column was allowed to empty by gravity flow. After incubation time, the filtered lysate was applied to the QIAGEN tip and allowed to enter the resin by gravity. The QIAGEN-tip was then washed with 10 mL QC wash buffer (1.0M NaCl, 50mM

MOPS, pH 7.0, 15% isopropanol) twice. The DNA was finally eluted with 5 mL of elution buffer QN (1.6M NaCl, 50 mM MOPS pH 7.0, 15% isopropanol). To precipitate the eluted DNA, 3.5 mL of room temperature isopropanol were added to the DNA. The mixture was centrifuged immediately at 4600 rpm for 90 min. After centrifugation, the supernatant was carefully decanted and the pellet was washed with 3 mL of endotoxin-free 70% ethanol and centrifuged for 20 min at 4600 rpm. The pellet was then air-dried for 10-15 min and the DNA was redissolved in 100 μl of endotoxin-free buffer TE (10mM Tris-Cl, pH 8.0, 1mM EDTA). The pellet was allowed to resuspend overnight at 4°C. Concentration of the extracted plasmids was then measured with a NanoDrop 1000 spectrophotometer (Thermo Fisher Scientific), which quantifies nucleic acids in the sample by reading its absorbance at 260 nm.

2.2 Cell culture

2.2.1 General cell culture procedures

2.2.1.1 Cell maintenance

The ARPE-19 cells were purchased from the American Type Culture Collection (CRL-2302^{TM}, ATCC) and cultured in standard culture medium Dulbecco's Modified Eagle's Medium with Ham's F-12 Nutrient Mixture (DMEM/F12, Sigma Aldrich, Gillingham, UK), supplemented with 10% fetal bovine serum (FBS; Invitrogen, Paisley, UK), 1% penicillin–streptomycin (Sigma Aldrich) and 1% L-Glutammine (Sigma Aldrich). Cells were kept in culture up to passage 30 and incubated at 37°C, 5% CO_2 and 90% humidity. Growth media was routinely replaced every 48 h and cells were subcultured when they reached 90% confluence in the flasks. Cell growth was checked under an optical microscope to determine confluence. For sub-culturing, growth medium was removed and cells were washed with Dulbecco's phosphate buffer saline (DPBS), in order to remove traces of serum proteases that would have inhibited trypsin activity. 1X Trypsin EDTA (Sigma Aldrich) was added directly to the cells and the flask was incubated at 37°C for 5 min. Following trypsin digestion, the same volume of complete medium was added to the flask to stop the enzyme digestion activity. Cells were then collected

in a 15 mL Falcon tube and centrifuged at 1500 rpm at 15°C for 5 min. After spinning, medium was removed and cells were resuspended in 1 or 2 mL fresh pre-heated DMEM-F12. Depending on the nature of the experiments, cells were plated onto different supports at the required densities: glass-bottom petri dishes (Ibidi) for imaging and photostimulation; 24-well plates (Corning) for flow cytometry; 96-well plates for cytotoxicity studies.

2.2.1.2 Preparation of frozen stocks and cell revival

Frozen stocks were prepared to keep renewing the pool of cells. ARPE-19 cells were trypsinised to detach from the flask and centrifuged at 1500 rpm to obtain cell pellet. The pellet was resuspended in 1 to 5 mL, depending on cell confluence, complete medium supplemented with 10% DMSO (Di-methyl sulfoxide), used as a cryoprotective agent. Cell suspension was transferred into sterile cryovials and allowed to freeze gradually in the -80°C freezer before long-term storage in liquid nitrogen vapour. Cells from frozen aliquots were thawed by swirling in the water bath at 37°C. The content of the cryovial was then quickly transferred into a 15 mL centrifuge tube and the suspension was centrifuged at 1500 rpm for 5 min to obtain the cell pellet and remove DMSO, detrimental to the cells, from the suspension. The so-obtained pellet was resuspended in 1 or 2 mL of fresh pre-heated growth medium and cells were seeded on the different supports as needed depending on experiments. Cells were allowed to recover from the freezing/thawing process for at least two passages before proceeding with experimental work.

2.3 Cytotoxicity assessments

2.3.1 MTS assay: opsin cytotoxicity

The MTS *in vitro* cytotoxicity assay is a convenient method for assessing cell viability [Morgan, 1998], based on the reduction by dehydrogenases of a tetrazolium compound by viable cells to generate a purple formazan product that is soluble in cell culture media [Fotakis and Timbrell, 2006]. It therefore provides a sensitive quantification of viable cells in proliferation. Its main components are 3-(4,5-dimethyl-thiazol-2-yl)-5-

(3-carboxymethoxyphenyl)- 2-(4-sulfophenyl)-2H-tetrazolium (or MTS) and an electron coupling reagent (phenazine ethosulfate; PES).

The main features of this assay are its ease of use, accuracy and rapid indication of toxicity. Therefore, the number of viable cells is directly proportional to the amount of formazan produced and it can be quantified by measuring its absorbance at 490 nm.

For the present study, CellTiter 96® AQueous One Solution (Promega, Southampton, UK) was used. Briefly, cells were seeded in a 96-well plate at a density of 10^4 cells per well and incubated at 37°C, 5% CO_2 for 24 h. Seeding density was chosen as it produces an absorbance value within the linear range of the assay, as recommended by the manufacturer. After 24 h, cells were exposed to Lipofectamine 3000 (Invitrogen) and opsin plasmids, separately and together, to test if any of the reagents involved in the expression, besides optogenetic proteins themselves, could have any cytotoxic effect. Two days post-transfection, 20 μl of MTS reagent were added to 200 μl of cell culture medium and the plate was incubated for 4 h at 37°C. After incubation time, absorbance was recorded on a microplate reader (Biorad-Model 680) at 490 nm. A cell-culture buffer, in this case HBSS (Hank's Balanced Salt Solution, Sigma Aldrich) served as a negative control while a known toxic compound, in this case Distel (formerly Trigene, a halogenated tertiary amine compound with a blend of surface active disinfectants and detergents), supplied the positive controls. All conditions were repeated in triplicates and means calculated for each set of measurements; background readings of culture medium without cells were subtracted from the values obtained. The relative cell metabolic activity (%) was calculated using the following equation:

$$CV = \frac{(S - T)}{(H - T)} \times 100 \tag{2.1}$$

where: CV= cell viability, based on relative metabolic activity, S= absorbance for the tested samples, T= absorbance with toxic compound (in this case Distel, formerly known as Trigene), positive control, H= absorbance with HBSS, negative control. Cell viability values $\geq$ 80% are considered non-toxic [Malich et al., 1997].

2.3.2 Live/dead assay: all-trans retinal (ATR) cytotoxicity

All-trans retinal (ATR) as a chromophore for the functionality of rhodopsins for optogenetic purposes has been mainly supplemented to non-mammalian organisms (such as *Drosophila melanogaster* and *Caenorhabditis elegans*) for optogenetic experiments, although there are reports of ATR supplementation to HEK-293 [Yu et al., 2015] cells and cardiomyocytes[Arrenberg et al., 2010].

Considering ATR's diverse roles in different tissues, it is important to evaluate its potential negative effects on cell viability. Calcein AM and propidium iodide dyes, commonly referred to as live/dead stains, were used in this study to assess cytotoxicity [Youn et al., 2011]. The live/dead assay is a routinely-used assay to study cell viability following treatments and the 96-well plate is an ideal vessel for preliminary results. Evaluation of cytotoxicity was performed in a 96-well plate using calcein AM, a membrane permeable dye, which is esterified by cellular esterases of live cells, and propidium iodide, a membrane-impermeable dye that shifts its fluorescence and increases its signal 20-fold when bound to damaged DNA from dead cells.

Briefly, ARPE-19 cells were seeded at a density of 10^4 cells per well in a black 96-well plate with transparent bottom (3603, Corning Costar, Flintshire, UK). Cells were kept in culture for 48 h in ATR-supplemented medium with ATR concentrations ranging from 0.1 to 30 μM. Viability of cells grown under these conditions was compared to viability of cells grown in standard growth medium (DMEM F12-Ham, 10% FBS, 1% Penicillin/Streptomycin, 1% L-Glu). Cells were stained with the dye solution (HBSS-HEPES 20 mM, calcein AM, 2μM; Propidium Iodide, 2μM; Hoechst 33342, 2μM, all from Thermo Fisher Scientific) and incubated at room temperature for 30-45 min. The dye solution was not washed after incubation to prevent loss of dead floating or detached cells. The plate was imaged with the ImageXpressUltra (BioTek) confocal microplate reader, which allows simultaneous recording of fluorescence intensity and acquisition of images of the cells in the wells.

2.4 Transfection

2.4.1 Transfection optimisation

Optimisation of plasmid expression in mammalian cells depends on optimising plasmid DNA uptake, which was pursued using a battery of methods to achieve the highest transfection efficiency.

2.4.1.1 Lipofection

Lipofection is a lipid-nanoparticle based technique designed to target exogenous genetic material into eukaryotic cells (see 1.3). The main advantages of lipofection are its high efficiency, its ability to transfect all types of nucleic acids in a wide range of cell types, its ease of use, reproducibility and low toxicity. In addition, this method is suitable for both transient and stable transfection, i.e. the genetic material can be temporarily or permanently expressed by the cells.

Lipoplexes Lipofectamine 3000 (Invitrogen) is an advanced lipid-based transfection reagent. It has been optimised for hard-to-transfect cell lines and shows high transfection efficiencies varying from one cell line to another. ARPE-19 cells were seeded to be 80-90% confluent at the moment of transfection and the procedure was carried out following manufacturer's instructions. Briefly, plasmid DNA was mixed with P3000 reagent to enhance the formation of stable complexes to be incorporated in the lipid carriers. DNA-lipofectamine ratio throughout experiments was 1:3, while DNA-P3000 ratio was 1:2. Lipid-DNA complexes were formed in serum-free medium (Optimem) and incubated at room temperature for approximately 15 min. Growth medium was replaced at least 2 h before transfection with the antibiotic-free medium. Following incubation, the lipoplexes were added to the cultured cells dropwise. Cells were incubated at 37°C for 24-48 h prior to evaluation of transfection outcomes.

Lipoplexes/Polyplexes DreamFectGold (OZ Biosciences) is a transfection reagent based both on cationic lipids (lipoplexes) and polymers (polyplexes), designed on the so-called Tee-Technology (Triggered Endosomal Escape), which combines and exploits

the properties of both entities to achieve extremely efficient nucleic acid delivery into the target cells. This new generation of lipopolyamines contains a hydrophobic part and a charged polyamine moiety. These components allow the release of large nucleic acid amounts in the cytosol and increase DNA nuclear uptake. Briefly, cells were seeded on a 24-well plate to be 70% confluent on the day of transfection. DNA-polyamine complexes were prepared following the manufacturer's instructions. Briefly, DNA and recommended amounts of DreamFectGold were mixed and incubated at room temperature for 20 min. Following incubation, the mixture was added to the cells, which were then incubated for 24-48 h at 37°C before analysis.

2.4.1.2 Magnetofection

Magnetic nanoparticles/polyplexes PolyMagNeo (OZ Biosciences) is a novel magnetofection reagent in which iron oxide magnetic nanoparticles are coated with cationic molecules. DNA-nanoparticles complexes were prepared following the manufacturer's instructions, incubated at room temperature for 20 min and then added to the cells. The cells were then incubated at room temperature for 20 min on the magnetic plate (see Figure 2.8) and, once removed the plate, put back into the incubator, until analysis 24-48 h later.

Magnetic nanoparticles/lipoplexes CombiMag (OZ Biosciences) is a magnetofection reagent which can be combined with any other commercially available transfection system, in order to improve their efficiency. It works as an enhancer employing a magnetic field to deliver genetic material into the cells. In this study, CombiMag was combined with Polyplus JetPrime and DreamFectGold. Magnetofectamine, another magnetic transfection reagent, is the association of Lipofectamine 2000 (Life Technologies) and CombiMag reagents. DNA-nanoparticle complexes were prepared following the manufacturer's instructions (OZ Biosciences) and were then added to the cells, seeded on a 24-well plate on the previous day, in order to be 70-90% confuent at the moment of transfection. The cells were then incubated at room temperature for 20 min on the magnetic plate and subsequently put back into the incubator, until analysis 24-48 h later 2.8.

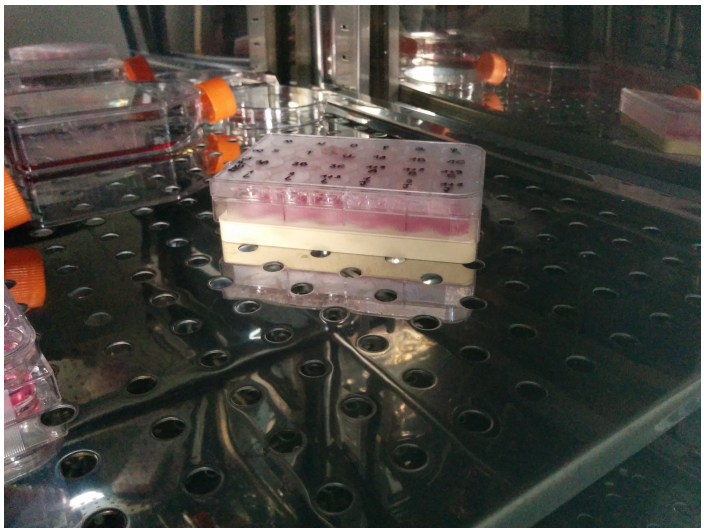


Figure 2.8: **Cells transfected with magnetofection reagents shown on the magnetic plate used to induce the process.** ARPE-19 cells on 24-well plate on the magnetic plate used for magnetofection are shown inside the incubator. The plate generates a powerful magnetic field, which, by interacting with the iron-oxide magnetic nanoparticles conjugated with the optogenetic plasmids, drives the genetic material inside the cells.

2.4.1.3 Polymer-based Transfection

Polymers Polyplus JetPrime (Polyplus Transfection) is a novel polymer-based transfection reagent designed to increase endocytosis of DNA complexes into primary or hard to transfect cells. Cells were plated on a 24-well plate on the day prior to transfection, in order to be 70-90% confluent after 24 h. JetPrime-DNA complexes were prepared following the manufacturer's instructions and the percentage of positive transfected cells was evaluated 48 h post transfection with MoFloAstrios flow cytometer (see relative section). Moreover, JetPrime was also used together with CombiMag for Magnetofection (see CombiMag section), in order to enhance its efficiency.

2.4.2 Evaluation of transfection efficiency

Efficiency of transfection was evaluated with two complementary approaches: flow cytometry and fluorescence imaging. In both methodologies, fluorescence of mCherry and EYFP markers was interrogated to confirm successful delivery of the optogenetic constructs to the ARPE-19 cells. On the one hand, flow cytometry allows for rapid screening of numerous cells, whilst fluorescence imaging enables visualisation of patterns of expression in the cells. The fluorescent tags of ChR2 and eNpHR were used as marker

to assess the rate of success of the transfection process. Flow cytometry was also used to compare efficiencies of the different delivery methods used.

2.4.2.1 Flow cytometry

To confirm and quantify efficiencies of the transfection protocols, transfected ARPE-19 cells were analysed on a flow cytometer. Flow cytometry is a reliable technique, which has been used for a variety of applications in the life sciences, from cell cycle analysis to immunology [Burchiel et al., 2000; Pozarowski and Darzynkiewicz, 2004; Riccardi and Nicoletti, 2006]. In the present work, flow cytometry was performed on a MoFlo AStrios (Beckman Coulter), equipped with filters for mCherry and EYFP identification. A 561nm laser was used for the excitation of ChR2/mCherry, combined with a 604-624 nm bandpass emission filter. On the other hand, a 488nm laser was combined with a 500-526 nm bandpass filter for eNpHR/EYFP detection. Samples were prepared in the following way: 48 h post-transfection, cells were trypsinised and centrifuged at 1500 rpm for 5 min. After discarding the supernatant, the pellet was resuspended in 500 μl fresh medium and the cell suspension was kept on ice until analysis on the flow cytometer. At least 50·000 events were analysed for each sample. Briefly, the cell solution is uptaken by the microfluidic system in the flow cytometer and analysed as it passes by the laser light, one cell at a time. When emission of the desired fluorescence is recorded, the electronics register one cell count on the graph generated by the total cell count and calculate percentage of cells positive for the specific marker.

2.4.2.2 Fluorescence microscopy

Fluorescent tags for ChR2 and NpHR were imaged either on a LeicaDMIRE2 fluorescence or confocal systems, equipped with 561 nm and 488 nm lasers and filter sets for mCherry (emission 610 nm) and EYFP (emission 530 nm). Expression levels were studied at 24, 48, 72, 144 h post transfection (hpt), following fixation with 4% paraformaldehyde (PFA) in order to study expression patterns at different time points and address the window with maximal transient transfection efficiency.

2.5 Localisation study

Although many efforts have been devoted to the optimisation of protein trafficking, opsin travel in the cells can still be influenced by a great variety of factors and assessment of protein localisation at different time points might be crucial to determine the best time window to perturb membrane potential using these tools [Allen et al., 2015]. For this purpose, wheat germ agglutinin (WGA) was used as a membrane stain, in order to study sub-cellular localisation of optogenetic proteins. In fluorescence confocal microscopy, colocalisation refers to observation of the spatial overlap between two (or more) different fluorophores, each having a distinct emission wavelength, to see if the different targets are located in the same area of the cell or in close proximity. WGA is a lectin, that is a carbohydrate-binding protein; it binds to N-acetyl-D-glucosammine and sialic acid, components which are highly abundant in chitin of insects and the cell membrane of yeast and bacteria, thus protecting wheat from insects or microrganisms. WGA can be tagged with different fluorophores and used as a membrane stain since it binds to carbohydrates on the outer surface of the cell membrane [Greenaway and LeVine, 1973]. WGA CF 405 (Biotium) is a blue-fluorescent labelled version of WGA whose spectra do not overlap with any of the other fluorescent molecules in the system (EYFP, mCherry, activation spectra of ChR2 or eNpHR). Briefly, ARPE-19 cells were transfected as previously described; cells were incubated with lipid-DNA complexes for the first two days in antibiotic-free medium and in complete growth medium the following days. On the fourth day following transfection, cells were stained with WGA CF 405 following the manufacturer's instructions, fixed with 4% PFA and imaged with a Laser Scanning Microscope LSM 800 (Zeiss).

2.6 Optogenetic stimulation: calcium imaging

Functionality of optogenetic channels was confirmed using ion-sensitive fluorescent dyes to monitor ion flow through the cell membrane after opening of the photoswitchable proteins. To study the response of Channelrhodopsin-2 mutants after blue light stimulation, calcium imaging experiments were performed on an inverted fluorescence mi-

croscope. ARPE-19 cells were grown in 35 mm glass-bottom petri dishes (ibidi μ-dish) and transfected with the desired ChR2 mutant 24 to 72 h before imaging. Frozen desiccated Fura-2 AM (Invtrogen) was diluted to a stock concentration in 100% DMSO (Dimethylsulfoxide) and loaded in the cells to a final concentration of 5 μM, exposing the cells to 0.1% DMSO. Cells were loaded with Fura-2 AM for 40 min at 37^{o}C in medium containing FBS to help internalisation of the dye. Following incubation time, samples were washed thoroughly with HBSS to remove excess of the dye and imaging was performed in HBSS, supplemented with extra $CaCl_2$ as needed.

Photostimulation experiments were performed on a Zeiss Axiovert 135TV equipped with fluorite optics (Zeiss) and a Ludl MAC2000 double filter wheel (LEP-Ludl Electronic Products) and an Andor LucaR CCD camera (Andor Technologies). Imaging experiments were controlled by MetaFluor (Molecular Devices) or μManager [Stuurman et al., 2007] softwares. Metafluor was also used for analysis of the images acquired during experiments. Supplemental image analysis was performed using FIJI [Schindelin et al., 2012]. During calcium imaging experiments, data were acquired as a set of images of the cells in the field of view. For processing, ROIs (Regions of interest) were drawn in the software around cells expressing the optogenetic channel (confirmed by fluorescent marker fluorescence) or untransfected cells (to be used as controls in the same field of view). Average fluorescence over time collected during the experiment was then exported as an array of data, which were further analysed via GraphPad Prism (GraphPad Software). Optogenetic stimuli were delivered using a xenon-mercury lamp filtered through a 475/40 nm bandpass filter for ChR2. Cells expressing ChR2 were visualised by mCherry fluorescence using a 560/40 nm excitation filter and a 635/60 nm emission filter (AT39010, Chroma Technology Corp). Simultaneous ChR2 activation and Fura-2 calcium imaging were performed using a 495 nm dichroic mirror that allowed delivery of blue light for photostimulation and excitation of Fura-2 dye from the same back port on the microscope. Fura-2 was excited at 340/15 nm and 380/15 nm and fluorescence emission was recorded at 510/40 nm.

2.7 Microscopy

2.7.1 Development of the imaging system

Optogenetic photostimulation was carried out on a Zeiss Axiovert 135TV inverted light microscope modified to perform the different tasks required from light delivery to recording of ion dynamics (Figure 2.9).

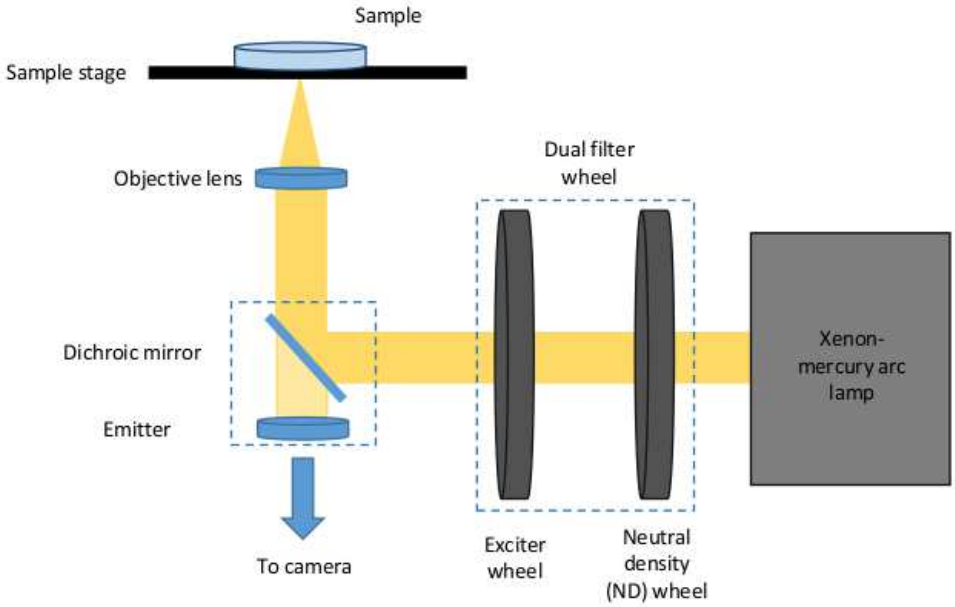


Figure 2.9: **Schematics of the imaging setup used for photostimulation and calcium imaging experiments, developed around a Zeiss Axiovert inverted light microscope.** Light from the xenon-mercury lamp was filtered by optical filters for the delivery of activation photostimuli for optogenetic channels and simultaneous recording of ion dynamics. *Original drawing.*

The microscope presents two illumination paths, one from the top, for brightfield, phase contrast and DIC (Differential Interference Contrast), and one from the bottom, used for fluorescence imaging and stimulation of the optogenetic actuators. Fluorescence illumination was provided by a xenon-mercury arc lamp allocated at the back port of the microscope. The system was equipped with a dual filter wheel (LEP Ludl Electronic Products Ltd) and an Andor LucaR emCCD camera (Andor Technologies). The dual filter wheel was controlled by a Ludl MAC2000 interface unit, managing communications to and from a computer via RS232 connections. Of the two filter wheels, one was equipped with neutral density (ND) filters to modulate intensity of the Xenon-mercury lamp delivered to the sample; the second wheel contained the excitation filters for the opsins and fluorophores used for photo-stimulation and calcium imaging exper-

iments. Dichroic mirrors and emitter filters were organised in a manual filter slider located underneath the sample stage. For photostimulation of the light-gated channel ChR2, a 475/40 nm exciter was used (XF1073-GlenSpectra, Horiba). Delivery of blue ChR2 stimulation and excitation of Fura-2 dye were assessed via the same filter cube. The standard Fura-2 dichroic, a 400 nm long-pass filter, was substituted with a 495 long-pass filter at 45°, in order to achieve simultaneous delivery of 470 nm light to open ChR2 channel and detection of calcium flows in the cells with Fura-2 (exc. 340/15 and 380/15 nm; em: 510/40 nm). Moreover, due to the ultraviolet wavelengths used for Fura-2 excitation, the microscope was equipped with UV-capable objectives (Zeiss), for maximum throughput and colour-correction. mCherry fluorescent tag used for the visualisation of ChR2-mCherry fusion protein was imaged with an AT39010 filter set (Chroma Technology Corp), composed of a 560/40 nm exciter, a 600 nm long-pass dichroic mirror and a 635/60 nm emitter, optimised for the detection of mCherry fluorophore. A schematic list of the filters used and the fluorophores imaged in the optogenetic stimulation experiments can be found in Table 2.2 and Figure 2.10.

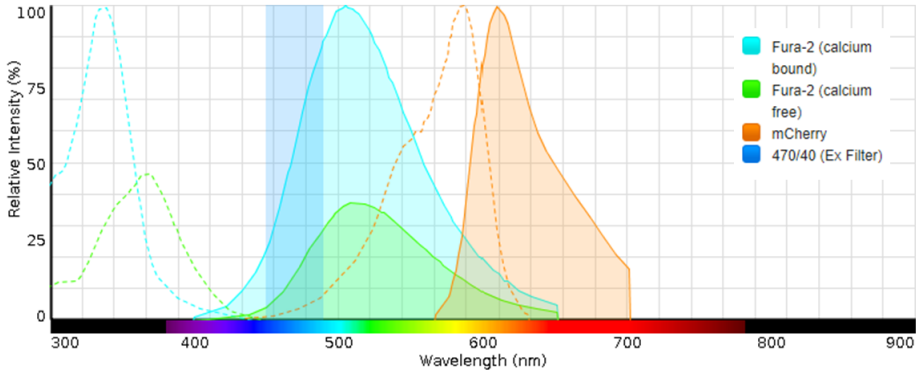


Figure 2.10: **Fluorescence spectra of the optical fluorophores and light-gated protein used in photostimulation and ratiometric calcium imaging experiments in the present study.** Overlay of the spectra shows distinction of the wavelengths used and compatibility of the fluorescent molecules for combined visualisation without crosstalk. Dotted lines and solid lines represent excitation and emission spectra, respectively. Image generated with SpectraViewer (ThermoFisher Scientific).

TARGET	FILTER	BANDWIDTH	COMPANY
ChR2	XF1073	475/40 nm	Horiba
mCherry	AT39010	exc. 560/40 nm 600 nm LP em. 635/60 nm	Chroma Tech Corp
Fura-2	XF1093 XF1094	340/15 nm 380/15 nm	Horiba

Table 2.2: **Table of optical filters used in the present study for optogenetic phosostimulation experiments of ChR2 light-gated channel and simultaneous Fura-2 ratiometric calcium imaging measurements.**

In later experiments requiring higher acquisition speed, the filter wheel imaging configuration was substituted with a multi-wavelength LED unit for calcium imaging experiments. FuraLED (CairnResearch Ltd) was used as an LED light source, optimised for ratiometric Fura-2 experiments at 340/380 nm. It was combined with a TwinLED unit containing a 470 nm LED and a powerful white LED for visualisation of the fluorescent marker mCherry, via the suitable filter set AT39010 (Chroma Technology Corp.). The LED unit was used in this thesis principally for the characterisation of ChR2 mutants generated by site-directed mutagenesis (Section 4.3.2). Illumination and emCCD gain were optimised to preserve fluorescent signal from photobleaching while providing adequate imaging speed.

2.7.2 Power measurements

Optical power of the illumination sources used for photostimulation of ChR2 at 475 nm was measured with an S120VC sensor (200-1100 nm wavelength range) and a handheld digital power meter (Thorlabs, Germany). Total power of the xenon-mercury arc lamp delivered via the exciter 475/40 nm (XF1073; Glen Spectra) was detected by placing the photodetector at the sample plane of the 10X, 20X and 40X objectives of the Zeiss Axiovert 135TV, prior to experiments, characterising the delivered power via the range of ND filters provided. Activation of ChR2 channel requires very specific irradiance values, reported to be between 0.1 and 10 mW/mm^2 [Murawski et al., 2016]. To accurately calculate power densities at different magnifications and with different neutral density filters, a 100 μm pinhole (Thorlabs) was interposed in the light path and the following formula was used for conversion of power data from the power meter

(W) to irradiance (W/m^2):

$$\text{Power density} = \text{power}(KW)/\text{area}(cm^2) \tag{2.2}$$

Data were then converted to mW/mm^2 for comparison with previous irradiance levels reported in the literature and are reported in Table 2.3.

ND FILTER	**LIGHT TRANSMISSION** (%)	**10X** (mW/mm^2)	**20X** (mW/mm^2)	**40X** (mW/mm^2)
None	100	6.6	18	41
0.56T	50	3.6	11	18
0.32T	30	1.36	5.3	9
0.1T	10	0.57	2.5	3.7
0.01T	1	0.09	0.22	0.3

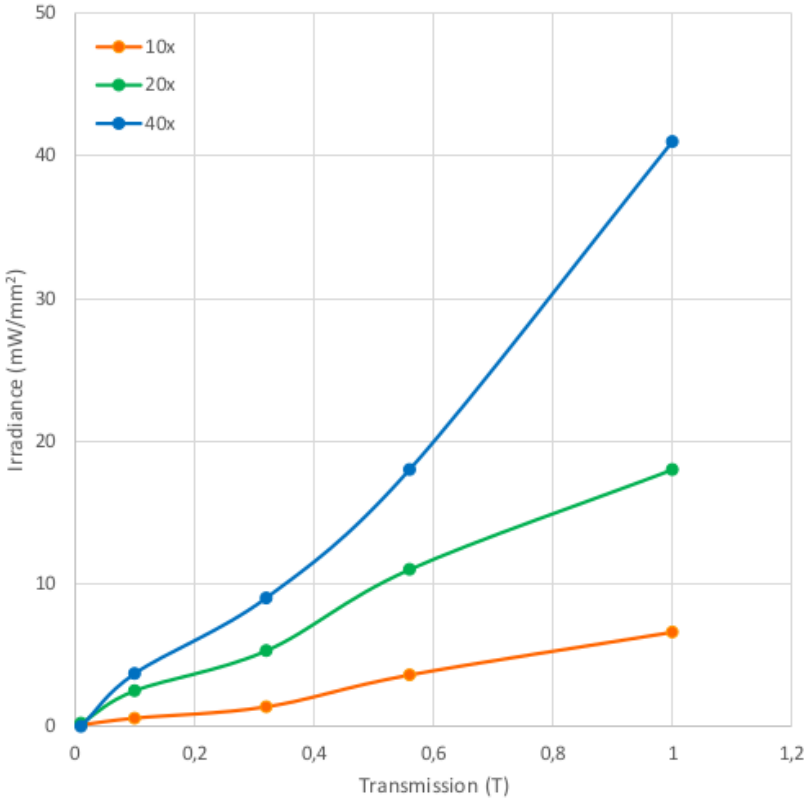


Table 2.3: **Table of power measurements of the blue light used for photostimulation of ChR2.** Light intensity was calibrated at the sample plane using a handheld power meter (Thorlabs). 475/40 nm filtered light was focused by 10X, 20X and 40X air objectives and power output was measured through a 100 μm pinhole (Thorlabs). Light intensity was modified by filtering the light path through different neutral density (ND) filters, ranging from 0.01 T (1% transmission) to 0.56 T (50% transmission). Full power of the arc lamp was measured without any ND filter. The graph reports data from the table for the three objective lenses.

Power delivered by the FuraLED/TwinLED unit (CairnResearch) was measured using the same procedure while the power of the LED was controlled remotely by varying the applied current under control of a Data Acquisition (DAQ) board and National Instruments MAX software; power density values calculated with the Formula 2.2 are reported in table 2.4.

VOLTAGE (mV)	**POWER DENSITY (40X)** ($mW/mm^{2)}$)
30	0.1
50	0.4
100	0.8
200	2.5
300	3.7
500	9
1000	14

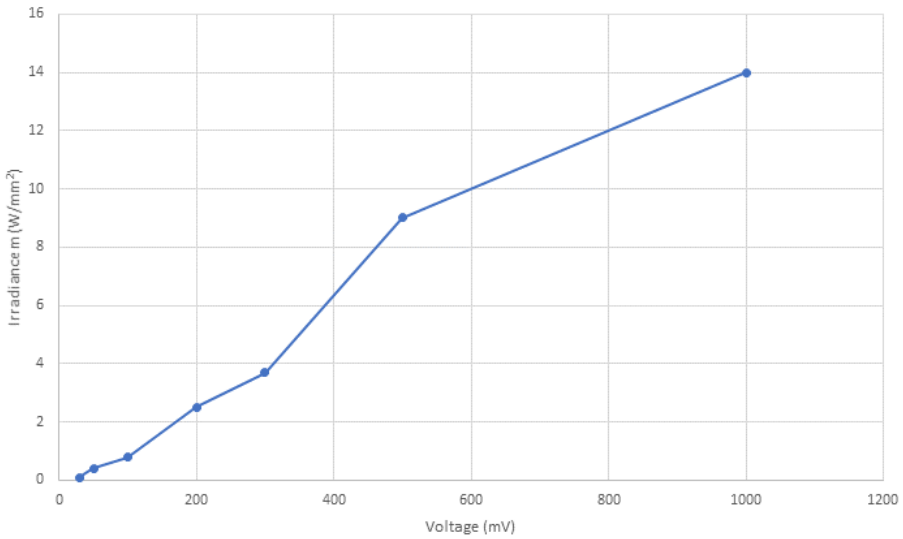


Table 2.4: **Table of power measurements of the blue light used for photostimulation of ChR2 in the FuraLED/TwinLED unit (CairnResearch Ltd).** FuraLED/TwinLED (Cairn Research) was employed as an alternative light source for the microscope for simultaneous photostimulation of optogenetic construct ChR2 and Fura-2 calcium imaging. The blue (470 nm) LED in the TwinLED unit was calibrated for its output light intensity with a handheld power meter (Thorlabs). Power of the LED was controlled remotely through a DAQ board and National Instruments MAX software. The input voltage to the LED was tuned and output power was filtered through a 100 μm pinhole (Thorlabs) and measured at the sample plane. The graph plots the data from the table.

2.8 Statistical analysis

Data reported in this thesis are representative of at least two or three replicates of the same conditions, unless otherwise specified. Statistical analysis was performed using GraphPad Prism (GraphPad Software). Flow cytometry analysis was performed

on $> 50{\cdot}000$ cells and independent replicates were performed to generate statistical significance. Fluorescence and confocal images shown in this thesis are representative of a variety of samples presenting comparable features. For calcium imaging results, data from $n > 5$ cells from two separate experiments are reported as mean values $\pm$ SEM (standard error of the mean), unless data from the response of a single cell are shown.

Chapter 3

Optimising the expression of optogenetic actuators in ARPE-19 cells

Introduction

Optogenetic control of cellular functions has revolutionalised the field of neuroscience in the past 15 years, by providing the means to genetically engineer cells to respond to light stimuli, triggering (ChR2) or inhibiting (HR) in subsets of neurons.[Boyden et al., 2005; Tye and Deisseroth, 2012b; Yizhar et al., 2011]. Outside the neuroscience, also the skeletal and the heart muscle have been investigated with optogenetic tools [Arrenberg et al., 2010; Bruegmann et al., 2015]. Optogenetics harness a family of light-sensitive channel proteins, called rhodopsins, naturally occurring in microorganisms, to provide light-triggered gating of ion permeabilities through the cellular membrane, causing depolarisation or hyperpolarisation depending on the optogenetic actuator deployed.

This Chapter presents the first evidence of the expression of the optogenetic actuators Channelrhodopsin-2 (ChR2) from green algae *Chlamydomonas reinhardtii* and Halorhodopsin (eNpHR) from the bacterium *Natronomonas pharaonis* in epithelial cells from the human retina, *in vitro*, with the final goal of exploiting such molecules to precisely manipulate ion and water fluxes. There is novelty in such a task, since ChR2/HR have so far seen wide use mainly in excitable cells. Similar approaches have

only recently been described, where optogenetic channels and pumps have been used to study epithelial cell morphogenesis, epithelial-mesenchimal transition, polarity or barrier function [Deneke et al., 2019; Efetova et al., 2013; Krueger et al., 2018; Makadia et al., 2018; Sato et al., 2017].

The first part of the work focused on optimising the delivery of ChR2 and eNpHR to a model epithelial cell line from the human eye, the ARPE-19 cell line. A variety of transfection strategies were attempted in order to introduce opsin genes in epithelial cells and they were examined and compared in efficiency, in order to deliver a reliable expression of optogenetic actuators within epithelial cultures *in vitro*. Expression patterns and localisation of the proteins after internalisation of the genetic material were assessed, with the aim of confirming expression of these exogenous proteins and correct targeting to the membrane compartment, where the proteins may be probed for functional activity. Subsequently, functionality of light-gated ChR2 in ARPE-19 cells was assessed by monitoring calcium dynamics within cells following activation of the optogenetic channel.

3.1 Optimisation of delivery of wtChR2 and eNpHR genes to the retinal pigment epithelial cell line ARPE-19

To achieve the first expression of optogenetic actuators to manipulate membrane ion dynamics in epithelial cells, efforts were exerted towards optimisation of delivery and expression procedures. Different gene delivery methods were tested in order to find and select the best approach for the application.

3.1.1 Flow cytometric evaluation of transfection efficiency

Flow cytometry is a reliable and well-established technique that allows for the rapid analysis of a vast population of cells with minimal sample preparation requirements. It is routinely used to quantify the number of cells with specific features within a population. In this study, flow cytometry was used to quantify the percentage of ARPE-19 cells expressing the optogenetic proteins after transfection. Flow cytometry allowed for the automated counting of a higher number of cells simultaneously, while

fluorescence microscopy was used to characterise the intracellular distribution of the transfected proteins. The two complementary approaches, when combined, allow for quantitative and qualitative analysis of both relative expression and location within cells.

Due to the untested ability of the wild type optogenetic actuators to express in epithelia (specifically the ARPE-19 cell line), a range of different methods and reagents were tested and compared for their ability to deliver and express the optogenetic constructs, in order to select the most efficient approach. No viral delivery method was attempted in this study; viral delivery, the harnessing of viruses to introduce genetic material inside the cells, can reach higher efficiencies, but can exert undesirable side effects, such as mutagenesis, toxicity and uncontrolled overexpression of the protein encoded by the transduced gene [Nayerossadat et al., 2012; Thomas et al., 2003]. Non-viral methods have been preferred to minimise side effects and work has been focused on maximising expression without damaging the cells' wellbeing.

Gene delivery screening

The screening of the reagents involved a lipid-based compound (Lipofectamine 3000), a cationic/lipid-based reagent (DreamFect Gold) and a polymer-based methodology (JetPrime). Three magnetic-nanoparticle based kits (Magnetofectamine, CombiMag, PolyMagNeo) were further tested in their ability to enhance expression by driving the construct into the cells, as described in Section 2.4.1. Cells were analysed for the expression of the optogenetic proteins 48 h after transfection using a flow cytometer. To compare transfection efficiency, cells expressing the given marker were counted against the total number of analysed cells, resulting in a percentage of positively-transfected cells. Figure 3.1 shows such values as the mean efficiencies referring to two or three replicates, each of 5 x 10^4 cells.

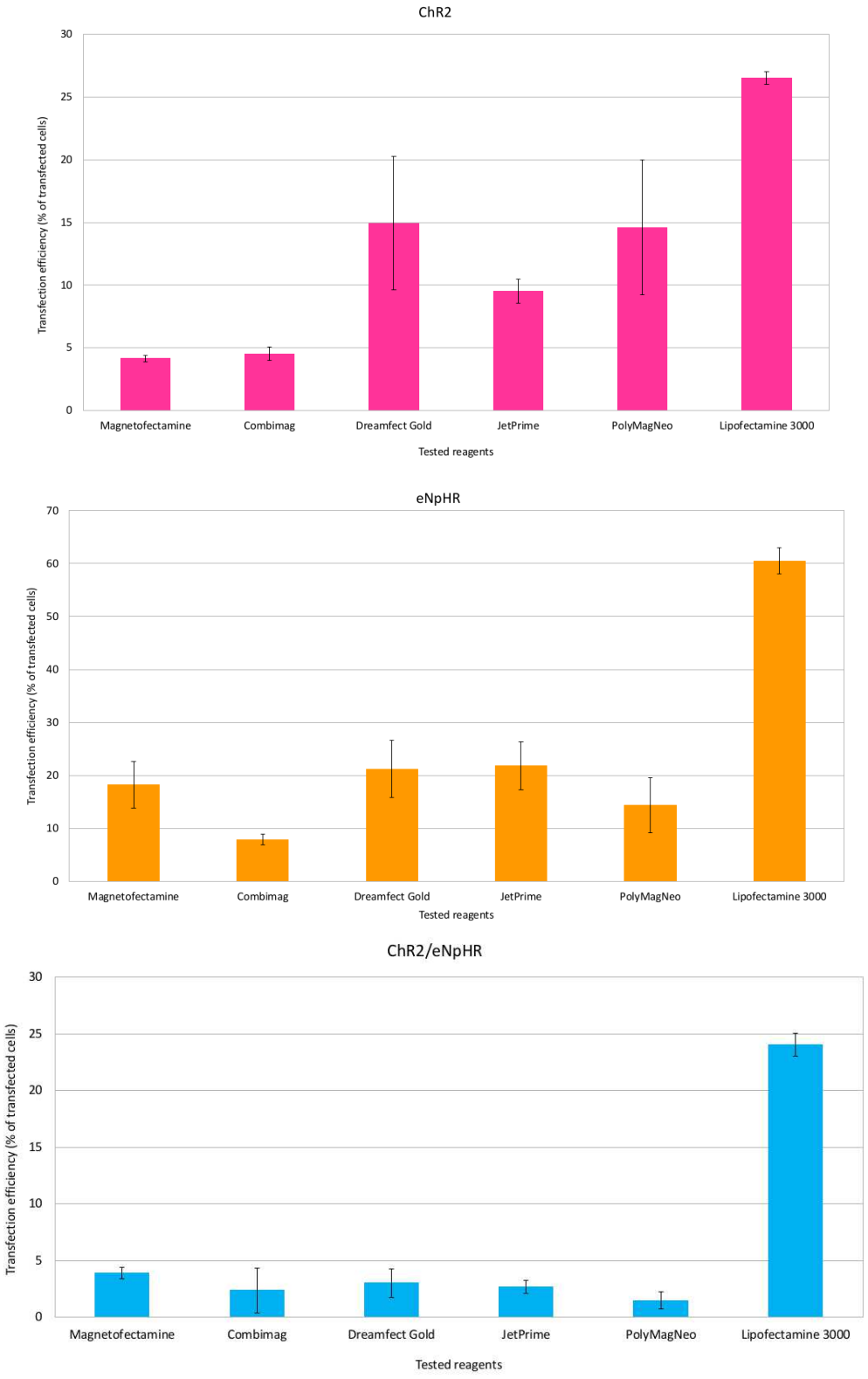


Figure 3.1: **Transfection optimisation: comparison of transfection reagents to select the most efficient method for the delivery of optogenetic constructs to the ARPE-19 cell line.** Comparison of transfection efficiency for the different tested commercial reagents. Histograms show percentage of cells expressing ChR2 (top, magenta), eNpHR(middle, orange) or both channels (bottom, blue) and are based on flow cytometry results.

PolyMagNeo and DreamFect Gold transfection efficiencies were similar to Lipofectamine 3000 ones for ChR2; however, they showed lower efficiencies, in the range of 15-20%, for eNpHR, compared to the 60% of transfected cells transfected by Lipofectamine 3000. Efficiencies for the combined transfection of optogenetic constructs were extremely low for all tested reagents, apart from Lipofectamine 3000, which showed a success rate similar to that for ChR2 plasmid only. Considering the results of the comparison, summarised in Figure 3.1, lipofection with Lipofectamine 3000 showed the highest efficiencies for both ChR2 and eNpHR (individually as well as together) was chosen as the method for the delivery of the optogenetic constructs to the ARPE-19 cell line.

Lipofectamine-mediated transfection

Representative results for ChR2 and eNpHR expression using Lipofectamine 3000 as a delivery method are summarised in Figure 3.2 in the form of dot plots and in Figure 3.3 in the form of histograms. Non-transfected ARPE-19 cells were used as a control to configure analysis parameters on the flow cytometer and to gate the healthy cells, excluding cell debris and clusters of cells, based on the forward (FSC) and side scatter (SSC) values (not shown). Gating performed on untransfected cells (Figure 3.2 A) was applied to transfected ARPE-19 cells to calculate the number of cells expressing the optogenetic channels. Both dot plots and histograms report successful expression of ChR2 and eNpHR, individually and simultaneously, by ARPE-19 cells. Histogram data are mean values ± SEM representative of three replicates for ChR2 and eNpHR single transfectants and two replicates for the combined transfection.

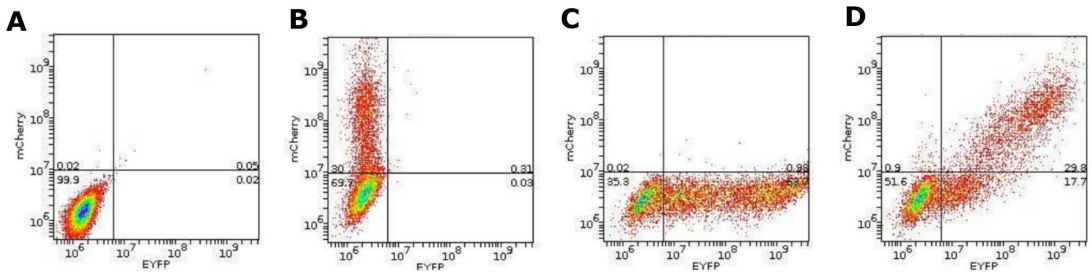


Figure 3.2: **Flow cytometry data for evaluation of transfection efficiency of wild type Channelrhodopsin-2 and *Natronomonas pharaonis* Halorhodopsin.** Dot-plots showing transfection efficiency for ChR2 **B**, NpHR **C** and co-transfection of both constructs simultaneously **D**. Analysis was performed on a MoFlo Astrios cell sorter (Beckman Coulter). Untrasfected ARPE-19 cells were used as unlabeled controls **A** to select analysis parameters on Weasel software. Expression of ChR2 and eNpHR was confirmed by reporter fluorescence of mCherry and EYFP, respectively.

Figure 3.3 reports efficiencies of Lipofectamine-mediated transfection for wtChR2 and eNpHR individually and simultaneous co-transfection with the two plasmids. Transfection efficiency of wtChR2, reported in magenta, was in the range of 25-30%, with an average of 26.5 ± 0.5%, while eNpHR-positive cells, in orange, reached a mean efficiency of 60 ± 2.5% of the total population. Combined transfection with the two optogenetic constructs, in blue in the figure, showed a similar transfection efficiency to wtChR2 alone, of 24.5 ±0.9%.

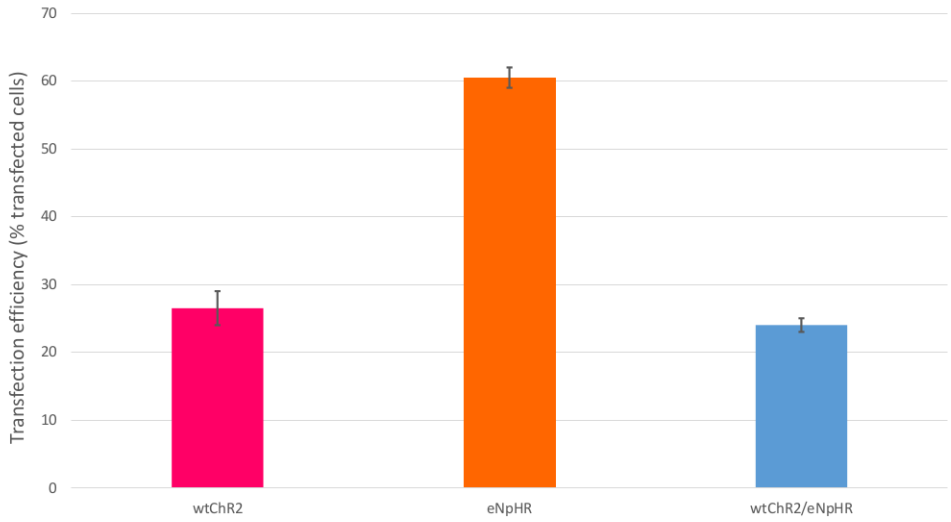


Figure 3.3: **Histograms showing efficiency of Lipofectamine-mediated transfection of wtChR2 and eNpHR.** In magenta and orange, wtChR2 and eNpHR individual transfection efficiencies. In blue, data for combined delivery of both optogenetic plasmids. All data are representative of replicates ± SEM.

3.1.2 Evaluation of cytotoxicity of optogenetic actuators in epithelia

Introducing genetic material into a cell and expression of the resulting protein can potentially cause cytotoxicity or even cell death. It is therefore important to assess cell health after delivery of transgenes, particularly where phototoxicity may be a confounding factor. This is the first evidence of the expression of ChR2 and eNpHR in the ARPE-19 cell line, therefore a test to assess toxicity of opsin proteins or any reagent involved in the process of gene delivery was performed to exclude excessive cell death following transfection.

A simple, cost- and time-effective colorimetric test was chosen to check cell viability 48 h post transfection (see Section 2.3.1). In general, the optogenetic constructs administered to the cells and the compounds used for their delivery did not significantly influence MTS absorption, indicating minimal toxicity of the expression in ARPE-19 cells, as it is reported in Figure 3.4.

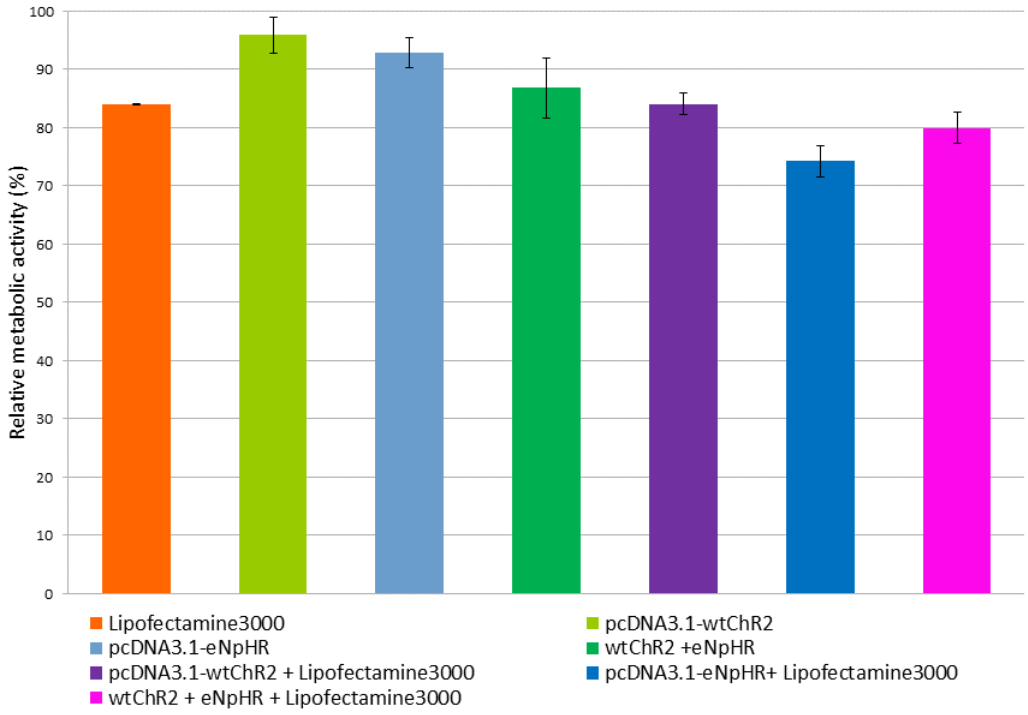


Figure 3.4: **Cytotoxicity assessment of optogenetic constructs.** Quantitative analysis of potential cytotoxicity effects of wtChR2 and eNpHR proteins and molecules involved in their delivery to ARPE-19 cells. Data were normalised to positive and negative controls (data not shown) to calculate relative percentage of cell viability. The histograms show no major reductions in cellular metabolic activity for all tested conditions. Data are representative of replicates ± SEM.

A slight reduction in MTS production by the cells can be explained as a decrease

of their physiological metabolic activity as a consequence of the transfection procedure itself. The expression of a transgenic protein in a cell can in fact slow down the cellular metabolic machinery, especially if characterised by high expression levels, such as in the case of eNpHR [Tye and Deisseroth, 2012b].

3.1.3 Expression study of optogenetic actuators by fluorescence imaging

To evaluate at a single cell level the expression patterns of the optogenetic proteins, fluorescence imaging was used. The two channel sequences were tagged with a fluorescent marker for visualisation: mCherry for ChR2 and EYFP for eNpHR. Fluorescence detection of these tags was employed to identify the cells expressing the light-responsive proteins. The cells were counterstained for the cell nuclei with Hoechst33342 and fixed in 4% paraformaldehyde 48 h post transfection before proceeding to imaging.
Fluorescent images confirmed successful expression of the optogenetic constructs ChR2 and eNpHR in ARPE-19 cells, as shown in Figures 3.5 and 3.6.

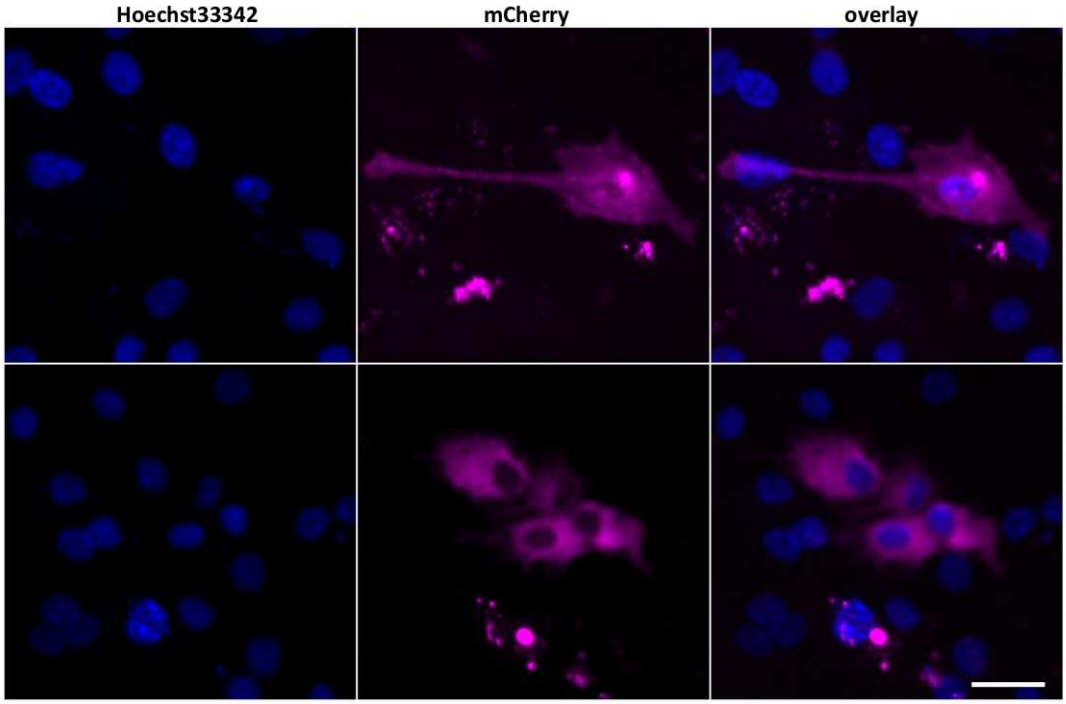


Figure 3.5: **Fluorescent images of ARPE-19 cells expressing the optogenetic construct wild-type ChR2.** To confirm succesful expression of the optogenetic constructs in the ARPE-19 cell line, the fluorescent tags mCherry (magenta) was used to visualise ChR2-expressing cells 48 h after transfection with Lipofectamine 3000. Hoechst33342 (blue) was used as a counterstain for the cell nuclei. Scale bar is 10 μm.

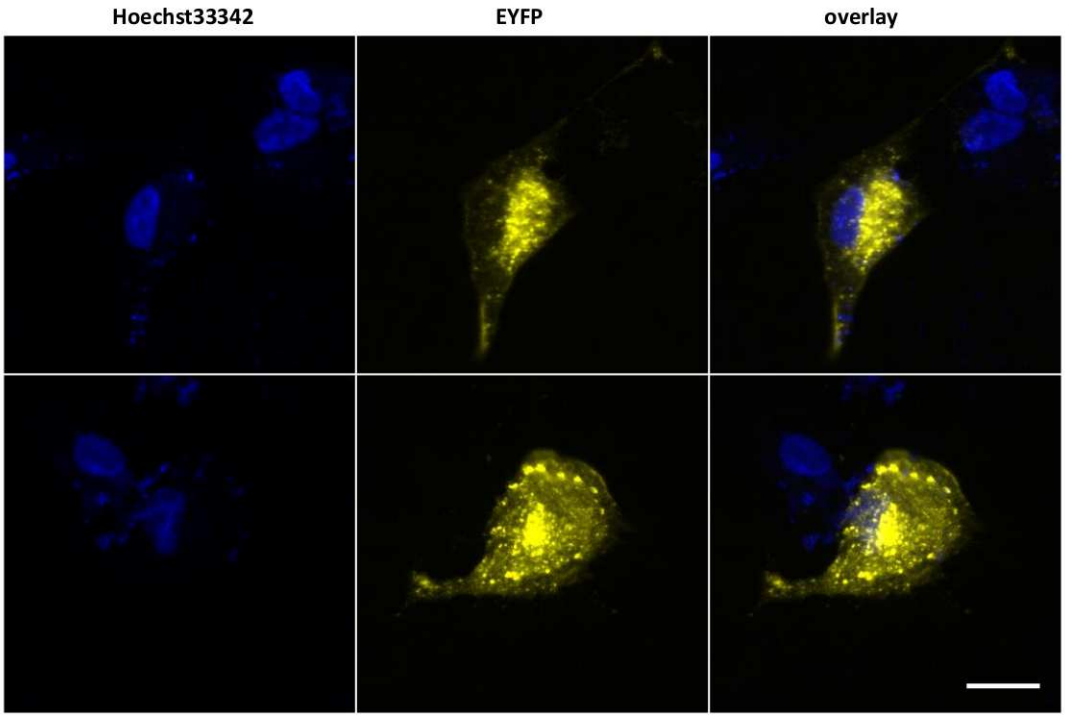


Figure 3.6: **Fluorescent images of ARPE-19 cells expressing the optogenetic construct eNpHR.** To confirm succesful expression of the optogenetic constructs in the ARPE-19 cell line, the fluorescent tag EYFP (yellow) was used to visualise eNpHR-expressing cells 48 h after transfection with Lipofectamine 3000. Hoechst33342 (blue) was used as a counterstain for the cell nuclei. Scale bar is 10 μm.

Cytoplasmic accumulation of fluorescence in the form of vesicles is appreciable in the images, both in the perinuclear region and in proximity to the membrane compartment. This observation is in line with previous data from other research groups [Arrenberg et al., 2009; Figueiredo et al., 2014]. Accumulation of a protein in agglomerates, mostly in the ER and Golgi structures, has in fact been reported for the expression of opsins, especially for Halorhodopsin [Gradinaru et al., 2008; Zhang et al., 2007; Zhao et al., 2008]. Localisation of the vesicles on the post-translational trafficking path responsible for the transport of synthesised proteins from the nucleus to the ER to their specific target structure in the cells is encouraging. Proteins retained in vesicles may eventually be transported to the plasma membrane [Bezzerides et al., 2004; Cymer et al., 2015], where they might be embedded as functional channels, therefore renewing the pool of optogenetic actuators in the cells.

Co-transfection of ChR2/eNpHR in the same cells was also successful, as shown in Figure 3.7. The spectral distinction of the activation wavelengths for ChR2 and eNpHR makes them an ideal protein duo to achieve ON/OFF control of cellular functions. One

of the future aims of this research is to combine the expression of the two constructs in the same cells and tune vectorial ion and fluid transports ON and OFF using light, although the function of HR was not fully elucidated by the current work. The future feasibility of this dual-actuator approach in ARPE-19 cells using co-transfected ChR2 and eNpHR appears encouraging.

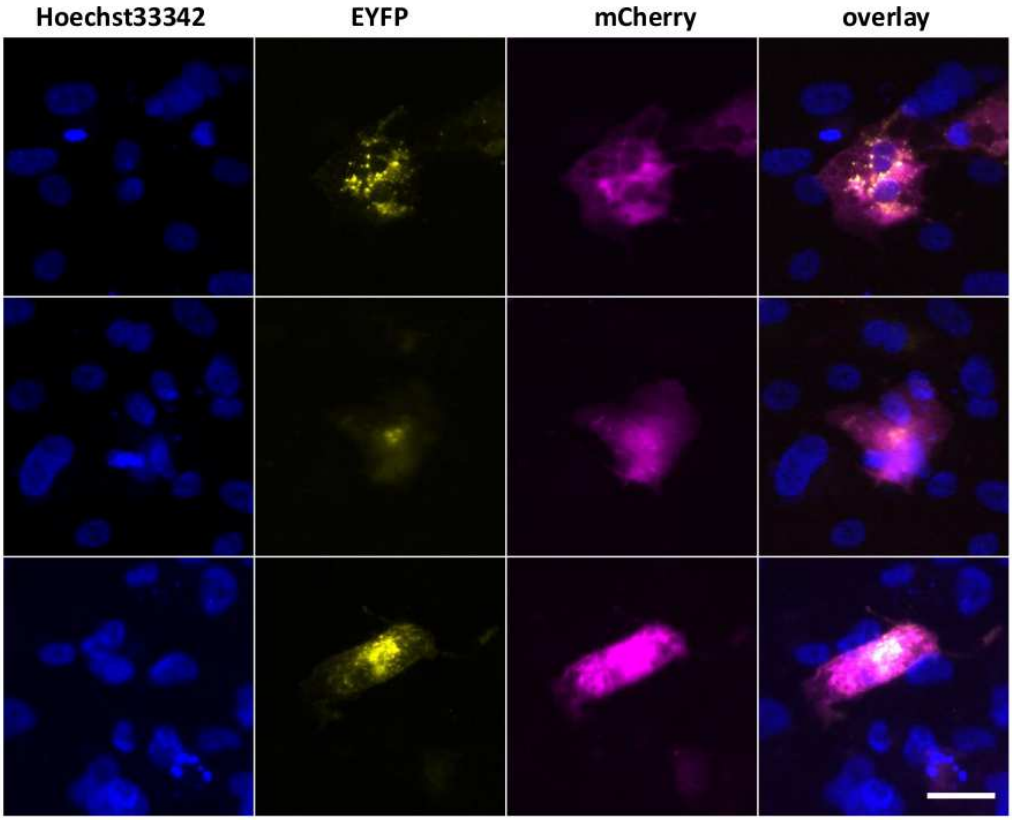


Figure 3.7: **Fluorescent images of ARPE-19 cells co-expressing wtChR2 and eNpHR.** ARPE-19 cells were co-transfected with the two pcDNA3.1 vectors encoding for wild-type ChR2 and eNpHR and imaged for the expression of the fluorescent tags mCherry and EYFP, therefore of the optogenetic channels, 48 h post Lipofectamine-mediated delivery of the plasmids. Images were acquired on a LeicaDMIRE2 fluorescent microscope equipped with the filter sets for mCherry and EYFP. Cells were counterstained with Hoechst33342 for visualisation of cell nuclei. Scale bar is 10 μm.

3.1.4 Membrane localisation study

The data reported above, were performed in a population of cells to confirm expression in a quantitative manner (Section 3.1.1) and to confirm non-cytotoxicity of the optogenetic constructs in ARPE-19 cells (Section 3.1.2). Subsequently, the correct localisation of the proteins in the plasma membrane, crucial for their functionality, was investigated with a single-cell imaging approach. To study membrane localisation, a membrane-specific dye was used. The blue fluorophore CF405-conjugated carbohydrate-binding

lectin Wheat Germ Agglutinin (WGA) (Biotium, Fremont, California) was employed [Greenaway and LeVine, 1973]. WGA binds to carbohydrates in the cell membrane and the dye CF405 allows for visualisation. Localisation of the opsins was assessed through fluorescence of their protein tags mCherry for ChR2 and EYFP for eNpHR in comparison to WGA fluorescence at the membrane domain.

Figure 3.8 shows a confocal image of an ARPE-19 cell expressing wild-type ChR2, determined by mCherry marker fluorescence (in magenta), stained with the membrane marker WGA. Perinuclear staining is visible in the cells, possibly caused by binding of WGA to N-acetyl-glucosamine or sialic acid at the nuclear membrane level. Overlay of WGA (blue) and mCherry (magenta) or EYFP (yellow) signals appears to confirm membrane localisation of wtChR2 and eNpHR, respectively.

Confocal images show intracellular aggregates of ChR2, mostly in the form of vesicles in the area surrounding the nucleus, which could be attributed to synthesised proteins travelling to the plasma membrane or recycling back after their life cycle. Analysis was assessed 4 days post transfection, confirming both persistence of the protein at this time point and expression at the membrane level and throughout the trafficking apparatus. Figure 3.9 confirms membrane localisation of Halorhodopsin with the same approach, by simultaneous visualisation of EYFP marker and WGA membrane stain. Also in the case of eNpHR, a certain degree of protein accumulation in vesicles can be noted. It can be speculated that such vesicles are part of the secretory pathway, from the nucleus through the ER, crucial for surface expression of membrane proteins. Figure 3.10 presents results for the co-transfectants, that is cells transfected with both ChR2 and eNpHR plasmids, simultaneously. Similar expression patterns as the single transfectants are appreciable in the figure, although a mixed population of cells in generated, where some have internalised and expressed only one of the two optogenetic channels or both. Figure 3.11 reports the distribution analysis performed on Figures 3.8 and 3.9. Panels 3.11 C and F show intensity profile of lines drawn on the optogenetically-modified cells and the fluorescent images for the membrane dye WGA; overlay of the profiles confirms sub-cellular localisation at the membrane level for both wtChR2 and eNpHR.

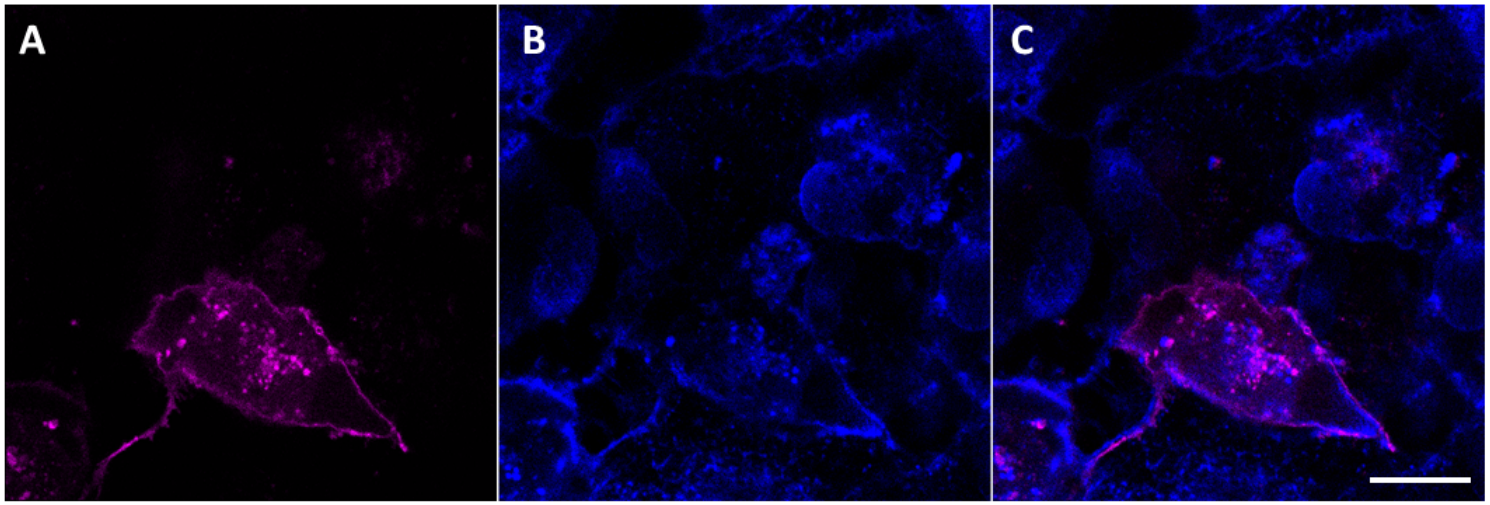


Figure 3.8: **Membrane localisation study of wtChR2 in ARPE-19 cells. A** mCherry reporter fluorescence (magenta) shows expression of wtChR2-mCherry fusion protein in ARPE-19 cells. **B** Membrane stain WGA-CF405 (blue) highlights extracellular membrane borders by binding sialic acid and N-acetyl-glucosamine on the cell surface. **C** Overlay of the two channels confirms membrane localisation of wtChR2 in ARPE-19 cells. Scale bar is 10 μm.

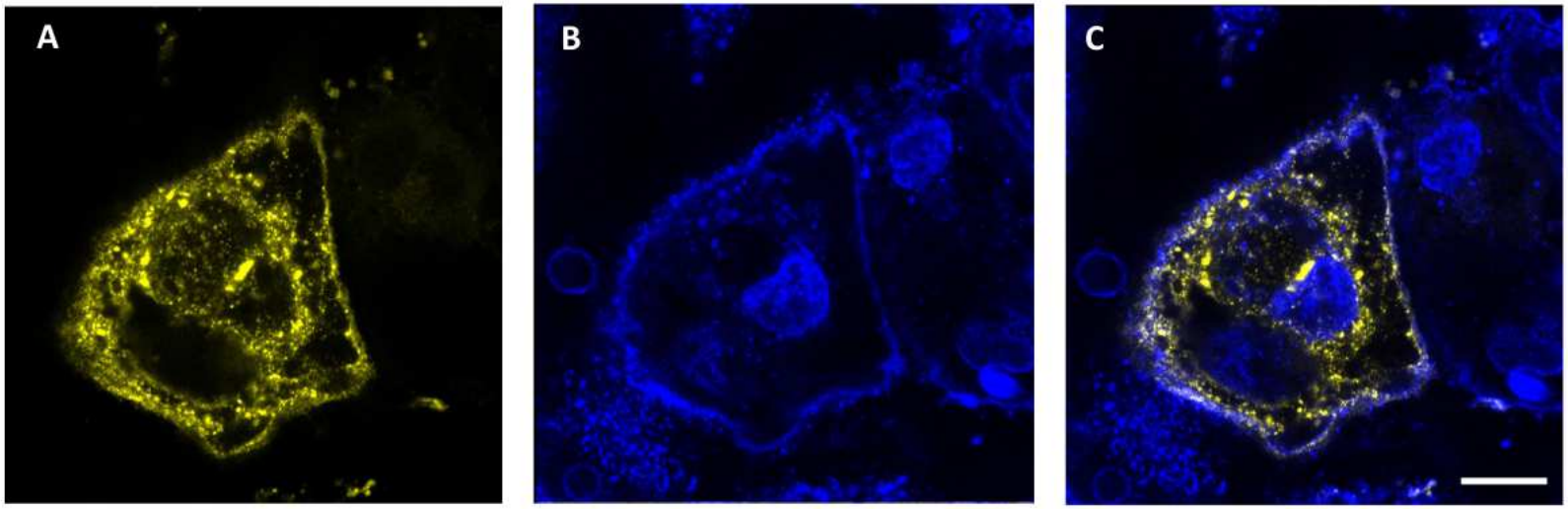


Figure 3.9: **Membrane localisation study of eNpHR2.0 in ARPE-19 cells. A** EYFP reporter fluorescence (yellow) shows expression of eNpHR-EYFP fusion protein in ARPE-19 cells. **B** Membrane stain WGA-CF405 (blue) highlights extracellular membrane borders by binding sialic acid and N-acetyl-glucosamine on the cell surface. **C** Overlay of the two channels confirms membrane localisation of eNpHR in ARPE-19 cells. Scale bar is 10 μm.

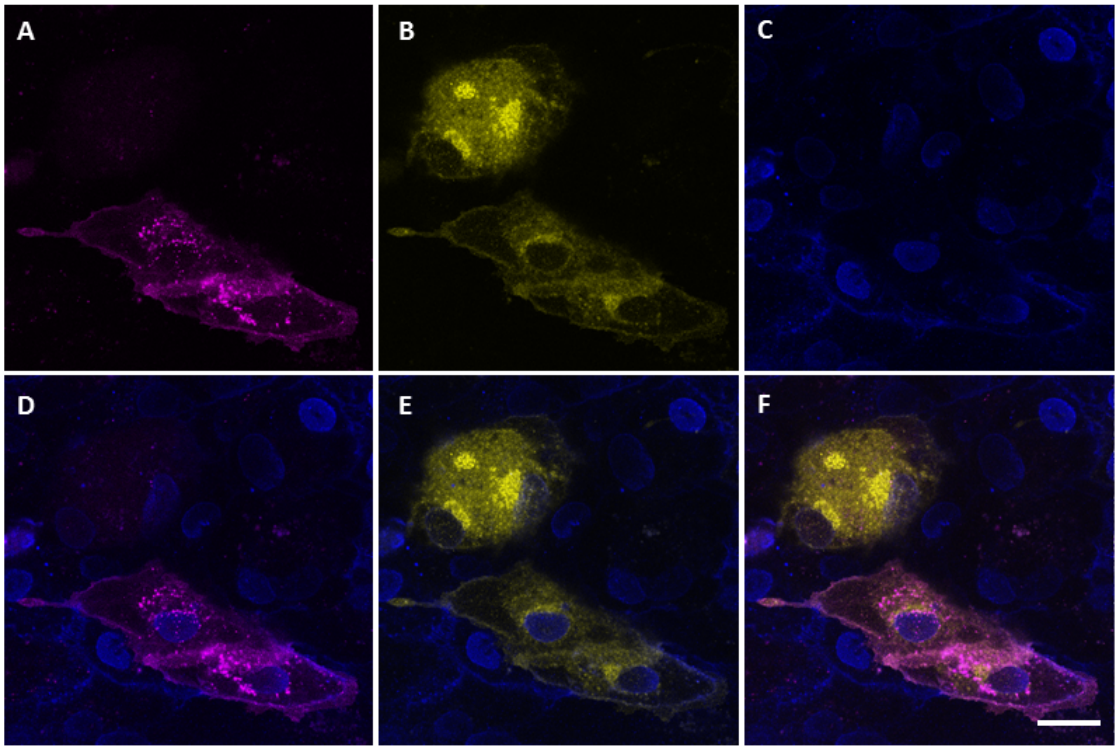


Figure 3.10: **Confocal images showing membrane localisation study of wtChR2 and eNpHR cotransfected in ARPE-19 cells.** pcDNA3.1 plasmids containing the sequences for wtChR2-mCherry and eNpHR-EYFP were simultaneously transfected in ARPE-19 cells. Confocal images of fluorescent markers mCherry (magenta) and EYFP (yellow) and of the membrane stain WGA-CF405 (blue) confirmed localisation of opsins in the plasma membrane domain. All images are referring to the same field of view. **A** Cells expressing wtChR2 characterised by mCherry fluorescence (magenta); **B** eNpHR-positive cells are visualised by EYFP fluorescence (yellow); **C** WGA-CF405 stains the cell membrane by binding negatively-charged sugars (blue). **D, E** Overlay of opsin markers and WGA stain highlight membrane localisation of ChR2 and eNpHR, respectively. **F** Overlay of the three channels shows two cells have internalised both optogenetic plasmids and are co-expressing ChR2 (magenta) and eNpHR (yellow). Scale bar is 10μm.

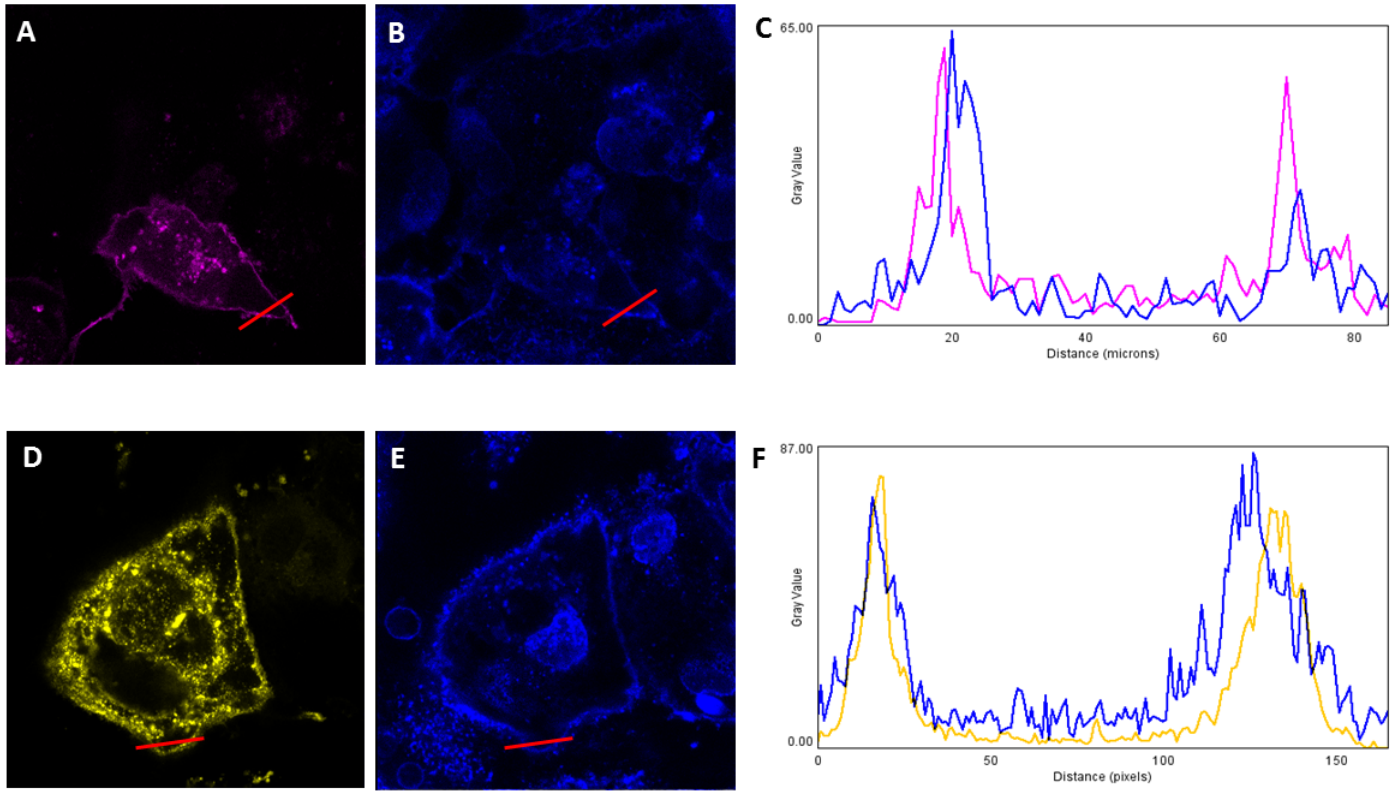


Figure 3.11: **Localisation study of wtChR2 and eNpHR in ARPE-19 cells.** Membrane localisation of wid-type ChR2 and eNpHR was assessed on FIJI, exploiting fluorescence intensities of mCherry-ChR2 (magenta, **A**), eNpHR-EYFP (yellow, **D**) and WGA-CF405 (blue, **B,E**). The plotted curves show intensity profiles of membrane-bound WGA (blue) and mCherry-tagged ChR2 (magenta **C**) or EYFP-tagged eNpHR (yellow **F**); overlay of the peaks confirms membrane localisation of the optogenetic proteins.

3.2 Functionality of wtChR2 in ARPE-19 cells assessed with calcium imaging

After optimisation of gene delivery (Section 3.1) and confirmation of opsin location in the cell membrane (Section 3.1.4), functionality of the optogenetic constructs in ARPE-19 cells was investigated. At first, assessment of channel light-responsiveness focused on the non-selective cation channel ChR2. Imaging of calcium dynamics has been reported as a reliable method to investigate functionality of ChR2, both *in vitro* and *in vivo* [Renault et al., 2015; Shipley et al., 2014]. ChR2 is, in fact, a non-selective cation channel and, therefore, its opening changes membrane calcium permeability. Increase in intracellular calcium can be monitored with the use of calcium-sensitive indicators, fluorescent molecules which, once internalised by the cells, are extremely sensitive to calcium variations in the intracellular environment. Upon photostimulation of ChR2 with blue light, opening of the channel should result in an increase of intracellular calcium concentration, therefore a rise in Fura-2 emission ratio when the dye is excited at 340 nm and 380 nm.

When exposed to pulses of 470 nm light, ChR2 failed to cause calcium transients in ARPE-19 cells expressing the wild type light-gated channel, as shown by the lack of Fura-2 ratio increase in Figure 3.12. Optimal Fura-2 concentration was investigated prior to experiments in ARPE-19 cells, to conclude 5 μM as the most suitable dye concentration for calcium imaging experiments on the developed imaging system. Different parameters were modified in order to test ChR2 functionality. Extracellular calcium concentration ($[Ca^{2+}]_o$) was varied from 2 mM to 90 mM, light power intensity was modulated from 0.5 to 40 mW/mm^2 and duration of the stimulus was tuned from 10 ms to 15 s. Intervals between stimuli were increased up to 5 s in order to allow the channel to return to its activatable state and sample preparation was performed in minimal illumination, in order to prevent undesired opening of ChR2. Despite attempting to activate ChR2-expressing cells in the described conditions, a range of 15 experiments incorporating $>$ 60 mCherry-positive cells failed to show a single significant elevation of $[Ca^{2+}]$ in response to 470nm stimulation of ChR2. Acetylcholine (Ach) addition to the imaging buffer (red arrow in Figure 3.12) caused an increase in intracellular calcium,

which was monitored by the dye Fura-2 in the same cells, demonstrating ability of the dye and the imaging system to record calcium fluctuations. Ach is a chemical messenger able to trigger a receptor-mediated rise in $[Ca^{2+}]_i$ in cultured retinal epithelial cells [Fischer et al., 1998; Osborne et al., 1991].

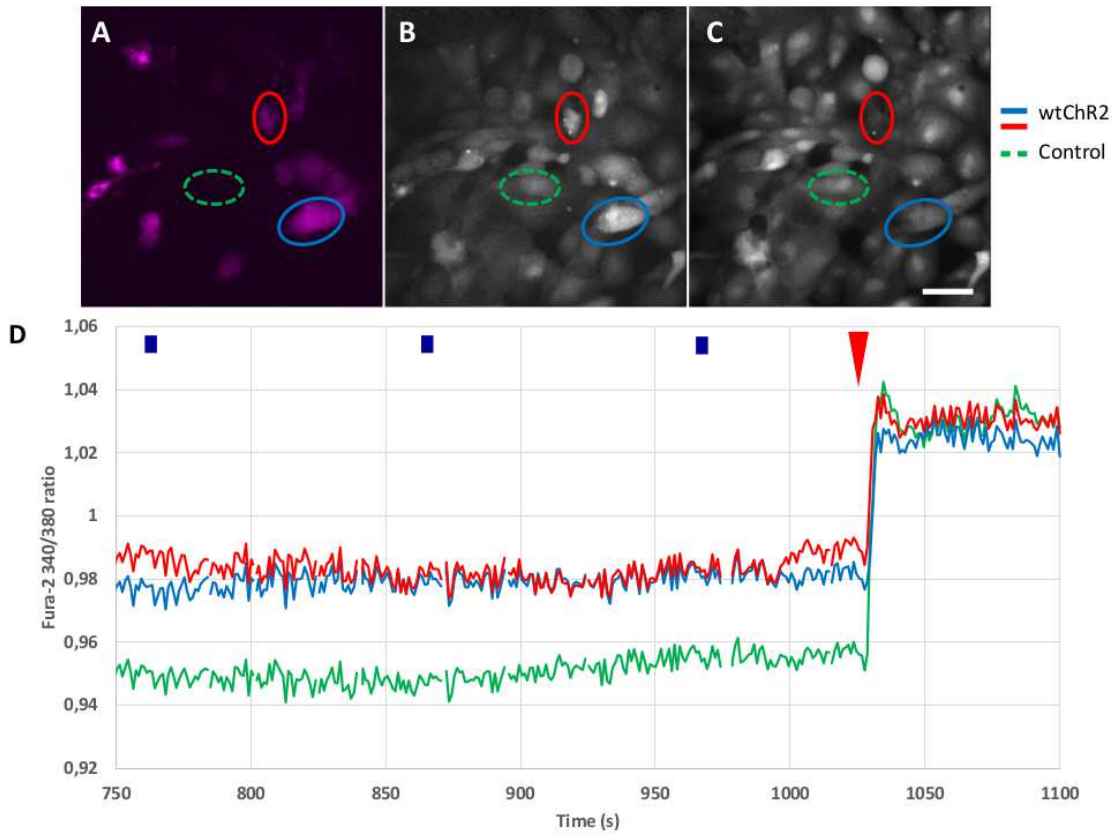


Figure 3.12: **Fura-2 ratiometric measurements of Ca^{2+} dynamics in ARPE-19 cells expressing wtChR2.** **A** Cells expressing ChR2-mCherry. Images of Fura-2 fluorescence excited at 340 nm**B** and 380 nm **C** show internalisation of the calcium-sensitive dye and allow for visualisation of untransfected cells in the same field of view. Scale bar is 50 μm. **D** Representative graph of the behaviour of wtChR2-expressing ARPE-19 cells following 2-second light stimuli (blue bars). Red arrow represents 10 μM acetylcholine supplementation to the imaging buffer.

Discussion

To summarise, this chapter has described the different steps towards the optimisation of the delivery and the expression of optogenetic constructs wtChR2 and eNpHR in the retinal pigment epithelial cell line, ARPE-19 (Sections 3.1.1 and 3.1.4). Finally, functionality of the non-selective cation channel wtChR2 in ARPE-19 cells was evaluated by the use of a calcium-sensitive indicator(Section 3.2). Flow cytometry (Section 3.1.1) and fluorescence imaging showed that both wtChR2 and eNpHR were successfully expressed by ARPE-19 cells, reaching a satisfying level of expression (25% and 60%, respectively). Confocal fluorescence images with the membrane stain WGA showed membrane localisation of the optogenetic proteins, confirming correct post-translational trafficking to the compartment where microbial rhodopsins are functional (Section 3.1.4). A certain degree of accumulation of eNpHR in vesicles was appreciable, as previously reported in the literature [Gradinaru et al., 2008]. Further investigation of the nature of such vesicles might provide interesting insights on the fate of the cytosolic eNpHR. Halorhodopsin (eNpHR) functionality was not investigated in the present study but expression levels and location of the protein in the cell membrane are encouraging data for further assessments of its activity. It is interesting to note that the population resulting from the co-transfection procedure shown in Figure 3.10, is heterogeneous: some cells present both ChR2 and eNpHR, while others are expressing only one channel or the other. Co-transfection generated a mixed population of optically-targetable cells that would provide the possibility to investigate different scenarios in the same batch of cells. For instance, effects of short pulses of blue light might be investigated in the same field of view on cells expressing ChR2 only or both ChR2 and eNpHR, to study if and how the presence of the other channel alters the cells' behaviour. If such a variety of expression patterns is not desirable, approaches to ensure stoichiometric expression of the two opsins could be taken: for instance, a single vector containing both genes for ChR2 and eNpHR connected by a joining sequence could be introduced into the cells instead of two separate vectors [Kleinlogel et al., 2011b].

Flow cytometry (Section 3.1.1) and confocal fluorescence (Section 3.1.4) were used to confirm the first four days following transfection as the most suitable time window for

photostimulation experiments, where a range of 25-30 % of ARPE-19 cells expressed the optogenetic channels in the membrane compartment. Evaluation of opsin functionality focused at first on wtChR2, mainly because optical requirements for this channel were readily accessible on the optical system. Photostimulation of the light-sensitive channel did not cause calcium transients in ARPE-19 cells, as shown in the exemplar in Figure 3.12.

Possible reasons lie in the low channel conductance, as previously reported for the wild-type ChR2 originally used for optogenetic purposes [Nagel et al., 2003] and/or in the level of membrane localisation of the protein at the time of experimental interrogation of its functionality. Desensitisation, that is the inactivation of the channel following exposure to excessive light intensities, might represent another limitation of the wild-type ChR2, which could explain the lack of calcium transients [Lin, 2011; Nagel et al., 2003]. Another explanation could lie in limitations in the imaging configuration used for calcium imaging experiments; the kinetics of wtChR2 in the microsecond time-scale may be missed at the sampling rates available using the current hardware, therefore compromising reliable detection. Approaches to improve acquisition speed and minimise hardware delays were considered and will be discussed in the following chapter.

Having discovered limitations of wtChR2 in manipulating epithelial [Ca^{2+}] dynamics I decided to modify wtChR2 structure to enhance its performance. The next part of this study will describe the process of selecting and optimising the best candidates among ChR2 variants to be employed for application in epithelial cell lines, specifically in retinal pigment epithelial cells. To date, ChR2 has mainly been optimised for expression and use in neurotropic vectors, both for applications *in vitro* and in living animals [Bernstein and Boyden, 2011; Betley and Sternson, 2011; Packer et al., 2013; Yizhar and Adamantidis, 2018]. Published resources, such as plasmids and vectors, are mainly tailored to expression in the brain and the genes are driven by neuron-specific promoters, which would result in poor expression levels in other lineages [Hioki et al., 2007]. To widen the application range of optogenetic tools, as discussed in the following chapter, the generation of novel optogenetic constructs was attempted in a less neuron-

specific vector, driven by the CMV promoter, which is efficiently expressed in epithelia [Yew et al., 1997], besides a variety of mammalian cultured cells *in vitro* [Foecking and Hofstetter, 1986].

Chapter 4

Creation and characterisation of ChR2 mutants in the ARPE-19 cell line

Introduction

Interrogation of light-gated wild type Channelrhodopsin-2 (wtChR2) activity in the retinal epithelial cell line ARPE-19 did not appear to alter calcium dynamics, as reported in 3.2. It was hypothesised that driving epithelial processes such as ion and fluid transport may require a different optimisation of channel behaviour (strong DC conductance) compared with that required to photoactivate excitable cells (rapid activation and inactivation kinetics). In addition, epithelia in general display strong homeostatic behaviour, which may act to actively resist the requisite ion dynamics required to perturb their physiology. In order to overcome literature-reported limitations of the wild type, among them low channel conductance and strong desensitisation [Lin, 2011], I focused on identifying appropriate single amino acid mutations in the sequence of ChR2, which would result in a more suitable channel performance in epithelial cells. The mutated amino acids were chosen because of their involvement in critical interactions with the retinal chromophore in the active site of the protein and are therefore crucial for channel properties (Section 1.2.1.3). Four variants of ChR2, namely E123T, C128A, L132C and T159C were generated via site-directed mutagenesis. Following generation

of ChR2 variants, expression patterns, localisation and activity of the mutants in the epithelial cell model were tested with the same methodologies used for the wild type in Chapter 3. Additionally, mutagenesis-generated variants were compared to an established construct, H134R from Addgene, studied alongside for expression and activity in epithelial cells. ChR2 mutants which proved to modify calcium permeability across ARPE-19 cells were further characterised for their specific features in this cell line.

4.1 Genetic engineering of ChR2 mutants for applications in epithelial physiology

4.1.1 Screening of ChR2 mutants

The last decade has seen the rise of genetic engineering of microbial rhodopsins for optogenetic applications. Modification and rearrangements in the sequences of the numerous nature-occurring light-gated channels and pumps have refined the spectrum of the optogenetic tools available to researchers [Lin, 2011; Lin et al., 2013; Prigge et al., 2012].

Modifications of single amino acids in the retinal binding pocket of channelrhodopsins has resulted in a variety of proteins with modified kinetics, activation wavelengths or ion permeability, as shown in Figure 1.30. Following screening of previously reported channelrhodopsin variants, this study focused on the mutants that would present the most appealing properties for the application of optogenetic techniques in epithelial cells *in vitro*.

Variants resulting from point mutations of *C. reinhardtii* ChR2 were preferred to ChRs with comparable features from other organisms. This decision was made for two reasons. First, a versatile vector (pcDNA3.1) with the ChR2 sequence fused to mCherry was already available, thus reducing the risks of the mutagenesis procedure. Moreover, the use of different variants of the same exact protein would make comparison of their characteristics more robust. For instance, ChETA [Gunaydin et al., 2010] was preferred to ChD (ChimeraD of Channelrhodopsin) [Lin et al., 2009b; Wang et al., 2009], generated by chimeragenesis of ChR1 and ChR2; they share similar properties in terms of

kinetics and recovery but ChETA can be engineered directly from wtChR2.

Selection of the mutants was based both on their published kinetics and conductance and on parameters interesting to be controlled non-invasively in epithelial cells, mostly the ARPE-19 cell line. These cells present in fact a plethora of ion channels and transporters and their ability to counteract perturbation of ionic equilibrium is potent. Therefore, mutants with slower off-kinetics of the channel, such as C128A [Berndt et al., 2008], would allow for prolonged fluxes of ions through the cell membrane and detection despite native channel activity to restore equilibrium. Similarly, mutation T159C [Berndt et al., 2011], which generates higher photocurrents in neurons, could potentially be exploited to increase the flow of ions through the open channel, therefore perturbing even more the intracellular environment and amplifying the signal for detection. On the other hand, a ChR2 variant characterised by increased permeability for calcium ions, like L132C (or CatCh-Calcium Translocating ChR2) [Kleinlogel et al., 2011a] might represent the perfect candidate for calcium imaging experiments. Similarly, a variant with a slight red-shifted (495nm) excitation, like ChETA (E123T mutation) would couple well with Fura-2 imaging experiments, avoiding cross-activation by the UV wavelengths used for calcium detection [Lin et al., 2009b].

4.1.2 Generation of ChR2 variants with modified channel properties for applications in epithelial physiology

Four variants of ChR2 were generated via site-directed mutagenesis on the wtChR2-mCherry pcDNA3.1 vector after screening of the point mutations known to have an effect on the channel kinetics and conductance.

Figure 4.1 shows alignments of the mutant sequences with the wt one, highlighting the mutation sites. In the DNA alignments, mutated nucleotides or triplets are demonstrating successful site-directed mutagenesis; they can in fact be compared with the mutagenic primers in Table 2.1.

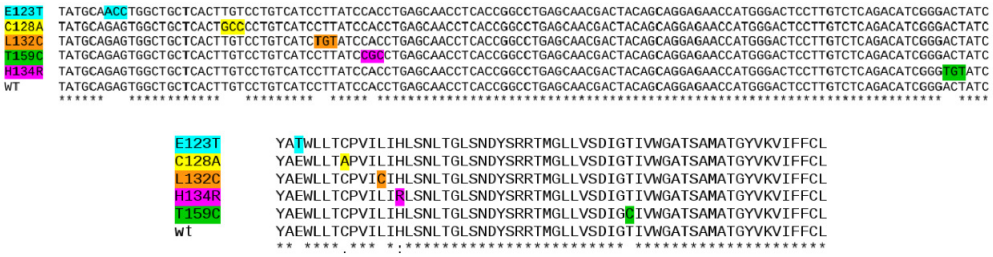


Figure 4.1: **DNA and protein sequences validation of ChR2 mutants created by site-directed mutagenesis.** Partial alignment of wtChR2-mCherry fusion protein DNA and protein sequence with the sequences of the mutants generated with the Quikchange II XL Site-Directed Mutagenesis kit (Agilent Technologies). Alignment was performed with Clustal Omega (EMBL-EBI) multiple sequence alignment tool. The highlighted mutations, both in the sequences of nucleotides and amino acids, confirm successful generation of point mutations in wtChR2 structure. The different point mutations are colour-coded (yellow for C128A, green for T159C, orange for L132C, blue for E123T and pink for H134R).

Whole sequence alignment in ClustalW confirmed preservation of the gene structure outside the mutation sites, together with the integrity of the fusion protein with the fluorescent marker mCherry, as shown in Figure 4.3. Figure 4.2 shows partial chromatograms obtained from the Sanger sequencing and by analysis with FinchTV software, compared with the wild type sequence, where succesful mutagenesis is demonstrated.

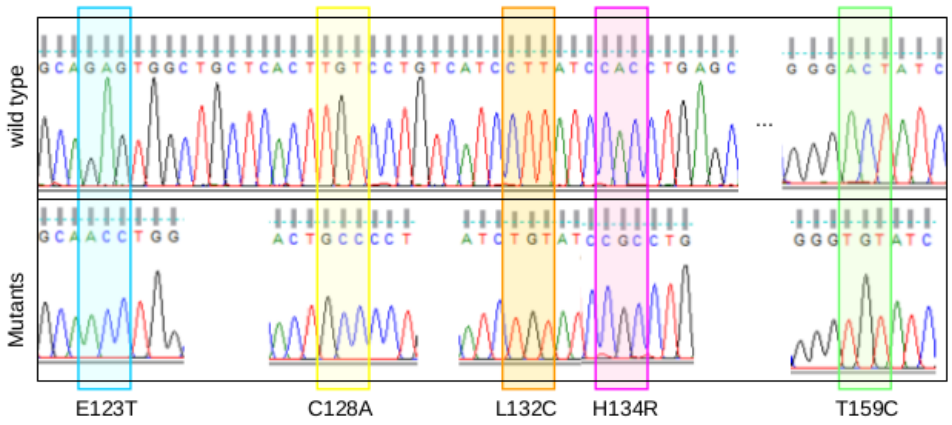


Figure 4.2: **Partial chromatograms showing successful mutations in the ChR2 sequence.** Left to right: E123T, C128A, L132C, H134R and T159C. Chromatograms were obtained with FinchTV software after Sanger sequencing analysis. Mutated triplets are highlighted in coloured boxes and they can be compared with the wild type sequence above them.

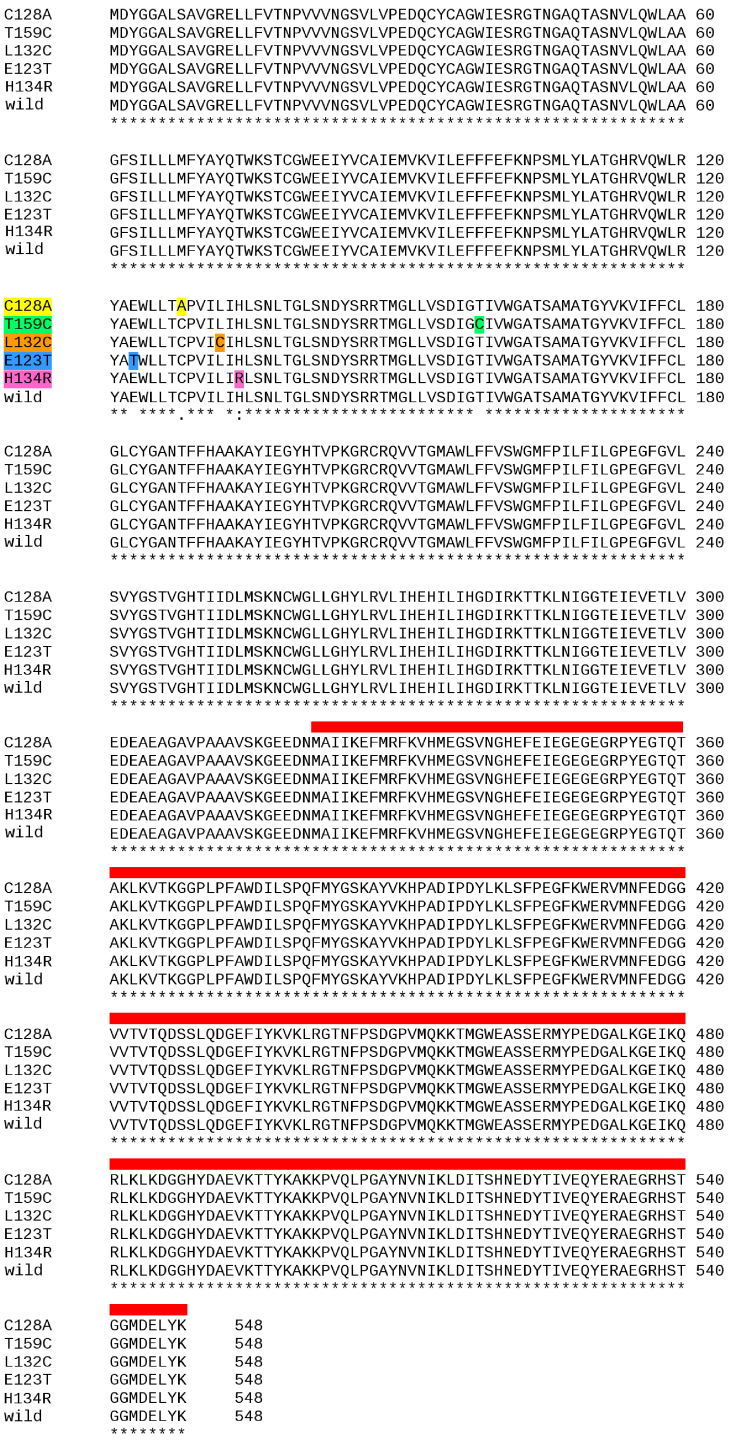


Figure 4.3: **Complete sequence alignment of ChR2 wild-type protein sequence (wild) with the mutants generated with the Quikchange II XL Site-Directed Mutagenesis kit (Agilent Technologies).** The alignment confirmed successful mutagenesis in the desired point of the sequences (highlighted in different colours for each mutant) and integrity of the fusion with mCherry fluorophore (highlighte in red).

4.1.3 Cytotoxicity study of *all-trans* retinal

Since ChR2 expression in the retinal pigment epithelial cell line ARPE-19 is novel, a cytotoxicity study was performed to assess effects of the supplementation of increasing

concentrations of *all-trans* retinal (ATR), required by microbial rhodopsins for their functionality [Patel et al., 2004], to the cell growth media. There are reports, in a number of optogenetic studies, of ATR supplementation both to mammalian cells and non-mammalian cells or animals [Grimm et al., 2017a; Kralj et al., 2012; Nagel et al., 2003].

In order to study the potential cytotoxic impact of ATR in the present study, a live/dead assay, was chosen, based on a similar evaluation by Yu and colleagues [Yu et al., 2015]. Calcein/Propidium Iodide (PI) live/dead assay is based on the principle that only live cells will be able to metabolise calceinAM and generate green fluorescence, while PI will only cross the membrane of dead cells and emit red fluorescence once bound to their damaged DNA.

In this case, ATR in concentrations ranging from 0.1 μM to 30 μM was incubated with the cells for 24 and 48 h in a 96-multiwell plate. Figure 4.4 reports representative fluorescence images of propidium iodide (red) and calceinAM (green) stains of ARPE-19 after 48 h incubation with 0.1 μM ATR and 30 μM ATR in the cell medium. Calcein fluorescence is abundant when cells are grown in low ATR concentrations (Figure 4.4 C), while it is reduced when $> 15\mu$M ATR was supplemented to the cell medium (Figure 4.4 D). Conversely, PI fluorescence is low and sparse at lower ATR concentrations (Figure 4.4 A) and intensifies upon increase of cell death as a consequence of higher toxicity of ATR (Figure 4.4 B).

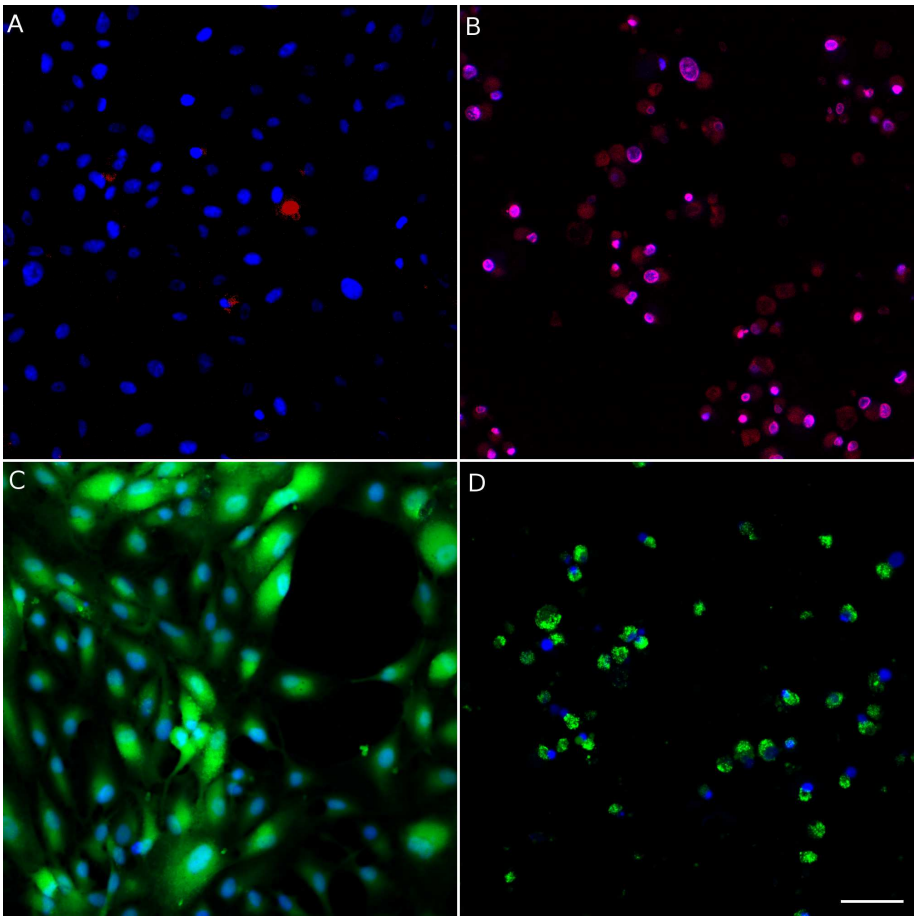


Figure 4.4: **Fluorescence images representative of calcein and propidium iodid fluorescence in ARPE-19 cells grown with increasing concentrations of ATR.** Effects of *all-trans* retinal on the health of ARPE-19 cells were evaluated with a live/dead assay based on propidium iodide and calcein. Panel **A** and **B** compare PI-stained cells (red) among population (labelled with Hoechst-stained nuclei-blue) grown in 0.1 μM and 30 μM ATR, respectively. Panel **C** and **D** show calcein-dyed cells (green) grown in 0.1 μM and 30 μM ATR, respectively. Blue represents Hoechst-labelled cell nuclei. Images were acquired with a MicroPlate Reader IX Ultra (ThermoFisher). Scale bar is 50 μm.

Data for the full range of concentrations tested are summarised in Figure 4.5. The graph is representative of two separate wells in the multiwell plate used to assess viability in the Microplate IX Ultra Reader, where 4 randomised spots were measured for PI fluorescence intensity. Cytotoxicity of ATR was established based on the number of dead cells (PI-positive) in the population of cells stained for their nuclei (Hoechst) in four fields of view in two wells with the same concentration of ATR. ATR concentrations ranging from 0.1 to 10 μM did not significantly affect cell health, with less than 10% dead cells. When massive doses of ATR (15-30 μM) were added to the growth medium, most of the cells in culture died, with percentages ranging from 20% to almost 80% for 20 and 30 μM.

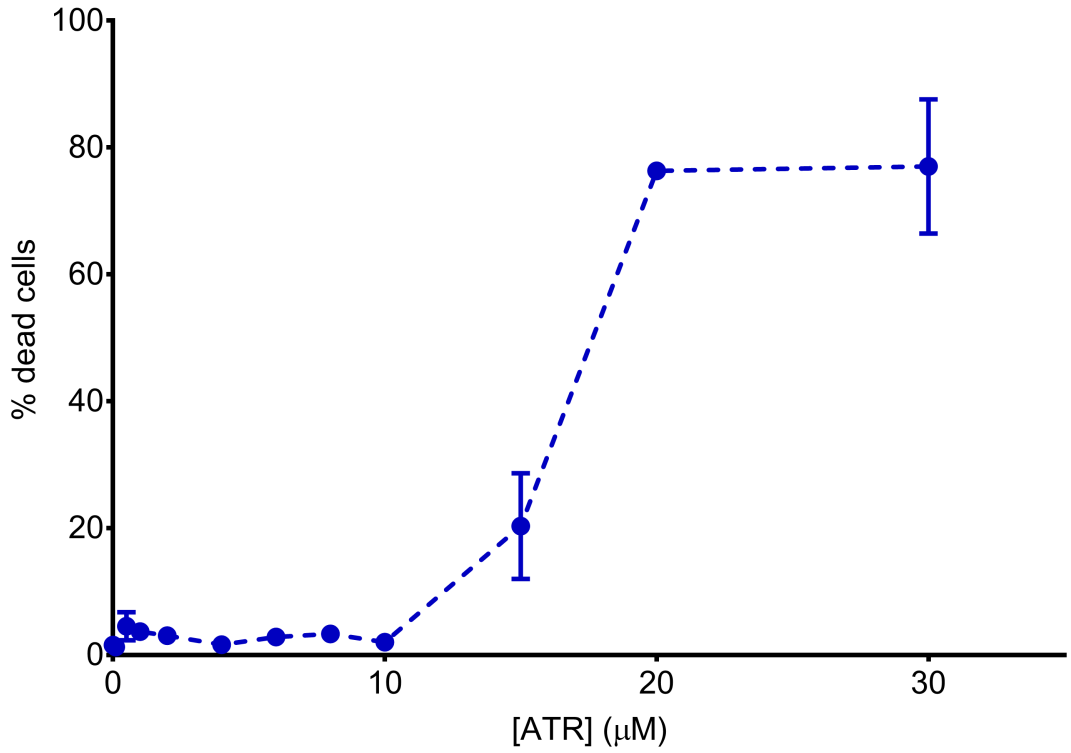


Figure 4.5: **Study of cytotoxicity of *all-trans* retinal in the ARPE-19 cell line.** Cytotoxicity of *all-trans* retinal (ATR) was evaluated with a live/dead assay. Assessment was performed in a 96-well plate and fluorescence of propidium iodide (PI) was read on a multiplate reader IXUltra following 48 h incubation with ATR concentrations ranging from 0.1μM to 30 μM. Data are representative of averages of replicates for each condition ± SEM.

From the outcome of the cytotoxicity assay, concentrations of ATR between 0.1 and 10 μM appear to be safe for supplementation to ARPE-19 cells for experiments assessing the functionality of the optogenetic channels without affecting growth or health. For experiments described in further sections , a concentration of 1μM ATR was chosen for supplementation into the cells' growth medium, unless otherwise stated.

4.2 Expression of ChR2 mutants in the ARPE-19 cell line

4.2.1 Flow cytometric evaluation of mutant ChRs expression in ARPE-19 cells

Following validation of the ChR2 mutants sequences generated via site-directed mutagenesis, reported in Section 4.1.2, all the plasmids were tested for expression levels in the ARPE-19 cell line. Data reported in this section show transfection efficiency of ChR2 mutants in pcDNA3.1 plasmids with and without ATR supplementation, anal-

ysed 48 h post transfection.

Figure 4.6 shows that 25-40% of ARPE-19 cells expressed the different exogenous mutants after delivery of genetic material, regardless of ATR supplementation. These expression levels are encouraging for assessment of the functionality of mutagenesis-generated ChR2 mutants in ARPE-19 cells and are comparable to transfection efficiencies reported in Section 3.1.1. Interestingly, improvement in the expression of T159C and C128A mutants was observed, which is comparable to the expression of the mutant H134R, purchased from Addgene.

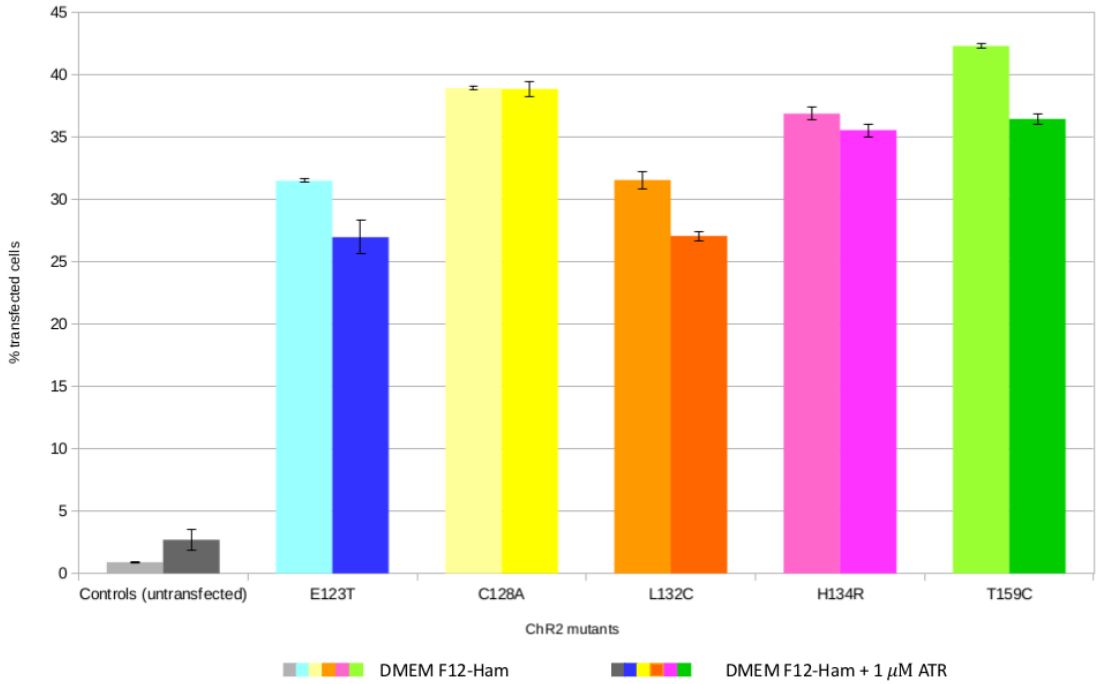


Figure 4.6: **Flow cytometry data showing transfection efficiency of ChR2 mutants constructs delivered by Lipofectamine3000 (ThermoFisher, Invitrogen) with or without supplementation of 1μM *all-trans* retinal in the growth medium.** Cells were analysed on a MoFlo Astrios cell sorter (Beckman Coulter) where ChR2 expression was confirmed by mCherry reporter fluorescence (ex. 587nm/em. 610nm). Data shown are representative for two independent sets of experiments both for the no-ATR medium and the supplemented one. Untransfected cells grown in the same conditions were used as controls (grey). Data represent mean values from replicates ± SEM.

4.2.2 Study of expression levels of ChR2 mutants by fluorescence imaging

Following flow cytometry, successful expression of ChR2 mutants generated by site-directed mutagenesis in ARPE-19 cells was confirmed by fluorescence microscopy. Fluorescence of mCherry reporter, fused to ChR2 mutants sequences, was used as a marker

for expression of the opsins in ARPE-19 cells.

Figure 4.7 shows representative fluorescent images reporting expression of ChR2 mutants E123T, C128A, L132C, H134R and T159C in ARPE-19 cells. Images were acquired with a Zeiss Axiovert 135TV equipped with an mCherry (excitation: 587nm, emission: 610 nm) filter set (Chroma Technology Corp).

Expresion patterns over time of a representative mutant were investigated to study time-course of the expression in ARPE-19 cells. Monitoring of the expression of ChR2 H134R was performed using mCherry fluorescent marker, tagged to the protein, to assess presence of ChR2 in ARPE-19 cells at 24, 48, 72 h and then at 6 days post-transfection.

Confocal images show fluorescence of mCherry fluorophore, excited at 560 nm and recorded at 610 nm, confirming expression of ChR2 H134R in ARPE-19 cells. Cells from the same batch were seeded on different glass-bottom petri dishes and transfected at day 0; they were then fixed with 4% PFA at increasing time points after lipofection and then imaged on a Leica DMIRE2 confocal microscope. Images were acquired both at 20X magnification, to analyse a bigger population, and at 63X magnification, to visualise expression patterns at the single-cell level. Figure 4.8 highlights a decreasing number of cells expressing the optogenetic channel over time. At 24 h, in fact, a considerable population of the cells in the field of view has internalised the genetic material and is expressing ChR2 H134R. After 48 h, no major difference is appreciable, but at 72 h post transfection most of the cells expressing the channel have died, leaving only a reduced population of ChR2-H134R-expressing cells. Six days (144 h) from transfection, only the minority of the cells is presenting the optogenetic protein ChR2 H134R. These data are in line with the time-course of transient transfection, which is normally attenuated within a week from the delivery of the genetic material [Meissner et al., 2001; Tucker et al., 2003].

Figure 4.9 shows similar images to Figure 4.8, but acquired at higher magnification to highlight sub-cellular localisation of ChR2/H134R-mCherry. Interestingly, after 72 h, increased presence of the optogenetic channel at the cell's outer boundaries is appreciable.

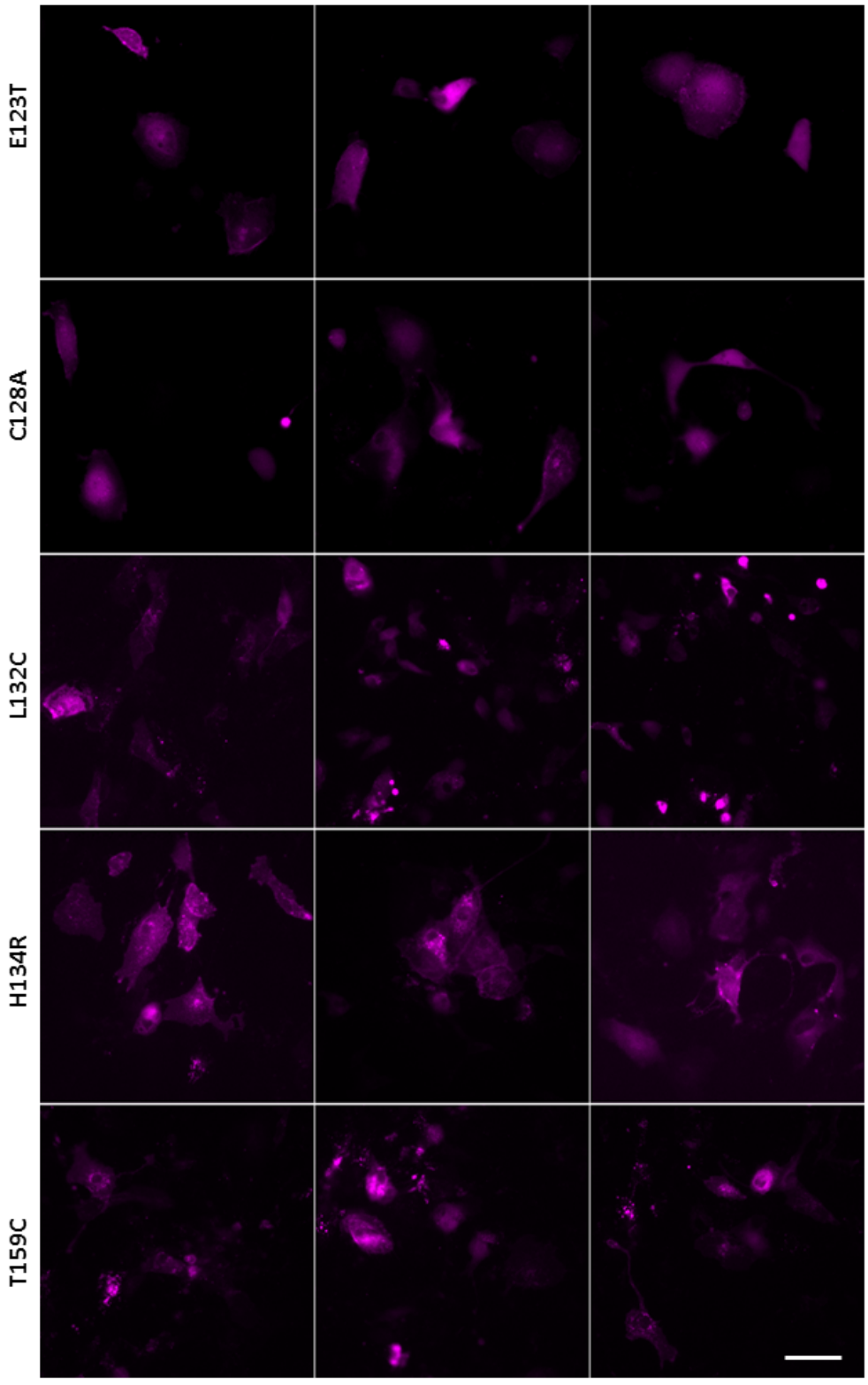


Figure 4.7: **Study of the expression patterns of mutants generated by site-directed mutagenesis.** ChR2 mutants E123T, C128A, L132C, H134R and T159C are expressed by the ARPE-19 retinal pigment cell line. Images report 3 randomised fields of view of ARPE-19 cells 48 h post transfection. Fluorescence of mCherry confirms expression of all ChR2 mutants generated by site-drected mutagenesis in live ARPE-19 cells. Scale bar is 50 μm.

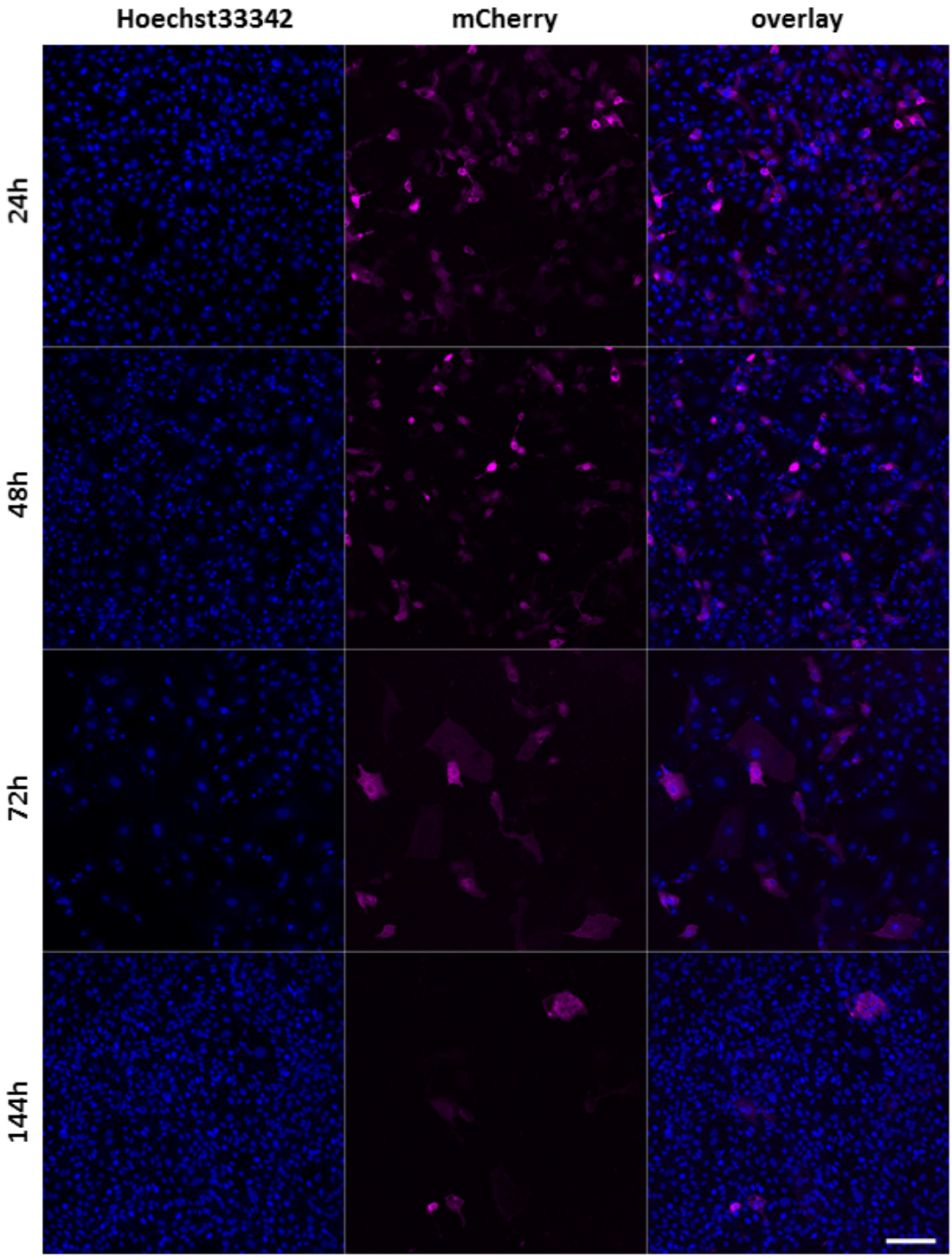


Figure 4.8: **Study of expression levels of ChR2(H134R) mutant at different time points post-transfection.** Lipofectamine3000-mediated expression of ChR2 H134R construct in ARPE-19 cells assessed with confocal microscopy at increasing time points after transfection. Cells were fixed with 4% paraformaldehyde at 24, 48, 72 and 144 h following transfection and counterstained with Hoechst33342 for nuclei labelling. mCherry fluorescence shows the distribution of ChR2 expression. Scale bar is 50 μm.

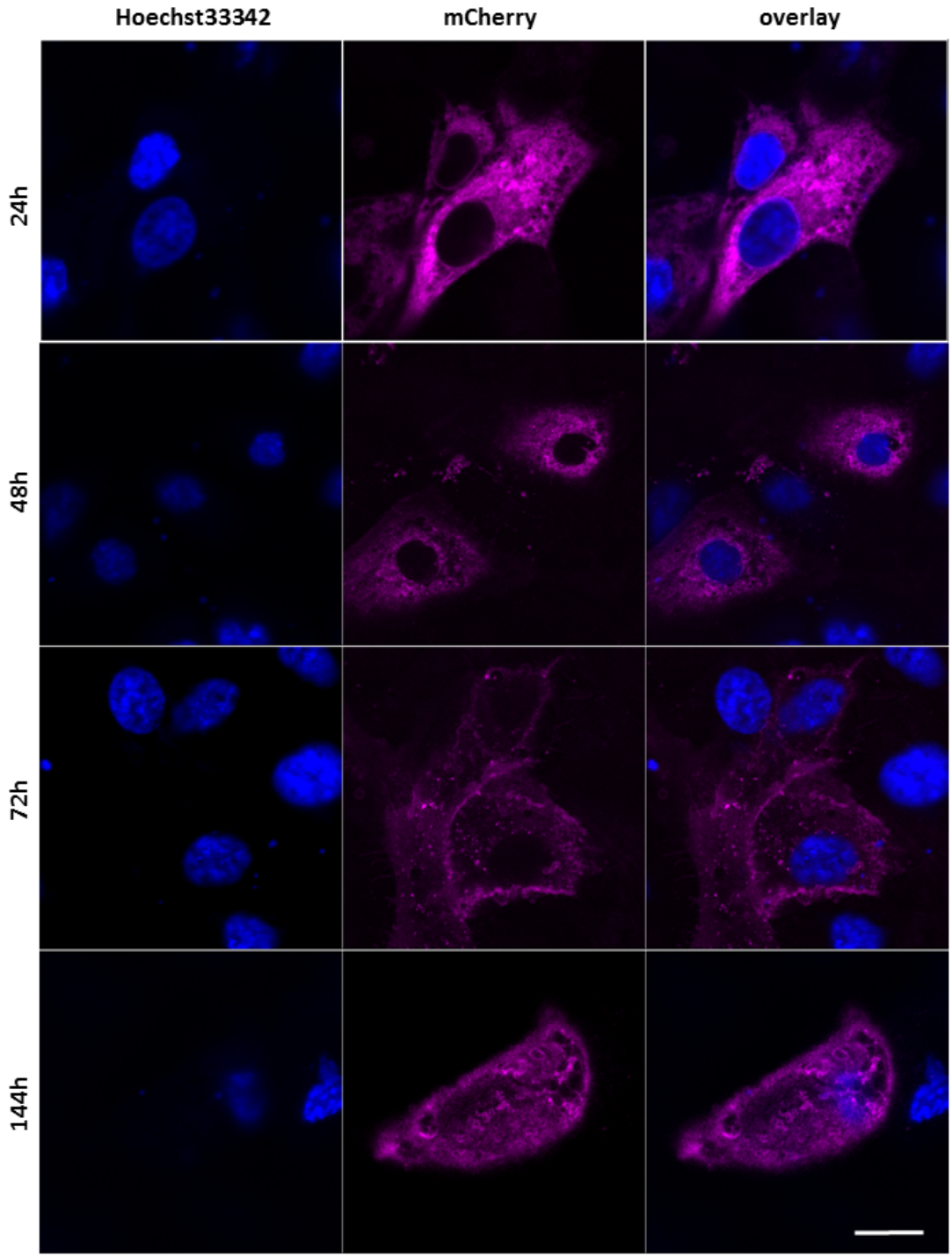


Figure 4.9: **Study of expression levels of ChR2(H134R) at different time intervals following transfection.** Lipofectamine3000-mediated expression of ChR2 H134R construct in ARPE-19 cells assessed with confocal microscopy (63X magnification) at increasing time points after transfection. Cells were fixed with 4% paraformaldehyde at 24, 48, 72 and 144 h following transfection and counterstained with Hoechst33342 for nuclei labelling. mCherry reporter fluorescence confirmed expression of ChR2 protein. Scale bar is 10 μm.

In summary, these results, together with data from the literature, highlighted the time interval between 24 and 72 h as the best range for performing experiments to assess functionality of the optogenetic channels, because of the maximum expression

reported by the fluorescent marker.

4.2.3 Membrane localisation study of the expression of ChR2 mutants in the ARPE-19 cell line

To study membrane expression patterns of the ChR2 mutants generated by site-directed mutagenesis, the blue fluorophore-conjugated wheat germ agglutinin, WGA-CF405, was again used as a membrane stain to assess subcellular distribution of the transgenic proteins, as in Section 3.1.4. ChR2 mutants were analysed for their membrane expression 36 h post transfection. Confocal images shown in figure 4.10 report fluorescence of the mCherry reporter, marker of ChR2 expression and localisation, and WGA-CF405, which binds to the negatively-charged carbohydrates in the cell membrane. At the time point chosen for assessment, subcellular localisation of ChR2 at the membrane compartment is appreciable by the overlay of WGA and mCherry fluorescence. Cytosolic fluorescence can also be noted, and it could indicate both synthesised ChR2-mCherry on the post-translational trafficking pathway from the nucleus to the membrane compartment or ChR2-mCherry on its recycling path from the membrane.

Figure 4.11 shows membrane distribution study performed on Figure 4.10 of ChR2 variants using FIJI software. Briefly, lines were drawn across optogenetically-modified cells on the fluorescence images for mCherry and WGA. The profile of such lines provides an index of overlay of the two fluorophores, therefore of the co-distribution of the ChR2 mutants and the plasma membrane. Despite cytosolic presence of ChR2-mCherry, the channels are also localised to the cell compartment where they are functionally active. These observations are consistent with the analysis of the expression levels of ChR2 H134R, suggesting the interval between 24 and 72 h as the most suitable window for experimental procedures assessing functionality of the channel, such as calcium imaging experiments, described in the following section 4.3.

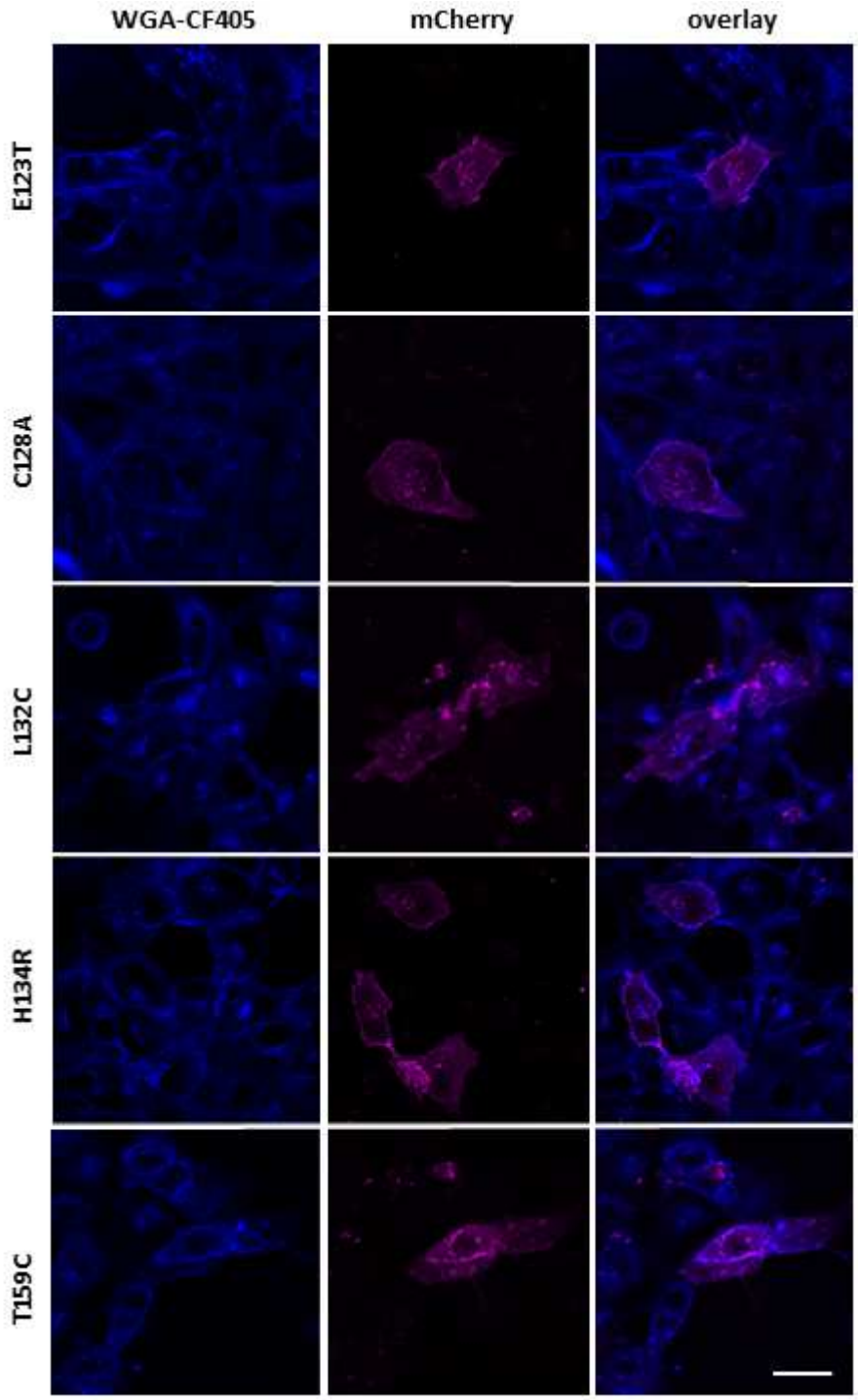


Figure 4.10: **Confocal images showing sub-cellular localisation of ChR2 mutants in ARPE-19 cells.** Confocal images show membrane localisation of ChR2 mutants (top to bottom) E123T, C128A, L132C, H134R and T159C. Blue fluorophore-conjugated wheat-germ agglutinin (WGA-CF405) highlights membrane compartment by binding to negatively-charged carbohydrates on the cell surface (left column). ChR2 mutants localisation was assessed by fluorescence of mCherry (magenta) reporter fused to the protein sequence (middle column). Overlay of the two channels shows partial localisation of the proteins to the plasma membrane domain. Scale bar is 20 μm.

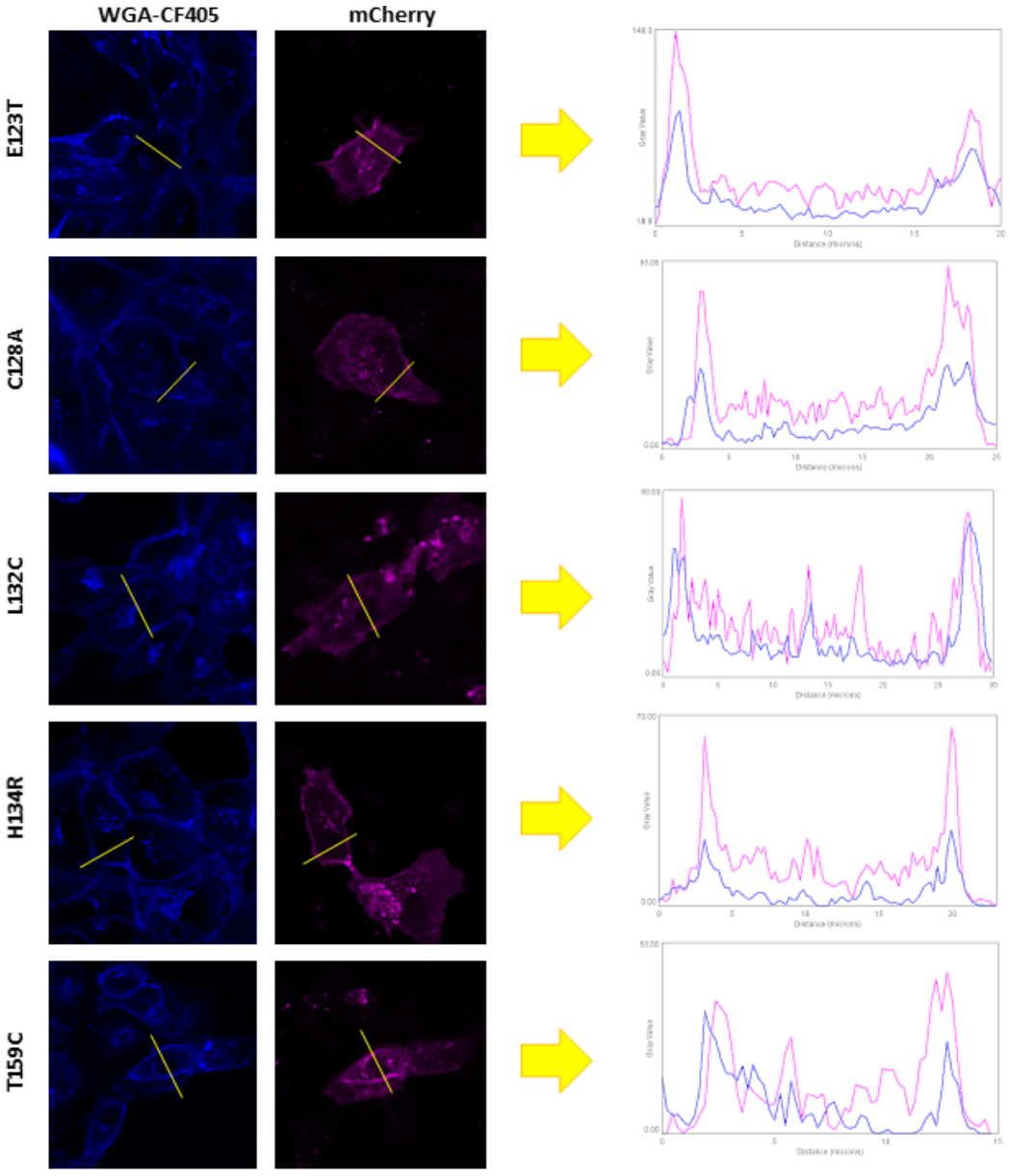


Figure 4.11: **Membrane localisation study of ChR2 mutants.** Membrane localisation of ChR2 mutants was assessed on FIJI, exploiting fluorescence intensities of mCherry-ChR2 (magenta) and WGA-CF405 (blue). Plots show intensity profiles of lines drawn across ChR2-expressing cells. The plotted curves show membrane-bound WGA (blue) and mCherry-tagged ChR2 mutants (magenta); overlay of the peaks confirms membrane localisation of the optogenetic proteins.

4.3 Functionality of ChR2 mutants in retinal epithelial cells

4.3.1 Fura-2 ratiometric calcium imaging of ChR2 mutants

Channelrhodopsin-2 (ChR2) is a non-selective cation channel permeable to sodium, potassium, protons and calcium. Monitoring of ion dynamics across the plasma membrane has been reported as a reliable method for confirmation of ChR2 channel activity [Renault et al., 2015; Shipley et al., 2014].

Functionality of ChR2 mutants in this study was assessed via ratiometric calcium imaging using the calcium-sensitive dye Fura-2 [Roe et al., 1990]. ARPE-19 cells in glass-bottom petri dishes (Ibidi μdishes) for optimal light propagation, were imaged on a Zeiss Axiovert 135TV inverted light microscope, equipped with a filter set for Fura-2 (dual excitation = 340 and 380 nm, emission = 510 nm) and an additional exciter for ChR2 activation light (475/40 nm). Expression of the optogenetic channels was confirmed by detection of mCherry ($\lambda_{\text{excitation}}$ = 587 nm; $\lambda_{\text{emission}}$ = 610 nm), fluorescent tag of the protein.

Stimulation with blue (470 nm) light for 2 s in an extracellular solution containing 80 mM $CaCl_2$ generated calcium transients in ARPE-19 cells expressing the mutants L132C (Figure 4.12), T159C (Figure 4.15) and H134R (Figure 4.17). No calcium transient was detected in untransfected cells exposed to the same light stimuli in the same field of view, while all cells responded to the addition of 10 μM ACh (positive control). The variant E123T failed to change calcium membrane permeability of ARPE-19 cells (Figure 4.19), or such change was too small to be detected. E123T mutation in ChR2 is characterised by reduced desensitisation compared to the wild type but decreased photocurrent amplitudes have also been reported [Lin, 2011].

C128A, one of the bistable channelrhodopsin mutants characterised by slower off-kinetics [Berndt et al., 2008], also appeared to modify calcium permeability (Figure 4.18). Different parameters were manipulated in order to optimise functionality of the ChR2 mutants in ARPE-19 cells, such as power intensity (0.3-40 mW/mm^2), imaging time post-transfection (from 24 h to 72 h), calcium concentration in the extracellular

solution (from 2 mM to 90 mM) and ATR supplementation to the medium (1 μM, 5 μM or no supplementation).

The present section summarises activities of the five ChR2 mutants in ARPE-19 cells described in this thesis, whilst the following section will compare the variants H134R, L132C and T159C for their properties in ARPE-19 retinal pigment epithelial cells *in vitro*.

Unless otherwise stated, the cells were grown in growth medium supplemented with 1μM ATR for 24 h before transfection and imaged 36 h following delivery of opsin plasmid DNA. Power used for blue (475/40 nm) light stimuli was, unless specified, 9 mW/mm^2.

L132C, Calcium Translocating Channelrhodopsin (CatCh)

Figure 4.12 shows representative Fura-2 measurements of calcium dynamics in ARPE-19 cells expressing the ChR2 mutant L132C, or CatCh (Calcium-Translocating Channelrhodopsin) in 80 mM extracellular calcium solution. Fluorescent imaging of mCherry marker for identification of ChR2/L132C-expressing cells in a wider population of untransfected cells is shown in Figure 4.12A. Fluorescence of the calcium-sensitive dye Fura-2 was exploited to visualise all the cells in the field of view and control untransfected cells were compared to response of optogenetically-modified cells (Figure 4.12 B and C). No brightfield imaging was performed on the cells, to prevent undesired photoactivation of ChR2 and subsequent desensitisation of the channel. Repeated 2s blue (470 nm) stimuli from the filtered light of the fluorescence xenon-mercury lamp were delivered to the cells through a 40X objective and Fura-2 fluorescence responses were recorded. Upon light stimulation, opening of the ChR2 pore causes a rapid rise in intracellular calcium concentration, as reported by changes in the ratiometric measurement of Fura-2 dye (Figure 4.12). No change in calcium permeability was recorded in neighbouring cells, simultaneously exposed to the same light stimuli (475/40 nm,9 mW/mm^2), which covered the full imaging field. After termination of the stimulus, the signal decayed exponentially towards the baseline, that is to pre-stimulus calcium concentrations. Homeostatic concentrations of intracellular calcium can be restored

either by uptake to the endoplasmic reticulum stores by means of the SERCA (Sarcoplasmic/Endoplasmic Reticulum Calcium ATPase) enzyme or by native membrane channels in ARPE-19 cells, such as the PMCA (Plasma Membrane Calcium ATPase).

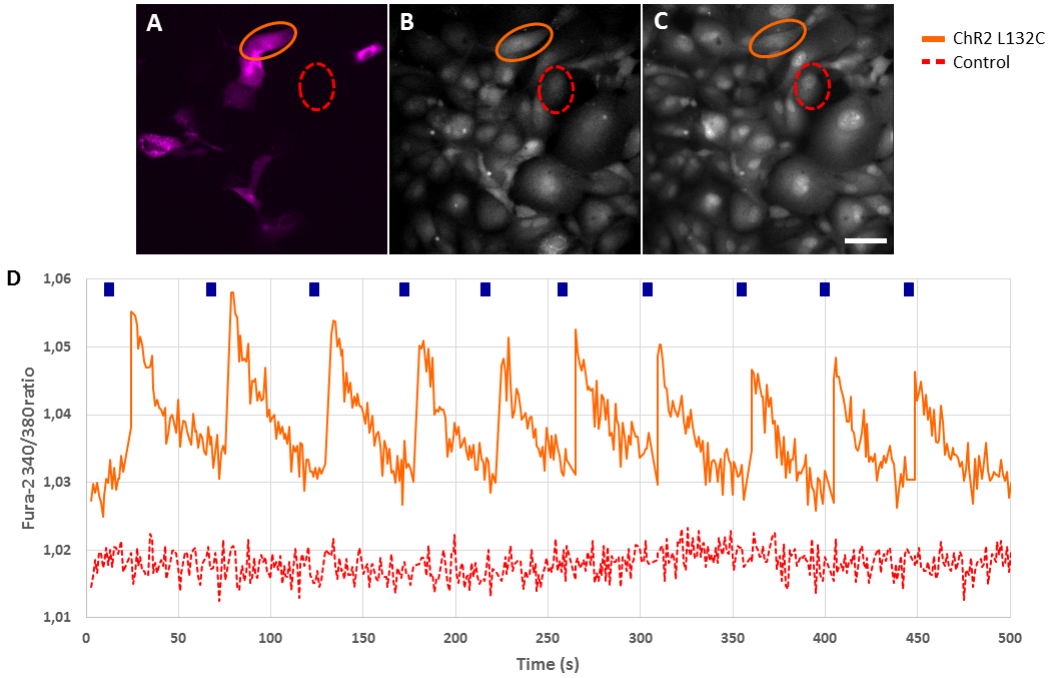


Figure 4.12: **Fura-2 ratiometric measurements of Ca^{2+} influx in ARPE-19 cells expressing ChR2 L132C mutant.** ChR2 L132C activation causes Ca^{2+} transients in ARPE-19 cells. **A** mCherry channel showing ChR2-expressing retinal epithelial cells; **B** Fura-2 340 nm and **C** 380 nm channels show intracellular loading of the calcium indicator. Scale bar is 50 μm. **D** ChR2 L132C response to 2-second blue light stimuli (blue bars, 475 nm, 9 mW/mm^2) delivered through the 40X/0.75NA objective. Cells were bathed in 80 mM extracellular Ca^{2+} solution. Representative trace of ChR2(L132C) cell is compared to the absence of calcium flow in an untransfected cell in the same field of view, acting as a control.

Recent evidence in the literature support the theory, which describes ATR as an enhancer of opsin performance [Grimm et al., 2017b; Yu et al., 2015]. To investigate ATR effect on optical response of ChR2 mutant L132C, the same functional analysis with Fura-2 indicator was conducted on L132C-transfected ARPE-19 cells grown in 0 μM or 1 μM-ATR DMEM. Figure 4.13 reports comparison of a calcium transient generated by a 2s photostimulus in ARPE-19 cells grown in the presence or absence of the retinal chromophore. L132C mutant reliably caused calcium transients, regardless of external sources of ATR. ATR supplementation did not alter the amplitude of the response but appeared to result in a faster off-rate of the channel, i.e. a quicker return to baseline calcium levels. Such difference might depend on the synthesis of a more stabilised channel, as reported for cardiac cells in culture [Yu et al., 2015].

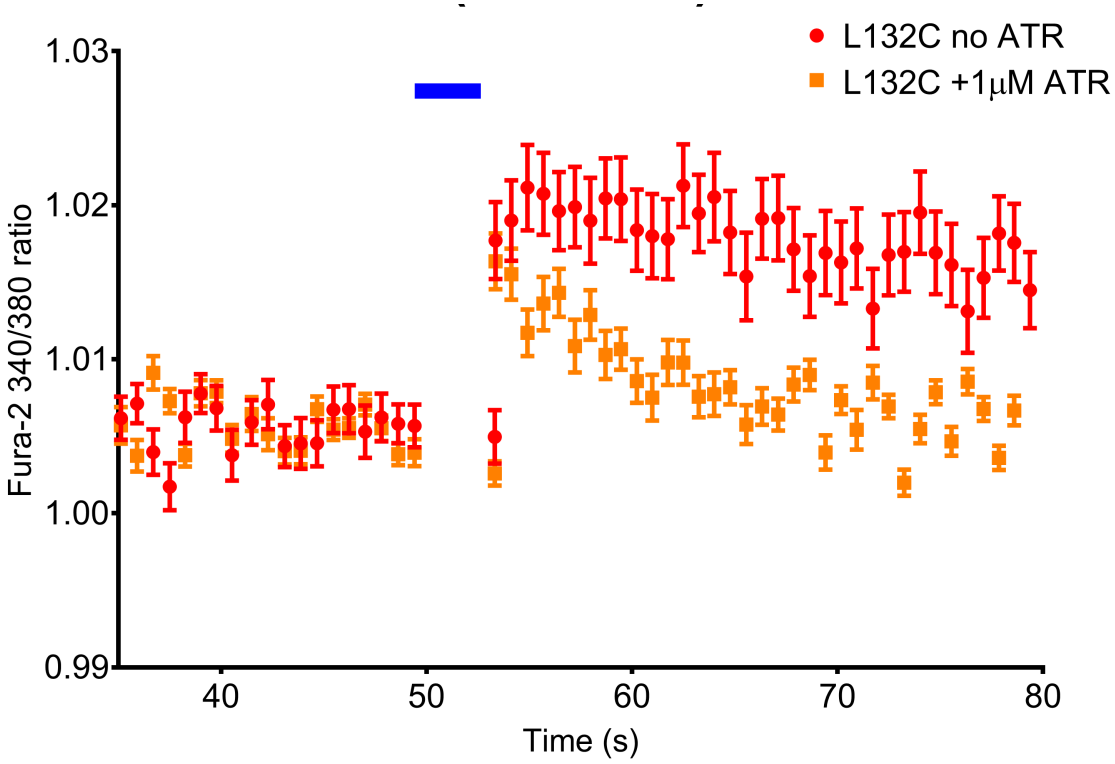


Figure 4.13: **Effects of *all-trans* retinal (ATR) supplementation on the activity of ChR2 mutant L132C.** The graph shows the response of ChR2 L132C mutant expressed in ARPE-19 cells grown in 1 μM ATR (orange) or in the absence of ATR (red). Calcium imaging was performed in 80 mM $CaCl_2$ extracellular solution. Two-second blue (470 nm) light stimulus is represented as a blue bar on the graph. Data are representative of average responses of n=10 cells for each condition. Data are presented as mean ± SEM at each point for each data set.

As shown by both Figure 4.12 and 4.13, repeated stimuli triggered precise response in ARPE-19 cells expressing ChR2 L132C. Up to 15 pulses were delivered to the optogenetically-modified cells and ChR2 L132C reliably changed calcium permeability.

Figure 4.14 shows Fura-2 measurements of ARPE-19 cells expressing L132C mutant in a 2 mM extracellular calcium solution. Although calcium transients were detected, such behaviour was recorded for <5% transfected cells, therefore less reliable than cells bathed in higher extracellular calcium, where >50% of the ChR2-expressing cells manifested changes in calcium permeability.

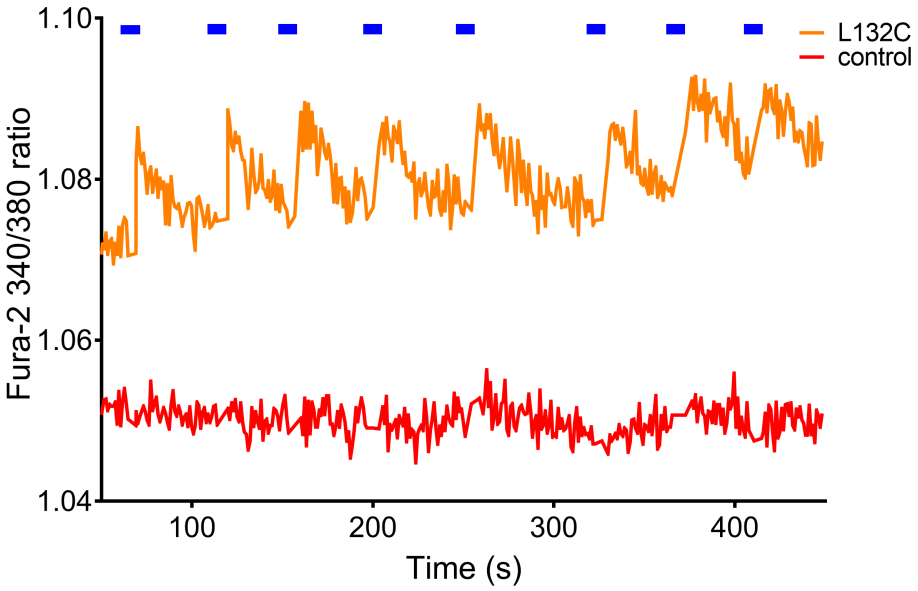


Figure 4.14: **L132C causes calcium transients in ARPE-19 cells in 2 mM Ca^{2+} solution.** The graph shows the response of ChR2 L132C mutant expressed in ARPE-19 cells in an extracellular solution containing 2 mM calcium chloride. Two-second blue (470 nm) light stimuli is represented as blue bars on the graph. The graph represents a single optogenetically-modified cell response (orange trace) and an untransfected control-cell response (red trace) in the same field of view.

T159C

Figure 4.15 reports a representative trace highlighting calcium flow dynamics in ARPE-19 cells expressing ChR2 variant T159C in an extracellular solution containing 80 mM $CaCl_2$. Similarly to L132C variant, T159C mutant successfully modified calcium permeability through the cell membrane, when exposed to subsequent pulses of light. Generation of calcium transients was reliable for at least 10 consecutive stimuli, ensuring recovery of the protein and return of signals to baseline calcium levels.

Figure 4.16 shows representative response to 2-second blue light stimulus of T159C-expressing ARPE-19 cells grown with and without ATR supplementation in the cell growth medium. Supplementation of ATR did not appear to alter the ChR2 T159C response, neither in its amplitude, nor its kinetics, suggesting that this mutant is less affected by the presence of exogenous ATR in the medium.

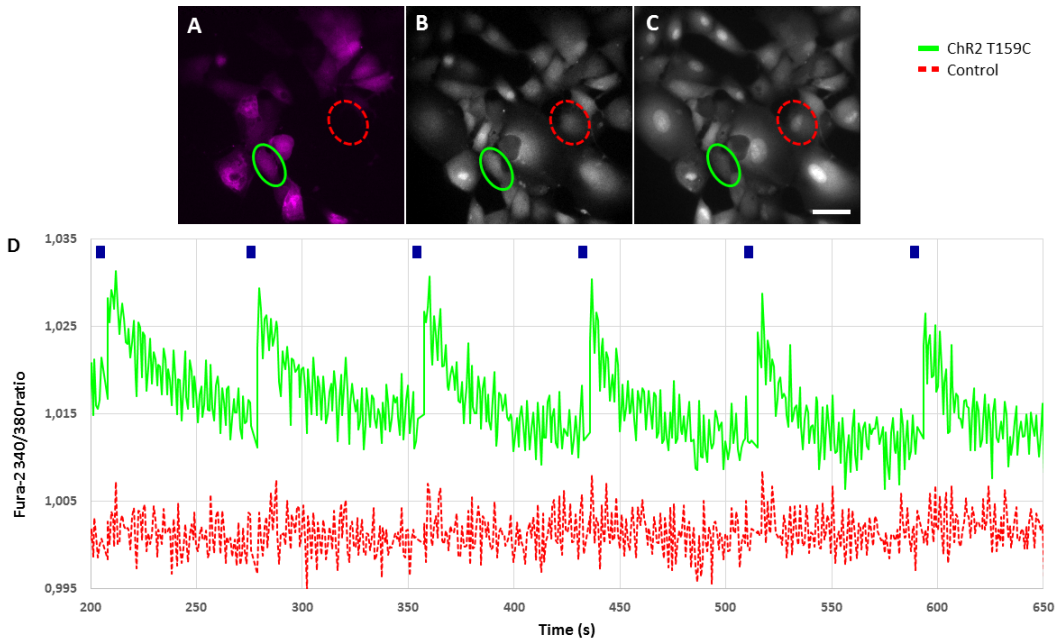


Figure 4.15: **Fura-2 ratiometric measurements of Ca^{2+} influx in ARPE-19 cells expressing ChR2 T159C mutant.** ChR2 T159C activation causes Ca^{2+} transients in ARPE-19 cells. **A** mCherry channel shows ChR2-expressing retinal epithelial cells; **B** Fura-2 340 nm and **C** 380 nm channels show internalisation of the calcium-sensitive dye by the cells. Scale bar is 50 μm. **D** ChR2-T159C expressing cell (green trace) response to 2-second blue light stimuli (blue bars, 475 nm, 9 mW/mm^2) delivered through the 40X/0.75NA objective. Untransfected cell (red trace) is shown in the same field of view and used as a control.

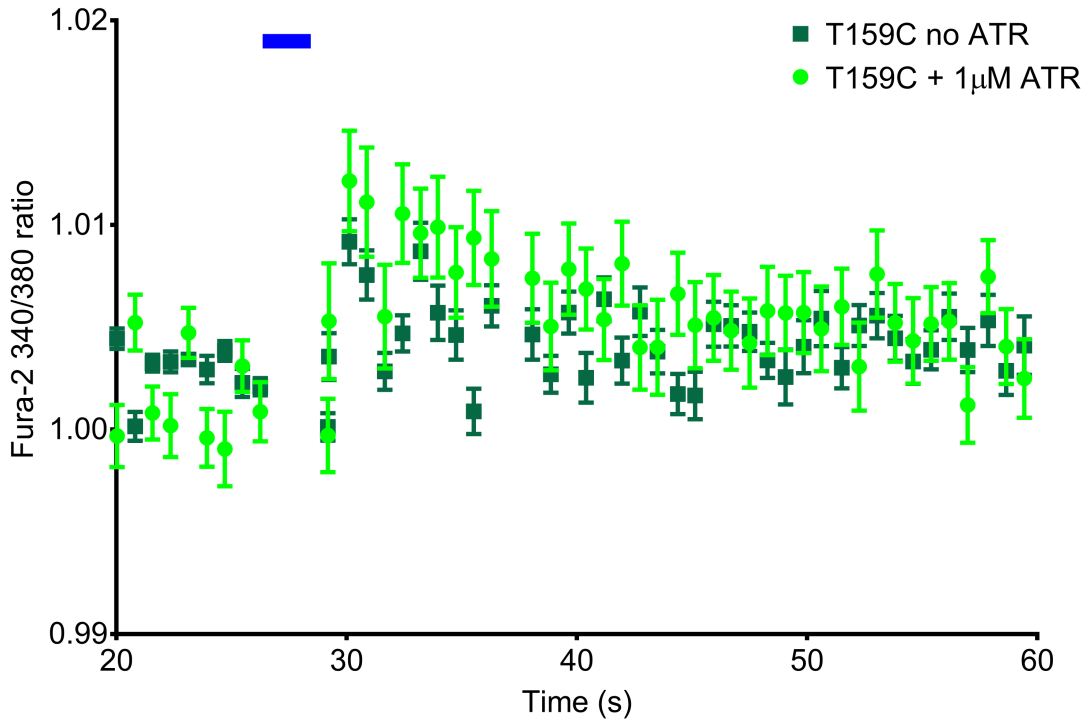


Figure 4.16: **Effects of *all-trans* retinal (ATR) supplementation on the activity of ChR2 mutant T159C.** The graph shows the response of ChR2 L132C mutant expressed in ARPE-19 cells grown in 1 μM ATR (green) or in the absence of ATR (dark green). Calcium imaging was performed in 80 mM $CaCl_2$ extracellular solution. Two-second blue (470 nm) light stimulus is represented as a blue bar on the graph. Data are representative of average responses of n>8 cells for each condition. Data are presented as mean ± SEM at each point for each data set.

H134R

Figure 4.17 reports calcium dynamics in ARPE-19 cells transfected with the ChR2 mutant H134R. Intracellular calcium concentration transiently increased upon activation of the light-sensitive channel, confirming functionality of the H134R mutant in the retinal epithelial cells. Similarly to L132C and T159C variants, calcium equilibrium was subsequently restored and Fura-2 signal returned to pre-stimuli levels. There appears to be an accumulation of intracellular calcium for this mutant, as suggested by the increase in Fura-2 ratio, which will require further investigation.

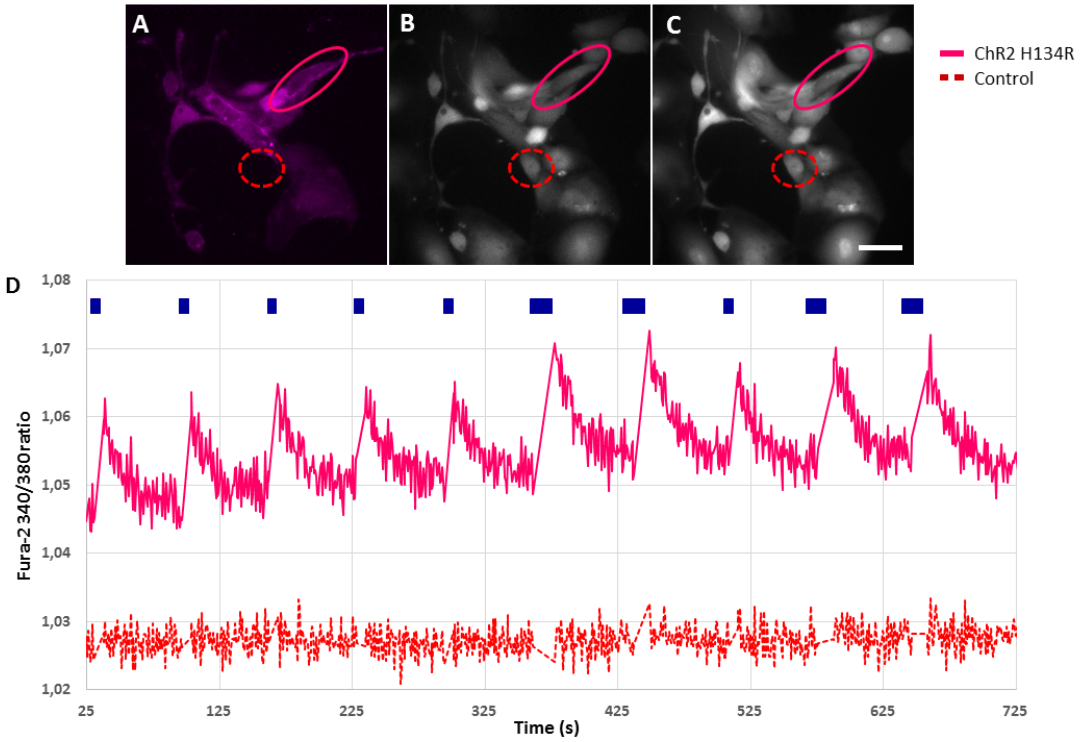


Figure 4.17: **Fura-2 ratiometric measurements of Ca^{2+} influx in ARPE-19 cells expressing ChR2 H134R mutant.** ChR2 H134R activation causes Ca^{2+} transients in ARPE-19 cells. **A** mCherry channel shows ChR2-expressing retinal epithelial cells; **B** Fura-2 340 nm and **C** 380 nm channels show intracellular distribution of the calcium-sensitive dye. Scale bar is 50 μm. **D** Fura-2 ratiometric measurements of ChR2-H134R-expressing cell (magenta) and untransfected cell (red) to blue (475nm, 9 mW/mm^2) light stimuli in the same field of view. Blue light stimuli of the duration of 5, 10 and 15 seconds are represented by blue marks on top of the graph.

C128A

C128A-expressing cells behaviour following light stimulation is reported in Figure 4.18. Intracellular calcium appeared to rise after light delivery but did not return to baseline levels (Figure 4.18 D). C128A is characterised by much slower off-kinetics when

compared to wtChR2 and τ_{off} of the channel has been reported to be longer than 50 seconds [Berndt et al., 2008]. Closure of the channel was attempted by delivering a short pulse of green (530 nm) light, which has been reported to accelerate channel off-kinetics in *Xenopus laevis* oocytes and hippocampal neurons. The 50 ms green light pulse contributed to the closure of the channel, although there is no complete return to baseline levels. Further characterisation of the mutant is needed to investigate the nature of the signals. Delivery of the green stimulus was complicated by the optical configuration in use, since this additional wavelenth was not automatically selectable within the system, requiring a manual intervention.

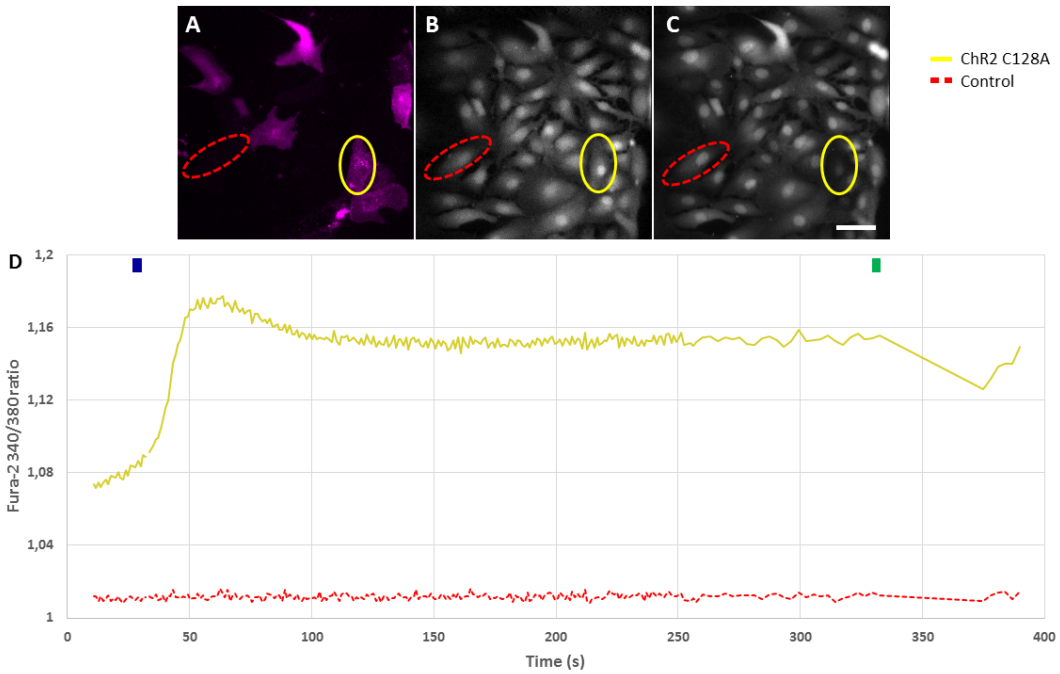


Figure 4.18: **Fura-2 ratiometric measurements of Ca^{2+} influx in ARPE-19 cells expressing ChR2 C128A mutant.** ChR2 C128A activation causes Ca^{2+} transients in ARPE-19 cells. **A** mCherry channel shows ChR2-expressing retinal epithelial cells; **B** Fura-2 340 nm and **C** 380 nm channels show internalisation of the calcium-sensitive dye. Scale bar is 50 μm. **D** Fura-2 ratiometric measurements of ChR2-C128A-expressing cell (yellow solid line) and untransfected control cell (red dotted line) to 10-millisecond blue (475 nm, 9 mW/mm^2) light stimuli delivered through the 40X/0.75NA objective. The channel is closed with 50-millisecond green (530 nm, 9 mW/mm^2) light pulse.

E123T (ChETA)

Figure 4.19 reports a representative response of ARPE-19 cells expressing ChR2 mutant E123T (ChETA). Photo-stimulation of E123T resulted in no significant calcium transient in ARPE-19 cells. Lack of activity of this mutant might be due to its reduced photocurrent amplitudes, compared to wtChR2.

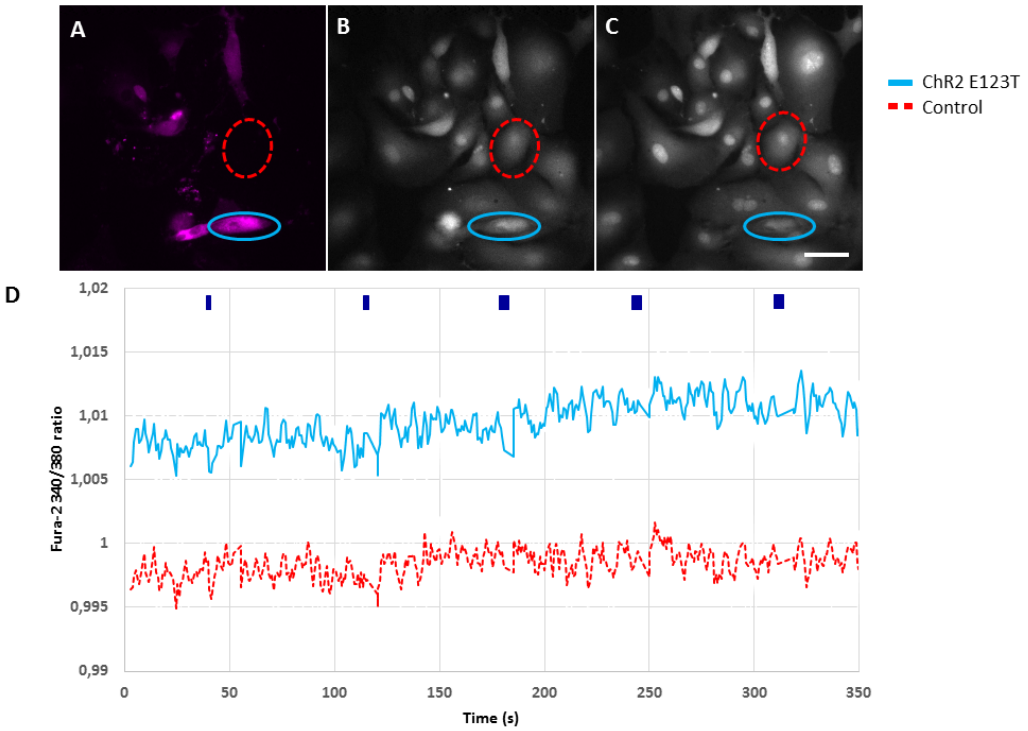


Figure 4.19: **Fura-2 ratiometric measurements of ARPE-19 cells expressing the ChR2 mutant E123T.** No significant calcium transient is recorded in ARPE-19 cells expressing ChR2 E123T in response to 10-millisecond or 2-second light stimuli (blue bars). **A** mCherry channel shows ChR2-expressing retinal epithelial cells; **B** Fura-2 340 nm and **C** 380 nm channels show calcium dye loading of the cells. Scale bar is 50 μm. **D** Fura-2 ratiometric measurements of ChR2-E123T-expressing cell (blue solid line) and control untransfected cell (red dotted line) to 10 ms and 2 s blue light stimuli (blue bars, 490 nm, 9 mW/mm^2) delivered through the 40X/0.75NA objective.

Following results on the functionality of ChR2 variants in ARPE-19 cells, the mutants L132C, H134R and T159C, which showed the ability to modify calcium dynamics within living ARPE-19 cells, were further analysed and characterised for their peculiar properties in this retinal epithelial cell line.

4.3.2 Characterisation of ChR2 mutants L132C, T159C and H134R properties in the ARPE-19 cell line

Behaviour of the mutants in terms of their response to blue light stimuli of different durations (10 ms to 15s) and of increasing light power intensities (mW/mm^2) were studied. Recovery kinetics of the channels were also investigated.

Figure 4.20 compares Fura-2 calcium transients of the mutants H134R, L132C and T159C in response to a 10 s 470 nm light stimulus. Data are representative of the mean response of n$>$ 8 cells (error bars have been omitted for ease of visualisation).

Whereas T159C and H134R were comparable in the amplitude of their responses, L132C

was characterised by a higher calcium influx compared to the other mutants. Such behaviour might be attributed to increased permeability to calcium ions of L132C compared to other ChRs, due to a larger channel pore formed by the substitution of a leucine with a cysteine in position 132 in the retinal-binding pocket [Kleinlogel et al., 2011a].

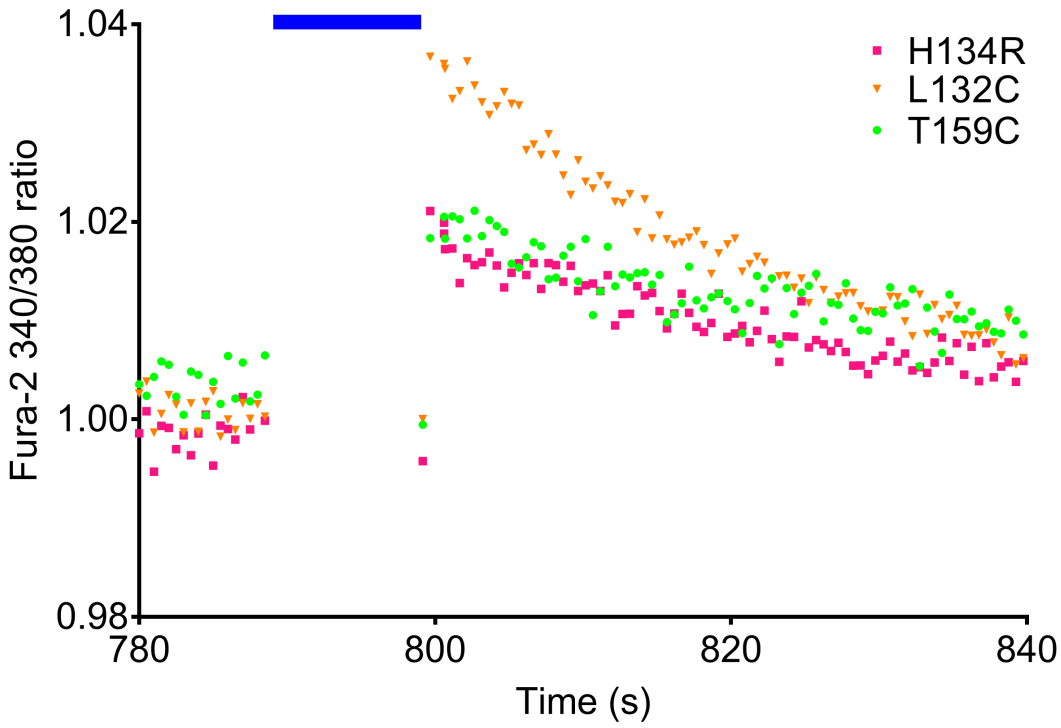


Figure 4.20: **Comparison of ChR2 mutant H134R, L132C and T159C responses to a 10-s light stimulus in ARPE-19 cells.** Fura-2 ratiometric measurements of Ca^{2+} influx in retinal pigment epithelial cells (ARPE-19) expressing ChR2 mutants in response to a 10s light stimulation (blue bar) in an extracellular solution containing 80 mM $CaCl_2$. Data are representative of the mean response from n> 8 cells for each mutant (error bars are omitted for ease of visualisation).

Figures reported below respresent the average behaviour of at least two separate experiments where n >7 cells responded to light stimulations. Data were acquired using the FuraLED/TwinLED unit (Cairn Research Ltd, Faversham, UK) as a light source, a multiwavelength LED unit designed for the combination of optogenetic stimulation and calcium imaging experiments. By removing the need for mechanical movement from one filter position to another, as needed for the filter wheel employed for previous experiments, this LED-based device is characterised by higher speed and reduces previously-described delays.

Figure 4.21 shows the amplitude of responses of ChR2 mutants H134R, L132C and T159C when exposed to increasing lengths of exposure to blue light of a fixed power (9

mW/mm^2). Stimuli were delivered at a fixed time interval, chosen to be longer than several time constants, allowing for channel photocycle completion and return of the signal to baseline levels. Stimuli lasting 10, 50, 100, 500 ms elicited reduced responses in the cells for all three mutants. The L132C mutant was characterised by larger amplitude responses compared to T159C and H134R. H134R and L132C responses appear to decrease slightly when exposed to 15s pulses, hinting at the range 2-10s as the most suitable for further experimentation. On the other hand, T159C responses continue to increase when exposed to longer pulses of blue light and stimuli ranging from 5s to 15s appear promising for the triggering of higher photo-currents.

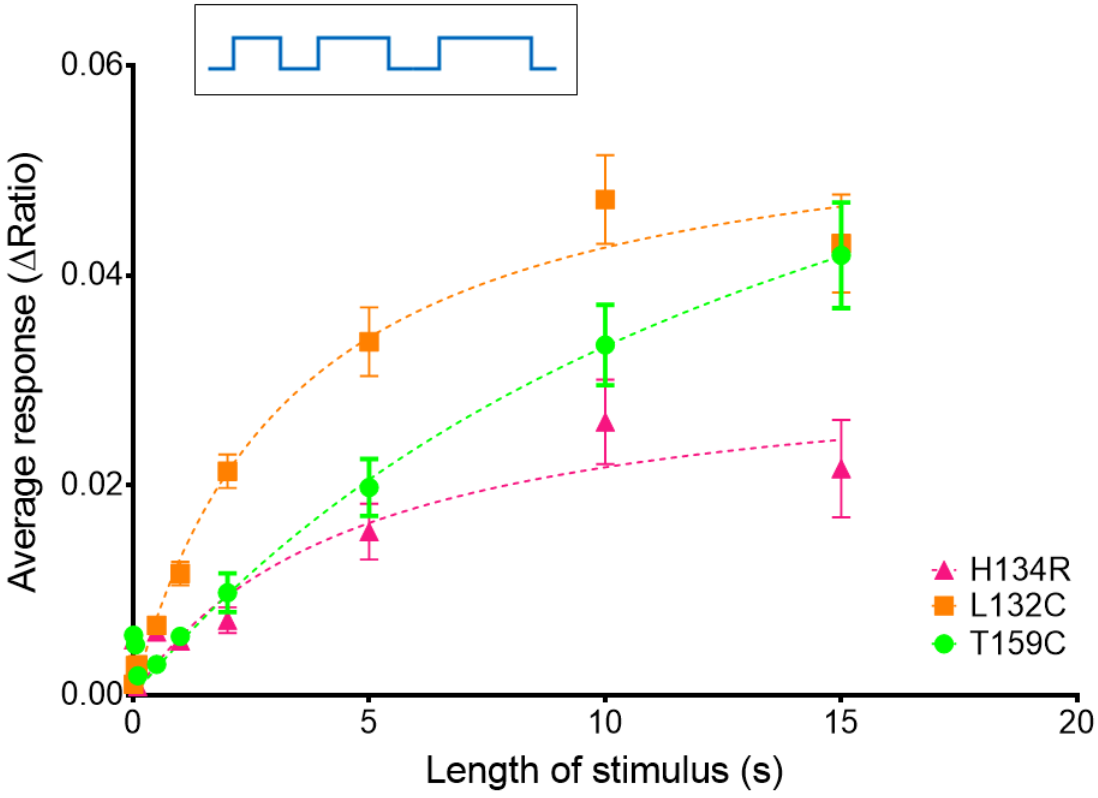


Figure 4.21: **Comparison of ChR2 mutant H134R, L132C and T159C response amplitudes to increasing length of blue (470 nm, 9 mW/mm^2) light stimulus reported as average Δ in Fura-2 ratio.** Blue (470 nm) light stimuli of increasing duration were delivered to ARPE-19 cells expressing ChR2 mutants H134R, L132C and T159C. Fura-2 ratiometric calcium imaging was performed 36 h post transfection. Data represent mean responses of n> 10 cells from two separate experiments ± SEM. Inset shows delivered photostimuli.

Correlation of mutant responses to the delivered light intensities was performed by controlling voltage applied to the 470 nm LED in the TwinLED unit from 0.03 V to 1 V, resulting in calibrated power densities at the sample ranging from 0.1 mW/mm^2 to 15 mW/mm^2 (Table 2.4). Figure 4.22 reports behaviour of mutants L132C, H134R

and T159C when exposed to increasing irradiance levels. Mutant H134R appears to respond well to the whole range of tested illumination power and be less influenced by higher light intensities. On the other hand, L132C and T159C response appears to be reduced when exposed to irradiances above 20 mW/mm^2.

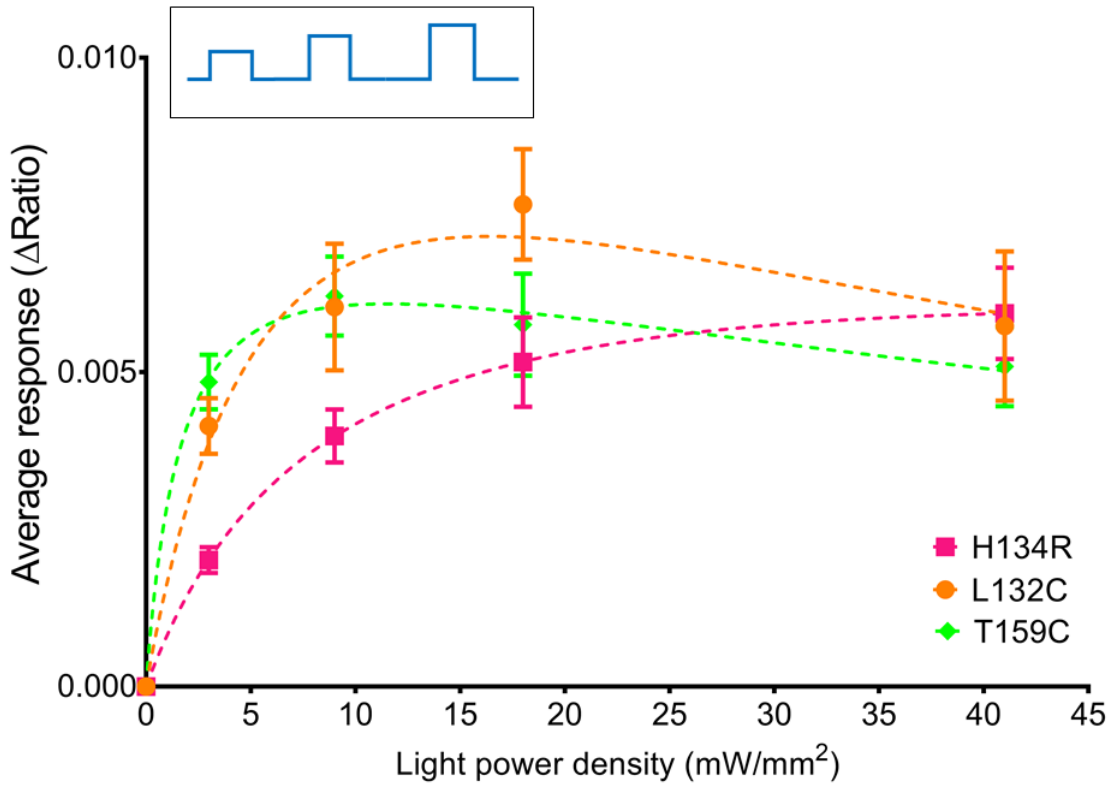


Figure 4.22: **Comparison of ChR2 mutant H134R, L132C and T159C response against increasing light intensities of blue (470 nm) light stimulus reported as average increase in Fura-2 ratio.** Blue (470 nm) light stimuli of increasing irradiance (mW/mm^2) were delivered to ARPE-19 cells expressing ChR2 mutants H134R, L132C and T159C. Fura-2 ratiometric calcium imaging was performed 36 h post transfection. Data represent mean responses of n > 10 cells from two separate experiments for each mutant ± SEM. Inset shows delivered photostimuli.

Figure 4.23 reports the comparison of the recovery kinetics for the ChR2 mutants L132C, H134R and T159C, i.e. the time required in between stimuli for the protein to recover and successfully initiate another calcium transient. L132C and H134R appeared to have a similar τ_{rec} of about 4 seconds, while T159C was characterised by a longer recovery time. τ_{rec} was extracted from the plotted data using GraphPad Prism (GraphPad Software) and represents the time needed by the mutant under examination to recover to 50% of its original maximum response, normalised in Figure 4.23 to 1.

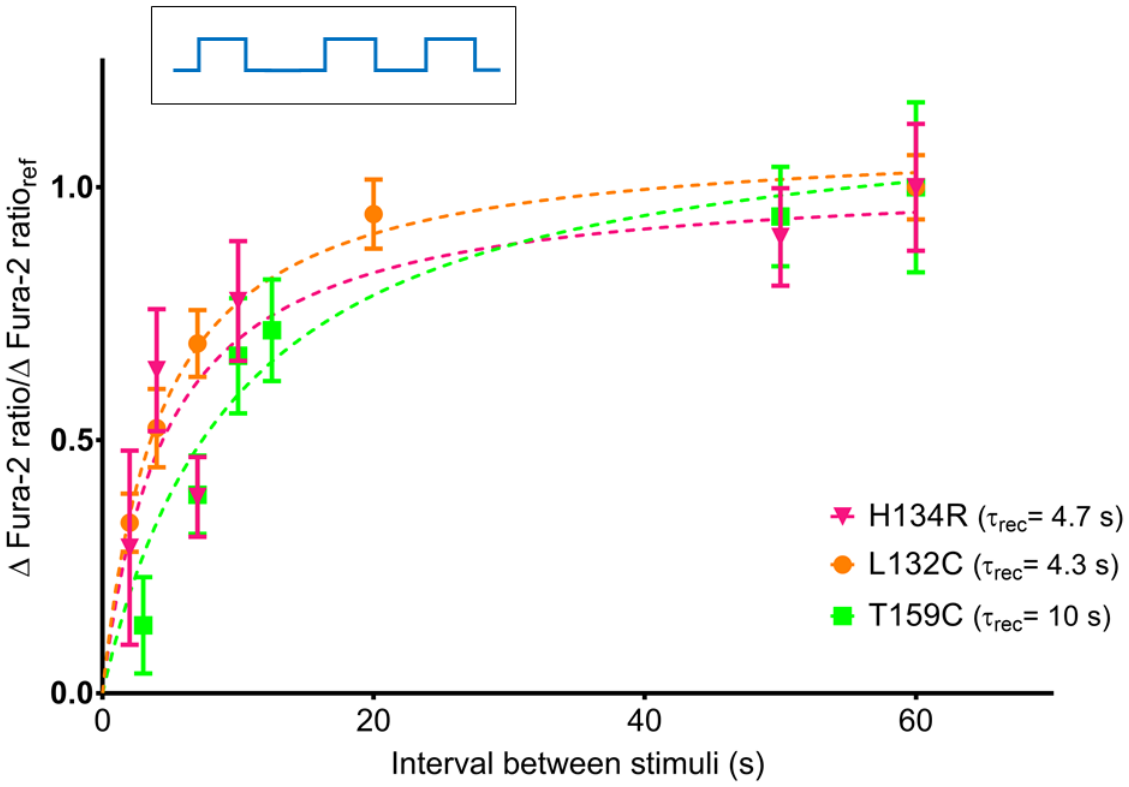


Figure 4.23: **Comparison of the recovery kinetics of ChR2 mutants H134R, L132C and T159C in response to blue light photostimulation. Data are reported as average increase in normalised Fura-2 ratio.** Blue (470 nm, 9 mW/mm^2) light stimuli were delivered to ARPE-19 cells expressing ChR2 mutants H134R, L132C and T159C at decreasing intervals in between subsequent stimulations. Fura-2 ratiometric calcium imaging was performed 36 h post transfection. Data represent mean responses of n> 7 cells from two separate experiments for each mutant ± SEM. Inset shows delivered photostimuli.

Discussion

In this chapter, I have described the successful mutagenesis of wtChR2 resulting in the generation of four point mutants with modified channel properties. I decided to genetically engineer wtChR2 following its performance in the ARPE-19 cell line, where no significant calcium influx was recorded with the calcium-sensitive dye Fura-2.

My research to select the most suitable mutations to overcome wtChR2 limitations, started with the screening of the literature for the numerous "designer channelrhodopsins". Mutations in channelrhodopsin sequence and structure have been tailored to applications in the brain, heart and muscle, mostly *in vivo* [Arrenberg et al., 2010; Boyden et al., 2005; Bruegmann et al., 2015; Tye and Deisseroth, 2012b]. Conversely, the present study investigated the most appropriate candidates to enable control of epithelial ion and water transport *in vitro*.

The ChR2 variant L132C was chosen for its increased permeability for calcium, in order to combine it with calcium imaging experiments. To a similar end, the E123T mutation in ChETA appeared as a beneficial feature to couple with Fura-2 calcium imaging experiments, based on its red-shifted (495 nm) spectral peak response, which prevents cross-activation by the UV wavelengths used for the excitation of the calcium dye. T159C was chosen because of its ability to generate higher photocurrents in mammalian cells, a property that may be of use for simultaneous optogenetic stimulation and electrophysiology of the epithelial layer. C128A presented interesting characteristics both due to its slower off-kinetics, which would allow substantial flow of cations from the extracellular environment, and to its dual-wavelength optical gating of the interconversion between conducting and non-conducting state. H134R was not generated via site-directed mutagenesis but purchased from Addgene, where it was readily accessible in a pcDNA3.1 vector, fused to the mCherry reporter gene. Numerous studies have reported activity of such a construct in mammalian cells [Arrenberg et al., 2010; Grossman et al., 2010; Lignani et al., 2013], therefore I decided to include it in the present study to validate results from the other mutants generated from pcDNA3.1-wtChR2-mCherry and to test it in the ARPE-19 cell line.

Integrity of the protein sequence following mutagenesis was assessed via Sanger sequencing, a robust methodology routinely used to study gene sequences. Although point mutations reported in the present work were already available to the scientific community, their expression was mainly driven by excitatory-neuron specific promoters (CaMKIIa) and they were optimised for viral delivery to the nervous system. Mutagenesis inside the pcDNA3.1 was performed to create a pool of mutants in this versatile, epithelia-appropriate vector, which could easily be transfected in mammalian cells of various origins. Following complete characterisation, I intend to deposit the optogenetic constructs in an open-source repository, in order to disseminate the outputs of the present work, providing a suite of novel tools appropriate to the light-mediated study of epithelial physiology.

Expression of the newly-generated constructs was assessed via flow cytometry and fluorescence imaging to confirm successful delivery and translation of the opsin proteins,

both quantitatively and qualitatively. Correct post-translational trafficking of ChR2 mutants to the plasma membrane, essential for protein functionality, was investigated with a membrane-targeting fluorescent dye.

Before proceeding with functional analysis of ChR2 mutants, *all-trans* retinal (ATR) effects on the cells and on the expression of the opsins were characterised. Exogenous supplementation of ATR has been considered fundamental only for non-mammalian organisms, such as for optogenetic behavioural studies of the fruit fly *Drosophila melanogaster*. ATR supplementation to heterologously-expressed ChR2 functionality are still debated and recent investigations have confirmed its beneficial effects also on mammalian cells [Grimm et al., 2017b; Kralj et al., 2012; Yu et al., 2015]. Interestingly, flow cytometry assessment of mutant expression revealed an increase in background autofluorescence for cells grown in ATR-supplemented medium, as reported in Figure 4.24.

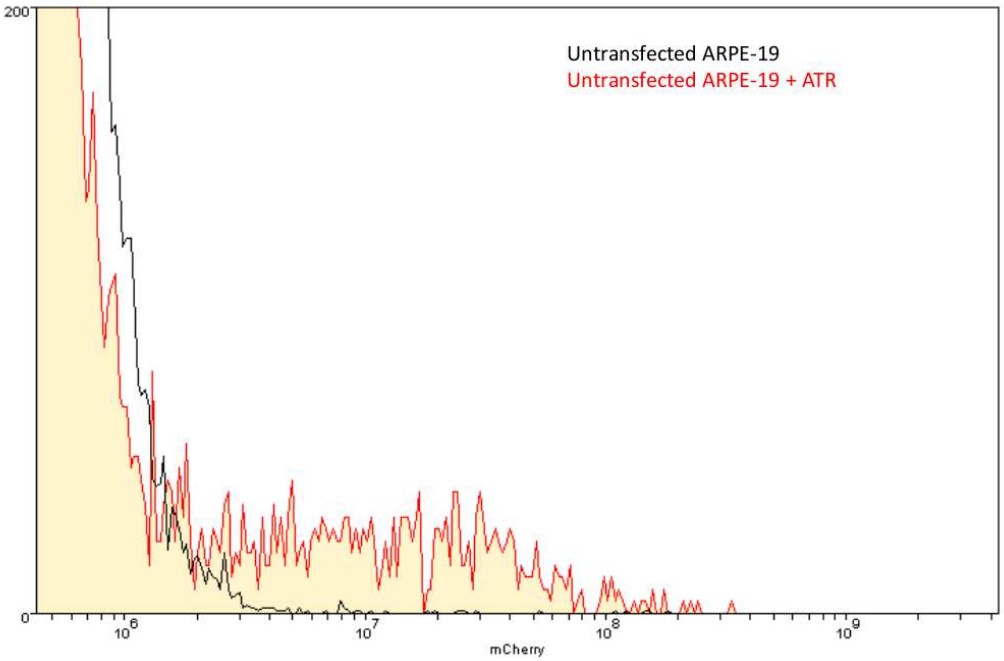


Figure 4.24: **Effects of *all-trans* retinal (ATR) supplementation on ARPE-19 autofluorescence.** Histogram showing untransfected ARPE-19 cells grown with (red trace) or without (black trace) supplementation of ATR in the cell growth medium. The y axis reports cell count.

Such change in the background autofluorescence could be attributed to the pigment lipofuscin, which is a product of the RPE retinoid metabolism [Brunk and Terman, 2002], highlighted in Figure 4.25.

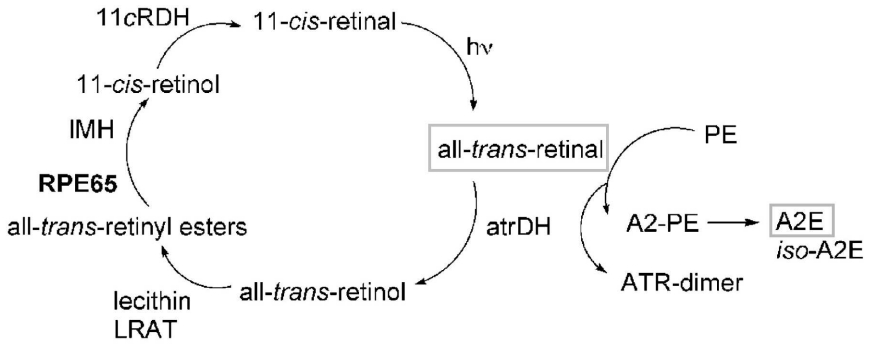


Figure 4.25: **Retinal cycle and by-production of the fluorophore A2E.** The visual cycle and A2E by-production. A2E, the main constituent of RPE pigment lipofuscin, is synthesised from *all-trans* retinal (ATR) escaping re-isomerisation to *11-cis* retinal *in vivo*. From ATR in excess, RPE produce A2E by reaction with phospatidylethanolamine, leading to accumulation of toxic lipofuscin and, eventually, degeneration of the tissue.

Retinal lipofuscin is a heterogeneous mixture of proteins, lipids and fluorescent molecules, mainly derived from vitamin A [Kennedy et al., 1995]; it has been investigated for its involvement in ageing and other retinal diseases [Sparrow and Boulton, 2005]. In the human eye, lipofuscin mainly originates from the phagocytosis of lipid-rich photoreceptor outer segments (POS), that is one of the main tasks of the RPE layer to ensure homeostasis in the retinal environment. *In vitro* models of the RPE, such as the ARPE-19 cell line, lack this source of lipofuscin but can produce it as a by-product of vitamin A or its derivatives, such as ATR [Jung et al., 2007]. One of the main hydrophobic components of lipofuscin is the fluorophore A2E (N-retinyledin-N-retinylethanolamin) which originates from phosphatidylethanolamine (PE) and *all-trans* retinal that is not reduced in the cells.

Supplementation of the growth medium with ATR might have provided extra substrate for this reaction, thus explaining the increased red autofluorescence of ATR-treated cells compared to the untreated [Di Guardo, 2015]. Accumulation of A2E, which shares mCherry excitation/emission spectra, as shown in Figure 4.26, might in fact explain the stronger background autofluorescence which is creating a population of false positively-transfected cells in the untransfected ARPE-19 cells grown in the presence of ATR (red trace in Figure 4.24). Confirmation of this speculation would require detailed chemoanalysis of the cell layer following ATR exposure, which was beyond the scope of this study but will be an interesting avenue for future work.

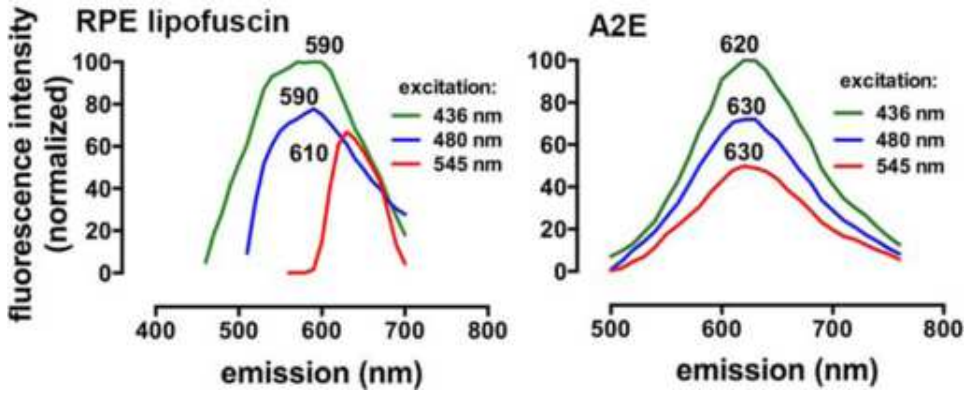


Figure 4.26: **Fluorescence spectra of lipofuscin and A2E fluorophores, by-products of the retinoid metabolism in the Retinal Pigment Epithelium (RPE).** Lipofuscin and its main lipophilic component, A2E, are both characterised by fluorescence in the amber/red region of the spectrum. Upon excitation at different wavelengths, fluorescence emission shifts for both molecules. Red lines in both graphs show emission of A2E and lipofuscin when excited at 545 nm.

To confirm the ability of optogenetic tools to change ion permeabilities across the membrane of epithelial cells, I chose to monitor calcium dynamics with the ratiometric calcium-sensitive dye Fura-2. Whereas electrophysiology techniques interrogate single cells, ratiometric calcium imaging allows simultaneous recording of calcium fluctuations from numerous cells and has been successfully coupled with optogenetic activation of ChRs [Shipley et al., 2014]. Furthermore, ratiometric calcium imaging is non-invasive, eliminating the need for microelectrodes, and it enables an all-optical evaluation of optogenetic actuators on a relatively simple fluorescent microscope. Nonetheless, ChR2 permeability is not limited to calcium, therefore different ion-sensitive fluorophores may be of use for the study of other ion dynamics in epithelial cells.

Preliminary data on ChR2 mutants in ARPE-19 cells reported successful generation of calcium transients by means of L132C, H134R and T159C. Although E123T and C128A did not significantly change calcium permeability across the membrane of ARPE-19 cells, further investigation of their activity will be required. The L132C variant performed as the best Ca^{2+}-conducting ChR2 in the present study. I believe further characterisation of the optogenetic actuators presented in this work and implementation of the optical system with faster and more reliable light-delivery instrumentation, may result in a useful tool for the study of epithelial transport of solutes and water, as discussed in Chapter 5.

To conclude, I demonstrated how light-gated channels and pumps from the microbial

world may provide useful tools for the future, in order to provide insights on the contribution of single ions to physiological processes, such as epithelial transport, reducing the invasineness of conventional methodologies.

Chapter 5

Conclusions and Future Work

In conclusion, this thesis has described the creation and optimisation of a novel optogenetic toolkit, culminating in genetically modified epithelial cells expressing light-gated ion channels in their membranes capable of altering their internal ion dynamics. Photostimulation of the engineered cells resulted in changes in the membrane ion permeabilities (Section 4.3) and enabled control over the temporal component of ion fluxes, with possibility of extending control to the spatial domain.

Due to the novel nature of the study, experimental work focused on optimising delivery and expression of the optogenetic actuators ChR2 and eNpHR in the cell line chosen for the study, the retinal pigment epithelium ARPE-19 cell line (Chapter 3). Subsequently, ChR2 variants with improved characteristics were designed and engineered via site-directed mutagenesis. Mutants were successful in the generation of calcium transients in the ARPE-19, demonstrating functionality of the optogenetic channel in the retinal epithelial cells (Chapter 4). Because of time limitations, the optogenetic constructs herein described could not be tested for their effects on ion and water transepithelial transport in ARPE-19 cells but the results presented in Chapter 4 are proof of concept for further investigations towards this direction.

The experimental cell model was chosen since it is generally regarded as the in vitro counterpart of the RPE, the retinal pigmented epithelium located at the back of the eye [Dunn et al., 1996]. The RPE expresses *in vivo* a variety of ion channels, transporters and pumps [Wimmers et al., 2007], on which the functionality of this epithelium is based [Strauss, 2005]. Deficiencies in such molecules or impairments in their homeo-

static regulation are at the foundations of different ophtalmological diseases [Beatty et al., 2000; Liang and Godley, 2003a; Marmor, 2000; R Sparrrow et al., 2010]. The rationale behind this thesis lay in the fact that, at their molecular base, optogenetic actuators such as ChR2 and eNpHR are nothing more than ion gates that can be operated by light [Nagel et al., 2003; Schobert and Lanyi, 1982]. Therefore, they can provide insights into physiological dynamics, especially in complex systems where numerous channels and transporters play a key role and where varying, reversible and repeated purturbations may be needed to uncouple different physiological responses under investigation. Epithelia represent an ideal candidate for the application of these techniques, as they rely on ion dynamics to exploit one of their most important functions, i.e. vectorial epithelial transport of solutes and water [Hamann, 2002; Joseph and Miller, 1991; Quinn and Miller, 1992; Tarran, 2004].

Future plans involve deposition of the optogenetic constructs in the pcDNA3.1 vector in an open-source plasmid repository, such as Addgene, where the vector will be available to other researchers to test. Despite lack of significant responses from the mutants E123T and C128A in the ARPE-19 cells, these variants could still be useful for other applications in different cell lines. Moreover, availability of the protein variants in the pcDNA3.1 will expand its pool for usage; it includes in its sequence, a ubiquitous CMV promoter, suitable to maximise expression in all mammalian cells, not only of neuronal lineage, conversely to the cell type-specific CaMKIIa promoter, found in most available optogenetic vectors.

Future directions include testing the functionality of eNpHR in the ARPE-19 cells, for which expression levels have already been optimised in this study (Chapter 3). The chloride-sensitive dye MQAE (N-(Ethoxycarbonylmethyl)-6-Methoxyquinolinium Bromide) [Ikeuchi et al., 2018; Verkman, 1990] will be used to investigate eNpHR ability to drive chloride ions through the membrane of the ARPE-19 cells when exposed to amber light at 580 nm. Distinction between acivation spectra of eNpHR and MQAE excitation (reported in Figure 5.1) make this dye a suitable candidate for monitoring chloride dynamics following opening of Halorhodopsin. MQAE is a second-generation chloride indicator, whose fluorescence is inversely proportional to the concentration

of intracellular chloride, a mechanism called diffusion-limited collisional quenching. When intracellular chloride increases, for example after gating of the chloride pump halorhodopsin (eNpHR), fluorescence of the dye will decrease, due to close interactions of the chloride ions with the MQAE molecule.

Alternatively, voltage sensitive dyes could be employed for monitoring of membrane voltage changes following activation of optogenetic proteins. Genetically-encoded calcium indicators (GECIs) [Mank and Griesbeck, 2008; McCombs and Palmer, 2008; Tian et al., 2012] or voltage-sensitive probes [Alford et al., 2013; Dugué et al., 2012; Mutoh et al., 2011] might also be exploited in an all-optogenetic approach to record outputs of optically-controlled cells.

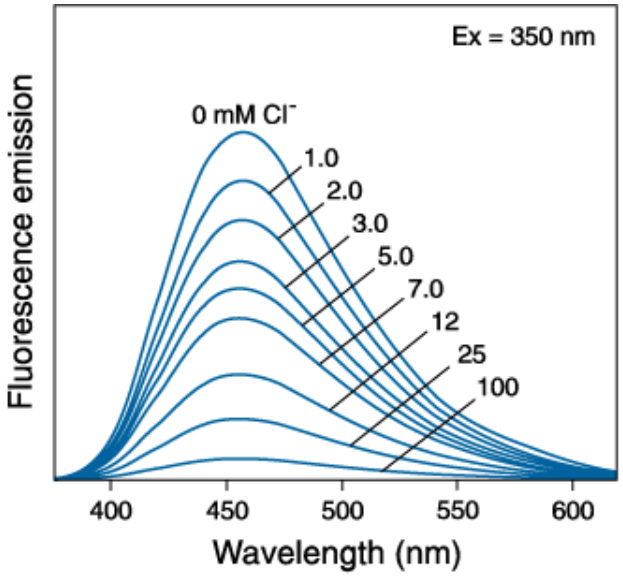


Figure 5.1: **Fluorescence emission spectra of chloride-sensitive indicator MQAE at different chloride concentrations.** MQAE, a second-generation chloride-sensitive indicator, changes its fluorescence upon variations in chloride concentrations in the intracellular environment. $[Cl^-]_i$ increase results in an indirectly-proportional quenching of the dye fluorescence. Image from Thermo Fisher Scientific.

Future directions include the possibility of hijacking epithelial vectorial transport by targeting different optogenetic actuators to the apical or basolateral compartments of the epithelial cell membrane. Epithelial functional polarity depends in fact on the selective segregation of specific proteins and lipids in one of the two membrane domains, distinguished by the tight junctions' complexes. Several mechanisms are involved in the correct delivery of channels, transporters, adhesion proteins to the correct compartment [Matter and Mellman, 1994; Simons and Wandinger-Ness, 1990]. These include:

specific amino acid sequences, like the tyrosine-based signals (NPXY, YXRF) and the dileucine motifs (LL) [Legouis et al., 2003] for basolateral delivery; post-translational modifications, such as the N-glycosilation of proteins resulting in apical targeting [Weisz and Rodriguez-Boulan, 2009]; interaction with the cytoskeleton to drive delivery of the protein, for instance through the PDZ domain, an 80-90 amino acid sequence which is involved in anchoring proteins to actin filaments, clathrin-mediated processes [Deborde et al., 2008] and more. By mimicking one of the described mechanisms, for example by genetic engineering of the opsin sequences with specific target sequences from protein localised in one of the two membrane domains, selective expression of the optogenetic constructs can be achieved. Expressing Halorhodopsin in the apical membrane, for instance, would result in the ability to drive chloride ions inside the ARPE-19 cells from the apical extracellular environment. Subsequently, native chloride channels in the basolateral membrane will exclude chloride ions which would have accumulated in the cells, resulting in the osmotic drive of water across the cells. This combination would provide the unprecedented ability to drive, with light, the rate-limiting step of transepithelial fluid transport in a functioning tissue non-invasively under physiological conditions. A heterogeneous population of cells could be generated in order to develop a mosaic of light-responsive and light-insensitive cells, to study how changing membrane permeability to different ions in the optogenetic cells will affect the neighbour cells in the layer.

Apical and basolateral targeting of the light-gated proteins will require the growth of a polarised epithelium. Specifically-designed porous filters are available for the growth of epithelial cells on a suspended membrane bathed in medium on both sides; cells plated on the membrane will grow into a layer and develop polarity [Zegers et al., 2003]. Immunocytochemistry of tight junction complexes and an increase in TEER (Trans-Epithelial Electrical Resistance) measurements, both markers of a mature epithelium, will confirm polarity [Chen et al., 2015].

Following characterisation of ChR2 mutants, variants showing the best characteristics in terms of channel conductance and light responsiveness could be introduced permanently in the ARPE-19 cells to generate a stably-transfected optogenetic cell line. The

process will involve the selection of mutated cells based on the gene for the resistance to a specific antibiotic contained in the plasmid sequence internalised by the cells [Tao et al., 2002]. Following selection, all the cells should express the optogenetic actuator chosen, thus removing the need for delivering of the genes prior to experiments. At the same time, multiple cell lines could be generated, for instance expressing one optogenetic actuator at a time or both ChR2 and eNpHR at the same time for more complex combined experiments.

Optogenetic control of ion dynamics might be extended to other epithelia, in order to clarify or deepen our knowledge about their physiological processes. The airway epithelium, for instance, is strongly dependent on the activity of chloride channels, like CFTR (Cystic Fibrosis Transmembrane Regulator) [Sheppard and Welsh, 1999], whose mutations and dysfunctions cause the genetic disease cystic fibrosis [Cutting, 2015]. An optogenetic approach, by using electrogenic chloride pumps, would prove valuable to investigate the dynamics of chloride flow through lung epithelium cell lines, in order to follow ion fluctuations in the healthy and pathological scenarios.

A possible use for the molecular tools presented in this work might be in the view of the study of fluid transport across epithelia, a controversial topic in physiology. Optogenetic modifications of ion membrane permeabilities will result in perturbation of volume equilibrium, due to alterations of the ionic gradient inside the cells. Volume changes in epithelia have been monitored in a number of ways, including intracellular ion dilution of fluorescent indicator, measurements of impedance [Sun and Morgan, 2010] and optical approaches [McManus et al., 1993] but present considerable limitations, mainly due to the multifactorial and complex nature of the phenomenon. Volume fluctuations in cells can be studied optically by monitoring intracellular fluorescent dyes [Hamann et al., 2002], like the ones routinely used as ion indicators, for instance. Most of these dyes are in fact trapped in the intracellular environment after internalisation, due to cleavage by intracellular enzymes; alterations of the cell volume will therefore result in dilution or concentration of the dye, reflected in a decrease or increase in the relative average fluorescence intensity in that same cell. The dye Fura-2, used in this study to monitor calcium dynamics after ChR2 activation (Sections 3.2 and 4.3), allows for the

study of volume perturbations when excited at its isosbestic point, 360 nm, that is the calcium-insensitive region of its spectrum. At this wavelength, in fact, Fura-2 is not responsive to calcium transients, like at 340 and 380 nm, therefore fluctuation in the dye fluorescence can be attributed to dilution or concentration effects due to volume alterations. By recording emission at 510 nm when Fura-2 is excited at the isosbestic point, intensity fluctuates in response to variations in cell volume only [Altenberg et al., 1994]. Similar approaches can be implemented using a variety of fluorophores, provided they are trapped intracellularly, robust to photobleaching, and don't suffer from compartmentalisation (or this compartmentalisation is stable).

During this study, a basic inverted light microscope was upgraded and equipped with the most suitable optics to fulfil experimental needs, i.e. simultaneous optogenetic activation of opsin proteins and recording of their outputs in terms of changes in the fluorescence of ion-sensitive indicators. Future work around the microscope might explore the possibility to implement the system with electrophysiology instrumentation, in order to keep track of electrical dynamics during photostimulation in whole-cell patch clamp configuration. In this regard, brightfield illumination for the correct positioning of the microelectrodes should be replaced by filtered light outside the excitation spectrum of the optogenetic sensor under examination, to prevent cross-activation or even desesnsitisation of the light-gated channels. An Optopatcher device, combining a dual LED-coupled optical fibre and an electrode for electrophysiological recordings, could be used in this configuration, allowing light-gating of the channels and simultaneous recording of photocurrents at the tip of the same microelectrode [Katz et al., 2013].

Major improvements in the imaging configuration could be achieved by replacing the obsolescent dual filter wheel, characterised by at least a 200-ms mechanical delay between adjacent positions, with a multi-wavelength LED light source. Preliminary tests on the FuraLED/TwinLED illuminator (kindly provided by Cairn Research Ltd) reported at the end of this work in Section 4.3.2, showed promising results for the simultaneous activation and monitoring of the optogenetically-modified ARPE-19 cells, increasing signal to noise ratio and improving acquisition speed. The unit allows for additional LEDs, to achieve control of different opsins and ion indicators, concurrently.

Motorisation of the filter slider would be another beneficial improvement of the imaging configuration. Fluorescence indicators to be used in combination with optogenetic molecules were restricted by the requirement for manual movements of hardware parts in the microscope. Automation of the slider for dichroic mirrors and emitters, together with a multi-wavelength LED light source, will not only accelerate the imaging process, but also a broader spectrum of opsins and dyes could be taken into account for further experimentation.

In future it may also be possible to implement light-patterning techniques within the imaging system, allowing fast, spatially-resolved opsin activation at defined points within the sample in tissue or *in vitro* without the need for configuration changes in the optical path [Papagiakoumou, 2013]. Light-patterning devices such as Spatial Light Modulators (SLMs) and Digital Micromirror Devices (DMDs) have successfully been used for optogenetic stimulation of single cells in a population of opsin-expressing neurons or even for targeting of light stimuli to sub-cellular compartments [Ronzitti et al., 2017].

In conclusion, the present work has reported the first evidence of the expression of functional light-gated ion channels and pumps in the membrane of human retinal epithelial cells *in vitro*, in order to control and study a core mechanism of epithelia, i.e. transport of ions through the plasma membrane. The work focused on implementing a biotechnology technique, optogenetics, for an unprecedently-reported use in a cell model for epithelial cells from the human retina, optimising both the molecular and optical tools for this specific application. There are recent reports of optogenetic control of epithelial functions and mechanisms [Deneke et al., 2019; Efetova et al., 2013; Krueger et al., 2018; Makadia et al., 2018; Sato et al., 2017], proving the potential of such technique outside the explored fields. No evidence is present, to my knowledge, regarding the functional expression of ChR2 mutants in the human retinal epithelium. A suite of 4 different epithelial-applicable optogenetic constructs, capable of controlling calcium signaling within epithelial cells, was generated and characterised. Moreover, preliminary data on Halorhodopsin expression are encouraging for simultaneous dual

control together with ChR2. The outcome of this research will be available to the scientific community and has the potential to be transferred to other epithelial cell models in order to investigate, together with existing techniques, still-debated processes in these cells, such as fluid volume regulation and water transport, non-invasively using photonics.

Acknowledgements

The present work would have not been possible without the support of different people in the past four years. I would like to thank my supervisors for entrusting me with this great and interesting project and for the opportunity to work on this research. Thank you all for the help and guidance and encouraging support throughout these years and during the writing of this thesis. I would like to thank Matt Clark for the inspiring conversations and the possibility to work independently on the project. I would like to express my gratitude to Kevin Webb for his constant guidance, motivation and directions for exciting possibilities to test during and after this PhD. I would like to thank Jamie Twycross, who introduced me to the world of mathemical modelling and for his help in widening my knowledge. I would like to express my thankness to Emilia Moradi for her excellent advice, who taught me how to design and interpret experiments, besides being extremely supportive throughout my whole PhD. Thank you all for the advice which helped me growing both as a scientist and a person. I would also like to thank Richard Smith, Fernando Perez Cota, Rikesh Patel and Leonel Marques for the helpful conversations and hands-on experience which taught me to jump into techniques outside my comfort zone. I would like to acknowledge Tamar Guetta Baranes for her help during the molecular biology experiments in this thesis and for access to the Human Genetics lab facilities I needed for my experiments. I would like to thank Isabella Maiellaro for her support, encouragement and hospitality during my two-week stay in Germany. Thank you Ian Mellor and his students, Neville and Maria, for their help in the preliminary electrophysiology experiments and the use of their equipment. I would also like to acknowledge David Onion, Seema Rajani and Chris Gell for the help when using their lab facilities for the experiments in this work. Thank you to Rosanna Davies and all the guys at Cairn Research Ltd for the support with the instrumentation they kindly provided me with. I would also like to thank all the people in the Optics and Photonics research group I have worked with or talked to during my PhD.

I sincerely thank my parents Sandra and Luigi and my brother Fabiano for being the most wonderful family in the world (no offense to any other family) and for believing in

me, no matter what. I never find the right words to thank them enough but you are my inspiration. Thank you Paolo for being an amazing boyfriend and for all the positivity, support and love you have for me every day. Thank you for making our (rented) little flat feel like home and for the way you see me, which pushes me to be a better me. I wouldn't have done it without you. Thanks to all my family in Italy, you are the reason I am the person I am and why I get up after I fall. Thanks to my aunt Laura who always has a word of support for me and who has taught me so much. Thank you Martina for becoming an important member of our family. Thanks to Paolo's family for having embraced me as part of the family and for your support. Thanks to my friend Stefania for her > 15-year friendship and all the Skype calls/dinners we've had these years we've been far apart. Thanks to my friend Andrea for his madness and friendship. Thanks to Silvia, Giancarlo, Manuela, Stefano, Simone for being the crazy people we are and for all the laughters in these many years of friendship. Thanks to Daniella for her incredible kindness and encouragement and for the importance of drinking tea. Thanks to Rikesh for being a good friend and for the advice/conversations on so many different topics and for introducing me to the tradition of pub quizzing. Thanks to my SIOS mates Fernando, Rafael, Sal and Shakila for our chats in the office/lab and for all the time we spent together these years. Thanks to Pieter for our long chats in the corridors. Thanks to Mina for her inspiring positivity. Thanks to Sidahmed for his thoughful insights on experiments and life. Thanks to Luke and Ula and for being good friends and for the evenings spent together. Thanks to all the people who did acts of kindness to us while we were writing up (like giving us home-cooked food). Thanks to Ronnie James Dio, Eddie Vedder, Bruce Dickinson, Mark Knopfler and crochet for calming my soul.

I'm afraid the list could go on and I am surely forgetting someone but I will conclude here by saying that I am really grateful for this opportunity for studying and starting my journey in this wonderful word of discovery that is Research and I am looking forward to the adventures ahead.

Bibliography

Ablonczy, Z., Dahrouj, M., Tang, P. H., Liu, Y., Sambamurti, K., Marmorstein, A. D., and Crosson, C. E. (2011). Human Retinal Pigment Epithelium Cells as Functional Models for the RPE In Vivo. *Investigative Ophthalmology & Visual Science*, 52(12):8614–8620.

Adamantidis, A. R., Zhang, F., Aravanis, A. M., Deisseroth, K., and De Lecea, L. (2007). Neural substrates of awakening probed with optogenetic control of hypocretin neurons. *Nature*, 450(7168):420.

Adamis, A., Shima, D., Yeo, K.-T., Yeo, T., Brown, L., Berse, B., Damore, P., and Folkman, J. (1993). Synthesis and secretion of vascular permeability factor/vascular endothelial growth factor by human retinal pigment epithelial cells. *Biochemical and biophysical research communications*, 193(2):631–638.

Alford, S. C., Wu, J., Zhao, Y., Campbell, R. E., and Knöpfel, T. (2013). Optogenetic reporters. *Biology of the Cell*, 105(1):14–29.

Allen, B., Singer, A., and Boyden, E. (2015). Principles of designing interpretable optogenetic behavior experiments. *Learning & Memory*, 22:232–238.

Altenberg, G. A., Deitmer, J. W., Glass, D. C., and Reuss, L. (1994). P-glycoprotein-associated Cl-currents are activated by cell swelling but do not contribute to cell volume regulation. *Cancer research*, 54(3):618–622.

Anderson, D. H., Mullins, R. F., Hageman, G. S., and Johnson, L. V. (2002). A role for local inflammation in the formation of drusen in the aging eye. *American journal of ophthalmology*, 134(3):411–431.

Anderson, J. and Van Itallie, C. (1995). Tight junctions and the molecular basis for regulation of paracellular permeability. *American Journal of Physiology-Gastrointestinal and Liver Physiology*, 269(4):G467–G475.

Anderson, J. M. (2001). Molecular structure of tight junctions and their role in epithelial transport. *Physiology*, 16(3):126–130.

Aravanis, A. M., Wang, L.-P., Zhang, F., Meltzer, L. A., Mogri, M. Z., Schneider, M. B., and Deisseroth, K. (2007). An optical neural interface: in vivo control of rodent motor cortex with integrated fiberoptic and optogenetic technology. *Journal of neural engineering*, 4(3):S143.

Arber, W. and Linn, S. (1969). DNA modification and restriction. *Annual review of biochemistry*, 38(1):467–500.

Arrenberg, A. B., Del Bene, F., and Baier, H. (2009). Optical control of zebrafish behavior with halorhodopsin. *Proceedings of the National Academy of Sciences*, page pnas.0906252106.

Arrenberg, A. B., Stainier, D. Y. R., Baier, H., and Huisken, J. (2010). Optogenetic Control of Cardiac Function. *Science*, 330(6006):971.

Ashcroft, F. M. (1999). *Ion channels and disease*. Academic press.

Bagal, S. K., Brown, A. D., Cox, P. J., Omoto, K., Owen, R. M., Pryde, D. C., Sidders, B., Skerratt, S. E., Stevens, E. B., and Storer, R. I. (2012). Ion channels as therapeutic targets: a drug discovery perspective. *Journal of medicinal chemistry*, 56(3):593–624.

Balazs, D. A. and Godbey, W. (2011). Liposomes for use in gene delivery. *Journal of drug delivery*, 2011.

Bamann, C., Kirsch, T., Nagel, G., and Bamberg, E. (2008). Spectral characteristics of the photocycle of channelrhodopsin-2 and its implication for channel function. *Journal of molecular biology*, 375(3):686–694.

Barrett, K. E. and Keely, S. J. (2000). Chloride secretion by the intestinal epithelium: molecular basis and regulatory aspects. *Annual review of physiology*, 62(1):535–572.

Beatty, S., Koh, H.-H., Phil, M., Henson, D., and Boulton, M. (2000). The role of oxidative stress in the pathogenesis of age-related macular degeneration. *Survey of ophthalmology*, 45(2):115–134.

Berndt, A., Schoenenberger, P., Mattis, J., Tye, K. M., Deisseroth, K., Hegemann, P., and Oertner, T. G. (2011). High-efficiency channelrhodopsins for fast neuronal stimulation at low light levels. *Proceedings of the National Academy of Sciences*, 108(18):7595.

Berndt, A., Yizhar, O., Gunaydin, L. A., Hegemann, P., and Deisseroth, K. (2008). Bi-stable neural state switches. *Nature Neuroscience*, 12:229.

Bernstein, J. G. and Boyden, E. S. (2011). Optogenetic tools for analyzing the neural circuits of behavior. *Trends in Cognitive Sciences*, 15(12):592–600.

Betley, J. N. and Sternson, S. M. (2011). Adeno-associated viral vectors for mapping, monitoring, and manipulating neural circuits. *Human gene therapy*, 22(6):669–677.

Beyder, A. and Farrugia, G. (2016). Ion channelopathies in functional GI disorders. *American Journal of Physiology-Heart and Circulatory Physiology*.

Bezzerides, V. J., Ramsey, I. S., Kotecha, S., Greka, A., and Clapham, D. E. (2004). Rapid vesicular translocation and insertion of TRP channels. *Nature cell biology*, 6(8):709.

Bhutto, I. A., McLeod, D. S., Hasegawa, T., Kim, S. Y., Merges, C., Tong, P., and Lutty, G. A. (2006). Pigment epithelium-derived factor (PEDF) and vascular endothelial growth factor (VEGF) in aged human choroid and eyes with age-related macular degeneration. *Experimental eye research*, 82(1):99–110.

Bok, D. (1993). The retinal pigment epithelium: a versatile partner in vision. *J Cell Sci*, 1993(Supplement 17):189–195.

Bouck, N. (2002). PEDF: anti-angiogenic guardian of ocular function. *Trends in molecular medicine*, 8(7):330–334.

Boyden, E. S., Zhang, F., Bamberg, E., Nagel, G., and Deisseroth, K. (2005). Millisecond-timescale, genetically targeted optical control of neural activity. *Nature Neuroscience*, 8:1263.

Bradke, F. and Dotti, C. G. (1998). Membrane traffic in polarized neurons. *Biochimica et Biophysica Acta (BBA)-Molecular Cell Research*, 1404(1-2):245–258.

Brown, L. S. and Jung, K.-H. (2006). Bacteriorhodopsin-like proteins of eubacteria and fungi: the extent of conservation of the haloarchaeal proton-pumping mechanism. *Photochemical & Photobiological Sciences*, 5(6):538–546.

Bruegmann, T., van Bremen, T., Vogt, C. C., Send, T., Fleischmann, B. K., and Sasse, P. (2015). Optogenetic control of contractile function in skeletal muscle. *Nature Communications*, 6:7153.

Brunk, U. T. and Terman, A. (2002). Lipofuscin: mechanisms of age-related accumulation and influence on cell function. *Free Radical Biology and Medicine*, 33(5):611–619.

Burchiel, S. W., Edwards, B. S., Kuckuck, F. W., Lauer, F. T., Prossnitz, E. R., Ransom, J. T., and Sklar, L. A. (2000). Analysis of free intracellular calcium by flow cytometry: multiparameter and pharmacologic applications. *Methods*, 21(3):221–230.

Burg, M. B. and Orloff, J. (1968). Control of fluid absorption in the renal proximal tubule. *The Journal of clinical investigation*, 47(9):2016–2024.

Busskamp, V., Picaud, S., Sahel, J.-A., and Roska, B. (2012). Optogenetic therapy for retinitis pigmentosa. *Gene therapy*, 19(2):169.

Cereijido, M., Contreras, R. G., García-Villegas, M. R., González-Mariscal, L., and Valdés, J. (1996). Epithelial polarity. In Wills, N. K., Reuss, L., and Lewis, S. A., editors, *Epithelial Transport: A guide to methods and experimental analysis*, pages 49–69. Springer Netherlands, Dordrecht.

Cereijido, M., Contreras, R. G., Shoshani, L., Flores-Benitez, D., and Larre, I. (2008). Tight junction and polarity interaction in the transporting epithelial phenotype. *Biochimica et Biophysica Acta (BBA)-Biomembranes*, 1778(3):770–793.

Cereijido, M., Robbins, E., Dolan, W., Rotunno, C., and Sabatini, D. (1978). Polarized monolayers formed by epithelial cells on a permeable and translucent support. *The Journal of cell biology*, 77(3):853–880.

Cereijido, M., Valdés, J., Shoshani, L., and Contreras, R. G. (1998). Role of tight junctions in establishing and maintaining cell polarity. *Annual Review of Physiology*, 60(1):161–177.

Chagas, A. M., Prieto-Godino, L. L., Arrenberg, A. B., and Baden, T. (2017). The 100 lab: A 3d-printable open-source platform for fluorescence microscopy, optogenetics, and accurate temperature control during behaviour of zebrafish, Drosophila, and Caenorhabditis elegans. *PLoS biology*, 15(7):e2002702.

Chaudhary, G. and Singh, S. K. (2019). Global Status of Genetically Modified Crops and Its Commercialization. In *Biotechnology Products in Everyday Life*, pages 147–160. Springer.

Chen, S., Einspanier, R., and Schoen, J. (2015). Transepithelial electrical resistance (TEER): a functional parameter to monitor the quality of oviduct epithelial cells cultured on filter supports. *Histochemistry and cell biology*, 144(5):509–515.

Chihara, E. and Nao-i, N. (1985). Resorption of subretinal fluid by transepithelial flow of the retinal pigment epithelium. *Graefe's archive for clinical and experimental ophthalmology*, 223(4):202–204.

Clare, J. J., Tate, S. N., Nobbs, M., and Romanos, M. A. (2000). Voltage-gated sodium channels as therapeutic targets. *Drug discovery today*, 5(11):506–520.

Clausen, M. V., Hilbers, F., and Poulsen, H. (2017). The structure and function of the Na, K-ATPase isoforms in health and disease. *Frontiers in physiology*, 8:371.

Crabb, J. W., Miyagi, M., Gu, X., Shadrach, K., West, K. A., Sakaguchi, H., Kamei, M., Hasan, A., Yan, L., and Rayborn, M. E. (2002). Drusen proteome analysis: an approach to the etiology of age-related macular degeneration. *Proceedings of the National Academy of Sciences*, 99(23):14682–14687.

Cutting, G. R. (2015). Cystic fibrosis genetics: from molecular understanding to clinical application. *Nature Reviews Genetics*, 16(1):45.

Cymer, F., Von Heijne, G., and White, S. H. (2015). Mechanisms of integral membrane protein insertion and folding. *Journal of molecular biology*, 427(5):999–1022.

Davidson, A. E., Millar, I. D., Urquhart, J. E., Burgess-Mullan, R., Shweikh, Y., Parry, N., O'Sullivan, J., Maher, G. J., McKibbin, M., Downes, S. M., Lotery, A. J., Jacobson, S. G., Brown, P. D., Black, G. C., and Manson, F. D. (2009). Missense Mutations in a Retinal Pigment Epithelium Protein, Bestrophin-1, Cause Retinitis Pigmentosa. *The American Journal of Human Genetics*, 85(5):581–592.

de Ilarduya, C. T., Sun, Y., and Düzgüneş, N. (2010). Gene delivery by lipoplexes and polyplexes. *European journal of pharmaceutical sciences*, 40(3):159–170.

de la Cour Dornonville, M. (1993). Ion transport in the retinal pigment epithelium. A study with double barrelled ion-selective microelectrodes. *Acta ophthalmologica. Supplement*, (209):1–32.

Deborde, S., Perret, E., Gravotta, D., Deora, A., Salvarezza, S., Schreiner, R., and Rodriguez-Boulan, E. (2008). Clathrin is a key regulator of basolateral polarity. *Nature*, 452(7188):719.

Deisseroth, K. (2011). Optogenetics. *Nature methods*, 8(1):26.

Deisseroth, K. and Hegemann, P. (2017). The form and function of channelrhodopsin. *Science*, 357(6356):eaan5544.

Deneke, V. E., Puliafito, A., Krueger, D., Narla, A. V., De Simone, A., Primo, L., Vergassola, M., De Renzis, S., and Di Talia, S. (2019). Self-Organized Nuclear Positioning Synchronizes the Cell Cycle in Drosophila Embryos. *Cell*, 177(4):925–941.e17.

Di Guardo, G. (2015). Lipofuscin, lipofuscin-like pigments and autofluorescence. *European journal of histochemistry: EJH*, 59(1).

Dingermann, T. (2008). Recombinant therapeutic proteins: production platforms and challenges. *Biotechnology Journal: Healthcare Nutrition Technology*, 3(1):90–97.

Dubyak, G. R. (2004). Ion homeostasis, channels, and transporters: an update on cellular mechanisms. *Advances in physiology education*, 28(4):143–154.

Dugué, G. P., Akemann, W., and Knöpfel, T. (2012). A comprehensive concept of optogenetics. In *Progress in brain research*, volume 196, pages 1–28. Elsevier.

Dunlop, J., Bowlby, M., Peri, R., Vasilyev, D., and Arias, R. (2008). High-throughput electrophysiology: an emerging paradigm for ion-channel screening and physiology. *Nature Reviews Drug Discovery*, 7:358.

Dunn, K. C., Aotaki-Keen, A., Putkey, F., and Hjelmeland, L. (1996). ARPE-19, A Human Retinal Pigment Epithelial Cell Line with Differentiated Properties. *Experimental Eye Research*, 62(2):155–170.

Dustin, L. B. (2000). Ratiometric analysis of calcium mobilization. *Clinical and Applied Immunology Reviews*, 1(1):5–15.

Efetova, M., Petereit, L., Rosiewicz, K., Overend, G., Haußig, F., Hovemann, B. T., Cabrero, P., Dow, J. A., and Schwärzel, M. (2013). Separate roles of PKA and EPAC in renal function unraveled by the optogenetic control of cAMP levels in vivo. *J Cell Sci*, 126(3):778–788.

Ernst, O. P., Lodowski, D. T., Elstner, M., Hegemann, P., Brown, L. S., and Kandori, H. (2013). Microbial and animal rhodopsins: structures, functions, and molecular mechanisms. *Chemical reviews*, 114(1):126–163.

Ernst, O. P., Murcia, P. A. S., Daldrop, P., Tsunoda, S. P., Kateriya, S., and Hegemann, P. (2008). Photoactivation of channelrhodopsin. *Journal of Biological Chemistry*, 283(3):1637–1643.

Eveloff, J. L. and Warnock, D. G. (1987). Activation of ion transport systems during cell volume regulation. *American Journal of Physiology-Renal Physiology*, 252(1):F1–F10.

Falb, M., Pfeiffer, F., Palm, P., Rodewald, K., Hickmann, V., Tittor, J., and Oesterhelt, D. (2005). Living with two extremes: conclusions from the genome sequence of Natronomonas pharaonis. *Genome research*, 15(10):1336–1343.

Farrokh-Siar, L., Rezai, K., Semnani, R. T., Patel, S., Ernest, J., and Van Seventer, G. (1999). Human fetal retinal pigment epithelium suppresses the activation of CD4+ and CD8+ T-cells. *Graefe's archive for clinical and experimental ophthalmology*, 237(11):934–939.

Fastermann, D., Bolwien, C., Hehn, D., Schlesinger, R., and Heberle, J. (2000). Time-resolved vibrational spectroscopy of the halorhodopsin photocycle. *Biochemical Society Transactions*, 28(5):A188–A188.

Favre-Bulle, I. A., Preece, D., Nieminen, T. A., Heap, L. A., Scott, E. K., and Rubinsztein-Dunlop, H. (2015). Scattering of sculpted light in intact brain tissue, with implications for optogenetics. *Scientific reports*, 5:11501.

Feher, J., Kovacs, I., Artico, M., Cavallotti, C., Papale, A., and Gabrieli, C. B. (2006). Mitochondrial alterations of retinal pigment epithelium in age-related macular degeneration. *Neurobiology of aging*, 27(7):983–993.

Fendrihan, S., Legat, A., Pfaffenhuemer, M., Gruber, C., Weidler, G., Gerbl, F., and Stan-Lotter, H. (2006). Extremely halophilic archaea and the issue of long-term microbial survival. In *Life in Extreme Environments*, pages 125–140. Springer.

Figueiredo, M., Lane, S., Stout Jr, R. F., Liu, B., Parpura, V., Teschemacher, A. G., and Kasparov, S. (2014). Comparative analysis of optogenetic actuators in cultured astrocytes. *Cell Calcium*, 56(3):208–214.

Filipek, S., Stenkamp, R. E., Teller, D. C., and Palczewski, K. (2003). G protein-coupled receptor rhodopsin: a prospectus. *Annual review of physiology*, 65(1):851–879.

Finnemann, S. C., Leung, L. W., and Rodriguez-Boulan, E. (2002). The lipofuscin component A2e selectively inhibits phagolysosomal degradation of photoreceptor phospholipid by the retinal pigment epithelium. *Proceedings of the National Academy of Sciences*, 99(6):3842–3847.

Fischbarg, J. (2010). Fluid Transport Across Leaky Epithelia: Central Role of the Tight Junction and Supporting Role of Aquaporins. *Physiological Reviews*, 90(4):1271–1290.

Fischbarg, J. (2018). On the theory of solute-solvent coupling in epithelia. In *Water Transport and Biological Membranes*, pages 153–167. CRC Press.

Fischer, A. J., McKinnon, L. A., Nathanson, N. M., and Stell, W. K. (1998). Identification and localization of muscarinic acetylcholine receptors in the ocular tissues of the chick. *Journal of Comparative Neurology*, 392(3):273–284.

Foecking, M. K. and Hofstetter, H. (1986). Powerful and versatile enhancer-promoter unit for mammalian expression vectors. *Gene*, 45(1):101–105.

Forrester, J. V. and Xu, H. (2012). Good news–bad news: the Yin and Yang of immune privilege in the eye. *Frontiers in immunology*, 3:338.

Fotakis, G. and Timbrell, J. A. (2006). In vitro cytotoxicity assays: Comparison of LDH, neutral red, MTT and protein assay in hepatoma cell lines following exposure to cadmium chloride. *Toxicology Letters*, 160(2):171–177.

Frank, R. N. (1997). Growth factors in age-related macular degeneration: pathogenic and therapeutic implications. *Ophthalmic research*, 29(5):341–353.

Förster, C. (2008). Tight junctions and the modulation of barrier function in disease. *Histochemistry and cell biology*, 130(1):55–70.

Gollapalli, D. R., Maiti, P., and Rando, R. R. (2003). RPE65 operates in the vertebrate visual cycle by stereospecifically binding all-trans-retinyl esters. *Biochemistry*, 42(40):11824–11830.

González-Perrett, S., Kim, K., Ibarra, C., Damiano, A. E., Zotta, E., Batelli, M., Harris, P. C., Reisin, I. L., Arnaout, M. A., and Cantiello, H. F. (2001). Polycystin-2, the protein mutated in autosomal dominant polycystic kidney disease (ADPKD), is a Ca2+-permeable nonselective cation channel. *Proceedings of the National Academy of Sciences*, 98(3):1182–1187.

Gradinaru, V., Thompson, K. R., and Deisseroth, K. (2008). eNpHR: a Natronomonas halorhodopsin enhanced for optogenetic applications. *Brain Cell Biology*, 36(1):129–139.

Green, W. R., McDONNELL, P. J., and Yeo, J. H. (1985). Pathologic features of senile macular degeneratlon. *Ophthalmology*, 92(5):615–627.

Greenaway, P. and LeVine, D. (1973). Binding of N-acetyl-neuraminic acid by wheat-germ agglutinin. *Nature New Biology*, 241(110):191.

Grimm, C., Vierock, J., Hegemann, P., and Wietek, J. (2017a). Whole-cell Patch-clamp Recordings for Electrophysiological Determination of Ion Selectivity in Channelrhodopsins. *JOVE-Journal of Visualized Experiments*.

Grimm, C., Vierock, J., Hegemann, P., and Wietek, J. (2017b). Whole-cell patch-clamp recordings for electrophysiological determination of ion selectivity in Channelrhodopsins. *JoVE (Journal of Visualized Experiments)*, (123):e55497.

Grisshammer, R. (2006). Understanding recombinant expression of membrane proteins. *Current Opinion in Biotechnology*, 17(4):337–340.

Grossman, N., Poher, V., Grubb, M. S., Kennedy, G. T., Nikolic, K., McGovern, B., Palmini, R. B., Gong, Z., Drakakis, E. M., Neil, M. A. A., Dawson, M. D., Burrone, J., and Degenaar, P. (2010). Multi-site optical excitation using ChR2 and micro-LED array. *Journal of Neural Engineering*, 7(1):016004.

Grossniklaus, H. E. and Green, W. R. (2004). Choroidal neovascularization. *American journal of ophthalmology*, 137(3):496–503.

Grynkiewicz, G., Poenie, M., and Tsien, R. Y. (1985). A new generation of Ca2+ indicators with greatly improved fluorescence properties. *Journal of Biological Chemistry*, 260(6):3440–3450.

Guijarro, J., Engelhard, M., and Siebert, F. (2006). Anion uptake in halorhodopsin from Natromonas pharaonis studied by FTIR spectroscopy: consequences for the anion transport mechanism. *Biochemistry*, 45(38):11578–11588.

Gunaydin, L. A., Yizhar, O., Berndt, A., Sohal, V. S., Deisseroth, K., and Hegemann, P. (2010). Ultrafast optogenetic control. *Nature neuroscience*, 13(3):387.

Gundersen, D., Orlowski, J., and Rodriguez-Boulan, E. (1991). Apical polarity of Na, K-ATPase in retinal pigment epithelium is linked to a reversal of the ankyrin-fodrin submembrane cytoskeleton. *The Journal of cell biology*, 112(5):863–872.

Haas, M. and McManus, T. J. (1983). Bumetanide inhibits (Na+ K+ 2cl) co-transport at a chloride site. *American Journal of Physiology-Cell Physiology*, 245(3):C235–C240.

Hamann, S. (2002). Molecular mechanisms of water transport in the eye. In *International review of cytology*, volume 215, pages 395–431. Elsevier.

Hamann, S., Kiilgaard, J. F., Litman, T., Alvarez-Leefmans, F. J., Winther, B. R., and Zeuthen, T. (2002). Measurement of cell volume changes by fluorescence self-quenching. *Journal of fluorescence*, 12(2):139–145.

Han, X. and Boyden, E. S. (2007). Multiple-color optical activation, silencing, and desynchronization of neural activity, with single-spike temporal resolution. *PloS one*, 2(3):e299.

Hauck, T. S., Jennings, T. L., Yatsenko, T., Kumaradas, J. C., and Chan, W. C. (2008). Enhancing the toxicity of cancer chemotherapeutics with gold nanorod hyperthermia. *Advanced Materials*, 20(20):3832–3838.

Hay, E. D. (1993). Extracellular matrix alters epithelial differentiation. *Current opinion in cell biology*, 5(6):1029–1035.

Hübner, C. A. and Jentsch, T. J. (2008). Channelopathies of transepithelial transport and vesicular function. *Advances in genetics*, 63:113–152.

Hioki, H., Kameda, H., Nakamura, H., Okunomiya, T., Ohira, K., Nakamura, K., Kuroda, M., Furuta, T., and Kaneko, T. (2007). Efficient gene transduction of neurons by lentivirus with enhanced neuron-specific promoters. *Gene therapy*, 14(11):872.

Hires, S. A., Tian, L., and Looger, L. L. (2008). Reporting neural activity with genetically encoded calcium indicators. *Brain cell biology*, 36(1-4):69.

Horton, R. M. (1997). In vitro recombination and mutagenesis of DNA. In *PCR cloning protocols*, pages 141–150. Springer.

Huang, B., Bates, M., and Zhuang, X. (2009). Super-resolution fluorescence microscopy. *Annual review of biochemistry*, 78:993–1016.

Huang, X., Jain, P. K., El-Sayed, I. H., and El-Sayed, M. A. (2008). Plasmonic photothermal therapy (PPTT) using gold nanoparticles. *Lasers in medical science*, 23(3):217.

Hummler, E. (2003). Epithelial sodium channel, salt intake, and hypertension. *Current hypertension reports*, 5(1):11–18.

Ihara, K., Narusawa, A., Maruyama, K., Takeguchi, M., and Kouyama, T. (2008). A halorhodopsin-overproducing mutant isolated from an extremely haloalkaliphilic archaeon Natronomonas pharaonis. *FEBS letters*, 582(19):2931–2936.

Ikeda, Y., Yonemitsu, Y., Onimaru, M., Nakano, T., Miyazaki, M., Kohno, R.-i., Nakagawa, K., Ueno, A., Sueishi, K., and Ishibashi, T. (2006). The regulation of vascular endothelial growth factors (VEGF-A, -C, and -D) expression in the retinal pigment epithelium. *Experimental Eye Research*, 83(5):1031–1040.

Ikeuchi, Y., Kogiso, H., Hosogi, S., Tanaka, S., Shimamoto, C., Inui, T., Nakahari, T., and Marunaka, Y. (2018). Measurement of [Cl] i unaffected by the cell volume change using MQAE-based two-photon microscopy in airway ciliary cells of mice. *The Journal of Physiological Sciences*, 68(2):191–199.

Ikonen, E. (2001). Roles of lipid rafts in membrane transport. *Current opinion in cell biology*, 13(4):470–477.

Imamura, Y., Noda, S., Hashizume, K., Shinoda, K., Yamaguchi, M., Uchiyama, S., Shimizu, T., Mizushima, Y., Shirasawa, T., and Tsubota, K. (2006). Drusen, choroidal neovascularization, and retinal pigment epithelium dysfunction in SOD1-deficient mice: a model of age-related macular degeneration. *Proceedings of the National Academy of Sciences*, 103(30):11282–11287.

Ishizuka, T., Kakuda, M., Araki, R., and Yawo, H. (2006). Kinetic evaluation of photosensitivity in genetically engineered neurons expressing green algae light-gated channels. *Neuroscience research*, 54(2):85–94.

Iwai, Y., Honda, S., Ozeki, H., Hashimoto, M., and Hirase, H. (2011). A simple head-mountable LED device for chronic stimulation of optogenetic molecules in freely moving mice. *Neuroscience research*, 70(1):124–127.

Jardón-Valadez, E., Bondar, A.-N., and Tobias, D. J. (2014). Electrostatic interactions and hydrogen bond dynamics in chloride pumping by halorhodopsin. *Biochimica et Biophysica Acta (BBA) - Bioenergetics*, 1837(12):1964–1972.

Jay, D. G. and Sakurai, T. (1999). Chromophore-assisted laser inactivation (CALI) to elucidate cellular mechanisms of cancer. *Biochimica et Biophysica Acta (BBA)-Reviews on Cancer*, 1424(2-3):M39–M48.

Johnson, I. (1998). Fluorescent probes for living cells. *The Histochemical Journal*, 30(3):123–140.

Johnson, I. S. (1983). Human insulin from recombinant DNA technology. *Science*, 219(4585):632–637.

Jones, B., Pfeiffer, R., Ferrell, W., Watt, C., Marmor, M., and Marc, R. (2016). Retinal remodeling in human retinitis pigmentosa. *Experimental eye research*, 150:149–165.

Jones, S. (1993). Muscarinic receptor subtypes: modulation of ion channels. *Life sciences*, 52(5-6):457–464.

Joseph, D. and Miller, S. (1991). Apical and basal membrane ion transport mechanisms in bovine retinal pigment epithelium. *The Journal of Physiology*, 435(1):439–463.

Jung, T., Bader, N., and Grune, T. (2007). Lipofuscin: formation, distribution, and metabolic consequences. *Annals of the New York Academy of Sciences*, 1119(1):97–111.

Kato, H. E., Zhang, F., Yizhar, O., Ramakrishnan, C., Nishizawa, T., Hirata, K., Ito, J., Aita, Y., Tsukazaki, T., Hayashi, S., Hegemann, P., Maturana, A. D., Ishitani, R., Deisseroth, K., and Nureki, O. (2012). Crystal structure of the channelrhodopsin light-gated cation channel. *Nature*, 482:369.

Katz, Y., Yizhar, O., Staiger, J., and Lampl, I. (2013). Optopatcher—an electrode holder for simultaneous intracellular patch-clamp recording and optical manipulation. *Journal of neuroscience methods*, 214(1):113–117.

Kawedia, J. D., Nieman, M. L., Boivin, G. P., Melvin, J. E., Kikuchi, K.-I., Hand, A. R., Lorenz, J. N., and Menon, A. G. (2007). Interaction between transcellular and paracellular water transport pathways through Aquaporin 5 and the tight junction complex. *Proceedings of the National Academy of Sciences*, 104(9):3621–3626.

Kennedy, B. G. (1994). Volume regulation in cultured cells derived from human retinal pigment epithelium. *American Journal of Physiology-Cell Physiology*, 266(3):C676–C683.

Kennedy, C. J., Rakoczy, P. E., and Constable, I. J. (1995). Lipofuscin of the retinal pigment epithelium: a review. *Eye*, 9(6):763.

Kent, D., Vinores, S. A., and Campochiaro, P. A. (2000). Macular oedema: the role of soluble mediators. *British Journal of Ophthalmology*, 84(5):542–545.

Kevany, B. M. and Palczewski, K. (2010). Phagocytosis of retinal rod and cone photoreceptors. *Physiology*, 25(1):8–15.

Kiela, P. R. and Ghishan, F. K. (2016). Physiology of intestinal absorption and secretion. *Best practice & research Clinical gastroenterology*, 30(2):145–159.

Kim, J.-B. (2014). Channelopathies. *Korean journal of pediatrics*, 57(1):1.

Kim, T.-i., McCall, J. G., Jung, Y. H., Huang, X., Siuda, E. R., Li, Y., Song, J., Song, Y. M., Pao, H. A., and Kim, R.-H. (2013). Injectable, cellular-scale optoelectronics with applications for wireless optogenetics. *Science*, 340(6129):211–216.

Kleinlogel, S., Feldbauer, K., Dempski, R. E., Fotis, H., Wood, P. G., Bamann, C., and Bamberg, E. (2011a). Ultra light-sensitive and fast neuronal activation with the Ca2+-permeable channelrhodopsin CatCh. *Nature Neuroscience*, 14:513.

Kleinlogel, S., Terpitz, U., Legrum, B., Gökbuget, D., Boyden, E. S., Bamann, C., Wood, P. G., and Bamberg, E. (2011b). A gene-fusion strategy for stoichiometric and co-localized expression of light-gated membrane proteins. *Nature Methods*, 8:1083.

Knöpfel, T., Lin, M. Z., Levskaya, A., Tian, L., Lin, J. Y., and Boyden, E. S. (2010). Toward the second generation of optogenetic tools. *Journal of Neuroscience*, 30(45):14998–15004.

Koch, R. and Barish, M. (1994). Perturbation of intracellular calcium and hydrogen ion regulation in cultured mouse hippocampal neurons by reduction of the sodium ion concentration gradient. *Journal of Neuroscience*, 14(5):2585–2593.

Kolbe, M., Besir, H., Essen, L.-O., and Oesterhelt, D. (2000). Structure of the Light-Driven Chloride Pump Halorhodopsin at 1.8 Å Resolution. *Science*, 288(5470):1390.

Kotterman, M. A., Chalberg, T. W., and Schaffer, D. V. (2015). Viral vectors for gene therapy: translational and clinical outlook. *Annual review of biomedical engineering*, 17:63–89.

Kouyama, T., Ihara, K., Maki, K., and Chan, S. K. (2018). Three-step isomerization of the retinal chromophore during the anion pumping cycle of halorhodopsin. *Biochemistry*, 57(41):6013–6026.

Kouyama, T., Kanada, S., Takeguchi, Y., Narusawa, A., Murakami, M., and Ihara, K. (2010). Crystal structure of the light-driven chloride pump halorhodopsin from Natronomonas pharaonis. *Journal of molecular biology*, 396(3):564–579.

Kralj, J. M., Douglass, A. D., Hochbaum, D. R., Maclaurin, D., and Cohen, A. E. (2012). Optical recording of action potentials in mammalian neurons using a microbial rhodopsin. *Nature methods*, 9(1):90.

Kravitz, A. V., Freeze, B. S., Parker, P. R. L., Kay, K., Thwin, M. T., Deisseroth, K., and Kreitzer, A. C. (2010). Regulation of parkinsonian motor behaviours by optogenetic control of basal ganglia circuitry. *Nature*, 466:622.

Krueger, D., Tardivo, P., Nguyen, C., and De Renzis, S. (2018). Downregulation of basal myosin-II is required for cell shape changes and tissue invagination. *The EMBO journal*, 37(23):e100170.

Kubo, M. and Okada, Y. (1992). Volume-regulatory Cl-channel currents in cultured human epithelial cells. *The Journal of Physiology*, 456(1):351–371.

Ladha, S. (1998). Lipid heterogeneity and membrane fluidity in a highly polarized cell, the mammalian spermatozoon. *Journal of Membrane Biology*, 165(1):1–10.

Lang, F., Busch, G. L., Ritter, M., Volkl, H., Waldegger, S., Gulbins, E., and Haussinger, D. (1998). Functional significance of cell volume regulatory mechanisms. *Physiological reviews*, 78(1):247–306.

Lanyi, J. K. (1985). Halorhodopsin, the Light-Dependent Chloride Transport System of Halobacteria. In *Recent Advances in Biological Membrane Studies*, pages 393–407. Springer.

Lanyi, J. K. (2004). Bacteriorhodopsin. *Annu. Rev. Physiol.*, 66:665–688.

Larsen, E. H. and Hoffmann, E. K. (2016). Volume Regulation in Epithelia. In *Ion Channels and Transporters of Epithelia in Health and Disease*, pages 131–185. Springer.

Larson, M. and Spring, K. R. (1987). Volume regulation in epithelia. In *Current Topics in Membranes and Transport*, volume 30, pages 105–123. Elsevier.

Legouis, R., Jaulin-Bastard, F., Schott, S., Navarro, C., Borg, J., and Labouesse, M. (2003). Basolateral targeting by leucine-rich repeat domains in epithelial cells. *EMBO reports*, 4(11):1096–1100.

Lewis, S. and Wills, N. (1982). Electrical properties of the rabbit urinary bladder assessed using gramicidin D. *The Journal of membrane biology*, 67(1):45–53.

Lewis, S. A. (1996). Epithelial structure and function. *Epithelial Transport: A guide to methods and experimental analysis.*, pages pp 1–20.

Li, H., Sheppard, D. N., and Hug, M. J. (2004). Transepithelial electrical measurements with the Ussing chamber. *Journal of Cystic Fibrosis*, 3:123–126.

Li, R. and Gundersen, G. G. (2008). Beyond polymer polarity: how the cytoskeleton builds a polarized cell. *Nature reviews Molecular cell biology*, 9(11):860.

Li, X., Gutierrez, D. V., Hanson, M. G., Han, J., Mark, M. D., Chiel, H., Hegemann, P., Landmesser, L. T., and Herlitze, S. (2005). Fast noninvasive activation and inhibition of neural and network activity by vertebrate rhodopsin and green algae channelrhodopsin. *Proceedings of the National Academy of Sciences*, 102(49):17816–17821.

Liang, F.-Q. and Godley, B. F. (2003a). Oxidative stress-induced mitochondrial DNA damage in human retinal pigment epithelial cells: a possible mechanism for RPE aging and age-related macular degeneration. *Experimental Eye Research*, 76(4):397–403.

Liang, F.-Q. and Godley, B. F. (2003b). Oxidative stress-induced mitochondrial DNA damage in human retinal pigment epithelial cells: a possible mechanism for RPE aging and age-related macular degeneration. *Experimental Eye Research*, 76(4):397–403.

Liao, J. C., Roider, J., and Jay, D. G. (1994). Chromophore-assisted laser inactivation of proteins is mediated by the photogeneration of free radicals. *Proceedings of the National Academy of Sciences*, 91(7):2659–2663.

Lignani, G., Ferrea, E., Difato, F., Amaru‘, J., Ferroni, E., Lugara‘, E., Espinoza, S., Gainetdinov, R., Baldelli, P., and Benfenati, F. (2013). Long-term optical stimulation of channelrhodopsin-expressing neurons to study network plasticity. *Frontiers in Molecular Neuroscience*, 6:22.

Lin, J., Yang, J., and Tsien, R. (2009a). Development and characterization of channelrhodopsin variants for improved optical control of neuronal excitability. *Society for Neuroscience*.

Lin, J. Y. (2011). A user's guide to channelrhodopsin variants: features, limitations and future developments. *Experimental Physiology*, 96(1):19–25.

Lin, J. Y. (2012). Optogenetic excitation of neurons with channelrhodopsins: light instrumentation, expression systems, and channelrhodopsin variants. In *Progress in brain research*, volume 196, pages 29–47. Elsevier.

Lin, J. Y., Knutsen, P. M., Muller, A., Kleinfeld, D., and Tsien, R. Y. (2013). ReaChR: a red-shifted variant of channelrhodopsin enables deep transcranial optogenetic excitation. *Nature neuroscience*, 16(10):1499.

Lin, J. Y., Lin, M. Z., Steinbach, P., and Tsien, R. Y. (2009b). Characterization of engineered channelrhodopsin variants with improved properties and kinetics. *Biophysical journal*, 96(5):1803–1814.

Liu, J., Tian, J., Haas, M., Shapiro, J. I., Askari, A., and Xie, Z. (2000). Ouabain interaction with cardiac Na+/K+-ATPase initiates signal cascades independent of changes in intracellular Na+ and Ca2+ concentrations. *Journal of Biological Chemistry*, 275(36):27838–27844.

Madisen, L., Mao, T., Koch, H., Zhuo, J.-m., Berenyi, A., Fujisawa, S., Hsu, Y.-W. A., Garcia III, A. J., Gu, X., and Zanella, S. (2012). A toolbox of Cre-dependent optogenetic transgenic mice for light-induced activation and silencing. *Nature neuroscience*, 15(5):793.

Makadia, P. A., Najjar, S. A., Saloman, J. L., Adelman, P., Feng, B., Margiotta, J. F., Albers, K. M., and Davis, B. M. (2018). Optogenetic activation of colon epithelium of the mouse produces high-frequency bursting in extrinsic colon afferents and engages visceromotor responses. *Journal of Neuroscience*, 38(25):5788–5798.

Malich, G., Markovic, B., and Winder, C. (1997). The sensitivity and specificity of the MTS tetrazolium assay for detecting the in vitro cytotoxicity of 20 chemicals using human cell lines. *Toxicology*, 124(3):179–192.

Mandonnet, E., Winkler, P. A., and Duffau, H. (2010). Direct electrical stimulation as an input gate into brain functional networks: principles, advantages and limitations. *Acta neurochirurgica*, 152(2):185–193.

Mank, M. and Griesbeck, O. (2008). Genetically encoded calcium indicators. *Chemical reviews*, 108(5):1550–1564.

Mannermaa, E., Reinisalo, M., Ranta, V.-P., Vellonen, K.-S., Kokki, H., Saarikko, A., Kaarniranta, K., and Urtti, A. (2010). Filter-cultured ARPE-19 cells as outer blood–retinal barrier model. *European Journal of Pharmaceutical Sciences*, 40(4):289–296.

Manninen, A. (2015). Epithelial polarity–generating and integrating signals from the ECM with integrins. *Experimental cell research*, 334(2):337–349.

Marmor, M. (1990). Control of subretinal fluid: experimental and clinical studies. *Eye*, 4(2):340.

Marmor, M. F. (2000). Mechanisms of fluid accumulation in retinal edema. In *Macular Edema*, pages 35–45. Springer.

Masuzawa, T., Ohta, T., Kawamura, M., Nakahara, N., and Sato, F. (1984). Immunohistochemical localization of Na+, K+-ATPase in the choroid plexus. *Brain research*, 302(2):357–362.

Mathias, R. T. (1985). Epithelial water transport in a balanced gradient system. *Biophysical journal*, 47(6):823–836.

Matter, K. and Mellman, I. (1994). Mechamisms of cell polarity: sorting and transport in epithelial cells. *Current opinion in cell biology*, 6(4):545–554.

Maxam, A. M. and Gilbert, W. (1977). A new method for sequencing DNA. *Proceedings of the National Academy of Sciences*, 74(2):560–564.

McCarty, N. A. and O'Neil, R. G. (1992). Calcium signaling in cell volume regulation. *Physiological Reviews*, 72(4):1037–1061.

McCombs, J. E. and Palmer, A. E. (2008). Measuring calcium dynamics in living cells with genetically encodable calcium indicators. *Methods*, 46(3):152–159.

McIsaac, R. S., Bedbrook, C. N., and Arnold, F. H. (2015). Recent advances in engineering microbial rhodopsins for optogenetics. *Current opinion in structural biology*, 33:8–15.

McLeod, D. S., Grebe, R., Bhutto, I., Merges, C., Baba, T., and Lutty, G. A. (2009). Relationship between RPE and choriocapillaris in age-related macular degeneration. *Investigative ophthalmology & visual science*, 50(10):4982–4991.

McManus, M., Fischbarg, J., Sun, A., Hebert, S., and Strange, K. (1993). Laser light-scattering system for studying cell volume regulation and membrane transport processes. *American Journal of Physiology-Cell Physiology*, 265(2):C562–C570.

Meissner, P., Pick, H., Kulangara, A., Chatellard, P., Friedrich, K., and Wurm, F. M. (2001). Transient gene expression: recombinant protein production with suspension-adapted HEK293-EBNA cells. *Biotechnology and bioengineering*, 75(2):197–203.

Metzker, M. L. (2010). Sequencing technologies—the next generation. *Nature reviews genetics*, 11(1):31.

Miller, S. S. and Steinberg, R. H. (1977). Active transport of ions across frog retinal pigment epithelium. *Experimental eye research*, 25(3):235–248.

Minta, A., Kao, J., and Tsien, R. Y. (1989). Fluorescent indicators for cytosolic calcium based on rhodamine and fluorescein chromophores. *Journal of Biological Chemistry*, 264(14):8171–8178.

Mitic, L. and Anderson, J. (1998). Molecular architecture of tight junctions. *Annual review of physiology*, 60(1):121–142.

Mittelmeier, T. M., Boyd, J. S., Lamb, M. R., and Dieckmann, C. L. (2011). Asymmetric properties of the Chlamydomonas reinhardtii cytoskeleton direct rhodopsin photoreceptor localization. *The Journal of cell biology*, pages jcb–201009131.

Mizuno, M., Nakajima, A., Kandori, H., and Mizutani, Y. (2018). Structural Evolution of a Retinal Chromophore in the Photocycle of Halorhodopsin from Natronobacterium pharaonis. *The Journal of Physical Chemistry A*, 122(9):2411–2423.

Müller, M., Bamann, C., Bamberg, E., and Kühlbrandt, W. (2011). Projection structure of channelrhodopsin-2 at 6 Å resolution by electron crystallography. *Journal of molecular biology*, 414(1):86–95.

Morgan, D. M. (1998). Tetrazolium (MTT) assay for cellular viability and activity. In *Polyamine protocols*, pages 179–184. Springer.

Mostov, K., Su, T., and ter Beest, M. (2003). Polarized epithelial membrane traffic: conservation and plasticity. *Nature cell biology*, 5(4):287.

Mullis, K., Faloona, F., Scharf, S., Saiki, R., Horn, G., and Erlich, H. (1986). Specific enzymatic amplification of DNA in vitro: the polymerase chain reaction. volume 51, pages 263–273. Cold Spring Harbor Laboratory Press.

Murawski, C., Morton, A., Samuel, I. D., Pulver, S. R., and Gather, M. C. (2016). Organic Light-Emitting Diodes for Optogenetic Stimulation of Drosophila Larvae. pages JW4A–9. Optical Society of America.

Mutoh, H., Perron, A., Akemann, W., Iwamoto, Y., and Knöpfel, T. (2011). Optogenetic monitoring of membrane potentials. *Experimental physiology*, 96(1):13–18.

Nack, M., Radu, I., Gossing, M., Bamann, C., Bamberg, E., von Mollard, G. F., and Heberle, J. (2010). The DC gate in Channelrhodopsin-2: crucial hydrogen bonding interaction between C128 and D156. *Photochemical & Photobiological Sciences*, 9(2):194–198.

Nagel, G., Brauner, M., Liewald, J. F., Adeishvili, N., Bamberg, E., and Gottschalk, A. (2005a). Light activation of channelrhodopsin-2 in excitable cells of Caenorhabditis elegans triggers rapid behavioral responses. *Current Biology*, 15(24):2279–2284.

Nagel, G., Ollig, D., Fuhrmann, M., Kateriya, S., Musti, A. M., Bamberg, E., and Hegemann, P. (2002). Channelrhodopsin-1: a light-gated proton channel in green algae. *Science*, 296(5577):2395–2398.

Nagel, G., Szellas, T., Huhn, W., Kateriya, S., Adeishvili, N., Berthold, P., Ollig, D., Hegemann, P., and Bamberg, E. (2003). Channelrhodopsin-2, a directly light-gated cation-selective membrane channel. *Proceedings of the National Academy of Sciences*, 100(24):13940.

Nagel, G., Szellas, T., Kateriya, S., Adeishvili, N., Hegemann, P., and Bamberg, E. (2005b). Channelrhodopsins: directly light-gated cation channels.

Nathans, D. and Smith, H. O. (1975). Restriction endonucleases in the analysis and restructuring of DNA molecules. *Annual review of biochemistry*, 44(1):273–293.

Nathanson, J. L., Yanagawa, Y., Obata, K., and Callaway, E. M. (2009). Preferential labeling of inhibitory and excitatory cortical neurons by endogenous tropism of adeno-associated virus and lentivirus vectors. *Neuroscience*, 161(2):441–450.

Nathanson, M. H. and Boyer, J. L. (1991). Mechanisms and regulation of bile secretion. *Hepatology*, 14(3):551–566.

Nayerossadat, N., Maedeh, T., and Ali, P. A. (2012). Viral and nonviral delivery systems for gene delivery. *Advanced biomedical research*, 1.

Neyton, J. and Paoletti, P. (2006). Relating NMDA receptor function to receptor subunit composition: limitations of the pharmacological approach. *Journal of Neuroscience*, 26(5):1331–1333.

Niederkorn, J. Y. and Kaplan, H. J. (2007). *Immune response and the eye*, volume 92. Karger Medical and Scientific Publishers.

Nielsen, O. B. and Overgaard, K. (1996). Ion gradients and contractility in skeletal muscle: the role of active Na+, K+ transport. *Acta physiologica scandinavica*, 156(3):247–256.

Niessen, C. M. (2007). Tight junctions/adherens junctions: basic structure and function. *Journal of Investigative Dermatology*, 127(11):2525–2532.

Nikolic, K., Grossman, N., Grubb, M. S., Burrone, J., Toumazou, C., and Degenaar, P. (2009). Photocycles of channelrhodopsin-2. *Photochemistry and photobiology*, 85(1):400–411.

Nowak, J. Z. (2006). Age-related macular degeneration (AMD): pathogenesis and therapy. *Pharmacological Reports*, 58(3):353.

Oesterhelt, D. and Stoeckenius, W. (1971). Rhodopsin-like protein from the purple membrane of Halobacterium halobium. *Nature new biology*, 233(39):149.

Ohno-Matsui, K., Morita, I., Tombran-Tink, J., Mrazek, D., Onodera, M., Uetama, T., Hayano, M., Murota, S., and Mochizuki, M. (2001). Novel mechanism for age-related macular degeneration: An equilibrium shift between the angiogenesis factors VEGF and PEDF. *Journal of cellular physiology*, 189(3):323–333.

Okada, T., Sugihara, M., Bondar, A.-N., Elstner, M., Entel, P., and Buss, V. (2004). The retinal conformation and its environment in rhodopsin in light of a new 2.2 Å crystal structure. *Journal of molecular biology*, 342(2):571–583.

Oron, D., Papagiakoumou, E., Anselmi, F., and Emiliani, V. (2012). Two-photon optogenetics. In *Progress in brain research*, volume 196, pages 119–143. Elsevier.

Ortega, B. and Welling, P. A. (2018). Molecular Mechanisms of Polarized Protein Trafficking in Epithelial Cells. In *Physiology of the Gastrointestinal Tract (Sixth Edition)*, pages 1027–1050. Elsevier.

Osborne, N., FitzGibbon, F., and Schwartz, G. (1991). Muscarinic acetylcholine receptor-mediated phosphoinositide turnover in cultured human retinal pigment epithelium cells. *Vision research*, 31(7-8):1119–1127.

Packer, A. M., Roska, B., and Häusser, M. (2013). Targeting neurons and photons for optogenetics. *Nature neuroscience*, 16(7):805.

Palczewski, K. (2006). G protein–coupled receptor rhodopsin. *Annu. Rev. Biochem.*, 75:743–767.

Papagiakoumou, E. (2013). Optical developments for optogenetics. *Biology of the Cell*, 105(10):443–464.

Patel, A. B., Crocker, E., Eilers, M., Hirshfeld, A., Sheves, M., and Smith, S. O. (2004). Coupling of retinal isomerization to the activation of rhodopsin. *Proceedings of the National Academy of Sciences*, 101(27):10048–10053.

Peterson, L. W. and Artis, D. (2014). Intestinal epithelial cells: regulators of barrier function and immune homeostasis. *Nature Reviews Immunology*, 14(3):141.

Philp, N. J., Wang, D., Yoon, H., and Hjelmeland, L. M. (2003). Polarized expression of monocarboxylate transporters in human retinal pigment epithelium and ARPE-19 cells. *Investigative ophthalmology & visual science*, 44(4):1716–1721.

Pipe, S. W. (2008). Recombinant clotting factors. *Thrombosis and haemostasis*, 99(11):840–850.

Planells-Cases, R. and Jentsch, T. J. (2009). Chloride channelopathies. *Biochimica Et Biophysica Acta (BBA)-Molecular Basis of Disease*, 1792(3):173–189.

Plank, C., Schillinger, U., Scherer, F., Bergemann, C., Rémy, J.-S., Krötz, F., Anton, M., Lausier, J., and Rosenecker, J. (2003). The magnetofection method: using magnetic force to enhance gene delivery. *Biological chemistry*, 384(5):737–747.

Potrykus, I. (2001). Golden rice and beyond. *Plant physiology*, 125(3):1157–1161.

Pozarowski, P. and Darzynkiewicz, Z. (2004). Analysis of cell cycle by flow cytometry. In *Checkpoint Controls and Cancer*, pages 301–311. Springer.

Prakash, R., Yizhar, O., Grewe, B., Ramakrishnan, C., Wang, N., Goshen, I., Packer, A. M., Peterka, D. S., Yuste, R., and Schnitzer, M. J. (2012). Two-photon optogenetic toolbox for fast inhibition, excitation and bistable modulation. *Nature methods*, 9(12):1171.

Prigge, M., Schneider, F., Tsunoda, S. P., Shilyansky, C., Wietek, J., and Hegemann, P. (2012). Color-tuned Channelrhodopsins for Multiwavelength Optogenetics. *The Journal of Biological Chemistry*, (287):31804–31812.

Quinn, R. and Miller, S. (1992). Ion transport mechanisms in native human retinal pigment epithelium. *Investigative ophthalmology & visual science*, 33(13):3513–3527.

R Sparrrow, J., Hicks, D., and P Hamel, C. (2010). The retinal pigment epithelium in health and disease. *Current molecular medicine*, 10(9):802–823.

Radu, I., Bamann, C., Nack, M., Nagel, G., Bamberg, E., and Heberle, J. (2009). Conformational changes of channelrhodopsin-2. *Journal of the American Chemical Society*, 131(21):7313–7319.

Redmond, T. M., Yu, S., Lee, E., Bok, D., Hamasaki, D., Chen, N., Goletz, P., Ma, J.-X., Crouch, R. K., and Pfeifer, K. (1998). Rpe65 is necessary for production of 11-cis-vitamin A in the retinal visual cycle. *Nature genetics*, 20(4):344.

Rees, D. C., Chang, G., and Spencer, R. H. (2000). Crystallographic analyses of ion channels: lessons and challenges. *Journal of Biological Chemistry*, 275(2):713–716.

Regehr, W. G., Connor, J. A., and Tank, D. W. (1989). Optical imaging of calcium accumulation in hippocampal pyramidal cells during synaptic activation. *Nature*, 341(6242):533.

Rehm, B. (2001). Bioinformatic tools for DNA/protein sequence analysis, functional assignment of genes and protein classification. *Applied microbiology and biotechnology*, 57(5-6):579–592.

Renault, R., Sukenik, N., Descroix, S., Malaquin, L., Viovy, J.-L., Peyrin, J.-M., Bottani, S., Monceau, P., Moses, E., and Vignes, M. (2015). Combining microfluidics, optogenetics and calcium imaging to study neuronal communication in vitro. *PloS one*, 10(4):e0120680.

Reuss, L. (2001). Tight junction permeability to ions and water. *Tight junctions*, 2:61–88.

Reutsky-Gefen, I., Golan, L., Farah, N., Schejter, A., Tsur, L., Brosh, I., and Shoham, S. (2013). Holographic optogenetic stimulation of patterned neuronal activity for vision restoration. *Nature communications*, 4:1509.

Riccardi, C. and Nicoletti, I. (2006). Analysis of apoptosis by propidium iodide staining and flow cytometry. *Nature protocols*, 1(3):1458.

Rice, P., Longden, I., and Bleasby, A. (2000). EMBOSS: the European molecular biology open software suite. *Trends in genetics*, 16(6):276–277.

Ritter, E., Stehfest, K., Berndt, A., Hegemann, P., and Bartl, F. J. (2008). Monitoring light-induced structural changes of Channelrhodopsin-2 by UV-visible and Fourier transform infrared spectroscopy. *Journal of Biological Chemistry*, 283(50):35033–35041.

Rizzolo, L. J. (2007). Development and role of tight junctions in the retinal pigment epithelium. *International review of cytology*, 258:195–234.

Roberts, R. J. (2005). How restriction enzymes became the workhorses of molecular biology. *Proceedings of the National Academy of Sciences*, 102(17):5905–5908.

Roe, M., Lemasters, J., and Herman, B. (1990). Assessment of Fura-2 for measurements of cytosolic free calcium. *Cell calcium*, 11(2-3):63–73.

Rogers, D. F. (2007). Physiology of airway mucus secretion and pathophysiology of hypersecretion. *Respiratory care*, 52(9):1134–1149.

Ronzitti, E., Ventalon, C., Canepari, M., Forget, B. C., Papagiakoumou, E., and Emiliani, V. (2017). Recent advances in patterned photostimulation for optogenetics. *Journal of Optics*, 19(11):113001.

Rowan III, R., Warshel, A., Skyes, B., and Karplus, M. (1974). Conformation of retinal isomers. *Biochemistry*, 13(5):970–981.

Ruggeri, B. A., Camp, F., and Miknyoczki, S. (2014). Animal models of disease: pre-clinical animal models of cancer and their applications and utility in drug discovery. *Biochemical pharmacology*, 87(1):150–161.

Saint-Geniez, M., Kurihara, T., Sekiyama, E., Maldonado, A. E., and D'Amore, P. A. (2009). An essential role for RPE-derived soluble VEGF in the maintenance of the choriocapillaris. *Proceedings of the National Academy of Sciences*, 106(44):18751.

Sanger, F., Nicklen, S., and Coulson, A. R. (1977). DNA sequencing with chain-terminating inhibitors. *Proceedings of the national academy of sciences*, 74(12):5463–5467.

Santacroce, L., D'Agostino, D., Charitos, I. A., Bottalico, L., and Ballini, A. (2018). A short review about electrophysiology and bioimpedance: History and perspectives. 9(11):587.

Sato, M., Kubo, M., Aizawa, T., Kamo, N., Kikukawa, T., Nitta, K., and Demura, M. (2005). Role of putative anion-binding sites in cytoplasmic and extracellular channels of Natronomonas pharaonis halorhodopsin. *Biochemistry*, 44(12):4775–4784.

Sato, M. P., Higuchi, T., Nin, F., Ogata, G., Sawamura, S., Yoshida, T., Ota, T., Hori, K., Komune, S., and Uetsuka, S. (2017). Hearing loss controlled by optogenetic stimulation of nonexcitable nonglial cells in the cochlea of the inner ear. *Frontiers in Molecular Neuroscience*, 10:300.

Schindelin, J., Arganda-Carreras, I., Frise, E., Kaynig, V., Longair, M., Pietzsch, T., Preibisch, S., Rueden, C., Saalfeld, S., and Schmid, B. (2012). Fiji: an open-source platform for biological-image analysis. *Nature methods*, 9(7):676.

Schobert, B. and Lanyi, J. K. (1982). Halorhodopsin is a light-driven chloride pump. *Journal of Biological Chemistry*, 257(17):10306–10313.

Schoenlein, R., Peteanu, L., Mathies, R., and Shank, C. (1991). The first step in vision: femtosecond isomerization of rhodopsin. *Science*, 254(5030):412–415.

Shendure, J. and Ji, H. (2008). Next-generation DNA sequencing. *Nature biotechnology*, 26(10):1135.

Sheppard, D. N. and Welsh, M. J. (1999). Structure and function of the CFTR chloride channel. *Physiological reviews*, 79(1):S23–S45.

Shimomura, O. (2009). Discovery of green fluorescent protein (GFP)(Nobel Lecture). *Angewandte Chemie International Edition*, 48(31):5590–5602.

Shipley, F. B., Clark, C. M., Alkema, M. J., and Leifer, A. M. (2014). Simultaneous optogenetic manipulation and calcium imaging in freely moving C. elegans. *Frontiers in neural circuits*, 8:28.

Simons, K. and Wandinger-Ness, A. (1990). Polarized sorting in epithelia. *Cell*, 62(2):207–210.

Sineshchekov, O. A., Jung, K.-H., and Spudich, J. L. (2002a). Two rhodopsins mediate phototaxis to low- and high-intensity light in Chlamydomonas reinhardtii. *Proceedings of the National Academy of Sciences*, 99(13):8689–8694.

Sineshchekov, O. A., Jung, K.-H., and Spudich, J. L. (2002b). Two rhodopsins mediate phototaxis to low- and high-intensity light in Chlamydomonas reinhardtii. *Proceedings of the National Academy of Sciences*, 99(13):8689–8694.

Soria, B. and Ceña, V. (1998). *Ion channel pharmacology*. Oxford University Press, Oxford; New York.

Sparrow, J. R. and Boulton, M. (2005). RPE lipofuscin and its role in retinal pathobiology. *Experimental eye research*, 80(5):595–606.

Spilsbury, K., Garrett, K. L., Shen, W.-Y., Constable, I. J., and Rakoczy, P. E. (2000). Overexpression of vascular endothelial growth factor (VEGF) in the retinal pigment epithelium leads to the development of choroidal neovascularization. *The American journal of pathology*, 157(1):135–144.

Spring, K. R. (1998). Routes and mechanism of fluid transport by epithelia. *Annual review of physiology*, 60(1):105–119.

Spudich, J. L. (2006). The multitalented microbial sensory rhodopsins. *Trends in microbiology*, 14(11):480–487.

Srinivas, S., Bonanno, J. A., Larivière, E., Jans, D., and Van Driessche, W. (2003). Measurement of rapid changes in cell volume by forward light scattering. *Pflügers Archiv*, 447(1):97–108.

Srinivasan, B., Kolli, A. R., Esch, M. B., Abaci, H. E., Shuler, M. L., and Hickman, J. J. (2015). TEER measurement techniques for in vitro barrier model systems. *Journal of laboratory automation*, 20(2):107–126.

Stamer, W. D., Bok, D., Hu, J., Jaffe, G. J., and McKay, B. S. (2003). Aquaporin-1 channels in human retinal pigment epithelium: role in transepithelial water movement. *Investigative ophthalmology & visual science*, 44(6):2803–2808.

Steed, E., Balda, M. S., and Matter, K. (2010). Dynamics and functions of tight junctions. *Trends in cell biology*, 20(3):142–149.

Stehfest, K. and Hegemann, P. (2010). Evolution of the channelrhodopsin photocycle model. *ChemPhysChem*, 11(6):1120–1126.

Strauss, O. (2005). The Retinal Pigment Epithelium in Visual Function. *Physiological Reviews*, 85(3):845–881.

Strauss, O. (2011). The retinal pigment epithelium. In *Webvision: The Organization of the Retina and Visual System [Internet]*. University of Utah Health Sciences Center.

Stutzin, A. and Hoffmann, E. K. (2006). Swelling-activated ion channels: functional regulation in cell-swelling, proliferation and apoptosis. *Acta Physiologica*, 187(1-2):27–42.

Stuurman, N., Amdodaj, N., and Vale, R. (2007). microManager: open source software for light microscope imaging. *Microscopy Today*, 15(3):42–43.

Sugiyama, Y., Maeda, M., Futai, M., and Mukohata, Y. (1989). Isolation of a gene that encodes a new retinal protein, archaerhodopsin, from Halobacterium sp. aus-1. *Journal of Biological Chemistry*, 264(35):20859–20862.

Sun, T. and Morgan, H. (2010). Single-cell microfluidic impedance cytometry: a review. *Microfluidics and Nanofluidics*, 8(4):423–443.

Tao, W., Rein, D. H., Dean, B. J., Stabila, P. F., and Goddard, M. B. (2002). ARPE-19 as a platform cell line for encapsulated cell-based delivery.

Tarran, R. (2004). Regulation of airway surface liquid volume and mucus transport by active ion transport. *Proceedings of the American Thoracic Society*, 1(1):42–46.

Terentyuk, G. S., Maslyakova, G. N., Suleymanova, L. V., Khlebtsov, N. G., Khlebtsov, B. N., Akchurin, G. G., Maksimova, I. L., and Tuchin, V. V. (2009). Laser-induced tissue hyperthermia mediated by gold nanoparticles: toward cancer phototherapy. *Journal of biomedical optics*, 14(2):021016.

Theocharis, A. D., Skandalis, S. S., Gialeli, C., and Karamanos, N. K. (2016). Extracellular matrix structure. *Advanced drug delivery reviews*, 97:4–27.

Thomas, C. E., Ehrhardt, A., and Kay, M. A. (2003). Progress and problems with the use of viral vectors for gene therapy. *Nature Reviews Genetics*, 4(5):346.

Tian, L., Akerboom, J., Schreiter, E. R., and Looger, L. L. (2012). Neural activity imaging with genetically encoded calcium indicators. In *Progress in brain research*, volume 196, pages 79–94. Elsevier.

Tong, J.-P. and Yao, Y.-F. (2006). Contribution of VEGF and PEDF to choroidal angiogenesis: a need for balanced expressions. *Clinical biochemistry*, 39(3):267–276.

Triggle, D. J. (2007). Calcium channel antagonists: clinical uses—past, present and future. *Biochemical pharmacology*, 74(1):1–9.

Tsien, R. Y. (1989). Fluorescent indicators of ion concentrations. In *Methods in cell biology*, volume 30, pages 127–156. Elsevier.

Tsien, R. Y. (1998). The green fluorescent protein.

Tsuboi, S. (1987). Measurement of the volume flow and hydraulic conductivity across the isolated dog retinal pigment epithelium. *Investigative ophthalmology & visual science*, 28(11):1776–1782.

Tucker, T. A., Varga, K., Bebok, Z., Zsembery, A., McCarty, N. A., Collawn, J. F., Schwiebert, E. M., and Schwiebert, L. M. (2003). Transient transfection of polarized epithelial monolayers with CFTR and reporter genes using efficacious lipids. *American Journal of Physiology-Cell Physiology*, 284(3):C791–C804.

Tye, K. M. and Deisseroth, K. (2012a). Optogenetic investigation of neural circuits underlying brain disease in animal models. *Nature Reviews Neuroscience*, 13(4):251.

Tye, K. M. and Deisseroth, K. (2012b). Optogenetic investigation of neural circuits underlying brain disease in animal models. *Nature Reviews Neuroscience*, 13:251.

Vera-Díaz, F. A. and Doble, N. (2012). The human eye and adaptive optics. In *Topics in Adaptive Optics*. InTech.

Verhoefen, M., Bamann, C., Blöcher, R., Förster, U., Bamberg, E., and Wachtveitl, J. (2010). The Photocycle of Channelrhodopsin-2: Ultrafast Reaction Dynamics and Subsequent Reaction Steps. *ChemPhysChem*, 11(14):3113–3122.

Verkman, A. (1990). Development and biological applications of chloride-sensitive fluorescent indicators. *American Journal of Physiology-Cell Physiology*, 259(3):C375–C388.

Viola, H., Macdonald, W., Tang, H., and Hool, L. (2009). The L-type Ca2+ channel as a therapeutic target in heart disease. *Current medicinal chemistry*, 16(26):3341–3358.

Voipio, J., Pasternack, M., and MacLeod, K. (1998). Ion-sensitive microelectrodes. *pH and brain function. Wiley-Liss, New York*, pages 95–108.

Wagstaff, K. M. and Jans, D. A. (2007). Nucleocytoplasmic transport of DNA: enhancing non-viral gene transfer. *Biochemical Journal*, 406(2):185–202.

Wang, H., Sugiyama, Y., Hikima, T., Sugano, E., Tomita, H., Takahashi, T., Ishizuka, T., and Yawo, H. (2009). Molecular determinants differentiating photocurrent properties of two channelrhodopsins from chlamydomonas. *Journal of Biological Chemistry*, 284(9):5685–5696.

Weisz, O. A. and Rodriguez-Boulan, E. (2009). Apical trafficking in epithelial cells: signals, clusters and motors. *Journal of cell science*, 122(23):4253–4266.

White, B. and Cohen, J. (1992). Agonist-induced changes in the structure of the acetylcholine receptor M2 regions revealed by photoincorporation of an uncharged nicotinic noncompetitive antagonist. *Journal of Biological Chemistry*, 267(22):15770–15783.

Wietek, J. and Prigge, M. (2016). Enhancing channelrhodopsins: an overview. In *Optogenetics*, pages 141–165. Springer.

Wills, N. K. (1981). Antibiotics as tools for studying the electrical properties of tight epithelia. volume 40, pages 2202–2205.

Wilson, P. D., Sherwood, A., Palla, K., Du, J., Watson, R., and Norman, J. T. (1991). Reversed polarity of Na (+)-K (+)-ATPase: mislocation to apical plasma membranes in polycystic kidney disease epithelia. *American Journal of Physiology-Renal Physiology*, 260(3):F420–F430.

Wimmers, S., Karl, M. O., and Strauss, O. (2007). Ion channels in the RPE. *Progress in Retinal and Eye Research*, 26(3):263–301.

Wimmers, S. and Strauss, O. (2007). Basal Calcium Entry in Retinal Pigment Epithelial Cells Is Mediated by TRPC Channels. *Investigative Ophthalmology & Visual Science*, 48(12):5767–5772.

Witman, G. B. (1993). Chlamydomonas phototaxis. *Trends in cell biology*, 3(11):403–408.

Yawo, H., Kandori, H., and Koizumi, A. (2015). *Optogenetics: Light-Sensing Proteins and Their Applications*. Springer.

Yeste, J., Illa, X., Alvarez, M., and Villa, R. (2018). Engineering and monitoring cellular barrier models. *Journal of Biological Engineering*, 12(1):18.

Yew, N. S., Wysokenski, D. M., Wang, K. X., Ziegler, R. J., Marshall, J., McNeilly, D., Cherry, M., Osburn, W., and Cheng, S. H. (1997). Optimization of plasmid vectors for high-level expression in lung epithelial cells. *Human gene therapy*, 8(5):575–584.

Yin, H., Kauffman, K. J., and Anderson, D. G. (2017). Delivery technologies for genome editing. *Nature reviews Drug discovery*, 16(6):387.

Yizhar, O. and Adamantidis, A. (2018). Cell type-specific targeting strategies for optogenetics. In *Optogenetics: A Roadmap*, pages 25–42. Springer.

Yizhar, O., Fenno, L. E., Davidson, T. J., Mogri, M., and Deisseroth, K. (2011). Optogenetics in Neural Systems. *Neuron*, 71(1):9–34.

Yogeeswari, P., Ragavendran, J. V., Thirumurugan, R., Saxena, A., and Sriram, D. (2004). Ion channels as important targets for antiepileptic drug design. *Current drug targets*, 5(7):589–602.

Youn, H.-Y., McCanna, D. J., Sivak, J. G., and Jones, L. W. (2011). In vitro ultraviolet–induced damage in human corneal, lens, and retinal pigment epithelial cells. *Molecular vision*, 17:237.

Yu, J., Chen, K., Lucero, R. V., Ambrosi, C. M., and Entcheva, E. (2015). Cardiac Optogenetics: Enhancement by All-trans-Retinal. *Scientific Reports*, 5:16542.

Zegers, M. M., O'Brien, L. E., Yu, W., Datta, A., and Mostov, K. E. (2003). Epithelial polarity and tubulogenesis in vitro. *Trends in cell biology*, 13(4):169–176.

Zeissig, S., Bürgel, N., Günzel, D., Richter, J., Mankertz, J., Wahnschaffe, U., Kroesen, A. J., Zeitz, M., Fromm, M., and Schulzke, J. D. (2007). Changes in expression and distribution of claudin 2, 5 and 8 lead to discontinuous tight junctions and barrier dysfunction in active Crohn's disease. *Gut*, 56(1):61–72.

Zemelman, B. V., Lee, G. A., Ng, M., and Miesenböck, G. (2002). Selective photostimulation of genetically chARGed neurons. *Neuron*, 33(1):15–22.

Zhang, F., Wang, L.-P., Brauner, M., Liewald, J. F., Kay, K., Watzke, N., Wood, P. G., Bamberg, E., Nagel, G., and Gottschalk, A. (2007). Multimodal fast optical interrogation of neural circuitry. *Nature*, 446(7136):633.

Zhang, S., Xu, Y., Wang, B., Qiao, W., Liu, D., and Li, Z. (2004). Cationic compounds used in lipoplexes and polyplexes for gene delivery. *Journal of controlled release*, 100(2):165–180.

Zhao, S., Cunha, C., Zhang, F., Liu, Q., Gloss, B., Deisseroth, K., Augustine, G. J., and Feng, G. (2008). Improved expression of halorhodopsin for light-induced silencing of neuronal activity. *Brain cell biology*, 36(1-4):141–154.

Zhao, S., Ting, J. T., Atallah, H. E., Qiu, L., Tan, J., Gloss, B., Augustine, G. J., Deisseroth, K., Luo, M., and Graybiel, A. M. (2011). Cell type–specific channelrhodopsin-2 transgenic mice for optogenetic dissection of neural circuitry function. *Nature methods*, 8(9):745.